Structural and electronic chemistry : role of symmetrie and curvature

Julia Sabalot-Cuzzubbo

THÈSE

UNIVERSITE DE PAU ET DES PAYS DE L'ADOUR

École doctorale des Sciences Exactes et leurs Applications (ED 211 SEA)

Présentée et soutenue le 06 Avril 2022

par **Julia SABALOT-CUZZUBBO**

pour obtenir le grade de docteur
de l'Université de Pau et des Pays de l'Adour
Spécialité : Chimie Physique

CHIMIE STRUCTURALE ET ÉLECTRONIQUE : RÔLE DES SYMÉTRIES ET DE LA COURBURE

MEMBRES DU JURY

RAPPORTEURS

• Yannick CARISSAN	Maître de conférences - Université Paul Cézanne - Aix-Marseille III
• Sergey KRANOSHCHEKOV	Professeur - Moscow State University

EXAMINATEURS

• Karine COSTUAS	Directrice de recherches - Université de Rennes 1
• Alfonso SAN MIGUEL FUSTER	Professeur - Université Claude Bernard Lyon 1
• Corinne NARDIN	Professeur - Université de Pau et des Pays de l'Adour
• Panagiotis KARAMANIS	Chargé de recherches - Université de Pau et des Pays de l'Adour

DIRECTEURS

• Didier BEGUE	Professeur - Université de Pau et des Pays de l'Adour
• Jacky CRESSON	Professeur - Université de Pau et des Pays de l'Adour

UNIVERSITÉ DE PAU ET DES PAYS DE L'ADOUR

Contents

Remerciements

Je remercie l'ensemble des membres du jury et rapporteurs pour avoir bien voulu évaluer ce travail de thèse.

Je souhaite tout d'abord remercier mes encadrants de thèse, Pr Didier Bégué et Pr Jacky Cresson, pour m'avoir donné ma chance (surtout une seconde chance) et de m'avoir fait confiance tout au long de ces trois années. Je vous remercie pour nos longues réunions (plus ou moins préparées), nos discussions formelles ou informelles et nos échanges de mails (à toutes heures du jour et de la nuit!) qui nous ont permis d'avancer dans nos travaux. Je vous remercie d'avoir investi votre temps et d'avoir toujours été enthousiastes pour mes travaux de thèse.

Je remercie énormément aussi Dr Germain Salvato-Vallverdu, pour toute son aide, son investissement très précieux pour notre projet et sa patience (notamment en programmation!).

Merci également aux Dr William Lafrague-Dit-Hauret et Pr Michel Rerat pour leur réflexion et aide pour notre publication sur les états hélicoïdaux.

Je remercie également toute l'équipe de chimie théorique de l'IPREM pour son aide tout au long de ces trois années. Aussi, je remercie Dr Delphine Bessières et Pr Corinne Nardin pour avoir gentiment suivi mon travail durant tous mes comités de thèse. Merci Corinne pour tous vos conseils et votre écoute dans ma période de doutes pendant mon "faux départ".

Merci Jacky pour ta patience et ta pédagogie quand j'avais besoin d'explications sur certaines démonstrations mathématiques pendant ces trois années.

Merci Didier pour ta patience au début de la thèse quand le lancement de calculs n'était pas évident pour moi et pour nos discussions quotidiennes autour de sujets variés d'actualités ou bien que ce soit sur nos goûts musicaux, les ennuis de santé (le kiné quotidien!) ou le Covid!

Pour terminer, je tiens à remercier mes parents, sans qui, je ne serai certainement pas arrivée là. Merci d'avoir été là pour moi, d'avoir cru en moi durant toutes ces années d'études, merci pour votre soutien, votre présence et votre amour sans faille malgré les difficultés. Nona, je regrette ton absence pour la fin de ma thèse, tu aurais été fière *di tua piccola*.
Enfin, merci à toi aussi Benjamin pour ton soutien quotidien, ton écoute, ton optimisme et pour avoir su comprendre mes doutes pendant ce moment de ma vie.

General introduction

The research theme of this manuscript is part of a dynamic context of research of **new materials**. The current research needs in new materials can be explained by a growing desire to reduce the use of fossil resources to advance in terms of **energy transition**. Our research projects are based on an interdisciplinary collaboration involving **chemistry** and **mathematics**, and are particularly interested in fullerenes molecules, mainly carbon compounds with high potential, whose discovery has generated great interest. In order to exploit the complete potential of these materials, it is essential to understand the relationships between the structural arrangements and the physico-chemical behaviors, in other words their properties and reactivity.

Several challenges emerged when we chose to focus on these topics and we are at the very beginning of the theme project. It fundamental to set up a systematic and rigorous methodology to classify the different structural arrangements and the resulting properties. From classification and by exploiting the mathematical results, in the mid-term objective of the project it would be possible to isolate 3D structures with interesting electrical and mechanical properties. The long term objective is to develop a database that will allow us to propose materials of interest for the improvement of batteries [1] or the optimization of seawater purification membranes [2], to mention only two examples.

This manuscript represents a theoretical overview of **three years of work** and **initiates** investigations on these topics in our research team.

A first approach to these issues, prior to this thesis topic was to research and understand the possible deformations of graphene. Actually, it is known that deformations in the form of waves can modify the intrinsic molecule properties. The first simulations performed in 2018 by the CAPT research group of IPREM were able to show that deformations involving curvature influence the reactivity or conductivity of the material.

After a complete **reminder** in part I, the **second** major part of the work was focused on the study of **concepts** developed by **Robert C. Haddon** [3], a pioneer in the research of the relationship between **curvature** and **reactivity** of materials. He presents the question in both **geometrical and chemical terms**, and shows that the way the object is curved seems to play a major role in its reactivity, in particular on C_{60} fullerene. He proposes the construction of a **pyramidalization angle** associated with the curvature. However, his concept shows **limitations**, the angle cannot be defined in all possible situations. Based on these limitations, we have implemented an answer as generalist as possible, redefining most of R. C. Haddon's concepts and bringing a clarification to the **POAV1** (π-Orbital Axis Vector 1) theory. This preliminary work resulted in the publication of our first article [4] on this topic. This first article is illustrated by concrete examples from D. Tománek and Frederick's database [5]. Following this initial work, the study of other concepts developed by R. C. Haddon [6] became obvious. The notion of **POAV2** (π-Orbital Axis Vector 2) is a more generalized continuity of POAV1 and shows that the notions established by R. C. Haddon are not clear and require further and improved definitions. To allow the solving of some constraints, new and more precise definitions related to the reactivity of fullerenes are presented in this manuscript.

We can resume our first works such as the geometry of a system is not only a problem inherent to the geometry of the object. There is in fact a **coupling** between the **geometry and the orbital information**. It is then, possible to associate a discrete object with an object that can be called continuous "geometrical-chemical".

A **third** major part of this manuscript concerns the study of **aromaticity criteria** according to the theories stated by the researcher Erich Hückel. The properties of some carbon materials such as graphene are based on π-conjugation, aromaticity and therefore on the sp^2 hybridization of the constituent carbons. However, other visions in terms of aromaticity exist for cyclic molecules with sp^2 hybridized carbons. The study of these different notions, developed in the 1960's by Edgar Heilbronner [7] and Howard Zimmerman [8], are proved to be of fundamental importance in our developments.
Based on this work, which is well accepted in the theoretical chemistry community, we have re-established the general **energy equations** of the so-called Möbius systems as a function of the number of electrons π. The logical continuation of the work was the study of π-orbitals of **Möbius** type systems. Recent works of the research team of the famous Nobel prize laureate Roald Hoffmann [9], have particularly interested us. In effect, this work shows a relation between the orbitals of cyclic molecules called "Möbius" and the orbitals of molecules called [n]-cumulenes. Our work presented here, provides an explanation and a mathematical justification of the existence of this curiosity discovered by R. Hoffmann et al. [9] which is called: the **helical orbitals**.
Mathematical developments were complemented by **quantum calculations** performed by **DFT** (Density Functional Theory) and by multi-configuration calculations of the CASPT2 (Theory of Perturbation of the Complete Active Space) type aiming at clarifying and confirming the DFT results (in particular those previously carried out by the team of R. Hoffmann [9]).

From a more **applicative** point of view, our work presents numerous and varied possibilities. First in part II, we have performed precise cartographies of the properties of a large family of **fullerenes**, and **non-fullerenic** molecules, using the notions of pyramidalization angle, curvature, hybridization, and angular defect. It should be noted that the implementation of our illustrations is possible, with the support of a visualization program [10] available for free online, that was specially developed for the project by our research group at IPREM.
Then, in order to improve our understanding of the behavior of the curiosities represented by the **helical orbitals**, we have carried out an important visualization work on **[n]-cumulenes**, various molecules with and without hetero-atoms.

Publication and preprints associated to the thesis

- Relating the molecular topology and local geometry: Haddon's pyramidalization angle and the Gaussian curvature *(J. Sabalot-Cuzzubbo, G. Salvato-Vallverdu, D. Bégué, and J. Cresson. Relating the molecular topology and local geometry: Haddon's pyramidalization angle and the Gaussian curvature. Journal of Chemical Physics, 152:244310, 2020)*
- Etude des structures optimales et équivalentes de quelques molécules - le cas linéaire et le cercle pour la distribution nulle ou de Möbius *J. Sabalot-Cuzzubbo, J. Cresson, D. Bégué. 2020. Preprint)*
- Generation of helical states - Breaking of symmetries, Curie's principle, and excited states *(J. Sabalot-Cuzzubbo, D. Bégué, J. Cresson. 2021. Preprint hal-03360966f)*
- Haddon's POAV2 versus POAV theory for non-planar molecules *J. Sabalot-Cuzzubbo, J. Cresson, D. Bégué. 2021. Preprint)*

Part I

Reminders

This first part gives the necessary reminders for the understanding of the manuscript: reminders of geometry and chemistry.

The geometry reminder gives an overview of the geometric-chemical structure of the molecules according to the available information but also to give the criteria of a molecular skeleton.

The chemistry reminder includes the main points such as: the two Hückel methods with their characteristics, the definition of the geometry of a molecule from a chemical point of view, the interactions between atomic orbitals, and the context of Hückel matrices.

This last point gives a review of the:

- *Schrödinger equation,*
- *wave functions,*
- *atomic orbitals,*
- *Hamiltonian matrix,*
- *interaction assumptions,*
- *eigenvalues and energies of molecular orbitals.*

Finally, we present the necessary reminders concerning the methods of quantum computation.

0.1 Problem of geometry

0.1.1 Geometrical-chemical structure of molecules

Molecules can be described according to different information: geometrical, chemical and electronic.

- The geometrical data concerns the curve on which the atoms are arranged. This open or closed curve is of limited length in $\mathbb{R}^3$.
- The chemical data relates to the orbital structures specific to the molecule.
- The electronic data is about the electrons available in the molecule to form chemical bonds.

From a geometrical point of view we studied the cases of N atoms arranged either on straight line segments L_N we will discuss about a linear chain, or circles which will be assimilated to cycles S_N.

It should be noted that the geometrical point of view can be confusing. Indeed, the part we are interested in is related to the symmetry group of the molecule. The use of a curve to describe the arrangement of the atoms simplifies the study, but is not clearly representative of the molecule.

0.1.2 The skeleton of a molecule

For a molecule M made of N atoms noted A_i with $i = 1, ..., N$. We can characterize a molecule by a set of points $\mathscr{A}$ in $\mathbb{R}^3$ which will be represented by the position of the atoms. There exists a matrix $\mathscr{R}$ such that $R_{i,j} = 1$ if A_i and A_j form a bond and $R_{i,j} = 0$ if there is no binding. We then associate a molecule to $M = (\mathscr{A}, \mathscr{R})$.
We associate for a molecule M a geometrical representation called skeleton of the molecule. By definition, we define the skeleton as the geometrical object in $\mathbb{R}^3$ obtained by the plot of a segment between atoms A_i and A_j if $R_{i,j} = 1$. We note $S(M)$ the skeleton of M.

0.2 Problem of chemistry

From a chemical point of view, to correlate the adjacent matrices of the graphs associated with the molecules seen previously, we consider the Hückel matrices, then Hückel methods.

0.2.1 Hückel methods

The study of **Hückel matrices** provides a first approximation to study only the molecular interatomic distances but not the geometry, which requires further investigation of the Hückel method approach. A hierarchy between the matrices is organized according to the consideration of the neighboring atoms in the molecules. These matrices are associated with the graph theory.
A distinction is made between the **simple Hückel method** and the so-called **extended method** [11]. First, in the simple method, it is the interactions between atoms of the same nature that are of interest. In this case, only one orbital is involved, and finally allows the study of interatomic distances between first neighbors.
The simple method leads only to relations with parameters α, β. Where α is the coulombic integral, a negative parameter which represents the energy of the atomic orbital (AO) before interaction and β the negative resonance integral which is proportional to the overlap between two AOs and depends on the distance between atoms. A non-zero value of the β parameter shows the influence of the overlap, so the resonance integral must be used when two AOs are involved. It is then very complicated to solve the system. This method is therefore preferred in cases where only identical atoms are present and that only one AO is involved and that the interactions between neighbors are constant. The example of π-systems of hydrocarbons is to be preferred in this case. The advantage of the extended Hückel method is that it is applicable to all molecules and does not make any other approximation

than the monoelectronic Hamiltonian, but has some limitations. Indeed, the limitations are based on the simplification of the Hamiltonian, where, for example the differentiation of the energies of the distributions of two electrons between 2 degenerate molecular orbitals (MO) is not possible.

0.2.2 Geometry of molecules

As indicated at the beginning of the work 0.1.1, we consider molecules whose geometric structure is carried by a curve in $\mathbb{R}^3$ parameter such that: $\gamma : [0, l] \to \mathbb{R}^3$, where $l > 0$ is the length of the curve. We have then: $\Gamma = \gamma([0, l])$ the curve. *Note that we use the curvilinear coordinate tools.*

The atoms are uniformly positioned on the curve, we remind that N is the number of atoms whose position is given as :

$$t_i = (i-1)\left(\frac{l}{(N-1)}\right) \tag{1}$$

with i = 1, ..., N

The first and the last atom constitute the beginning and the end of the curve.

Note that the N atoms are arranged in $\mathbb{R}^3$, so if an atom has a bond or an interaction with another atom then it is connected by a segment. A polygonal curve is obtained which sometimes be replaced by a curve, a line or a circle.

We tried to describe the structure of the MOs of these molecules, so we used the Hückel methods as in 0.2.1.

0.2.3 Interaction with the atomic orbitals

Let us consider an atom and the family of atoms interacting with it. The interaction takes place between two AOs such that χ_a and χ_b. Two AOs interact to form an MO if their **overlap integral** is non-zero [11].

$$S_{a,b} = \langle \chi_a \mid \chi_b \rangle \tag{2}$$

This result is obtained from the formula of Wolsberg-Helmhotz described in [11].

The literature studies mostly simple geometries of molecules where the interactions between AOs are essentially between neighboring atoms arranged on the curve. In general, we consider an atom A_i and its interactions with A_{i-1} and A_{i+1}. Finally, the effective geometry does not play a role since everything occurs locally.
The existence of overlap between orbitals is also related to the molecular geometry.

Let us illustrate this with a helix where the N atoms are arranged. For a circular helix the parameters are:

$$\begin{cases} x(t) &= r\cos(t) \\ y(t) &= \epsilon r \sin(t) \\ z(t) &= bt \end{cases} \tag{3}$$

where ϵ is $+1$ or -1 which corresponds to the direction of the helix and $b > 0$ the pitch of the helix $2\pi b$.

The interaction between atoms is given by the length l_i which is the distance at which two atoms interact through their *AO*. The neighboring atoms of the curve will obviously interact and then we consider the first, second neighbors etc. It is then possible to filter the structure to take into account the longer interactions. The structure of the helix induces that if $2\pi b < l_i$ then, there will be interaction

with an atom positioned further on the curve. This, will have some consequence on the shape of the Hückel matrices for helical curves.

0.2.4 Hückel matrices

To be interested in Hückel matrices, we need to study the Schrödinger equation.

Schrödinger equation, wave functions and atomic orbitals

The **Schrödinger equation** associated to the **Hamiltonian** H is:

$$\boxed{H.[\Psi] = E.\Psi} \tag{4}$$

Ψ being the **MO** and solutions of the equation. Moreover, the wave functions are eigenfunctions of the Hamiltonian operator H.

The set of **wave functions** is defined as a vector space in $\mathbb{C}$, denoted by $\mathcal{O}$ and a scalar product defined for all ϕ and ψ such that:

$$\langle \phi, \psi \rangle = \int_{\Delta} \phi * \psi \mathrm{d}x \tag{5}$$

where dx is the volume element, Δ the space in which we work and $\phi* = \bar{\phi}$ the complex conjugate of ϕ.

Note χ_i $(i = 1, ..., n)$ are the **AOs** associated to atoms A_i.

They verify:

$$\langle \chi_i, \chi_i \rangle = 1 \tag{6}$$

and

$$\langle \chi_i, \chi_i \rangle = S_{i,j} \tag{7}$$

with i, j = 1, ..., N and where $S_{i,j}$ is the overlap integral of the AOs χ_i and χ_j.

Hückel's hypothesis consists in using the AOs as the basis of the vector space $\mathcal{O}$, i.e. to neglect the overlap between 2 distinct orbitals. Any wave function $\Psi \in \mathcal{O}$ is written as a linear combination of the AOs with coefficients in $\mathbb{C}$:

$$\Psi = \sum_{i=1}^{N} c_i \chi_i \tag{8}$$

with $c_i \in \mathbb{C}$.

The notion of **normalization** of Ψ is given by $\langle \Psi, \Psi \rangle = 1$ is:

$$\sum_{i=1}^{N} c_i^2 = 1 \tag{9}$$

The Hamiltonian : Matrix H

We also associate to the Hamiltonian operator H a matrix $\mathbf{H}$ using the orthonormal basis $\mathcal{O}$. We note this basis: $\phi_i, i = 1, ..., N$ and define such that:

$$\mathbf{H} = \begin{pmatrix} H_{11} & H_{12} & \dots & H_{1N} \\ H_{21} & H_{22} & \dots & H_{2N} \\ \dots & \dots & \dots & \dots \\ H_{N1} & H_{N2} & \dots & H_{NN} \end{pmatrix} \tag{10}$$

where column i is the vector $H[\phi_i]$.

The coefficients H_{ij} are obtained by the scalar product between ϕ_i and $H[\phi_i]$:

$$H_{ij} = \langle \phi_i \mid H \mid \phi_j \rangle = \langle \phi_i, H[\phi_j] \rangle \tag{11}$$

From a vector point of view the Schrödinger equation is written:

$$\mathbf{H}.\Psi = E.\Psi \tag{12}$$

The **eigenvalues** of the matrix **H** correspond to the eigenvalues of the operator H. The **eigenvectors** of **H** are the coefficients of the **eigenfunctions** of H in the basis $\{\phi_i\}_{i=1,\dots,N}$.
The matrix **H** has some properties. If only one type of atom is involved in the molecule, i.e. if it is homogeneous, we have for all i:

$$\mathbf{H}_{ii} = \alpha \tag{13}$$

where α depends only on the atom considered.

The mentioned parameter α (in 0.2.1) represents the **energy** of an electron in the considered AO and we have :

$$\mathbf{H}_{ij} = \mathbf{H}_{ji} \tag{14}$$

Thus, the matrix is symmetric. As a consequence, the eigenvalues are real and the eigenvectors orthogonal.

Interaction hypotheses, geometry and H matrix

Let us focus on the coefficients of the **H** matrix . The hypotheses are presented by Y. Jean and F. Volatron in [11] :

- if two AOs are not carried by bounded atoms we have : $H_{ij} = 0$,
- if two AOs are carried by bound atoms we have:

$$H_{ij} = \mu_{ij}\beta \tag{15}$$

*where β is the **total overlap** of the two AOs and μ_{ij} is $0 < \mu_{ij} \leq 1$ which depends of the overlap of the two AOs.*

Set :

$$\mu_{ij} = \cos(\phi_i) \tag{16}$$

where ϕ_i is the distribution of the orbitals.

The matrix **H** is written as:

$$\mathbf{H} = \alpha \mathbf{Id}_N + \beta \mathbf{A}_\phi \tag{17}$$

The matrix $\mathbf{A}_\phi$ is :

$$\mathbf{A}_\phi = \begin{pmatrix} 0 & \cos(\phi_1) & 0 & \dots & \dots & 0 & \cos(\phi_N) \\ \cos(\phi_1) & 0 & \cos(\phi_2) & 0 & \dots & \dots & 0 \\ 0 & \cos(\phi_2) & 0 & \cos(\phi_3) & 0 & \dots & 0 \\ \vdots & & & & & & \\ 0 & \dots & \dots & 0 & \cos(\phi_{N-2})\beta & 0 & \cos(\phi_{N-1}) \\ \cos(\phi_N) & 0 & \dots & \dots & 0 & \cos(\phi_{N-1}) & 0 \end{pmatrix} \tag{18}$$

We note $\nu_1(\phi) \leq \cdots \leq \nu_N(\phi)$ the real ordered **eigenvalues** of $\mathbf{A}_\phi$:

$$\lambda_i = \alpha + \beta\nu_i(\phi) \tag{19}$$

A_ϕ is of zero trace:

$$\sum_{i=1}^{N} \nu_i(\phi) = 0 \tag{20}$$

and

$$\sum_{i=1}^{N} \lambda_i = N\alpha. \tag{21}$$

Eigenvalues and energy of molecular orbitals

To find the **eigenfunctions** of the Schrödinger equation it is necessary to determine the solutions of the system: $\mathbf{H}\Psi = E\Psi$.

Consider then for all $E \in \mathbb{R}$ the matrix:

$$\mathbf{M}(E) = \mathbf{H} - E\mathbf{Id} \tag{22}$$

where $\mathbf{Id}$ *is the identity matrix of* $\mathbb{R}^N$.

An eigenfunction of H is equivalent to the existence of a non-zero solution of the linear system:

$$\mathbf{E}(E)\Psi = 0 \tag{23}$$

A necessary and sufficient condition is that the characteristic polynomial of $\mathbf{H}$ is zero in E:

$$P_{\mathbf{H}}(E) = \mid \mathbf{M}(\mathbf{E}) \mid = 0 \tag{24}$$

where $\mid . \mid$ *represents the determinant.*

Indeed, in this case the matrix $\mathbf{M}(E)$ has a non-zero kernel and therefore non-zero solutions.
The matrix $\mathbf{M}(E)$ is symmetric, its eigenvalues are real, so we can order them:

$$\lambda_1 \leq \lambda_2 \leq \cdots \leq \lambda_N \tag{25}$$

Also, the polynomial $P_{\mathbf{H}}(E)$ can be written by factorization:

$$P_{\mathbf{H}}(E) = (E - \lambda_1) \dots (E - \lambda_N) \tag{26}$$

For more details, about the characteristic polynomial of $\boldsymbol{H}$*, refer to Appendix 2 section 1.*

We can then determine the **total energy** E of the molecule such that:

$$\boxed{E = \sum_{i=1}^{N} g_i E_i} \tag{27}$$

where g_i *is the quantum number of the orbital* Ψ_i *which by the principle of exclusion of Pauli can take the values 0, 1, or 2 since each orbital can at most 2 electrons.*

Note $\pi(S)$ **the number of electrons** available to make bonds:

$$\sum_{i=1}^{N} g_i = \pi(S) \tag{28}$$

We can deduce the value of g_i according to the parity of $\pi(S)$:

- if $\pi(S) = 2m$ then $g_i = 2$ for $i = 1, \ldots, \frac{\pi(S)}{2}$ and $g_i = 0$ if $i = \frac{\pi(S)}{2} + 1, \ldots, N$
- if $\pi(S) = 2m + 1$ then $g_i = 2$ for $i = 1, \ldots, \frac{\pi(S)-1}{2}$, $g_i = 1$ for $i = \frac{\pi(S)+1}{2}, \ldots, N$ and $g_i = 0$ for $i = \frac{\pi(S)+1}{2} + 1, \ldots, N$.

Thus,

$$\boxed{E_i = \alpha + \beta\nu_i(\phi)} \tag{29}$$

We have:

$$\boxed{E = \pi(S)\alpha + \beta \sum_{i=1}^{N} g_i\nu_i(\phi)} \tag{30}$$

For more details, about the total energy of a molecule, refer to Appendix 2 section 2.

Distribution of a molecule

Associated to the notion of Hamiltonian, it is necessary to define the notion of **distribution of a molecule** which we will use in the following.

The distribution of a molecule is determined following steps:

- the Hückel matrix must be written,
- calculate the scalar products H_{ij} which are decomposed according to the formula 15.

The quantity corresponding to the distribution is then an angle ϕ_i, which is associated to $H_{i,i+1}$. As the angle is not clearly identified, we have to take into account the basis of the wave functions used with a vector basis in $\mathbb{R}^3$.

0.3 Quantum computing methods

In all the work presented in this manuscript, we have carried out calculations using *ab-initio* and **density functional theory (DFT)** implemented in the **Gaussian** code [12], we used in particular the DFT Hamiltonian type B3LYP [13, 14]. We mainly used Gaussian which is a popular and widely used quantum chemistry software. It is a gaussian based software ideally used for closed-shell systems and can be used with different methods (DFT, Hartree-Fock, Moller-Plesset,...). In order to obtain reliable energies on multi references systems calculations were also carried out in both CASSCF and CASPT2 levels of theory. These calculations were performed using Molpro program packages [15].

0.3.1 Description of electronic structure of molecules

When one wants to determine electronic properties of atoms and molecules by the point of view of **molecular modeling**, we have to remember that in the "quantum world" the Schrödinger equation is the master equation that describes the behavior of all the bodies in submicroscopic scale. Based on the De Broglie's observations on the wave-particle behavior of the matter, the Schrödinger equation is based on the fact that all bodies behave as waves with a certain wavelength.
This equation has some special characteristics:

- it is best solved as an algebraic partial differential equation, not as an analytical one
- it is an equation of eigenvalues, as the ones in algebraic mathematics and, for this, it needs linear operators and functions that describes vector in an algebraic space

- it needs the function to give the same function back, i.e., it needs a "guess" function to find this same function itself after a cycle of calculation.

The last item states the basis of what is called the **self-consistent field** . The guess function is used to solve Schrödinger equation, yielding eigenvalues and a function in a "better shape".
In a realistic world, solving this equation is not possible for a system with more than two electrons. It is in this point that "quantum chemistry" started to be developed more strongly with the introduction of approximations that allow one to solve the electronic structure of multi-electronic atoms and molecules. These approximations can be divided into physical-mathematical approximations and physical approximations. The **first physical approximation** is the **Born-Oppenheimer**, that states that as the nuclei of the atoms are much heavier than the electrons, they are much slower, so, they can be considered as statistic while the electrons move. This results in the decoupling of partial equations that would have needed to be calculated on both spatial coordinates (nuclei and electrons) before, and now, with such approximation, they need to be calculated only on the nuclei coordinates **or** on the electron coordinates.

By the third decade of XXth century, novel approaches have been proposed to determine the electronic structure of molecular systems and solids. The first one was proposed by D. R. Hartree and Vladimir A. Fock. The so-called **Hartree-Fock** method consists in treating the electrons and their wave-function as a determinant called Slater's determinant. This mathematics allowed the calculation to take place considering that the multi-electronic problem could be resolved as "multi" problems of one electron. This was introduced by an effective potential operator (Fock operator) which states a general field of electrons. This means that one electron is sensible to the electromagnetic field of the nuclei and the other N-1 electrons. This also does not take into account any relativistic effect that may happen.

This one-electron picture could then be implemented in a computational code to be solved iteratively (based on the self-consistent field scheme). The electrons could be translated into mathematical functions called **basis set** . These electrons could then be associated to specific orbitals (wave-functions) respecting the Pauli's exclusion theorem. The composition of the molecular orbitals was performed on the basis of a **linear combination of atomic orbitals** (LCAO method). The basis set can then be decorticated and designed to accommodate the needs of the physical problem being studied (number of core functions, polarization effects, felxibility to accomodate ionic clouds, etc).

Because of the one-electron picture, the Hartree-Fock method lacks of description of the electronic correlation in a many-body system. In this way, metallic systems and systems where electrons can delocalize over a region of the space are poorly-described by this method. Many others, called **post-Hartree-Fock** methods have tried, with different degrees of success, to incorporate these effects on the Hartree-Fock scheme. This, has been accomplished by **Perturbation theory**, as it is the case on nth order **Moller-Plesset perturbation theory** (MPn), coupled-cluster, configuration of interactions, multi-configuration methods, and semi-empirical ones.

A common point between these methods, exception made for the semi-empirical ones, is the limitation on the number of basis functions. These methods, although quite efficient on the description of the electronic structure of molecules, mainly, scale quickly with the number of atoms and in this way, are not practical for every system being studied, even though they would be very appropriate because the description of both exchange and correlation would be the appropriate in many cases. The semi-empirical methods, by their turn, can be employed for large systems, with a very low accuracy though. This is due to the fact that multi-center integrals are not calculated "on the fly" but are replaced by experimentally-obtained (or calculated with a higher level of theory method for model systems) values. This has been bypassed in parts by the introduction of **Density Functional Theory (DFT)** and this is discussed in the next section.

0.3.2 Density Functional Theory (DFT)

The use of **Density Functional Theory (DFT)** became a common-place in the molecular modeling of materials in the nanometric scale. In this method, the energy of a system is described as a functional of the electronic density, skipping the direct wave-function calculation in the process. While wave-function-based methods, such as Hartree-Fock (HF), solve a Schrödinger-like equation (the Fock equation), DFT is based on the assumption that there is a relationship between the total electronic energy and the overall electronic density.

Note that for the Fock equation, the same is valid for Perturbation Theory based methods, such as MP2, and Coupled-Cluster one.

The first basis of this idea was already present in the Thomas-Fermi model, however the breakthrough came by the Hohenberg-Kohn theorem in 1964, showing that the ground-state energy and other properties of a system were uniquely defined by the electron density. In other words, the energy E is hence a functional of the density $\rho(\vec{r})$ at the point $\vec{r}$. Based on the definition of the electric potential, one can write this as:

$$E[\rho(\vec{r})] = \int V_{ext}(\vec{r})\rho(\vec{r})d\vec{r} + F[\rho(\vec{r})] \tag{31}$$

The first term $V_{ext}(\vec{r})$ arises from the interaction of the electrons with the external potential produced by the Coulomb interaction with the nuclei. On the other hand, $F[\rho(\vec{r})]$ is the sum of the kinetic energy of the electrons and the contribution from inter-electronic interactions.

The **variational method** can be applied in the solving of this equation, in which the minimum value of $E[\rho(\vec{r})]$ represents the energy of the electron density of the ground-state. From this, it is a common-sense that DFT is intrinsically incapable of describing excited-states without further physical-mathematical considerations.

Then, in 1965, with the **Kohn-Sham** (KS) theorem, the term $F[\rho(\vec{r})]$ is suggested to be approximated as the sum of three terms in the form:

$$F[\rho(\vec{r})] = E_{KE}[\rho(\vec{r})] + E_H[\rho(\vec{r})] + E_{XC}[\rho(\vec{r})] \tag{32}$$

where $E_{KE}[\rho(\vec{r})]$ is the kinetic energy, $E_H[\rho(\vec{r})]$ the electron-electron Coulombic energy (also known as Hartree electrostatic energy), and $E_{XC}[\rho(\vec{r})]$ a term responsible for describing the exchange and correlation contributions.

The first term is further defined as the **kinetic energy** of a system of non-interacting electrons with the same density $\rho(\vec{r})$ as the real system. The second term associates the**electrostatic energy** as the classical interaction between two charged densities over all possible pairwise interactions. It is interesting to note that this term is classical and do not take into account the quantum *many-body* behavior of the electrons, i.e., as they are correlated to each other and the Heisenberg uncertainty principle, for instance.
Finally, the last term is then responsible for accounting for this quantum behavior of electrons and it is one of the master pieces of DFT, known as the exchange-correlation functional. As no analytical form of this functional is known, several approximations are proposed to treat this quantum mechanical problem and based on this, DFT cannot be considered always as an *ab initio* method, since the definition of this functional can take into account empirical parameters. However, even simple approximations to it can give favorable results and this is the key success of DFT.
Numerically, the electronic structure of the system is solved in a self-consistent way, in which a guess of a initial electronic density is fed into the above equations. The application of the variational approach allows one to reach the ground-state electronic density and, consequently, energy by a so-called

self-consistent field .
Calculating these specific energies for a multi-electronic system takes the form of multi-centered multi-index integrals, what is responsible for a ready increase in the computation time (often in the order of $O(N^4)$, where N is the number of atoms). In this way, treating large molecular systems becomes almost non-practical.
Moreover, the combination of these two equations bears a striking resemblance to those of Hartree-Fock theory. The difference between them is found on the fact that the HF has no correlation being calculated whereas KS is a correlated method. To go former to the latter, one only needs to replace the exchange energy by the exchange-correlation one.

0.3.3 The exchange-correlation functionals

The fact that the **exchange-correlation functional** is not known gives rise to the appearance of several difference ready to be employed by the user. Choosing the most appropriate demands testing it against the family of materials being studied and the nature of the physical-chemical issue.

The first functionals are based on two different approximations: the **Local Density Approximation** (LDA) and **Generalized Gradient Approximation** (GGA). For the former, the electron density varies locally whereas for the latter it also depends on gradient of it. In well-behaviored systems, the electron density is smooth, almost constant, thus, it does not depend on its gradient, justifying the use of LDA for these cases. For heteroatomic systems, this may not be true and GGA may become needed.
To refine even more the quality of the results, mainly the atomization energies, bond lengths and vibrational frequencies, functionals called **hybrid** have been developed over the three last decades. These functionals incorporate a portion of the exact exchange in HF theory with exchange and correlation from other sources such as LDA and GGA. These functionals are constructed by a linear combination of the HF exact exchange functional and any other exchange-correlation functional. The weight of participation of each component is typically found by fitting the predictions done by these functionals to experimental results.

The most used **hybrid functionals** are **B3LYP** [16, 17], **PBE0** [18, 19], **HSE** [20] and meta-hybrid **GGA** (as the Minnesota functionals) [21, 22]. Specifically, the B3LYP functional which has been used throughout this thesis, is written in the form of:

$$E_{XC}^{B3LYP} = E_X^{LDA} + a_0(E_X^{HF} - E_X^{LDA}) + a_x(E_X^{GGA} - E_X^{LDA}) + E_C^{LDA} + a_c(E_C^{GGA} - E_C^{LDA}) \quad (33)$$

Where E_{XC}^{B3LYP} stands for the exchange-correlation energy in the B3LYP scheme, E_X^{LDA} the exchange energy in the LDA scheme, E_X^{HF} the exchange energy of HF, E_X^{GGA} the exchange energy in GGA scheme, E_C^{LDA} the correlation energy in LDA scheme, and E_C^{GGA} the correlation energy in GGA scheme. The parameters a_0, a_x and a_c are the weight of participation of each component and assume the values of 0.20, 0.72 and 0.81, respectively. These parameters were determined beforehand by A. Becke by fitting the analogous B3PW91 functional to a set of molecular parameters [13].

This functional has been widely used for description of ground state properties of molecular systems. However, a serious low accuracy appears when trying to describe excited state properties and where the self-interaction problem becomes pathological.

Note that the self-interaction problem consists on the fact that a electron can interact with itself. This leads to problem of over-delocalization of the electron cloud since this electron tends to repulse itself.

This drawback has limited the use of B3LYP functional for charge-transfer systems and problems evolving the energies of the excited states for example.

0.3.4 Multi reference methods

Unlike the **Restricted Hartree-Fock (RHF)** solution which corresponds to the description of a **Slater** determinant made up of $\frac{N}{2}$ doubly occupied orbitals the exact solution that we are trying to describe by taking into account the correlation is in fact made up composed of an infinite number of configurations that can be thought of as excitations with respect to the N-electron RHF determinant in an infinitely large base. Of course, it is impossible to work in a complete or infinite basis. Various methods are then proposed by theoretical chemists to evaluate as accurately as possible this correlation. Three types of approaches are used :

- the methods aiming at solving variably the Schrödinger equation in the eigenstates by using a basis of Slater determinants or configurations. These are **Configuration Interaction (C.I.)** type approaches,
- perturbation methods requiring the definition of a minimal basis and a partition of the Hamiltonian operator adapted to ensure the convergence of the perturbation series in a Rayleigh-Schrödinger type approach,
- pairwise methods which consist in evaluating the correlation energy of pairs of electrons assumed without interactions (Independent Electron Pair Approximation - IEPA) or in interaction (Coupled Pair Theory).

These approaches have all in common that they build the basis for the development of the desired function from single-electron functions optimized at the **Hartree-Fock level** (generally monodeterminal ground state).

On the contrary, in the **Multi Configurational Self Consistent Field (MCSCF)** methods, the objective is to optimize with the use of a variational method both the monoelectronic functions used and the multiconfigurational development of the eigenfunction of the electronic Hamiltonian.

Among the numerous developments proposed, the **Complete Active Space Self Consistent Field (CASSCF)** approaches lead to the development of the multiconfigurational wave function on the totality of the configurations generated by the set of all possible excitations in a restricted space of occupied and virtual molecular orbitals (active space).

The purpose of this paragraph is not to present the mathematical details of all these computations method, but rather to set out the general considerations for the use of these approaches when one has to describe one or more electronic states of more or less strongly correlated electrons. Thus, in a system where static correlation is not involved, the RHF determinant remains a relatively good approximation for the description of the wave function. The addition of a method taking into account the dynamic correlation is done with this determinant (as for the DFT, methods ...). The RHF determinant is considered as the reference determinant. On the contrary, in the case of a system of strongly correlated electrons several Slater determinants must be considered to describe this state. The wave function used is most often a CAS wave function and the dynamic correlation is taken into account on the latter. This CAS wave function being made of several determinants, the system has several references. The term Multi-Reference (MR) thus translates the fact of considering the dynamic correlation on several reference determinants.

Part II

π-Orbital Axis Vectors theory

We dedicate this part to the theory of π-orbital axis vectors, as we are interested in the π-orbitals of molecules. Their interest, is that they are involved in molecular reactivity.

But how to get interested in them?

- *By using DFT calculation methods, however it is heavy and long in preparation and calculation time, and it is not possible for large molecules.*
- *Therefore, we are interested in the work of Robert C. Haddon's research team which proposes simple calculation tools but not sufficiently generalized.*

Thus, in this part of the manuscript we propose a detailed review, the extension and the interpretation of these different tools.

Introduction: Study of the Robert C. Haddon's concepts

The interest of this part concerns the issue of **reactivity** which is a fundamental point for the study of molecular structures. The goal is to carry out **cartographies** representing the reactivity. Many current topics depend on the knowledge of this reactivity as for instance in the case of hydrogen storage, or in some porous systems.
Generally, the obtention of these cartographies are performed by quantum calculations as DFT but they are sometimes complex in the case of molecules with a large number of atoms, or by molecular dynamics which is not sufficiently accurate.
To find the solution to these limitations, we must refer to the fundamental notions of reactivity. Chemically, the reactivity is connected to the π-system, it is therefore necessary to find one or more **tools** in order to determine this system, without quantum calculations, in an explicit and algorithmic way and in a not expensive way.

In the first chapter, we answer these questions by referring to the work of Robert C. Haddon, a pioneer on these topics. Initially, R. C. Haddon tried to identify the **planarity** of molecules, to answer this, he proposes a set of tools and notions.
The first notion is the **pyramidalization angle** well-known by chemists. First described by R. C. Haddon in regular cases in his article "C_{60}: sphere or polyhedron?" [3], we have chosen in this manuscript to work also in less regular cases.
Then, it is the notion of **π-Orbital Axis Vector 1 (POAV1)** illustrated by R. C. Haddon and L. T. Scott [23] related to the pyramidalization angle that we investigate. The POAV1 is the vector tool that best describes the direction of the π-system of a molecule. It provides a more precise access to the notion of system planarity even if the pyramidalization angle gives a first knowledge of it.
Hybridization, a well-known tool, is also studied in detail, in order to relate hybridization to the POAV1. However, despite all these tools, there are some limitations. Tools from mathematics, and more particularly from differential geometry, are useful. Concepts of **curvature**, and especially **spherical curvature** are given. In addition, we also consider the **angular defect**.
We study precisely all the concepts developed by the researcher and consider some of his concepts in a more general way with physical, geometrical and chemical meanings.

In the second chapter, we first explain the **methods of implementation** of the concepts that we have used throughout this work. Then, we expose the **application methods** that we have developed with the different concepts presented. We present among other things, our visualization program based on the concepts applied to a database of fullerene. Finally, we present a large number of our results according to all the notions on non-fullerenic molecules and along a reaction path of nitrile imine molecule (energy, minimum and maximum values of pyramidalization angle, hybridization, angular defect, spherical curvature, and the corresponding cartographies).

The third chapter, provides an opportunity to explore beyond the first concepts with a reflexion on the **POAV2** concept proposed by R. C. Haddon [6] as a complement to POAV1.
We conclude the chapter with an overview of possible applications of the concepts for the characterization of geometries, topologies, and reactivity of organic covalent molecules.
Then, we give a comparison between the two tools **POAV1** and **POAV2**, in order to show which is the most appropriate since there is no other method to characterize the π-system and more specifically the reactivity.

Chapter 1

The π-Orbital Axis Vector 1 (POAV1) theory

In this chapter, we consider and study 3 main points:

1. *the clarification of the notions of pyramidalization angle (Pyr), π-Orbital Axis Vector (POAV1), hybridization and curvature,*

2. *the extension to the notion of angular defect,*

3. *the properties of POAV1 and associated tools based on fullerenes and other non-fullerenic compounds.*

We used, among others [3][23][6], and results published in our first paper [4].

1.1 The π-Orbital Axis Vector (POAV1) of Robert C. Haddon

1.1.1 Pyramidalization angle and π-Orbital Axis Vector (POAV1)

Robert C. Haddon developed in 1990s the concept of **pyramidalization angle** (Pyr) and **π-Orbital Axis Vector (POAV1)** ([3, 23, 6]). In this series of articles, R. C. Haddon describes the concept for molecules such as fullerenes and more particularly the C_{60} fullerene. He introduces a **local concept**, i.e. specific to an atom. So from a geometrical point of view with respect to a vertex, since the fullerene (illustrated in first approximation as a soccer ball by Kroto et al.[24]) can be apprehended as a discrete sphere made of 20 hexagons and 12 polygons. We will then distinguish the use of the Pyr and π-Orbital Axis Vector (POAV1) in **regular trivalent** cases and in **non-regular trivalent** cases.

Regular trivalent case

The **trivalent regular case** is the simplest case that we can observe. It is the case studied by R. C. Haddon in [3]. In fact, R. C. Haddon studies the specific case of C_{60}, and assumes that all the carbon-carbon bonds are identical thus that they are of the same length and that the angles between bonds are equal.

The following figure illustrates the angle θ_{AB} associated to calculation of Pyr and the normal vector (n_a) in the specific case of C_{60}:

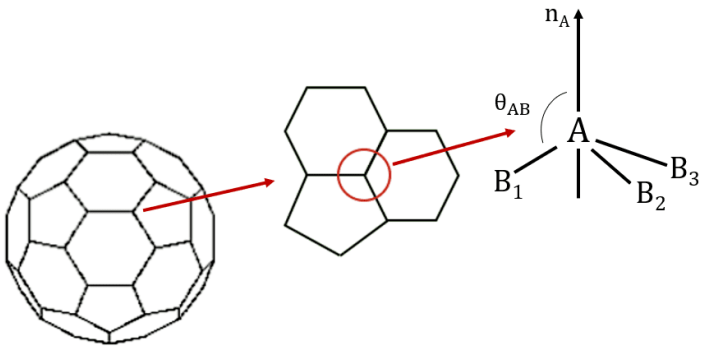

Figure 1.1: Representation of the pyramidalization angle in a regular case

Trivalent regular case means that all the bonds are of equal lengths and that each atom of the molecule is connected to three atoms.
In the case of any fullerene, the carbon atom studied are then always be bounded by 3 neighboring carbon atoms.

For the construction of Pyr we consider an atom and its three neighbors as a polyhedron with vertex A and the star of A ($\star(A)$) containing the three neighbors B. We can calculate the **angle of pyramidalization** in A such that :

$$\boxed{Pyr(A) = \theta_{AB} - \frac{\pi}{2}} \tag{1.1}$$

It should be noted that if $Pyr(A) = 0$ the molecule is considered as planar and if $Pyr(A) \neq 0$ the molecule is non-planar.

The Pyr is by definition obtained for a given atom A in a molecule associated with the existence of the particular vector called **POAV1(A) vector** which has the property to make a constant angle θ_{AB} with each neighbors B connected to A [25]. Where, B $\in \star(A)$ such that $\frac{\pi}{2} < \theta_{AB} < \pi$.

Thus, the vector POAV1(A) is the normal vector to the plane formed by the neighboring B atoms at the vertex A.

To prove the previous statements, let A be a given atom of the molecule M. As the molecule M is trivalent, we have three connected atoms B_1, B_2, B_3 connected to A. These three atoms define a plane $\mathcal{P}(A)$. As the three bonds are equivalents, the atom A belongs to the intersection of each mediating plane, then in particular to the line passing trough A and the intersection of the mediating line in the triangle defined by B_1, B_2 and B_3. Let us denote by I the intersection point of all mediating line in the plane $\mathcal{P}(A)$. We define POAV1(A) as the unique unitary vector directed from I to A.

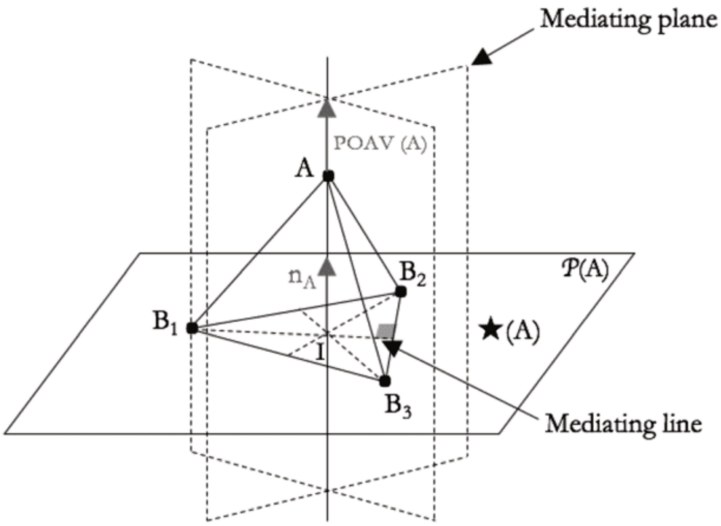

Figure 1.2: Construction in a trivalent regular case [4]

It remains to prove that POAV1(A) is such that the angle with each bond is constant. We first remark that the vector POAV1(A) is normal to the plane $\mathcal{P}(A)$. Indeed, the line (IA) belongs to the intersection of two intersecting planes which are normal to the plane $\mathcal{P}(A)$. It follows that POAV1(A) is a normal vector in A.

Let B be an atom of $\star(A)$ in $\mathcal{P}(A)$. Let us denote by l the bond length between A and atoms of $\star(A)$ and z_A the height IA of A with respect to the plane $\mathcal{P}(A)$. We denote by θ_{AB} the angle between POAV1(A) and the bond AB.

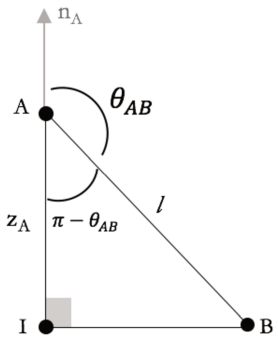

Figure 1.3: Angle between a bond and the POAV1(A) vector [4]

The angle θ_{AB} satisfies:

$$\cos(\pi - \theta_{AB}) = \frac{z_A}{l} \tag{1.2}$$

and,

$$\sin(\pi - \theta_{AB}) = \frac{IB}{l} \tag{1.3}$$

As θ_{AB} satisfies $\frac{\pi}{2} \leq \theta_{AB} < \pi$, we have $0 \leq \pi - \theta_{AB} < \frac{\pi}{2}$ and the value of the arccos is sufficient to determine $\pi - \theta_{AB}$ completely. As seen in the formula, the angle θ_{AB} depends only on z_A and l which are quantities independent of B. As a consequence, θ_{AB} is a quantity only depending on A and the length of the bond but independent of B. As a result, that the angle between the vector POAV1(A) and each bond is constant.

To finish, from a more mathematical point of view we can refer to the works of Liu's team [26] and Romon's manuscript [27]. Indeed, the existence of the vector POAV1(A) is associated with the existence of a cone in A, which is tangent to the faces containing A. This is a mesh property which can be denoted as cone mesh. All meshes whose vertices are trivalent are conical. Romon [27] also shows that a mesh whose vertices are of order 4 is conical. We then understand that in such a case the POAV1 can be determined.

Non-regular trivalent case

As we have just seen, R. C. Haddon defines the Pyr only in a certain case but not in a **non-regular trivalent case** [3, 23, 6]. The construction in a trivalent non-regular case will depend on the existence of a **regularized star** of a given atom in a molecule. Note that the POAV1 vector can be defined even for non-regular trivalent molecule.

In fact, for a trivalent molecule M, and A the considered atom of M. We define for each neighboring atom B $\in \star(A)$, a $Reg_\epsilon(B)$ with $\epsilon > 0$, a point of AB. We have then $Reg \star (A)$ i.e a **ϵ-regularized** $\star(A)$ as in the following figure 1.4.

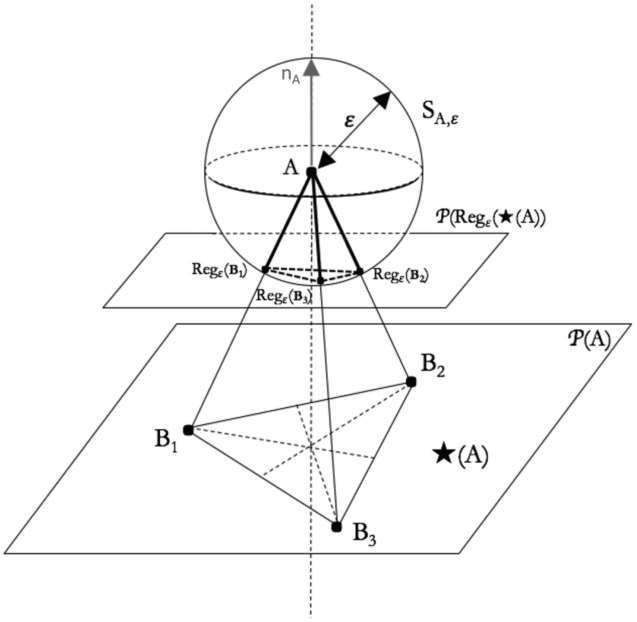

Figure 1.4: Representation of the regularized $\star(A)$ [4]

$Reg_\epsilon(B)$ is define by the relation:

$$\boxed{\overrightarrow{AReg_\epsilon(B)} = \frac{\epsilon}{AB}\overrightarrow{AB} \; \forall \in \star(A)} \tag{1.4}$$

with

$$\epsilon(A) = min_{B\in\star(A)}AB \tag{1.5}$$

which corresponds to the minimum of the bound lengths starting in A.

Finally, the regularization of the star of a given atom is **extendable** to the Pyr.
By definition, for a trivalent molecule M and A an atom of M, let $\epsilon > 0$, the ϵ-pyramidalization angle of M in A is defined as the Pyr associated with A and the ϵ-regularized star of A.
This definition depends only on ϵ, and this is not sufficient.

We have then, for the same type of trivalent molecule, a $\epsilon > 0$ and $\mathrm{POAV}_\epsilon(\mathrm{A})$ be the vector defined in 1.1.1. The $\mathrm{POAV}_\epsilon(\mathrm{A})$ is **independent** of ϵ.

The proof of this definition is developed in Appendix 2 section 3.

We can then deduce an essential point of the $\epsilon - Pyr$: for M a trivalent molecule and for $\epsilon > 0$, the $\epsilon - Pyr$ in A is **independant** of ϵ.

This property can be used to compute the Pyr in concrete cases where the bond lengths are not equals.

Note that this result is stated in the work of R. C. Haddon [3] p.1798.

1.2 Relationship with chemistry

The Pyr definition explained (1.1.1), is a **pure geometrical construction**. In fact, R. C. Haddon and L. T. Scott [23] expressed that the Pyr provides a *"convenient index of the degree of non-planirity"* of a given atom of a molecule. The major issue of R. C. Haddon is **chemistry** [3][23][6] and especially the chemical properties of the molecules related to the geometry. The need is to interpret the Pyr in this framework. As we seen in the previous section, the Pyr is related to the **POAV1** but also with others properties as the **hybridization** of atomic orbitals, and the measure of the **local distortion** of a given π-electron system in a given molecule.

1.2.1 Hybridization

The pyramidalization angle as defined previously, depends only on geometrical data and refers to the **non-planarity** of molecules. It is thus also related to the **hybridization** of AO.

We are interested in non-planar systems, so **non-planar conjugate systems**. We have the system of hybrid σ-orbitals. These hybrid orbitals (h_1, h_2, h_3) are linear combinations of the s and p_x, p_y, p_z orbitals. They are defined as:

$$h_i = c_{i,1}s + c_{i,2}p_x + c_{i,3}p_y + c_{i,4}p_z \tag{1.6}$$

The aim is to obtain the maximum **overlap** between orbitals, we must use p_i vectors allowing this condition.

We define the orbitals such that:

$$p_i = c_{i,2}p_x + c_{i,3}p_y + c_{i,4}p_z \tag{1.7}$$

with i = 1, 2, 3 and where c_i is a vector $c_i = (c_{i,2}, c_{i,3}, c_{i,4})$ and each p_i is directed along a internuclear axis between A and an atom B of $\star(A)$.

More generally, let :

$$\boxed{h_i = c_{i,1}s + \lambda_i p_i} \tag{1.8}$$

with i = 1, 2, 3.

Based on the work of R. C. Haddon and L. T. Scott [23] and the approach of Radziszewski et al. [28], we describe the **hybrid π-orbitals** as:

$$\boxed{h_\pi = c_\pi s + \lambda_\pi p_\pi} \tag{1.9}$$

Hybrid $\pi-$orbitals are related to the concept of **POAV1** (for reminder POAV1 makes equal angles with the σ-bonds of the neighboring atoms). The connection between POAV1 and hybridization is made by the angle $\theta_{i,\pi}$ *(with i = 1, 2, 3)*, which is the angle between p_π and p_i such that:

$$\theta_{1,\pi} = \theta_{2,\pi} = \theta_{3,\pi} \tag{1.10}$$

We take then the first relation of the Pyr (eq. 1.1):

$$\boxed{Pyr(A) = \theta_{\sigma,\pi} - \frac{\pi}{2}} \tag{1.11}$$

If we refer to the work of R. C. Haddon [6], we also show that the orbitals of the **σ-bonds** diverge from the internuclear axis when the angles between the σ-bonds are inferior or equal to **100**°. In the case of **π-orbitals** this is valid only when the angles between bonds are close. However when the σ-bonds are really different R. C. Haddon suggests the use of another tool that he calls **POAV2** , which takes into account the orthogonality between σ and π-orbitals. The POAV1 matches the POAV2 only if the bonds are **equal**.

To construct the geometrical model we have just described, we need to place it in a suitable reference frame. We also need to consider the POAV1, and p_π collinear to p_z as in eq. 1.9.

Thus, by indicating that the plane $\mathcal{P}$ is orthogonal to p_z, the σ-orbitals h_1, h_2 and h_3 make an angle made by $Pyr(A)$ with the plane $\mathcal{P}$ as : $\frac{\pi}{2} + Pyr(A)$.

If we refer to the work of R. C. Haddon and L. T. Scott [23], what we have just explained, can be summarized as an **intermediate hybridization** between sp^2 and sp^3 depending on the angle of Pyr. Then, we choose a reference frame to have the internuclear axis in the *(x, z)* plane such as:

$$\boxed{h_i = c_{i,1}s + c_{i,2}p_x + c_{i,3}p_y + c_{i,4}p_z} \tag{1.12}$$

with i = 1, 2, 3.

Orthogonality and normalization conditions

We define a condition of **orthogonality** between the **hybrid orbitals** described previously (section 1.2.1). In fact, the hybrid orbitals h_1, h_2, h_3, and h_π are orthogonal to each other.

The **orthogonality condition** is:

$$\boxed{c_{i,1}c_\pi + c_{i,4}\lambda_\pi = 0} \tag{1.13}$$

We also specify :

$$c_{i,1} = \mu_i \lambda_\pi \tag{1.14}$$

and

$$c_{i,4} = -\mu_i c_\pi \tag{1.15}$$

with i = 1, 2 3.

The angle between p_z and each h_i is the same, it implies:

$$\mu_1 = \mu_2 = \mu_3 = \mu \tag{1.16}$$

The expressions of the **σ-orbitals** are:

$$\begin{aligned} h_1 &= \mu(\lambda_\pi s - c_\pi p_z) + c_{1,2}p_x \\ h_2 &= \mu(\lambda_\pi s - c_\pi p_z) + c_{2,2}p_x + c_{2,3}p_y \\ h_3 &= \mu(\lambda_\pi s - c_\pi p_z) + c_{3,2}p_x + c_{3,3}p_y \end{aligned} \tag{1.17}$$

In order to **normalize** the **π-orbitals** we have:

$$\boxed{c_\pi^2 + \lambda_\pi^2 = 1} \tag{1.18}$$

In the same way the normalization according to s and p_z:

$$\begin{aligned} h_1 &= \frac{1}{\sqrt{3}}(\lambda_\pi s - c_\pi p_z) + c_{1,2}p_x \\ h_2 &= \frac{1}{\sqrt{3}}(\lambda_\pi s - c_\pi p_z) + c_{2,2}p_x + c_{2,3}p_y \\ h_3 &= \frac{1}{\sqrt{3}}(\lambda_\pi s - c_\pi p_z) + c_{3,2}p_x + c_{3,3}p_y \end{aligned} \tag{1.19}$$

The detailed proofs of the normalization are available in Appendix 2 section 4.

Relation between hybridization and the POAV1

We can determine the relationship between the **hybridization coefficients** presented just previously and the **POAV1** :

$$\boxed{c_\pi = \sqrt{3}c_{1,2}\tan(Pyr(A))} \tag{1.20}$$

and

$$\boxed{\lambda_\pi = \sqrt{1 - 3c_{1,2}^2\tan^2(Pyr(A))}} \tag{1.21}$$

We give the explicit formula of c_π and λ_π determining the **POAV1** vector. These coefficients are related by the normalization condition and their values depend on the Pyr.

The proofs of the development of the coefficients is given in Appendix 2 section 5.

We note that the works of R. C. Haddon and L. T. Scott [23] show the existence of c_π in the case of molecules with a C_{3v} symmetry.

We proven what R. C. Haddon and L. T. Scott [23] expose in terms of hybridization in the precise case of a C_{3v} **symmetry**.

This **specific symmetry** requires an adapted reference frame:

$$\begin{aligned} c_{2,2} &= c_{3,2} < 0 \\ c_{2,3} &= -c_{3,3} \end{aligned} \tag{1.22}$$

In this specific symmetry, there are three σ_v planes of symmetry in the plane (p_x, p_y) :

$$c_{2,2}^2 + c_{2,3}^2 = c_{1,2}^2 \tag{1.23}$$

This equality corresponds to the fact that we have an equilateral triangle with $c_{1,2} > 0$.

The σ-**orbitals** are:

$$\boxed{h_1 = \frac{1}{\sqrt{3}}(\lambda_\pi s - c_\pi p_z) + c_{1,2}p_x}$$

$$\boxed{h_2 = \frac{1}{\sqrt{3}}(\lambda_\pi s - c_\pi p_z) + c_{2,2}p_x + c_{2,3}p_y} \tag{1.24}$$

$$\boxed{h_3 = \frac{1}{\sqrt{3}}(\lambda_\pi s - c_\pi p_z) + c_{2,2}p_x - c_{2,3}p_y}$$

If we normalize according to the sp^3 **hybridization** conditions:

$$\begin{aligned} h_1 &= \frac{1}{\sqrt{3}}(\lambda_\pi s - c_\pi p_z) + \frac{\sqrt{2}}{\sqrt{3}}p_x \\ h_2 &= \frac{1}{\sqrt{3}}(\lambda_\pi s - c_\pi p_z) - \frac{1}{\sqrt{6}}p_x - \frac{1}{\sqrt{2}}p_y \\ h_3 &= \frac{1}{\sqrt{3}}(\lambda_\pi s - c_\pi p_z) - \frac{1}{\sqrt{6}}p_x + \frac{1}{\sqrt{2}}p_y \end{aligned} \tag{1.25}$$

The proofs of these sp^3 hybridization conditions is given in Appendix 2 section 6.

Relative weight and hybridization numbers

Knowing the hybridization of an atom, we have interested in the weight of each component of an orbital, this is called the **relative weight**. We consider an orbital of type:

$$\boxed{h = a_s s + a_x p_x + a_y p_y + a_z p_z} \tag{1.26}$$

with a_s, a_x, a_y, a_z the real coefficients and p_i the weight of the AO $p_i \in$ (s,x,y,z).

The aim is to compare the contribution of each orbital therefore, the relative weight between 2 given orbitals.

We consider the **relative weight** of the AO of s in MO h compared to the AO x in MO h as:

$$\boxed{w_{s,x}(h) = \frac{w_s(h)}{w_x(h)}} \tag{1.27}$$

In the others cases we have the same approach:

$$w_{s,y}(h) = \frac{w_s(h)}{w_y(h)} \tag{1.28}$$

$$w_{s,z}(h) = \frac{w_s(h)}{w_z(h)} \tag{1.29}$$

The **global weight** denoting by $p = a_x p_x + a_y p_y + a_z p_z$, is in this case the (s,p)-relative weight:

$$\boxed{w_{(s,p)} = \frac{w_s(h)}{w_x(h) + w_y(h) + w_z(h)}} \tag{1.30}$$

The important property of the relative weight is that there are **invariant** when the orbital is multiplied by a scalar $\mu \in \mathbb{R}$. This notion of weight for a given orbital can be extended to a finite family of orbitals

representing a particular local geometry.

The relative weight of a system of orbitals is given by:

$$w_{s,\star}(\mathfrak{h}) = \sum_{i=1}^{4} w_{s,\star}(h_i) \tag{1.31}$$

with $\mathfrak{h} = (h_i)_{i=1,...,4}$ *a family of orbitals,* $(s,\star)$ *the relative weight of* $\mathfrak{h}$ *and* $\star \in \{x,y,z\}$.

Still based on the work of R. C. Haddon and L. T. Scott [23], we are interested in **hybridization numbers** that determine the weight of each orbital in a molecular system.

We define:

$$m = \frac{1}{\tilde{\lambda_\pi^2}} \tag{1.32}$$

and

$$n = \tilde{\lambda_1^2} + \tilde{\lambda_2^2} + \tilde{\lambda_3^2} \tag{1.33}$$

with $\tilde{\lambda^2} = \frac{\lambda_\pi^2}{c_\pi^2}$.

We have the set of orbitals:

$$h_\pi = N_\pi(s + \tilde{\lambda}_\pi p_\pi) \tag{1.34}$$

$$h_i = N_i(s + \lambda_i p_i) \tag{1.35}$$

where $\| p_i \| = 1$ *for* i = 1,2,3.

Finally, the **hybridization numbers m** and **n** correspond to the relative weight of orbitals:

$$m = w_{s,z}(h_\pi) = \frac{w_s(h_\pi)}{w_z(h_\pi)} = \frac{1}{\tilde{\lambda_\pi^2}} = \frac{c_\pi^2}{\lambda_\pi^2} \tag{1.36}$$

$$n = w_{s,z}(\mathfrak{h}_\sigma) + w_x(\mathfrak{h}_\sigma) + w_y(\mathfrak{h}_\sigma) \tag{1.37}$$

$$\boxed{m = \frac{2\tan^2(Pyr(A))}{1 - 2\tan^2(Pyr(A))} = \frac{c_\pi^2}{\lambda_\pi^2}} \tag{1.38}$$

and,

$$w_x(\mathfrak{h}_\sigma) = w_y(\mathfrak{h}_\sigma) = 1, \tag{1.39}$$

then,

$$\boxed{n = 3m + 2} \tag{1.40}$$

From a computational point of view, the hybridization numbers can be used to describe the **hybridization** of the **σ-orbital**:

$$s^{\lambda_\pi^2} p_{x,y}^{n-3m} p_z^{c_\pi^2} \tag{1.41}$$

and the **π-orbitals** hybridization:

$$s^{c_\pi^2} p_z^{\lambda_\pi^2} \tag{1.42}$$

We are interested in the 2 classical cases of sp^2 and sp^3 **hybridizations.**

In the sp^2 case we have:

$$(sp^2_{x,y}p^0_z)_\sigma(s^0p^1_z)_\pi = (sp^2)_\sigma(p^1_z)_\pi$$

And in the sp^3 case, we have $\lambda_\pi = 0.866$ and $c_\pi = \frac{1}{2}$:

$$(s^{0.75}p^2_{x,y}p^{0.75}_z)_\sigma = (s^{0.75}p^{2.25})_\sigma(s^{0.25}p^{0.75})_\pi$$

To be more applicative, we will show in the continuation of the manuscript the illustrations of all the parameters described on fullerenes and non-fullerenic molecules.

From Robert C. Haddon's point of view [29], the **hybridization** of the π-orbitals will depend on the parameter m and the proportion of the weight of the s orbital to the p_z orbital as:

$$s^{c^2_\pi}p^{\lambda^2_\pi}_z \Longleftrightarrow s^{\frac{c^2_\pi}{\lambda^2_\pi}}p_z \tag{1.43}$$

If we consider the equation 1.38, again we find the parameter m : $\boxed{s^m p}$

In the case of **hybridization** of σ-orbitals , we fix $\tilde{n}$:

$$\tilde{n} = \frac{2}{\lambda^2_\pi} + m \tag{1.44}$$

Then, we have:

$$\tilde{n} = 3m + 2 \tag{1.45}$$

Thus, considering this new parameter, the average **hybridization** of the σ-orbitals is given by $\boxed{sp^{\tilde{n}}}$

We also define another parameter **Y** called **sigma hybridization** in relation to m which indicates the **deviation** of the conjugation of a system but also the contribution of the hybridization of the p_z orbital in each h_i orbital which will take into account the topology of the system such as the $Pyr(A)$:

$$\boxed{Y = m\frac{\lambda^2_\pi}{3} = \frac{c^2_\pi}{3}} \tag{1.46}$$

It is therefore possible to rewrite the hybridization of a system according to this new parameter, which will not change anything from a chemical point of view.

1.3 Limitations of the pyramidalization angle and the POAV1

As we have seen previously, the **pyramidalization angle** and the **POAV1** are closely related. The definition of the Pyr is connected to the existence of the POAV1 vector. Indeed, both are determined via an atom considered as a vertex in the molecule.

If we consider the case of the C_{60} fullerene proposed by R. C. Haddon [3], he places his work in a particular and well defined situation where it is admitted that the atoms are all identical, the bond lengths and the angles equal. However, it is obvious that the reality is different. We have therefore seen that the Pyr could not be defined for arbitrary molecules.

More precisely, the pyramidalization angle can not be extend outside the family of **admissible molecules**.

The existence of a POAV1(A) vector implies that POAV1(A) has to be normal to any plane $\mathcal{P}_\epsilon(A)$. In fact, if POAV1(A) exists and is different from n_A, the unique unitary vector to all plane $\mathcal{P}_\epsilon(A)$, then it makes a given angle $\alpha > 0$ with n_A. The POAV1(A) vector then generate a cone based in A by rotation around the axes n_A corresponding to all the vectors v such that v makes an angle α with the normal axe. As a consequence, for each bond corresponds a different vector, except when $\alpha = 0$ corresponding to the normal vector (figure 1.5).

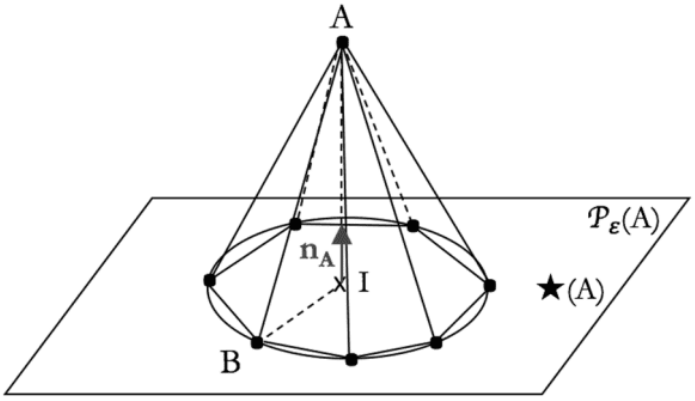

Figure 1.5: Representation of the pyramidalization angle [4].

From now, we assume that POAV1(A) is normal to any $\mathcal{P}_\epsilon(A)$. For each triple choice T of elements in $\text{Reg}_\epsilon(star(A))$, the explicit construction of the POAV1(A) vector (section 1.1.1) gives a unique vector POAV_T1(A) which is colinear to the vector I_TA where I_T is the intersection of the mediating line in the triangle defined by T. In general, other choice of triples will lead to different I_T. As A must belong to each line perpendicular to $\mathcal{P}_\epsilon(A)$ and passing trough I_T for each T, this is not possible in general unless all the I_T coincide, meaning that all the atoms of $\text{Reg}_\epsilon(\star(A))$ belong to a circle.

The two characteristics correspond to the definition of **admissible molecules**.

As a consequence, one must think to other characterizations of the local geometry of a molecule in order to study molecules of order ≥ 4 in some atoms.

Admissible molecules

We define an **admissible molecule** as:
a molecule M is said to be admissible if for each atom A of M and $\epsilon > 0$, there exists a plane $\mathcal{P}_\epsilon(A)$ such as $Reg_\epsilon(\star(A)) \subset \mathcal{P}_\epsilon(A)$.

The geometry of the previous conditions is resumed in figure 1.6. If the atom A does not belong to the same plane as the atoms of $Reg_\epsilon(\star(A))$, then it belongs to the intersection of all the mediating plane of the line segment between two arbitrary atoms of $Reg_\epsilon(\star(A))$.

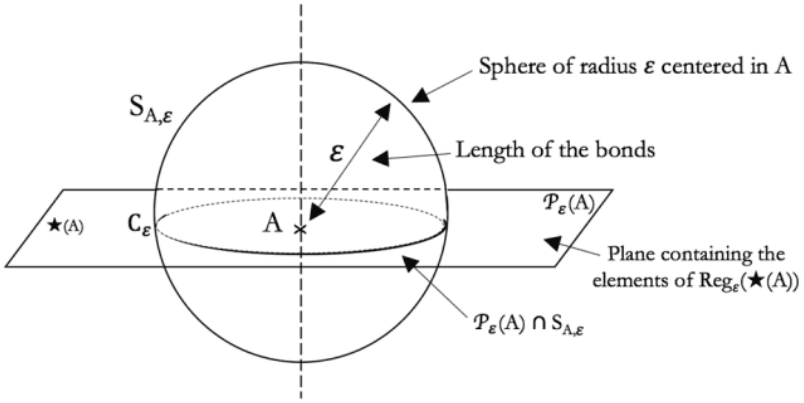

Figure 1.6: Geometry of an admissible molecule [4].

As the intersection of two planes define a line, it gives huge constraints on the positioning of each atom of $Reg_\epsilon(\star(A))$, in particular, they belong to a circle C_ϵ in the plane $\mathcal{P}_\epsilon(A)$. If we denote by O_ϵ the center of C_ϵ, then A belongs to the line passing through O_ϵ and normal to $\mathcal{P}_\epsilon(A)$.

The previous remark can be used to define the POAV1(A) vector in this general situation :
let M be an admissible molecule and A be an atom of M. Let $\epsilon > 0$ be given. We denote by C_ϵ the circle in $\mathcal{P}_\epsilon(A)$ such that $Reg_\epsilon(\star(A)) \subset C_\epsilon$. We denote by O_ϵ the center of C_ϵ. We denote by POAV1(A) the normal unitary vector to $\mathcal{P}_\epsilon(A)$ defined by:

$$POAV1(A) = \frac{\vec{O_\epsilon A}}{O_\epsilon A} \tag{1.47}$$

As usual, the POAV1 vector is defined through quantities depending on ϵ so that it is not *a priori* trivial that it gives a well-defined quantity. However, by construction, the set of points $Reg_\epsilon(\star(A))$ and $Reg_{\epsilon'}(\star(A))$ for two different ϵ, and ϵ' are homothetics as Reg_ϵ is a homothety of center A for all ϵ. In particular, homotheties are affine transformations that send a line to a parallel line.
As $Reg\epsilon(\star(A))$ belongs to a plane $\mathcal{P}_\epsilon(A)$, $Reg_{\epsilon'}(\star(A))$ belongs to a plane $\mathcal{P}_{\epsilon'}(A)$ parallel to $\mathcal{P}_\epsilon(A)$ and has the same normal vector. By normalization, we obtain a unique vector POAV1(A) normal to all the plane $\mathcal{P}_\epsilon(A)$ for $\epsilon > 0$.

Having the POAV1 vector, we can directly generalize the notion of *Pyr* as:
let M be an admissible molecule and A be a given atom of M. The *Pyr* in A denoted by Pyr(A) is the angle between the vector POAV1(A) and each bond AB, $B \in \star(A)$.

The proofs of this definition is given in Appendix 2 section 7.

1.4 Haddon's spherical Curvature

We note that the term **curvature** is well-defined in classical differential geometry for smooth (continuous) surfaces. On the other hand, in the discrete case, i.e. for polyhedral surfaces, the definition is more problematic. That is why, we are interested in the work of R. C. Haddon [3], especially concerning the **spherical curvature** which is related to the **pyramidalization angle**.

1.4.1 Spherical curvature

To represent the shape of a molecule, the notions of *Pyr* and curvature are often **confused**, that is

why R. C. Haddon expresses in his work [3] the notion of **spherical curvature**.

The simple notion of **curvature** is given for a smooth curve in $\mathbb{R}$ and related to the osculating circle. The curvature is given by the parameter $\frac{1}{R}$ where R is the radius of the **osculating circle**. The objective is to approximate locally up to order 2 the curve by an arc of a circle. In $\mathbb{R}^3$ it is necessary to approximate the surface by a portion of sphere but it is not so simple.

If we propose a definition:
for an osculating sphere, let M be a regular molecule trivalent. For each atom A, there exists a unique sphere $S(A)$ such as A $\in S(A)$ and for all B $\in \star(A)$, B $\in S(A)$. The sphere $S(A)$ is named the **osculating sphere** to M in A, the following figure 1.7 represents the notion. Thus, by definition, the **spherical curvature** is the quantity $\kappa(A)$:

$$\kappa(A) = \frac{1}{R_A} \tag{1.48}$$

where R_A is the radius of the osculating sphere to M in A.

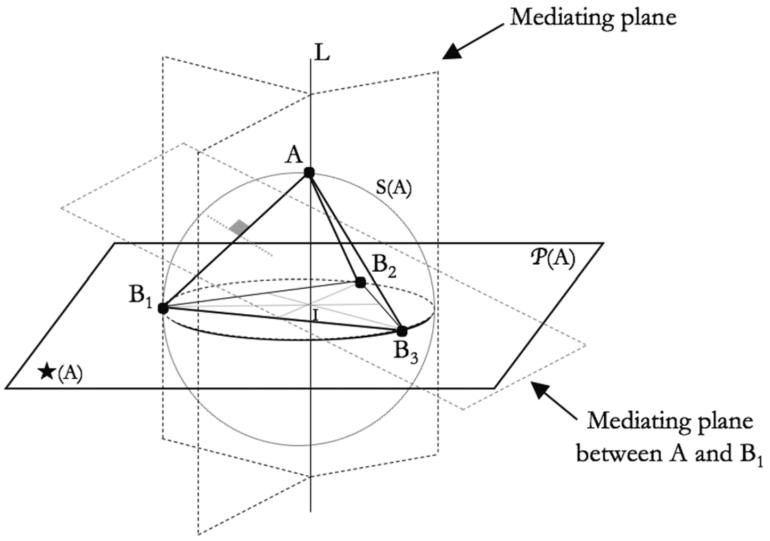

Figure 1.7: Representation of the osculating sphere and the spherical curvature [4]

We can therefore relate the spherical curvature to the Pyr by a **non-linear** relationship:

$$\boxed{\kappa(A) = \frac{2\sin(Pyr(A))}{a}} \tag{1.49}$$

The proofs of this relation is given in Appendix 2 section 8.

We have then, when the Pyr is small the previous relation which became **linear**:

$$\boxed{\kappa(A) \simeq \frac{2}{a} Pyr(A)} \tag{1.50}$$

1.4.2 Spherical curvature in non regular case

We can compute the spherical curvature in more **general cases**. The following figure describes the situation:

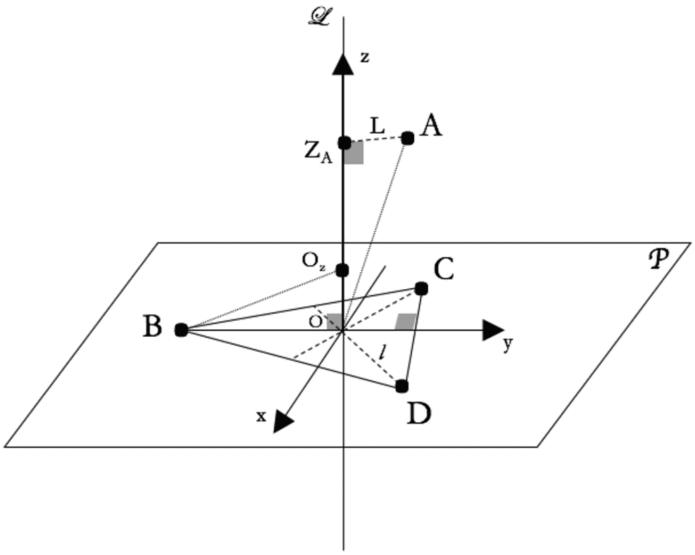

Figure 1.8: Spherical curvature in non-regular case [4]

In the case presented here, the osculating sphere is of center O_z ($O_z = (0, 0, z)$ such as:

$$\boxed{z = \frac{L^2 + z_A^2 - l^2}{2z_a}} \tag{1.51}$$

where z_A is the coordinate of A, $l = OB = OC = OD$ and $L = O_zA$.

Therefore, the spherical curvature is given by:

$$\boxed{\kappa(A) = \frac{1}{\sqrt{l^2 + \frac{(L^2+z_A^2-l^2)^2}{4z_A^2}}} = \frac{1}{\sqrt{l^2 + \frac{(OA^2-l^2)^2}{4z_A^2}}}} \tag{1.52}$$

The proofs of the relation in given in Appendix 2 section 9.

The spherical curvature gives access to the **non-planarity** of a molecule. However, we are always in the case of trivalent molecules.

1.4.3 Limitations of the spherical curvature

In the classical trivalent case, the **spherical curvature** provides a nice way to characterize the **non-planarity** of a given molecule. However, the generalization to molecules which are not trivalent leads to severe difficulties and is in general **impossible**.

If we consider a molecule which has atoms of order 4. Let A be an atom of this type. Then $\star(A)$ is made of 4 points B, C, D and E. In order to generalize the notion of spherical curvature, one has to construct a sphere interpolating the 5 points. The geometric construction of the osculating sphere made in section 1.4.2 for trivalent molecules determine a unique sphere interpolating 4 atoms. As a consequence, selecting any triple of points in $\star(A)$ denoted by T, one construct a unique **osculating sphere** in A with respect to T denoted by $S(A)_T$. In general, all these spheres are different and there exists no osculating sphere to the molecule in A.

Moreover, the spherical curvature describes the surface locally as a **dome** i.e a portion of a sphere. By consequence, this quantity is **not** sufficient to capture the **local geometry** of molecules that admit a

smooth representation, which have a negative **Gaussian curvature**, and that must be distinguished from a molecule with a positive Gaussian curvature.

1.5 Angular defect

The **angular defect** is a well-known notion in discrete differential geometry. This notion is always definable whereas the Pyr and the spherical curvature are not necessarily definable.
The angular defect is useful because it makes it possible to compute the **local shape** of a molecule.

To begin, we focus on the **Gaussian curvature** which can be defined as: a circle of radius r around p, which implies that for a given metric d on Σ, and a set of point $x \in \Sigma$ as $d(x,p) = r$ and $P(r)$ the circumference of the circle.

Note for more details that in terms of discrete curvature, the Gaussian curvature defines the local curvature for any type of polyhedron with a number of neighbors superior to 3. It gives a measure of how far the surface deviates from a plane surface at a vertex.

To determine the Gaussian curvature $G(p)$, we need to compare the circumference of a circle in the plane given by $2\pi r$ to the value of P on Σ.
The **Gaussian curvature** is given as:

$$\boxed{P(r) = 2\pi r - G(p)\pi\frac{r^3}{3} + \dots} \tag{1.53}$$

We consider the following quantity $K(p)$ to generalize what is mentioned above:

$$K(p) = 2\pi - \frac{P(r)}{r} \tag{1.54}$$

Related to the Gaussian curvature, the **angular defect** is defined as:

$$\boxed{K(A) = 2\pi - \sum_{T \in \mathcal{T}(A)} \alpha_T} \tag{1.55}$$

where α_T is the angle at the vertex A of the face $T \in \mathcal{T}(A)$, $\mathcal{T}(A)$ is the family of triangles T_i obtained by connecting the vertices in $\star(A)$ of two consecutive edges of A.

In reference to Romon's work [27], we know that the angular defect is related to the Gaussian curvature. Note that $K(A) = 0$ if and only if the surface is plane locally at a point A. If $K(A) < 2\pi$ the vertex A is spherical.

As for the other concepts presented in this manuscript, we show the relation between the **angular defect** and the Pyr.
Once again in the case of a **regular** molecule M and with l the length of the bond. We consider A an atom of the molecule, a triangle AB_1B_2 *(where B_1 and $B_2 \in \star(A)$)* and $\alpha_1(A)$, $\alpha_2(A)$, $\alpha_3(A)$ respectively the angles at the vertex A of triangles AB_1B_2, B_2AB_3 and B_3AB_1.

We have by definition:

$$\boxed{\alpha_1(A) + \alpha_2(A) + \alpha_3(A) = 2\pi - K(A)} \tag{1.56}$$

And, the relationship between the Pyr and the angular defect is given by:

$$\boxed{\cos(Pyr(A))\sum_{i=1}^{3}\sin\left(\frac{\theta_i(A)}{2}\right)=\sum_{i=1}^{3}\sin\left(\frac{\alpha_i(A)}{2}\right)} \tag{1.57}$$

$$\cos\alpha_F(A)=\cos^2 Pyr(A)\cos\theta_F(A)+\sin^2 Pyr(A) \tag{1.58}$$

and

$$\theta_1(A)+\theta_2(A)+\theta_3(A)=2\pi \tag{1.59}$$

with $(\alpha_i(A))_{i=1,2,3}$, $(\theta_i(A))_{i=1,2,3}$ and we note by $\mathcal{P}(A)$ the plane defined by $\star(A)$, by O the intersection of the median line of the triangle defined by $\star(A)$, by $\theta_1(A)$ the angle at vertex O of the triangle B_1OB_2, and similarly by $\theta_2(A)$ and $\theta_3(A)$ the angle at vertex O of the triangle B_2OB_3 and B_3OB_1.

The proofs of this relationship is given in Appendix 2 section 10.

To complete these relations, we know that: $\alpha_F(A)=\theta_F(A)$ if and only if $Pyr=0$. Furthermore, we show the relationship between $\kappa(A)$ and Pyr (eq. 1.57). The connection between the two notions is quite complex, using the **Taylor expansion** up to order 3, we can have an approximation of the relation:

$$\cos(Pyr(A))\left(\pi-\frac{1}{48}\sum_{i=1}^{3}\theta_i(A)^3\right)\simeq\frac{1}{2}K(A)-\frac{1}{48}\sum_{i=1}^{3}\alpha_i(A)^3 \tag{1.60}$$

1.6 Conclusion

This chapter provides a **complete** presentation (detailed, clarified, generalized and proven) of tools stated in many works of R. C. Haddon. We present the tools of **pyramidalization angle** and **POAV1** first in the **regular** (perfect) case which is limited to **trivalent** cases which is not necessarily realistic and rather limiting. And then, in the **non-regular** case (i.e. with different bond lengths) but still trivalent. It opens to more cases but still remains limiting. The **regularization** method gives the possibility to generalise a bit more.

The Pyr is a **geometrical** tool and the POAV1 gives access to the privileged direction of the π-orbitals within the system, which gives an indication on the probable deformation of the system, on the **local distortion**, hence the relation with chemistry and more particularly with **reactivity**.

We associate these tools with **hybridization**, it gives the characterization of σ and π-hybrid orbitals according to orthogonalization and normalization conditions and to highlight the intermediate hybridization between sp^2 and sp^3.

The study being complete: the **relative weights** and **hybridization numbers** (m and n) are described which give the composition of the hybrid orbitals involved in the planar or deformed systems. Finally, the **sigma hybridization** which is introduced, gives indications on the conjugation deviation of the system.

Obviously, these tools have some **limitations**, in particular we have defined the **admissible molecules** where these tools are clearly applicable.

These notions are associated with deformation, curvature, and in particular with **spherical curvature** which we prove in the non-regular cases which are the most close to reality but not totally since it remains in trivalent cases.

Finally, we showed that the **angular defect** tool is more universal since it is definable in most cases but has meaning only when it is associated with the Pyr. In effect, the Pyr gives access to the POAV1 which best represents the local reactivity.

All these tools provide access to information on the characterization of systems by their **deformation** and **reactivity**.

Chapter 2

Study of POAV1 over fullerenic and non-fullerenic compounds

In this second chapter, we expose how the different tools presented in the first chapter are used to carry out a complete and detailed study on various compounds:

1. *fullerenic molecules,*
2. *non-fullerenic molecules.*

We also present how the tools are used for an application on a reaction path of a ring expansion of a nitrile imine.

Then, a complete conclusion about these studies is given to explain more clearly the results.

To obtain our results we used a software "Pychemcurv" especially developed for the project thesis [10].

We used data from the database of Tománek and Frederick [5], and results from our first paper [4], but also results from publications of R. C. Haddon, A. R. Khamatgalimov et al. and C. Wentrup and al. [23, 6, 30, 31, 32].

2.1 Methods of implementation of the concepts

To apply the notions developed in chapter 1, we used a software developed by our research team at the Université de Pau et des Pays de l'Adour (UPPA) in the Institut des Sciences Analytiques et de Physico-Chimie pour l'Environnement et les Matériaux (IPREM) and the Institut Pluridisciplinaire de Recherches Appliquées (IPRA), under the supervision of Dr Germain Salvato-Vallverdu.

This collaboration with Dr Germain Salvato-Vallverdu allowed the effective implementation of the POAV1 theory concepts, on a set of fullerenic or more non-fullerenic molecules.

The **software** developed called ***Pychemcurv*** [10] is a python program for structural analyzes of molecular systems or solid state materials focusing on the **local curvature** at an atomic scale. The hybridization of molecular orbitals are obtained by the computation of the local curvature (calculated and mapped data). The software is easy to use since only the **cartesian** coordinates (*.xyz* file) of the systems are required. The program is therefore applicable to most molecular systems. When the *.xyz* files are loaded into the program, it gives access to all the local geometrical and hybridization properties : *Pyr, spherical curvature, angular defect,* c_π^2, λ_π^2, *m, n, hybridization, hybridization sigma.*

Note that the website dedicated to the software is available, which includes all the parameters accessible in an explicative way [10].

In the rest of the chapter we illustrate our results obtained from the software.

Notice that all the computational techniques used to carry out our results are given in Appendix 1.

2.2 POAV1 analysis of the Tománek and Frederick database

Following our interest in the work of R. C. Haddon [3] on the C_{60} fullerene, we chose to work on fullerenic molecular systems. We worked on a **set of molecules** without limiting only on the typical C_{60} fullerene.

To apply the different notions associated to POAV1, we used a very extensive **database** of C_n fullerenes [5] (with n being the number of atoms in the molecule). The database provides the cartesian coordinates and the energy (in electronvolts eV) of the fullerenes admissible from C_{20} to C_{720} according to their symmetries. The database is developed by Tománek and Frederick [5].
We remind that the associated energies of the database are defined according to the work of Guan et al. [33].
The database shows **three** families of fullerenes that we call: **small** (between the C_{20} and C_{60}), **medium** (between C_{60} and C_{100}) and **large** (between C_{100} and C_{720}).

We have focused our analysis on different fullerenes including the C_{32}, C_{40}, C_{60}, and C_{80} which are part of the **small** and **medium** fullerenes family.

2.2.1 Database analysis

The database of Tománek and Frederick [5] presents **2487 isomers** of fullerenes according to their symmetries. The following figure represents the set of isomers of the database:

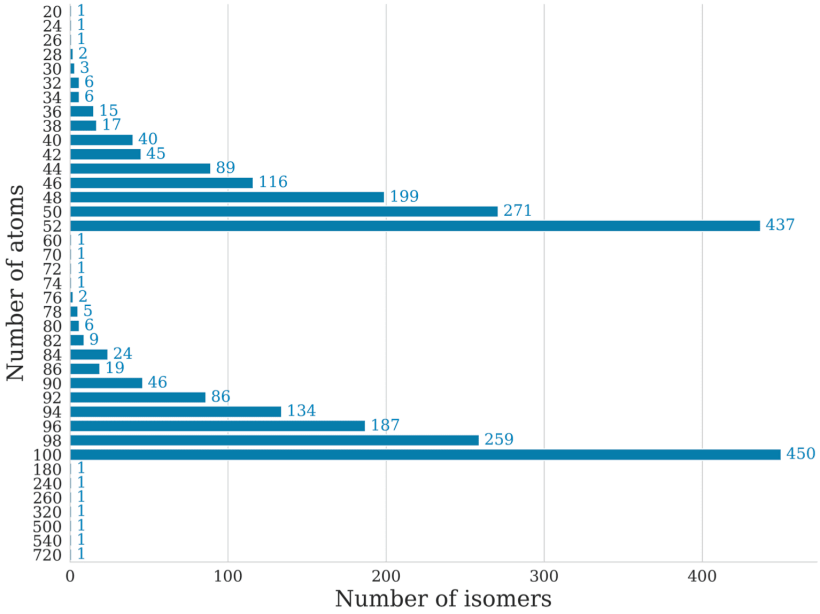

Figure 2.1: Representation of the number of atoms in function of the number of isomers in fullerenes [4]

We observe that C_{100} and C_{52} have the highest number of isomers followed by C_{50}, C_{98}, C_{46}, C_{94}.

On the contrary, the C_{20}, C_{24}, C_{26}, C_{60}, C_{70}, C_{72}, C_{74}, C_{180}, C_{240}, C_{260}, C_{320}, C_{500}, C_{540}, C_{720} present only one type of symmetry.

2.2.2 Analysis following the POAV1 notions

From a general point of view on the **complete database**, we note for our average parameters : a *Pyr* of **10.49°**, an angular defect (*Ang Def*) of **10.42°**, a spherical curvature (*Sph Curv*) of **0.262**, the hybridization coefficients c_π^2 and λ_π^2 are respectively of **0.074** and **0.926** and the hybridization numbers m and n are of **0.084** and **2.252**.
It allows to determine the hybridization (Hyb) as: $(s^{0.926}p_{x,y}^{2.000}p_z^{0.074})_\sigma$ $(s^{0.074}p_z^{0.926})_\pi$.

As mentioned in the section 0.3 and in the Appendix 1, we compute all the following results by using **DFT**, implemented in the Gaussian code with the Hamiltonian type B3LYP with the orbital base 6-31G*.
The following tables display all the **average parameters** (after geometrical optimization) that we have calculated for the fullerenes with only one symmetry.

Firstly for the **large** family of the database:

Fullerene	Pyr(A)	Ang Def	Sph Curv	c_π^2	λ_π^2	m	n	Hybridization
C_{180}	6.68	4.03	0.167	0.027	0.972	0.028	2.084	$(s^{0.0972}p_{x,y}^{2.000}p_z^{0.027})_\sigma$ $(s^{0.027}p_z^{0.972})_\pi$
C_{240}	5.78	3.03	0.145	0.021	0.979	0.021	2.063	$(s^{0.979}p_{x,y}^{2.000}p_z^{0.021})_\sigma$ $(s^{0.021}p_z^{0.979})_\pi$
C_{260}	5.56	2.80	0.140	0.019	0.981	0.019	2.058	$(s^{0.981}p_{x,y}^{2.001}p_z^{0.019})_\sigma$ $(s^{0.019}p_z^{0.981})_\pi$
C_{320}	5.02	2.29	0.126	0.015	0.985	0.016	2.047	$(s^{0.985}p_{x,y}^{1.999}p_z^{0.015})_\sigma$ $(s^{0.015}p_z^{0.985})_\pi$
C_{500}	4.03	1.49	0.101	0.010	0.990	0.010	2.030	$(s^{0.990}p_{x,y}^{2.000}p_z^{0.010})_\sigma$ $(s^{0.010}p_z^{0.990})_\pi$
C_{540}	3.89	1.38	0.098	0.009	0.991	0.009	2.028	$(s^{0.991}p_{x,y}^{2.001}p_z^{0.009})_\sigma$ $(s^{0.009}p_z^{0.991})_\pi$
C_{720}	3.38	1.07	0.086	0.007	0.993	0.007	2.021	$(s^{0.993}p_{x,y}^{2.000}p_z^{0.007})_\sigma$ $(s^{0.007}p_z^{0.993})_\pi$

Table 2.1: Average descriptor parameters for the large fullerene family

For the **medium** family:

Fullerene	Pyr(A)	Ang Def	Sph Curv	c_π^2	λ_π^2	m	n	Hybridization
C_{70}	10.79	10.42	0.270	0.073	0.927	0.080	2.238	$(s^{0.927}p_{x,y}^{1.998}p_z^{0.073})_\sigma$ $(s^{0.073}p_z^{0.927})_\pi$
C_{72}	10.70	10.38	0.268	0.073	0.927	0.080	2.239	$(s^{0.927}p_{x,y}^{1.999}p_z^{0.073})_\sigma$ $(s^{0.073}p_z^{0.927})_\pi$
C_{74}	10.48	9.81	0.262	0.069	0.931	0.074	2.222	$(s^{0.931}p_{x,y}^{2.000}p_z^{0.069})_\sigma$ $(s^{0.069}p_z^{0.931})_\pi$
C_{80}	10.16	9.40	0.246	0.066	0.934	0.071	2.213	$(s^{0.934}p_{x,y}^{2.000}p_z^{0.066})_\sigma$ $(s^{0.066}p_z^{0.934})_\pi$

Table 2.2: Average descriptor parameters for a selection of the medium fullerene family

And for the **small** family:

Fullerene	Pyr(A)	Ang Def	Sph Curv	c_π^2	λ_π^2	m	n	Hybridization
C_{20}	20.90	36.01	0.513	0.292	0.708	0.413	3.238	$(s^{0.708}p_{x,y}^{1.999}p_z^{0.292})_\sigma\ (s^{0.292}p_z^{0.708})_\pi$
C_{24}	18.90	30.77	0.465	0.244	0.756	0.340	3.021	$(s^{0.756}p_{x,y}^{2.001}p_z^{0.244})_\sigma\ (s^{0.244}p_z^{0.756})_\pi$
C_{26}	18.13	28.13	0.447	0.218	0.782	0.286	2.857	$(s^{0.782}p_{x,y}^{1.999}p_z^{0.218})_\sigma\ (s^{0.218}p_z^{0.782})_\pi$
C_{40}	14.73	19.45	0.352	0.145	0.855	0.177	2.531	$(s^{0.855}p_{x,y}^{2.000}p_z^{0.145})_\sigma\ (s^{0.145}p_z^{0.855})_\pi$
C_{60}	11.64	12.00	0.281	0.085	0.915	0.093	2.278	$(s^{0.915}p_{x,y}^{1.999}p_z^{0.085})_\sigma\ (s^{0.085}p_z^{0.915})_\pi$

Table 2.3: Average descriptor parameters for a selection of the small fullerene family

Pyramidalization angle: On the entire database, the **average** Pyr is **10.49°**. We notice that the Pyr varies between 3.38° and 20.90°.
The largest Pyr values are measured in the case of **small** fullerenes, for $n < 60$.
Actually, in the case of small fullerenes the constraints are more important which induces a more important curvature on the different vertices.
We note a clear difference between the family of large and medium fullerenes.
In the case of **large** fullerenes the Pyr values are lower and not close to the average value of C_{60} which can be used as a reference. These large fullerenes are less constrained and therefore have fewer vertices with strong pyramidalization.

The following figure displays the distribution of the Pyr values as a function of the number of atoms present in the fullerenes (for $n = 20$ to 100 on the basis of the isomers). We note in dashed line the value of the Pyr in the case of C_{60}, and the sp^2, sp^3 hybridization situations.

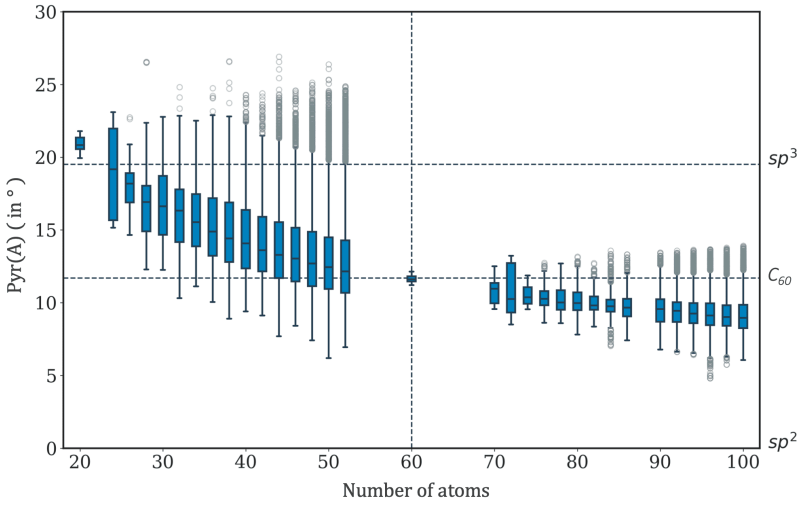

Figure 2.2: Boxplot representation of the pyramidalization angle (in degrees) in function of the number of atoms [4]

As mentioned by the graph, we observe that the Pyr angle decreases when the number of atoms increases. In the case of the family of small fullerenes there is a greater standard deviation of the Pyr than for the large family, this situation illustrates the presence of more isomers for the small fullerenes.

Angular defect, spherical curvature and pyramidalization angle: The **angular defect** follows the same behavior as the Pyr.

In the case of the **large** fullerene family, the $Ang\ Def$ is relatively small and decreases with the increasing of the number of atoms.

This is also the case for the family of **medium** fullerenes.
For fullerenes with $n < 60$ the $Ang\ Def$ is more important which is in accordance with the constraints imposed by the geometry of small fullerenes.

The **spherical curvature** shows the same trend and a **linear relationship** between the Pyr and the $Sph\ Curv$ as previously proven in eq. 1.50.

Hybridization and pyramidalization angle: We observed that on the 3 families, the Pyr is positioned in the situations commonly encountered between sp^2 and sp^3.
But some fullerenes have a hybridization **beyond** sp^3 for $Pyr > 19°$.

Fullerenes visualization-Cartographies

As presented in the previous section 2.1, the software *Pychemcurv* [10] provides cartographies with an adaptable color scale for each of the parameters.

We report here the **cartographies** that we carried out for the 3 families of fullerenes (small with C_{20}, medium with C_{70} and large with C_{180}, C_{60} is used as a reference) of the database. We observe the parameters presented in chapter 1: the pyramidalization angle , the angular defect , the spherical curvature and the hybridization.

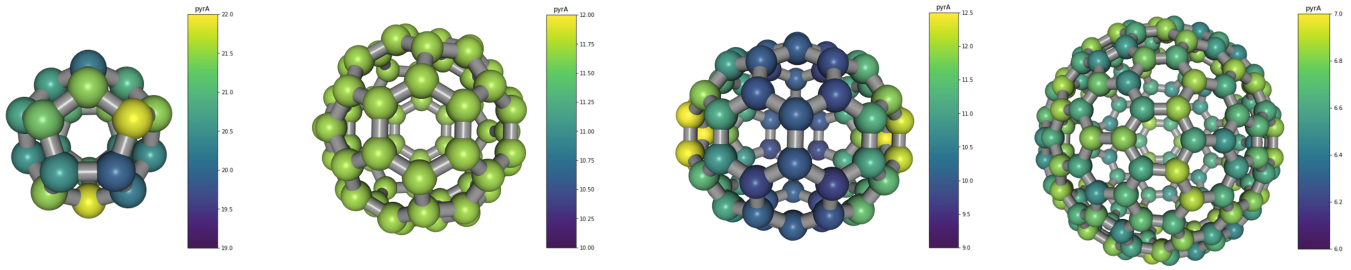

Figure 2.3: Cartographies of the pyramidalization angle for the fullerenes C_{20}, C_{60}, C_{70}, C_{180}

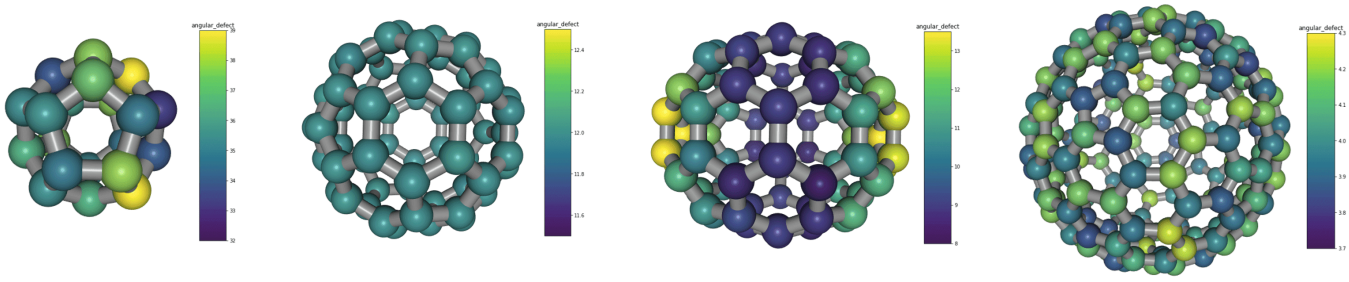

Figure 2.4: Cartographies of the angular defect for the fullerenes C_{20}, C_{60}, C_{70}, C_{180}

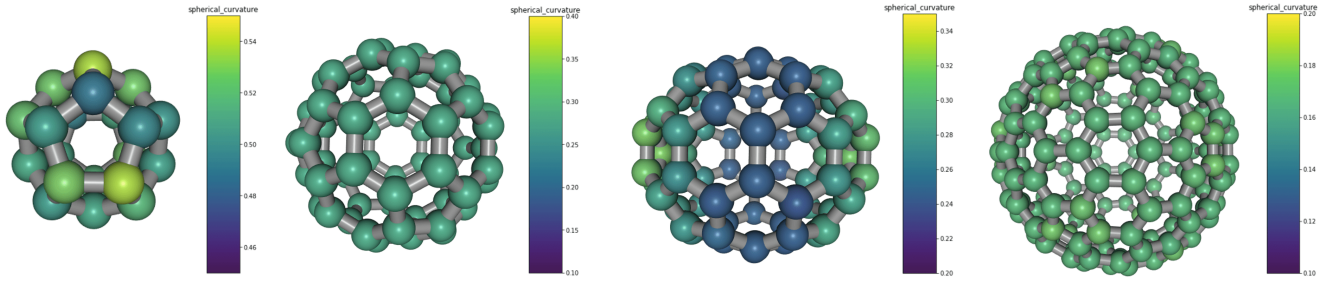

Figure 2.5: Cartographies of the spherical curvature for the fullerenes C_{20}, C_{60}, C_{70}, C_{180}

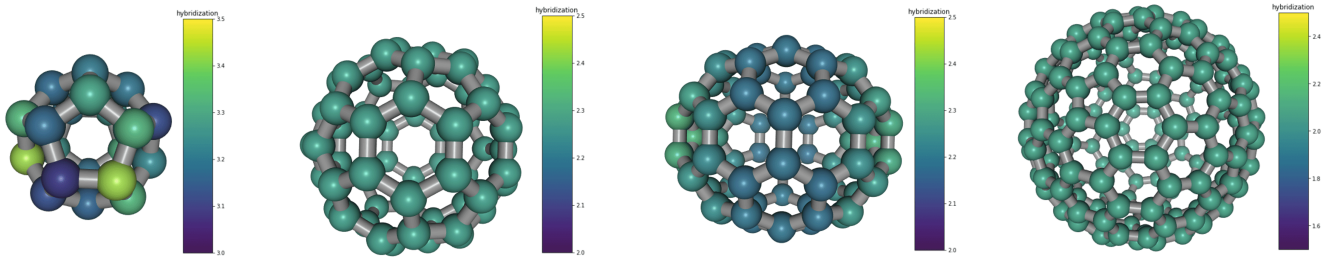

Figure 2.6: Cartographies of the hybridization for the fullerenes C_{20}, C_{60}, C_{70}, C_{180}

2.3 Application to other compounds

In this section, we used **non-fullerenic molecules** proposed by Robert C. Haddon in two of his works from 1986 [6] and 1990 [30]. We also studied molecules of a recent publication of the research team of A. R. Khamatgalimov concerning the **fullerenes** C_{50} [31] . We are also focusing on the interesting work of Han et al. [34] on **chlorofullerenes**.

In fact, all the POAV1 theory parameters presented in chapter 1 are applicable to both fullerenic and non-fullerenic molecules as we illustrate in the following by 25 examples.
The molecules have been studied following the same method, by DFT B3LYP/6-311G* calculations and visualizations of the properties of Robert C. Haddon's concepts as in the previous section.

For more details on computation techniques see the Appendix 1 section 1.

It should be noted that we are positioned in the so-called cases of the $\star(A)$, i.e. the atom we are interested in has **only 3 neighbors**. However, in some of the cases studied here we are in situations beyond 3 neighbors which does not define correctly the $\star(A)$. Our programs allow us to extract the data of the studied properties are based on 3 neighbors in the case of Pyr, hybridization and spherical curvature. Excluding the angular defect which permits to get free of the three neighbors situations.

2.3.1 Non-fullerenic molecules

Note that a geometry optimization was necessary for each of the molecules and the visualizations were carried out by the software VESTA [35].

Notice that the number in brackets corresponds to each of the molecules in abscissa on the figure 2.57.

- Molecule $C_{11}H_{10}$: 1,6-methano-[10]-annulene (n°1) [6]

The molecule presents 2 isomers. The first isomer (of Cs symmetry) has the following geometry (figure 2.7) including 2 bridged hexagons.

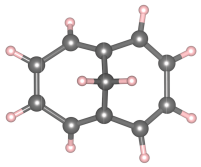

Figure 2.7: Representation of the molecule 1,6-methano-[10]-annulene ($C_{11}H_{10}$)

Parameter	Minimum	Maximum
Energy (u.a)	-425.23	
Pyr (°)	0.55	5.06
Hybridization	2.00	2.05
Angular defect (°)	-72.66	2.31
Spherical curvature	0.01	0.12

Table 2.4: Set of minimum and maximum values of parameters of the 1,6-methano-[10]-annulene ($C_{11}H_{10}$, Pyr, Hyb, $AngDef$, $SphCur$)

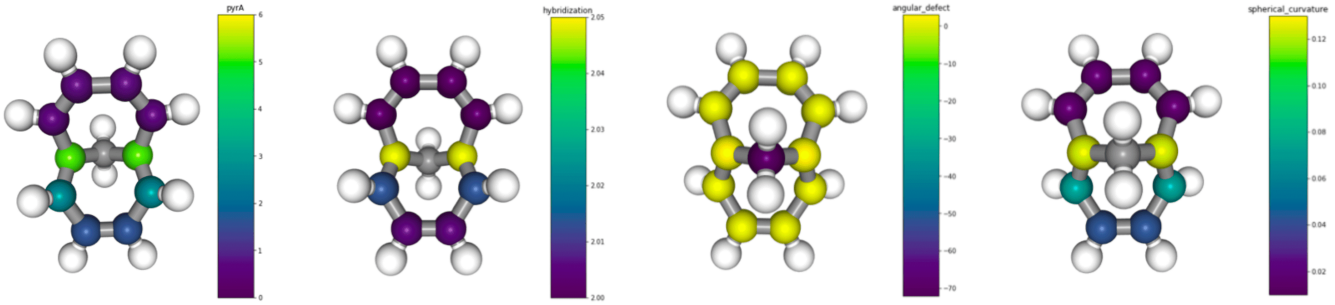

Figure 2.8: Cartographies of the parameters of 1,6-methano-[10]-annulene ($C_{11}H_{10}$)

We notice that the Pyr are higher on the carbons at the junction between the 2 hexagons than on the carbons constituting the hexagons. The hybridization is uniform in the whole molecule around 2.00. The angular defect gives access to situations where 4 neighboring atoms are present. Here we observe especially a very negative value on the central atom. Finally, the spherical curvature is also more pronounced at the junctions between hexagons and relatively weaker on the carbons of the remaining skeleton.

- Molecule $C_{11}H_{10}$: 1,5-methano-[10]-annulene (n°2) [6]

The second isomer has the geometry illustrated in the figure 2.9, with 2 different "geometrical" patterns of the molecule 1,6-methano-[10]-annulene:

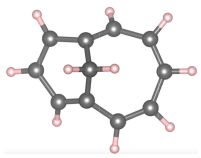

Figure 2.9: Representation of the molecule 1,5-methano-[10]-annulene ($C_{11}H_{10}$)

Parameter	Minimum	Maximum
Energy (u.a)	-425.20	
Pyr (°)	0.06	8.24
Hybridization	2.00	2.13
Angular defect (°)	-72.31	6.08
Spherical curvature	0.002	0.20

Table 2.5: Set of minimum and maximum values of parameters of the 1,5-methano-[10]-annulene ($C_{11}H_{10}$, Pyr, Hyb, $AngDef$, $SphCurv$)

This isomer of C_1 geometry, has an energy of lower than the isomer 1,6-methano-[10]-annulene.

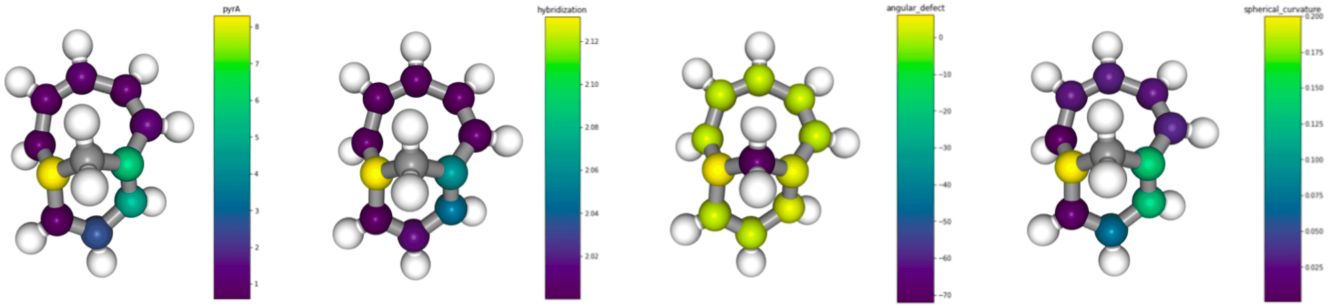

Figure 2.10: Cartographies of the parameters of 1,5-methano-[10]-annulene ($C_{11}H_{10}$)

Once again here, we remark that the Pyr values are higher at the carbons involved in the bridge than in the rest of the molecular skeleton. The hybridization is on the entire molecule of sp^2 type. The angular defect and the spherical curvature follow the same trend as the previous properties.

- Molecule $C_{11}H_8$: 7bH-cyclopenta-[cd]-indene (n°3) [6]

Composed by 2 pentagons and 1 hexagon the molecule has a C_1 symmetry:

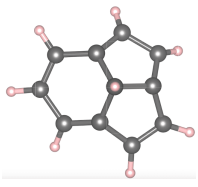

Figure 2.11: Representation of the molecule 7bH-cyclopenta-[cd]-indene ($C_{11}H_8$)

Parameter	Minimum	Maximum
Energy (u.a)	-424.01	
Pyr (°)	0.39	12.11
Hybridization	2.00	2.30
Angular defect (°)	-70.76	13.12
Spherical curvature	0.01	0.29

Table 2.6: Set of minimum and maximum values of parameters of the molecule 7bH-cyclopenta-[cd]-indene ($C_{11}H_8$, Pyr, Hyb, $AngDef$, $SphCurv$)

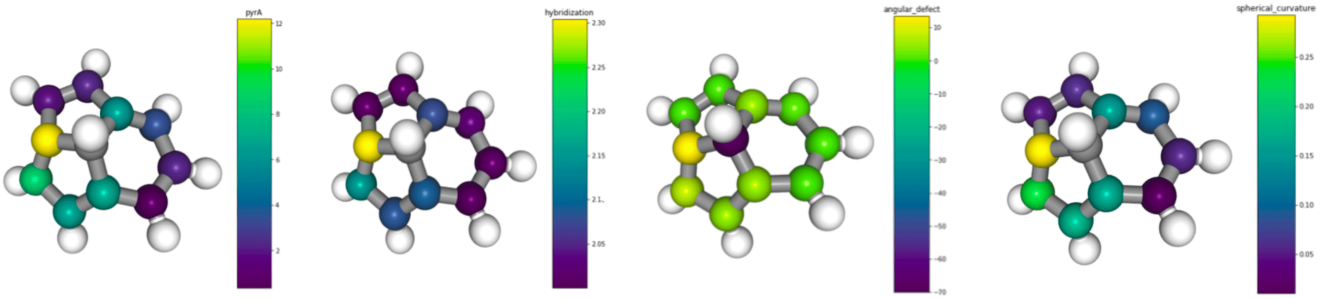

Figure 2.12: Cartographies of the parameters of 7bH-cyclopenta-[cd]-indene ($C_{11}H_8$)

Let us note here that the values of Pyr are the most important in the regions of junctions between geometrical patterns i.e. where the molecule tends to bend. The hybridization values remain in the same range, however we notice an increase concerning the carbon where the Pyr is the highest. The angular defect is once again, higher at the carbon with the maximum of Pyr. The spherical curvature is more important at the pentagon-pentagon junction where the curvature seems to be more significant.

- Molecule $C_{16}H_{14}$: *syn*-1,6,8,13-bismethano-[14]-annulene (n°4) [6]

This molecule (of symmetry C_1) is constituted of 3 hexagonal patterns bridged together.

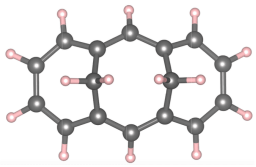

Figure 2.13: Representation of the molecule *syn*-1,6,8,13-bismethano-[14]-annulene ($C_{16}H_{14}$)

Parameter	Minimum	Maximum
Energy (u.a)	-618.19	
Pyr (°)	2.43	4.78
Hybridization	2.01	2.04
Angular defect (°)	-67.57	2.07
Spherical curvature	0.07	0.13

Table 2.7: Set of minimum and maximum values of parameters of the molecule *syn*-1,6,8,13-bismethano-[14]-annulene ($C_{16}H_{14}$, Pyr, Hyb, $AngDef$, $SphCurv$)

We observe here that the Pyr are more important at the extremities and in the core of the molecule and the hybridizations are relatively uniform of sp^2 type. The angular defect shows 2 trends. The skeleton as a whole has relatively small values between 0 and 2, and only the 2 atoms at the bridge vertices have much smaller values. The spherical curvature approximates the Pyr cartography in terms of the distribution of values within the molecule.

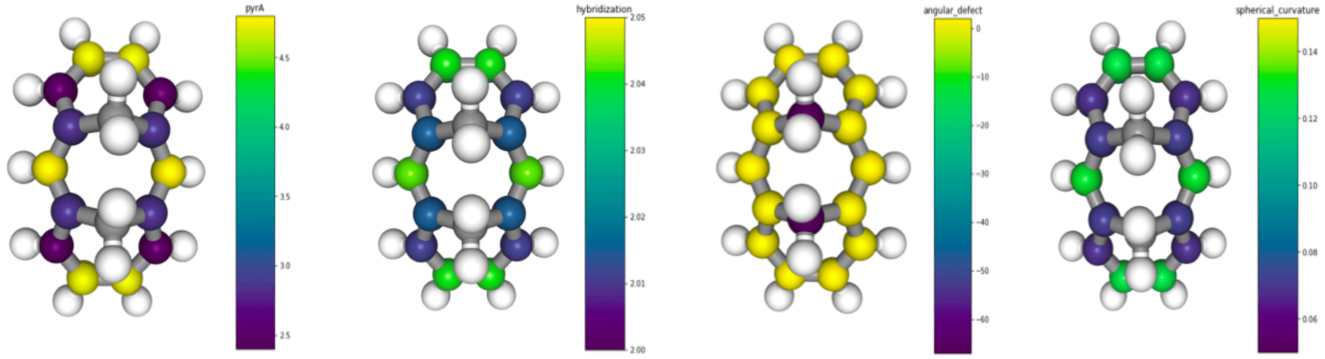

Figure 2.14: Cartographies of the parameters of *syn*-1,6,8,13-bismethano-[14]-annulene ($C_{16}H_{14}$)

- Molecule $C_{20}H_{20}$: *trans*-15,16-diethyldihydropyrene (n°5) [6]

This molecule has of formula $C_{20}H_{20}$ presents 2 substituents $-CH_2 - CH_3$, and has a symmetry C_1.

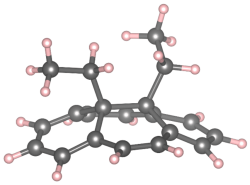

Figure 2.15: Representation of the molecule *trans*-15,16-diethyldihydropyrene

All the information of the different properties are available in the cartographies:

Parameter	Minimum	Maximum
Energy (u.a)	-774.28	
Pyr (°)	0.18	4.32
Hybridization	2.00	2.03
Angular defect (°)	-74.99	1.69
Spherical curvature	0.004	0.11

Table 2.8: Set of minimum and maximum values of parameters of the molecule *trans*-15,16-diethyldihydropyrene (Pyr, Hyb, $AngDef$, $SphCurv$)

We note that the Pyr are relatively low on the whole molecule. The hybridizations are close to 2.00 so of sp^2-type. The angular defect shows 2 trends with values close to 1 within the hexagonal units and very negative values on the atoms bonded to substituents. The spherical curvature is relatively low.

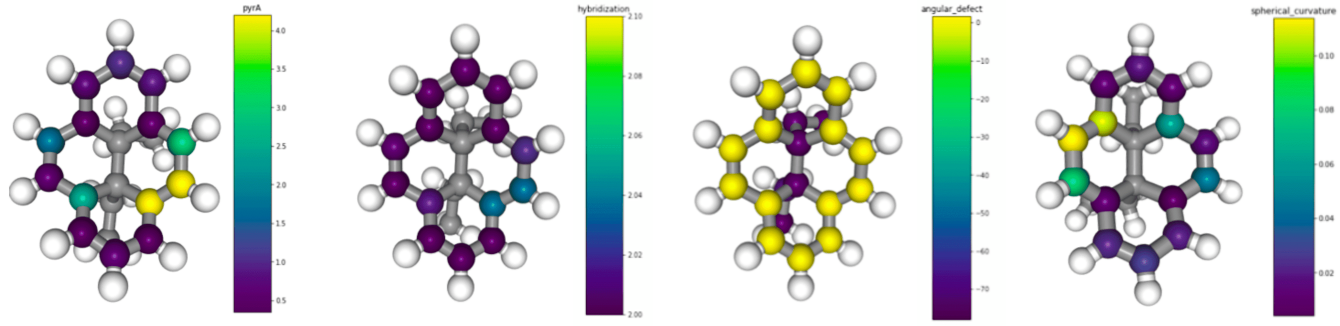

Figure 2.16: Cartographies of the parameters of *trans*-15,16-diethyldihydropyrene

- Molecule C_7H_{10}: bicyclo-[2.2.1]-hept-2-ene (n°6) [6]

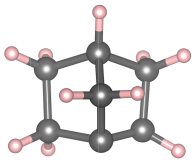

Figure 2.17: Representation of the molecule bicyclo-[2.2.1]-hept-2-ene

For this molecule of symmetry C_1 we get the following data:

Parameter	Minimum	Maximum
Energy (u.a)	-272.72	
Pyr (°)	14.21	23.07
Hybridization	2.44	3.71
Angular defect (°)	-75.02	49.28
Spherical curvature	0.38	0.53

Table 2.9: Set of minimum and maximum values of parameters of the bicyclo-[2.2.1]-hept-2-ene (Pyr, Hyb, $AngDef$, $SphCurv$)

This molecule has 4 neighbors atoms and only 2 trivalent atoms where our parameters are computable. The 2 calculated Pyr have quite high values and the hybridizations show situations higher than sp^2 and sp^3. The computable angular defects are negative on all atoms except the 2 atoms which are trivalent.

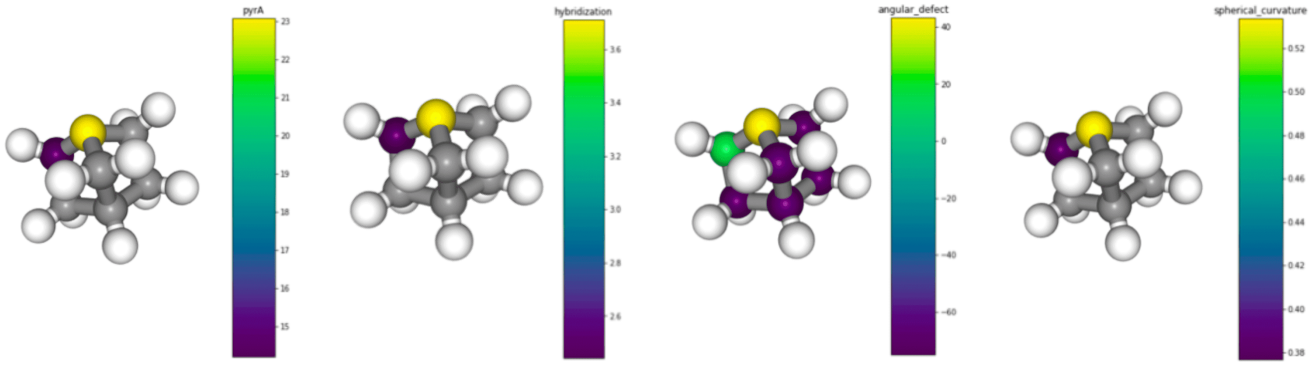

Figure 2.18: Cartographies of the parameters of bicyclo-[2.2.1]-hept-2-ene

- Molecule $C_{12}H_{16}$: Tricyclo[4.2.2.2^{2,5}]dodecane (n°7) [30]

The following molecule has a D_{2h} geometry:

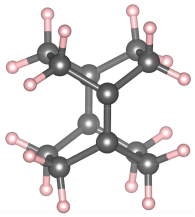

Figure 2.19: Representation of the molecule $C_{12}H_{16}$

For all the properties calculated next, we will note that only 2 values emerge, we thus identify carbons in the center of the molecule and the 4 other carbons of the extremities.

Parameter	Minimum	Maximum
Energy (u.a)	-466.93	
Pyr (°)	11.17	-
Hybridization	2.25	-
Angular defect (°)	-75.02	11.06
Spherical curvature	0.26	-

Table 2.10: Set of minimum and maximum values of parameters of the molecule $C_{12}H_{16}$ (Pyr, Hyb, $AngDef$, $SphCurv$)

A unique value of Pyr and spherical curvature in this molecule 11.17° and 0.26. The hybridization indicates a single carbon type with a sp^2 tendency. The angular defect is negative on the external carbons and positive on the central atoms.

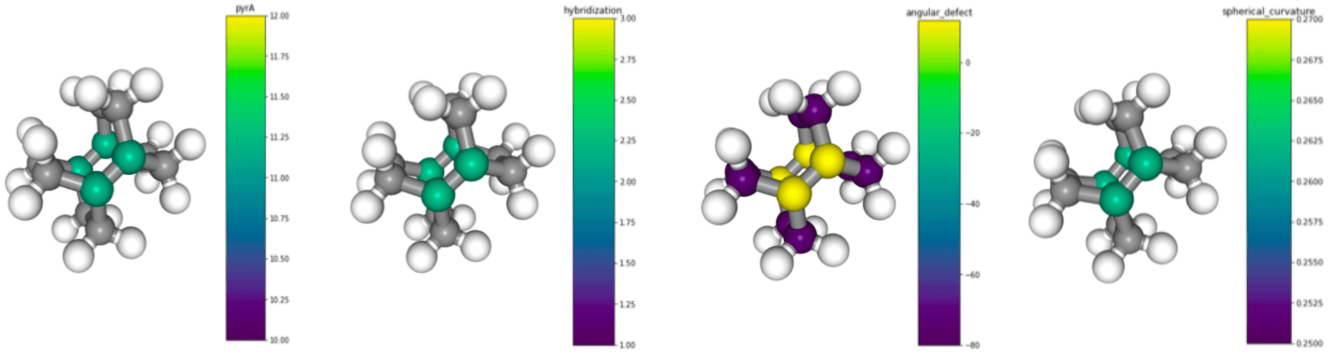

Figure 2.20: Cartographies of the parameters of Tricyclo[4.2.2.2$^{2.5}$]dodecane

- Molecule $C_{28}H_{16}$: 9,9',10,10'-tetrahydrodianthracene (n°8) [30]

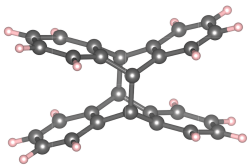

Figure 2.21: Representation of the molecule $C_{28}H_{16}$

Parameter	Minimum	Maximum
Energy (u.a)	-1076.74	
Pyr (°)	0.02	16.79
Hybridization	2.00	2.67
Angular defect (°)	0.00	24.05
Spherical curvature	0.0004	0.38

Table 2.11: Set of minimum and maximum values of parameters of 9,9',10,10'-tetrahydrodianthracene ($Pyra$, Hyb, $AngDef$, $SphCurv$)

Of C_{2h} symmetry, we notice that the Pyr are the highest in the center of the molecule at the junctions which present the most important curvature on the 4 carbons. A similar behavior is observed for

hybridizations close to 2.00 and increase up to 2.66 for the 4 central atoms. The situation is the same for the 2 other parameters.

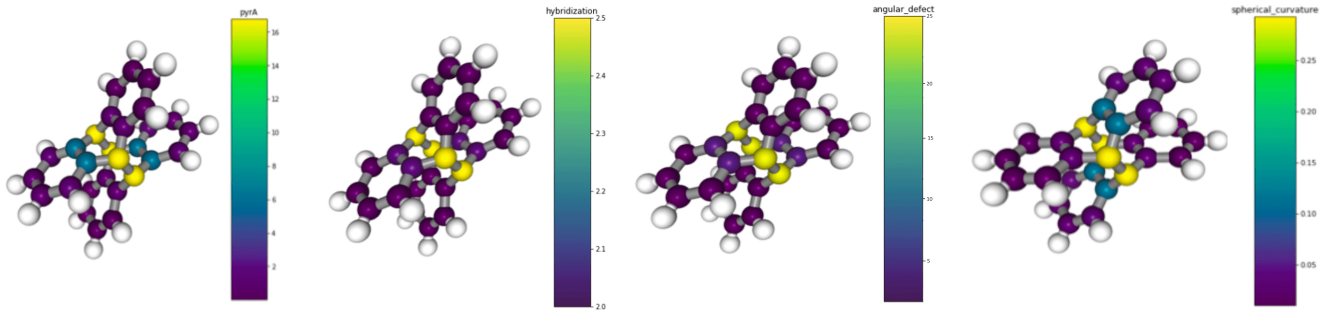

Figure 2.22: Cartographies of the parameters of 9,9',10,10'-tetrahydrodianthracene

- Molecule $C_{20}H_{20}$: Sesquinorbornatriene (bridged down) (n°9) [30]

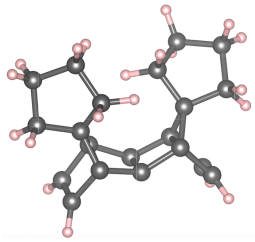

Figure 2.23: Representation of the molecule sesquinorbornatriene (bridged down)

Parameter	Minimum	Maximum
Energy (u.a)	-773.92	
Pyr (°)	4.04	18.12
Hybridization	2.03	2.82
Angular defect (°)	-75.21	33.19
Spherical curvature	0.11	0.42

Table 2.12: Set of minimum and maximum values of parameters of sesquinorbornatriene (bridged down) (Pyr, $Hybr$, $AngDef$, $SphCurv$)

The molecule is C_1 symmetry, the Pyr have higher values in the deformed zone of the molecule, the spherical curvature follows the same behavior but with values lower than 1. We observe 2 types of carbons sp^2 and sp^3. The angular defect is calculable on all carbons, the deformed zone has the highest values.

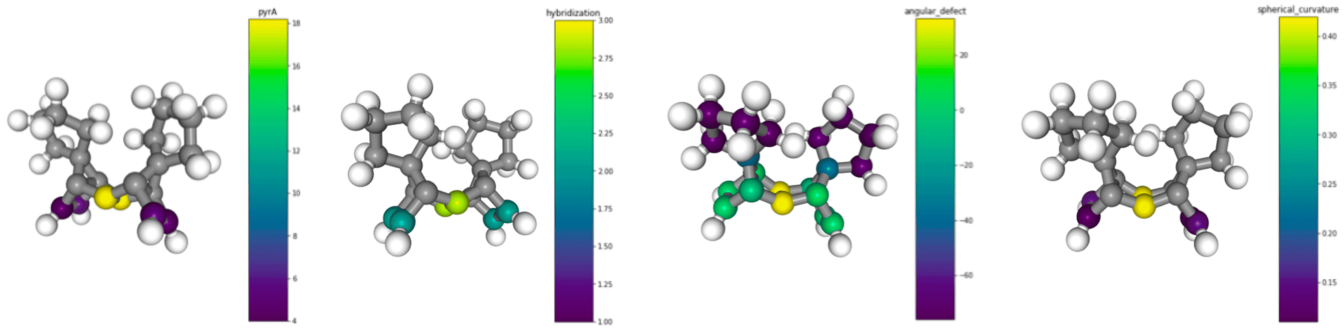

Figure 2.24: Cartographies of the parameters of sesquinorbornatriene (bridged down)

- Molecule $C_{20}H_{20}$: Sesquinorbornatriene (bridged to the top) (n°10) [30]

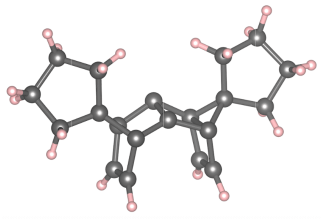

Figure 2.25: Representation of the molecule sesquinorbornatriene (bridged to the top)

Parameter	Minimum	Maximum
Energy (u.a)	-773.93	
Pyr (°)	0.01	27.88
Hybridization	2.00	5.81
Angular defect (°)	-74.71	71.74
Spherical curvature	0.0003	0.61

Table 2.13: Set of minimum and maximum values of parameters of the sesquinorbornatriene (bridged to the top) (Pyr, Hyb, $AngDef$, $SphCurv$)

The Pyr are in the same order of importance as in the top-bridged case but slightly lower. The hybridizations and the angular defect are higher. Finally, the spherical curvature is quite low, less than 1.

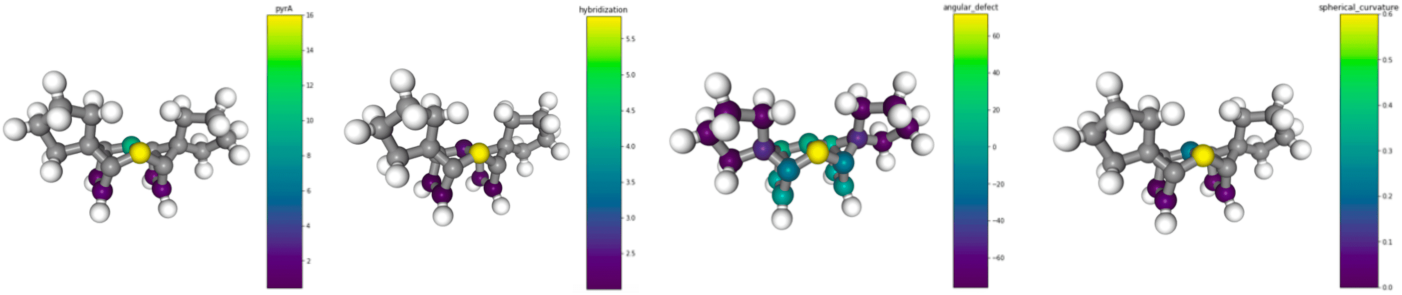

Figure 2.26: Cartographies of the parameters of sesquinorbornatriene (bridged to the top)

- Molecule C_8H_{14}: *Trans*-cyclooctene (n°11) [30]

Of symmetry C_1 the hybridization of the 2 carbon atoms is of type sp^2, the angular defect is negative and very weak except on the 2 trivalent atoms where it is lower than 1. The same behavior is observed with values lower than 0.5.

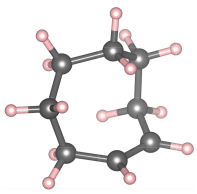

Figure 2.27: Representation of the molecule *Trans*-cyclooctene

Parameter	Minimum	Maximum
Energy (u.a)	-313.35	
Pyr (°)	1.41	3.10
Hybridization	2.00	2.02
Angular defect (°)	-78.60	0.87
Spherical curvature	0.04	0.08

Table 2.14: Set of minimum and maximum values of parameters of the *Trans*-cyclooctene (Pyr, Hyb, $AngDef$, $SphCurv$)

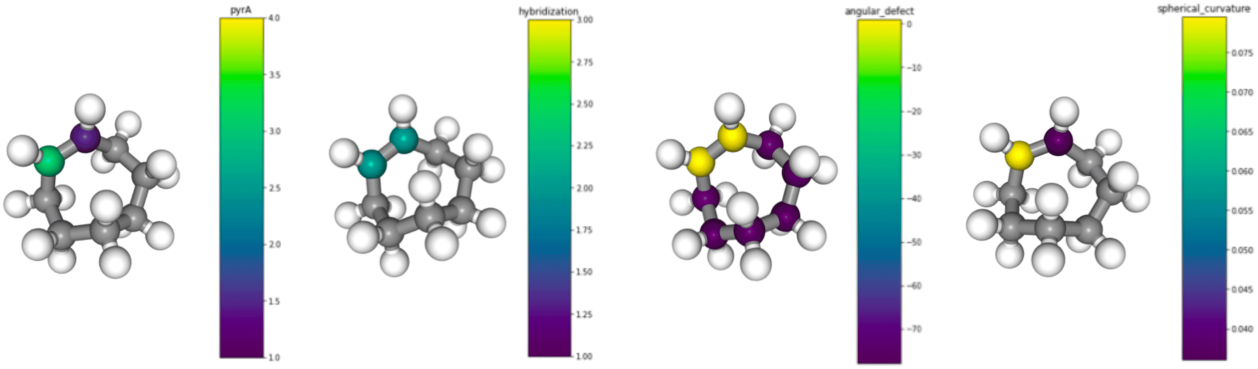

Figure 2.28: Cartographies of the parameters of C_8H_{14}: *Trans*-cyclooctene

- Molecule $C_{24}H_{24}$ (n°12) [30]

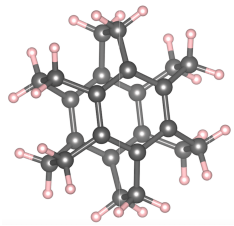

Figure 2.29: Representation of the molecule $C_{24}H_{24}$

Parameter	Minimum	Maximum
Energy (u.a)	-929.13	
Pyr (°)	7.05	-
Hybridization	2.09	-
Angular defect (°)	-76.26	4.46
Spherical curvature	0.17	-

Table 2.15: Set of minimum and maximum values of parameters of the molecule $C_{24}H_{24}$ (Pyr, Hyb, $AngDef$, $SphCurv$)

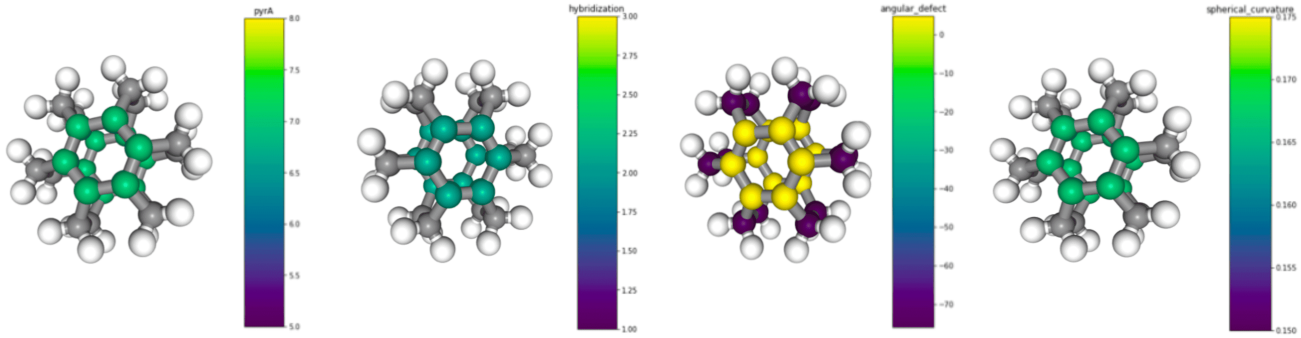

Figure 2.30: Cartographies of the parameters of $C_{24}H_{24}$

The extrema are summarized for a C_{6h} symmetry. The Pyr are identical throughout the molecule as the sp^2 hybridization. The angular defect is according to 2 values and the spherical curvature less than 1 uniformly.

- Molecule $C_{20}H_{10}$: Corannulene (n°13) [30]

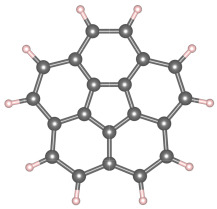

Figure 2.31: Representation of the molecule of corannulene

Parameter	Minimum	Maximum
Energy (u.a)	-768.32	
Pyr (°)	0.03	0.07
Hybridization	2.00	-
Angular defect (°)	0.000088	0.0004
Spherical curvature	0.008	0.002

Table 2.16: Set of minimum and maximum values of parameters of corannulene (Pyr, Hy, $AngDef$, $SphCurv$)

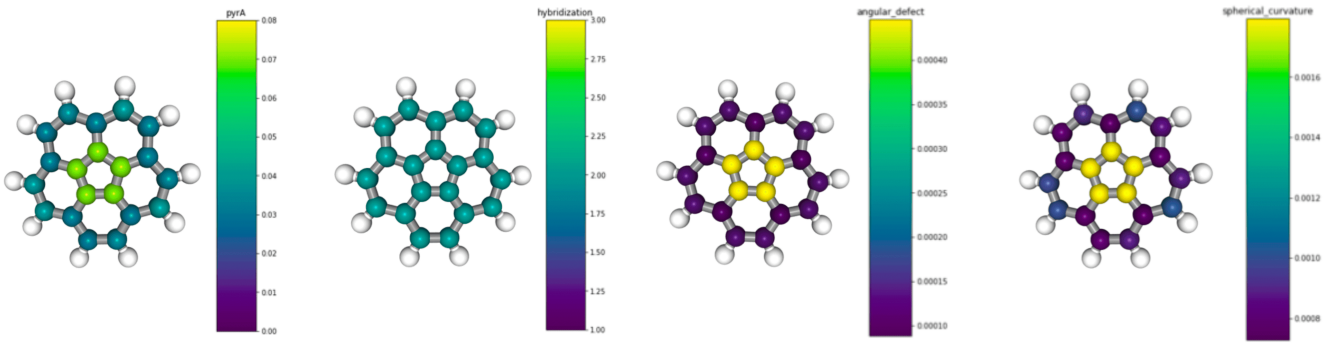

Figure 2.32: Cartographies of the parameters of the corannulene

The molecule of formula $C_{20}H_{10}$ of symmetry C_{5h}, includes 5 hexagonal patterns surrounding 1 pentagon. During the calculations we observe that the molecule bends progressively. The Pyr will be more pronounced in the center of the molecule than in its periphery. The hybridization is uniform showing a sp^2 character. The angular defect is rather reliable being weaker on the carbons in periphery than in the center. This agrees with the data of Pyr. The spherical curvature also correlates with the previous results with a greater spherical curvature on the atoms forming the pentagon.

2.3.2 Fullerenic molecules

- Molecule C_{50}-D_3 (n°14) [31]

This molecule is a C_{50} fullerene with D_3 symmetry, composed by pentagons and a majority of hexagons.

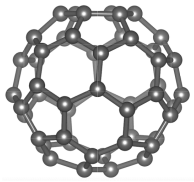

Figure 2.33: Representation of the molecule fullerene C_{50}-D_3

Parameter	Minimum	Maximum
Energy (u.a)	-1894.39	
Pyr (°)	12.06	13.86
Hybridization	2.30	2.42
Angular defect (°)	12.88	16.81
Spherical curvature	0.30	0.34

Table 2.17: Set of minimum and maximum values of parameters of the molecule fullerene C_{50}-D_3 (Pyr, Hyb, $AngDef$, $SphCurv$)

The Pyr data are quite uniform with relatively close minimum and maximum values. The hybridizations are also relatively similar around 2.3. The angular defect and the spherical curvature have a uniform behavior.

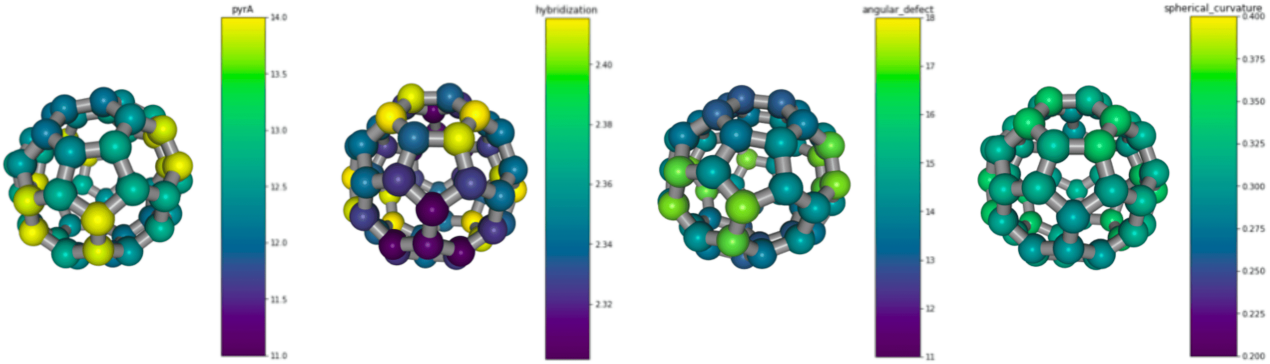

Figure 2.34: Cartographies of the parameters of fullerene C_{50}-D_3

- Molecule C_{50}-D_{5h} (n°15) [31]

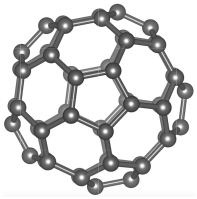

Figure 2.35: Representation of the molecule fullerene C_{50}-D_{5h}

This fullerene of D_{5h} symmetry consists of pentagons and a majority of hexagons. The Pyr are in a relatively close range of values, however we note that 2 pentagons on both sides of the molecule have lower angles around 11°. The hybridizations are uniform. The angular defect values are wider. Finally the spherical curvature remains lower than 0.5.

Parameter	Minimum	Maximum
Energy (u.a)	-1894.38	
Pyr (°)	11.12	13.59
Hybridization	2.25	2.40
Angular defect (°)	10.98	16.26
Spherical curvature	0.28	0.34

Table 2.18: Set of minimum and maximum values of parameters of the molecule fullerene C_{50}-D_{5h} (Pyr, Hyb, $AngDef$, $SphCurv$)

We note few differences between the values of parameters of the 2 isomers.

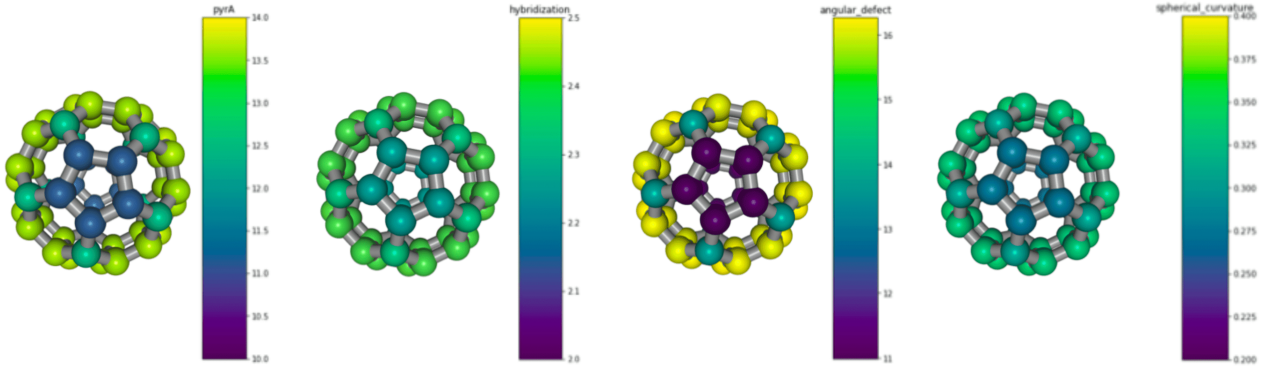

Figure 2.36: Cartographies of the parameters of fullerene C_{50}-D_{5h}

- Molecule Chlorofullerene $C_{50}Cl_{10}$-D_3 (n°16) [34]

This chlorofullerene, constituted of a C_{50} and 10 chlorine atoms on the equatorial zone, presents an original structure called "saturne". It should be noted that this fullerene exists under 2 different symmetries.

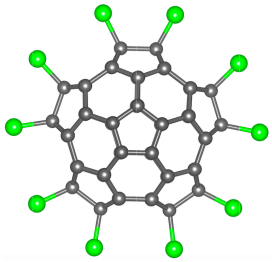

Figure 2.37: Representation of the fullerenic molecule $C_{50}Cl_{10}$-D_3

Parameter	Minimum	Maximum
Energy (u.a)	-6475.74	
Pyr (°)	9.66	10.92
Hybridization	2.18	2.24
Angular defect (°)	-72.60	10.54
Spherical curvature	0.24	0.27

Table 2.19: Set of minimum and maximum values of parameters of the fullerenic molecule $C_{50}Cl_{10}$-D_3 (Pyr, Hyb, $AngDef$, $SphCurv$)

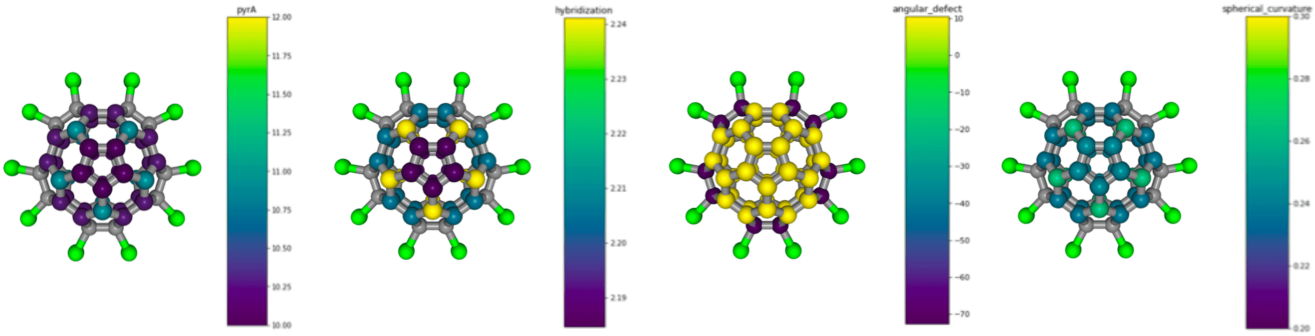

Figure 2.38: Cartographies of the parameters of cholorofullerene D_3

We observe 2 trends in the values of Pyr. The whole molecule is in the range of 10° except for the carbons where the chlorine atoms are added where the Pyr reaches 24°. The hybridizations are of the average of 2.2 on the quasi-totality of the molecule, however the carbons bounded with the chlorines have hybridization of almost 4. Finally the angular defect and the spherical curvature have the same behavior.

- Molecule Chlorofullerene $C_{50}Cl_{10}$-D_{5h} (n°17) [34]

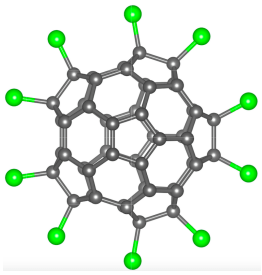

Figure 2.39: Representation of the fullerenic molecule $C_{50}Cl_{10}$-D_{5h}

Parameter	Minimum	Maximum
Energy (u.a)	-6475.74	
Pyr (°)	9.67	10.92
Hybridization	2.18	2.24
Angular defect (°)	-72.60	10.54
Spherical curvature	0.23	0.27

Table 2.20: Set of minimum and maximum values of parameters of the fullerenic molecule $C_{50}Cl_{10}$-D_{5h} (Pyr, Hyb , $AngDef$, $SphCurv$)

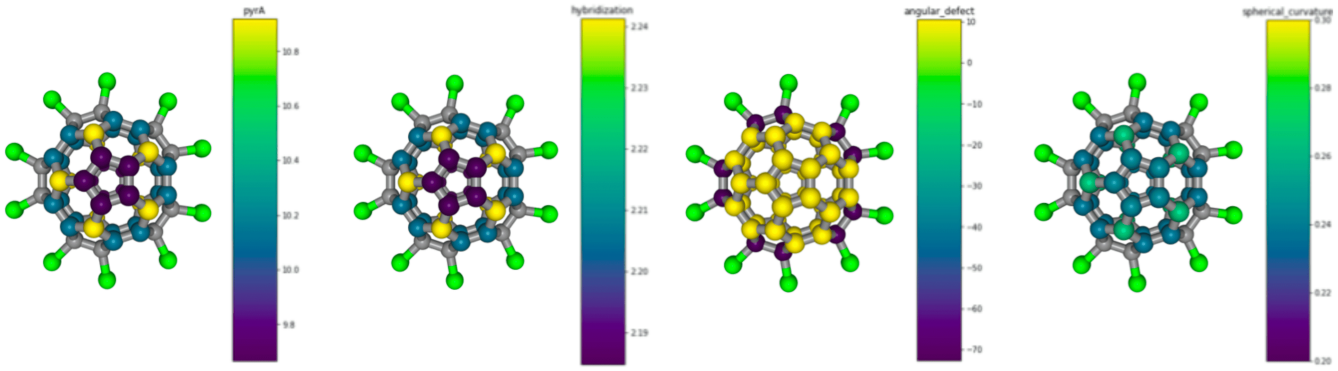

Figure 2.40: Cartographies of the parameters of cholorofullerene D_{5h}

This second molecule is similar but with a D_{5h} symmetry. In all the cartographies we observe the same behavior as for the previous molecule with lower values on the whole molecule but higher values on the carbon atoms of the equatorial part where the chlorine atoms are added.

- Molecule of fullerene C_{64}-C_{3v} (n°18) [34]

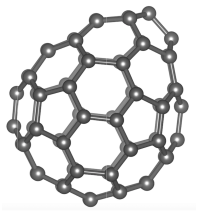

Figure 2.41: Representation of the molecule C_{64}-C_{3v}

Parameter	Minimum	Maximum
Energy (u.a)	-2424.79	
Pyr (°)	11.61	16.43
Hybridization	2.28	3.50
Angular defect (°)	11.94	40.17
Spherical curvature	0.28	0.53

Table 2.21: Set of minimum and maximum values of parameters of the molecule C_{64}-C_{3v} (Pyr, Hyb, $AngDef$, $SphCurv$)

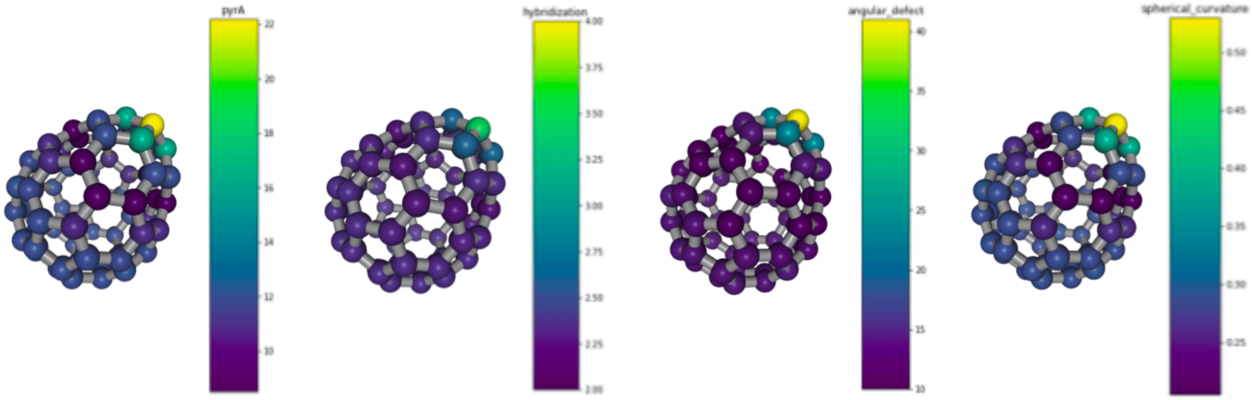

Figure 2.42: Cartographies of the parameters of the fullerene C_{64}-C_{3v}

This fullerene of 64 carbon atoms has a C_{3v} symmetry. This fullerene is not perfectly spherical and shows a deformation at one of its poles. We notice that the Pyr are the highest in 4 atoms at the top which is deformed. The hybridizations are uniform of sp^2 type but are beyond 3 at the top. For the angular defect and the spherical curvature the same behavior is observed at the top.

- Molecule of fullerene C_{64}-C_2 (n°19) [34]

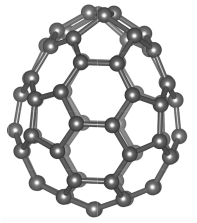

Figure 2.43: Representation of the molecule C_{64}-C_2

Parameter	Minimum	Maximum
Energy (u.a)	-2425.03	
Pyr (°)	7.06	22.97
Hybridization	2.10	3.68
Angular defect (°)	4.46	42.85
Spherical curvature	0.17	0.51

Table 2.22: Set of minimum and maximum values of parameters of the molecule C_{64}-C_2 (Pyr, Hyb, $AngDef$, $SphCurv$)

We note once again that this C_{64} is not perfectly spherical, which will certainly induce variations in the properties. The Pyr are more pronounced in the non-spherical regions. This deformed region also shows higher hybridizations close to 4 while the rest of the molecule has sp^2.

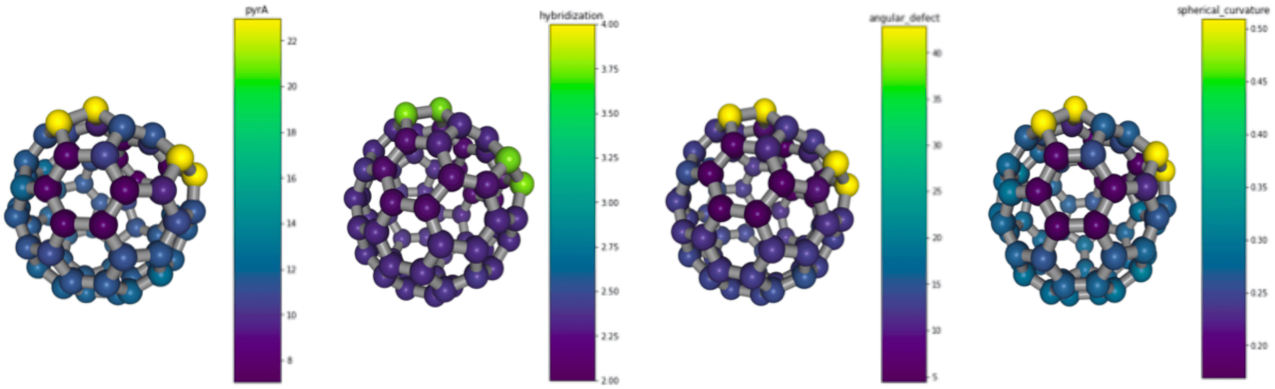

Figure 2.44: Cartographies of the parameters of the fullerene C_{64}-C_2

- Molecule of fullerene C_{64}-D_2 (n°20) [34]

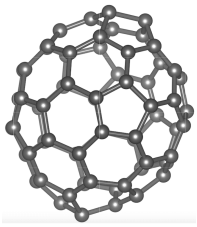

Figure 2.45: Representation of the molecule C_{64}-D_2

Parameter	Minimum	Maximum
Energy (u.a)	-2425.05	
Pyr (°)	7.77	22.79
Hybridization	2.12	3.64
Angular defect (°)	6.23	42.22
Spherical curvature	0.19	0.50

Table 2.23: Set of minimum and maximum values of parameters of the molecule C_{64}-D_2 (Pyr, Hyb, $AngDef$, $SphCurv$)

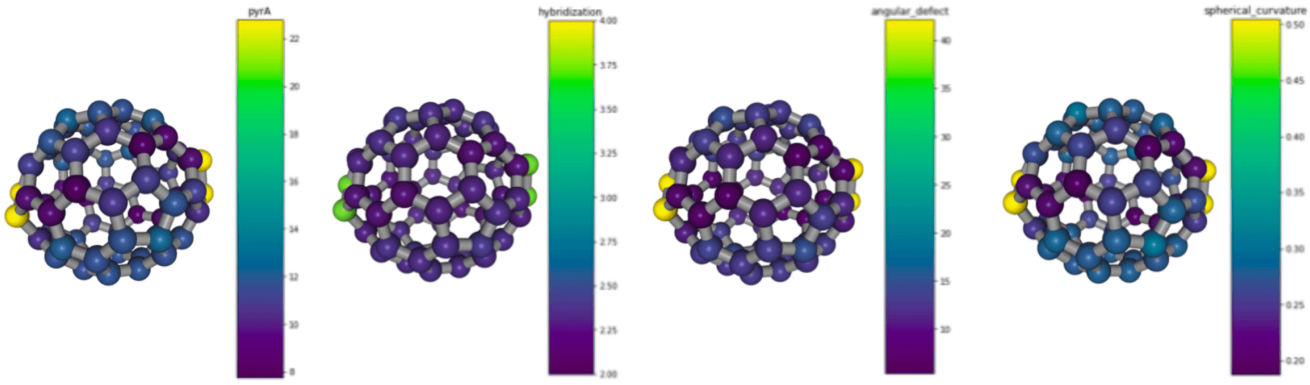

Figure 2.46: Cartographies of the parameters of the fullerene C_{64}-D_2

We observe once again that the fullerene is not perfectly spherical, in particular by the pyramidal angles which are clearly higher at the poles of the molecule. We note the same situation with the

hybridizations which are close to 2 on the whole molecule and beyond 3 at the vertices. Concerning the angular defect and the spherical curvature the situations are rather similar.

- Molecule of fullerene C_{64}-C_s (n°21) [34]

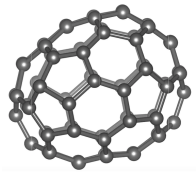

Figure 2.47: Representation of the molecule C_{64}-C_s

Parameter	Minimum	Maximum
Energy (u.a)	-2425.04	
Pyr (°)	6.94	22.79
Hybridization	2.09	3.64
Angular defect (°)	4.31	42.26
Spherical curvature	0.17	0.50

Table 2.24: Set of minimum and maximum values of parameters of the molecule C_{64}-C_s (Pyr, Hyb, $AngDef$, $SphCurv$)

Once again this C_{64} is not perfectly spherical. We thus observe higher pyramidal angles at the more deformed poles of the molecule. The hybridizations are around 2.2 on the whole molecule except on the extremities.

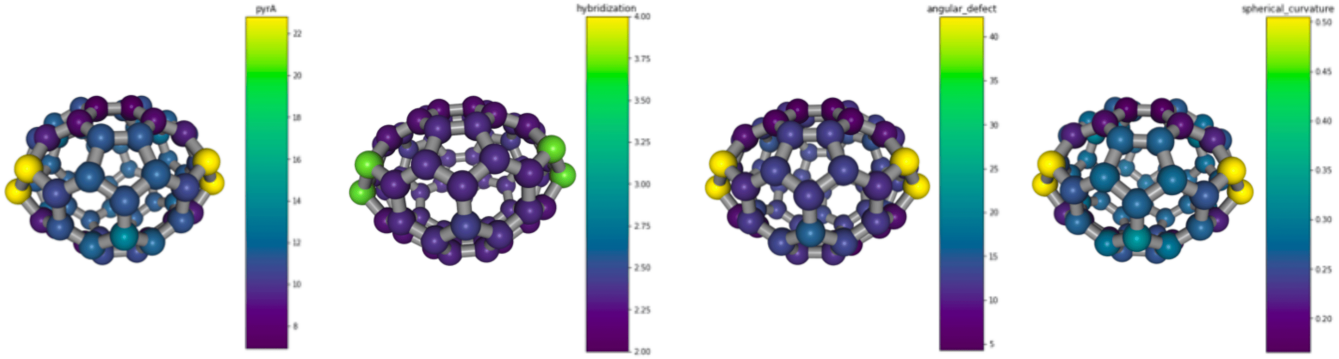

Figure 2.48: Cartographies of the parameters of the fullerene C_{64}-C_s

As for the $C_{50}Cl_{10}$ molecules of the 2008 [34] publication reports chlorofullerenes said to be "pineapple-shaped" from C_{64} and 4 chlorine atoms. We were able to study the possible cholofullerenes from the different C64 studied which are not found in the "pineapple" category.
The first cholorofullerene is the one constructed from C_{3v} symmetry which adopts the original shape described by the publication [34].

- Molecule of fullerene $C_{64}Cl_4$-C_{3v} (n°22) [34]

As already commented concerning the fullerene C_{64} the deformation of the molecule is accentuated with the addition of chlorine atoms. We thus observe a zone where the values of the properties will be more significant.

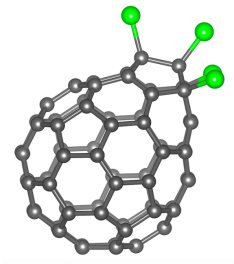

Figure 2.49: Representation of the molecule $C_{64}Cl_4$-C_{3v}

Parameter	Minimum	Maximum
Energy (u.a)	-4257.59	
Pyr (°)	7.43	11.92
Hybridization	2.11	2.29
Angular defect (°)	-78.45	12.59
Spherical curvature	0.18	0.29

Table 2.25: Set of minimum and maximum values of parameters of the molecule $C_{64}Cl_4$-C_{3v} (Pyr, Hyb, $AngDef$, $SphCurv$)

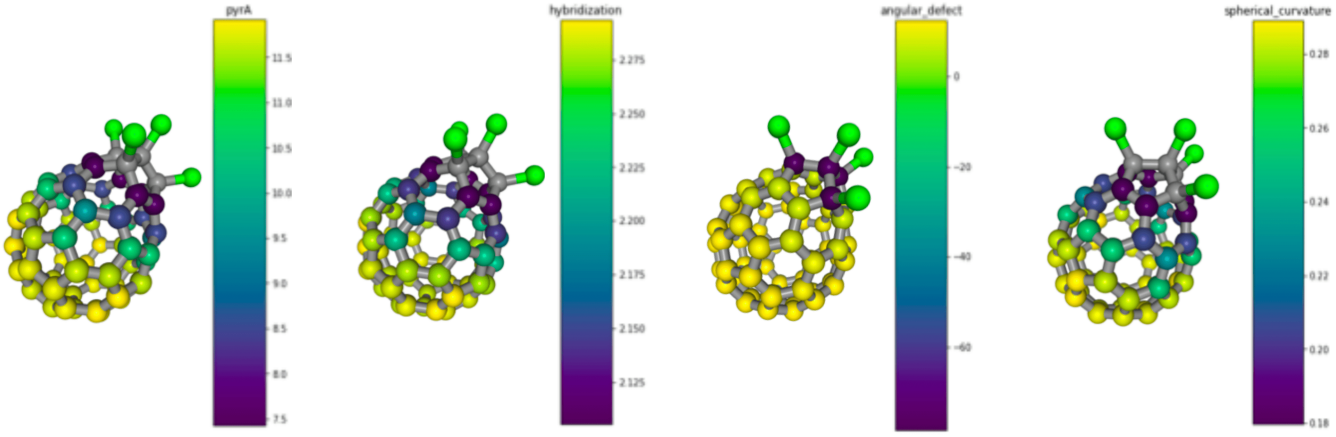

Figure 2.50: Cartographies of the parameters of the fullerene $C_{64}Cl_4$-C_{3v}

We note a maximum of 12° for the angles of pyramidalisation on the lower part of the chlorofullerene and smaller angles towards the top. The hybridizations follow the same behavior with a maximum hybridization of 2.3. The angular defect is calculable in each atom of the molecule, we note that it reaches 13° on the main part of the molecule until the top which shows negative values.

- Molecule of fullerene $C_{64}Cl_4$-C_s (n°23) [34]

This second molecule has a different geometry because the chlorine atoms are not added on the same carbon atoms as the previous molecule but on both sides of the molecule as we can see on the figure:

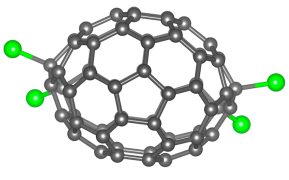

Figure 2.51: Representation of the molecule $C_{64}Cl_4$-C_s

Parameter	Minimum	Maximum
Energy (u.a)	-4257.52	
Pyr (°)	6.94	13.33
Hybridization	2.12	2.38
Angular defect (°)	-70.57	15.56
Spherical curvature	0.19	0.32

Table 2.26: Set of minimum and maximum values of parameters of the molecule $C_{64}Cl_4$-C_s (Pyr, Hyb, $AngDef$, $SphCurv$)

The pyrmidalization angles range from 7° to 13° on the whole molecule. The hybridizations are uniform on the whole molecule showing that the carbons are hybridized sp^2. The angular defect is positive on the whole carbon skeleton except on the 4 addition sites where the values are negative.

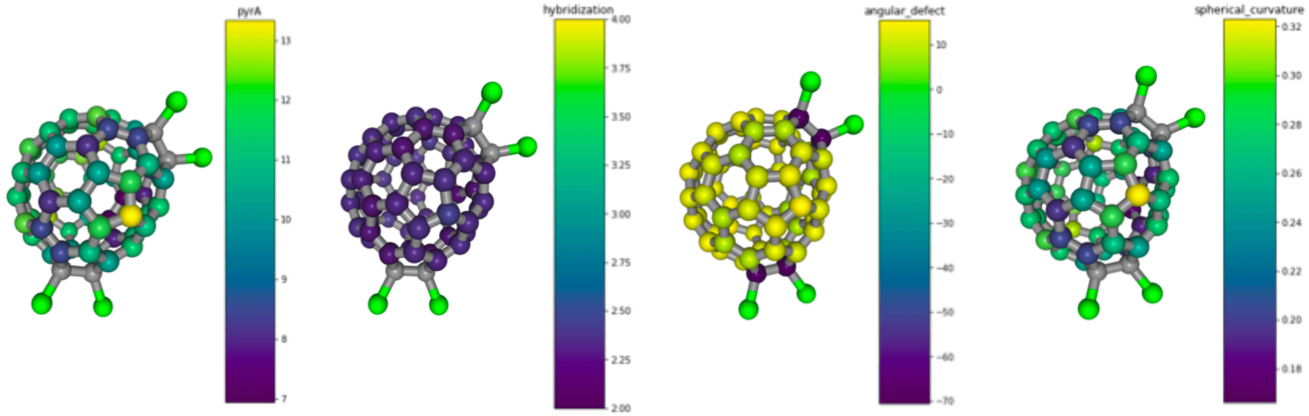

Figure 2.52: Cartographies of the parameters of the fullerene $C_{64}Cl_4$-C_s

- Molecule of fullerene $C_{64}Cl_4$-D_2 (n°24)[34]

This chlorofullerene is presented in the same way as the previous one with the addition of 2 chlorine atoms at each pole and presents the D_2 symmetry.

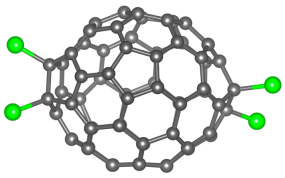

Figure 2.53: Representation of the molecule $C_{64}Cl_4$-D_2

Parameter	Minimum	Maximum
Energy (u.a)	-4257.51	
Pyr (°)	7.77	12.61
Hybridization	2.12	2.33
Angular defect (°)	-70.47	14.00
Spherical curvature	0.19	0.31

Table 2.27: Set of minimum and maximum values of parameters of the molecule $C_{64}Cl_4$-D_2 (Pyr, Hyb, $AngDef$, $SphCurv$)

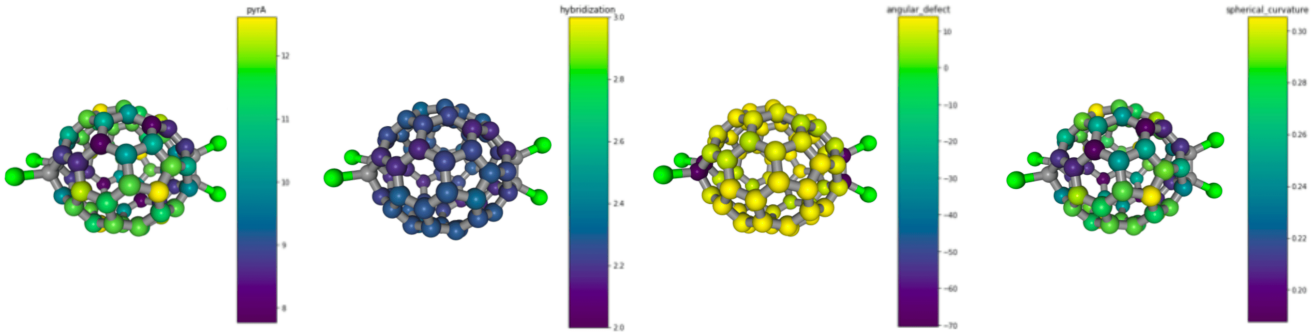

Figure 2.54: Cartographies of the parameters of the fullerene $C_{64}Cl_4$-D_2

Similar to the other chlorofullerenes, $C_{64}Cl_4$ with D_2 symmetry shows non-uniform Pyr throughout the molecule. The angular defect values are positive throughout the molecule but negative here as well at sites of chlorine atom addition. Finally, the spherical curvature is not very uniform on the whole molecule.

- Molecule of fullerene $C_{64}Cl_4$-C_2 (n°25) [34]

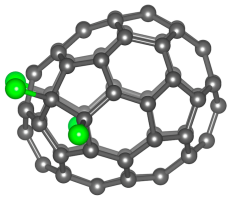

Figure 2.55: Representation of the molecule $C_{64}Cl_4$-C_2

Parameter	Minimum	Maximum
Energy (u.a)	-4257.51	
Pyr (°)	6.94	13.33
Hybridization	2.12	2.38
Angular defect (°)	-70.57	15.56
Spherical curvature	0.20	0.50

Table 2.28: Set of minimum and maximum values of parameters of the molecule $C_{64}Cl_4$-C_2 (Pyr, Hyb, $AngDef$, $SphCurv$)

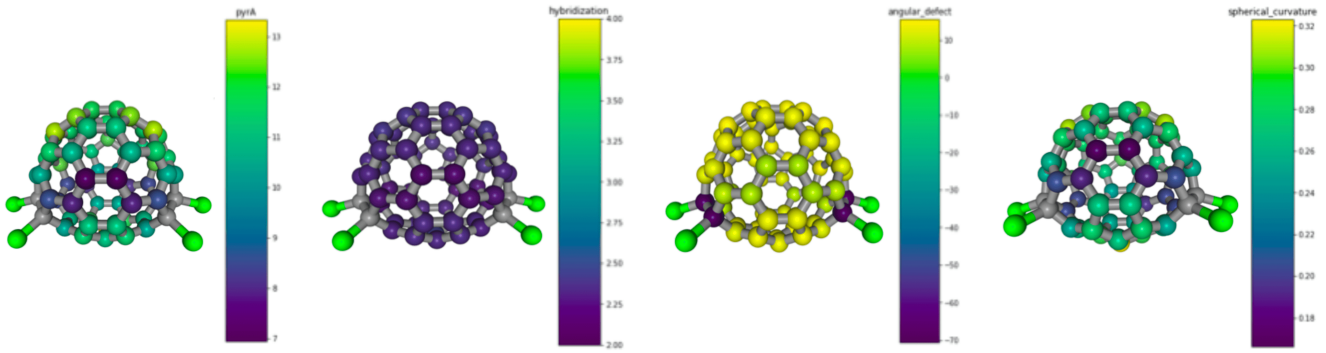

Figure 2.56: Cartographies of the parameters of the fullerene $C_{64}Cl_4$-C_2

We observe angles of pyramidalization between 7° and 13°. The hybridizations are uniform. In this case again the angular defect is positive on the molecule except on the 4 addition sites of the chlorine atoms.

Overview of the pyramidalization angle and hybridization: The two following graphs (figure 2.57) illustrate the data of the molecules according to the parameters of pyramidalization angle and hybridization, taking into account the neighboring environment and the hybridization of each carbon.

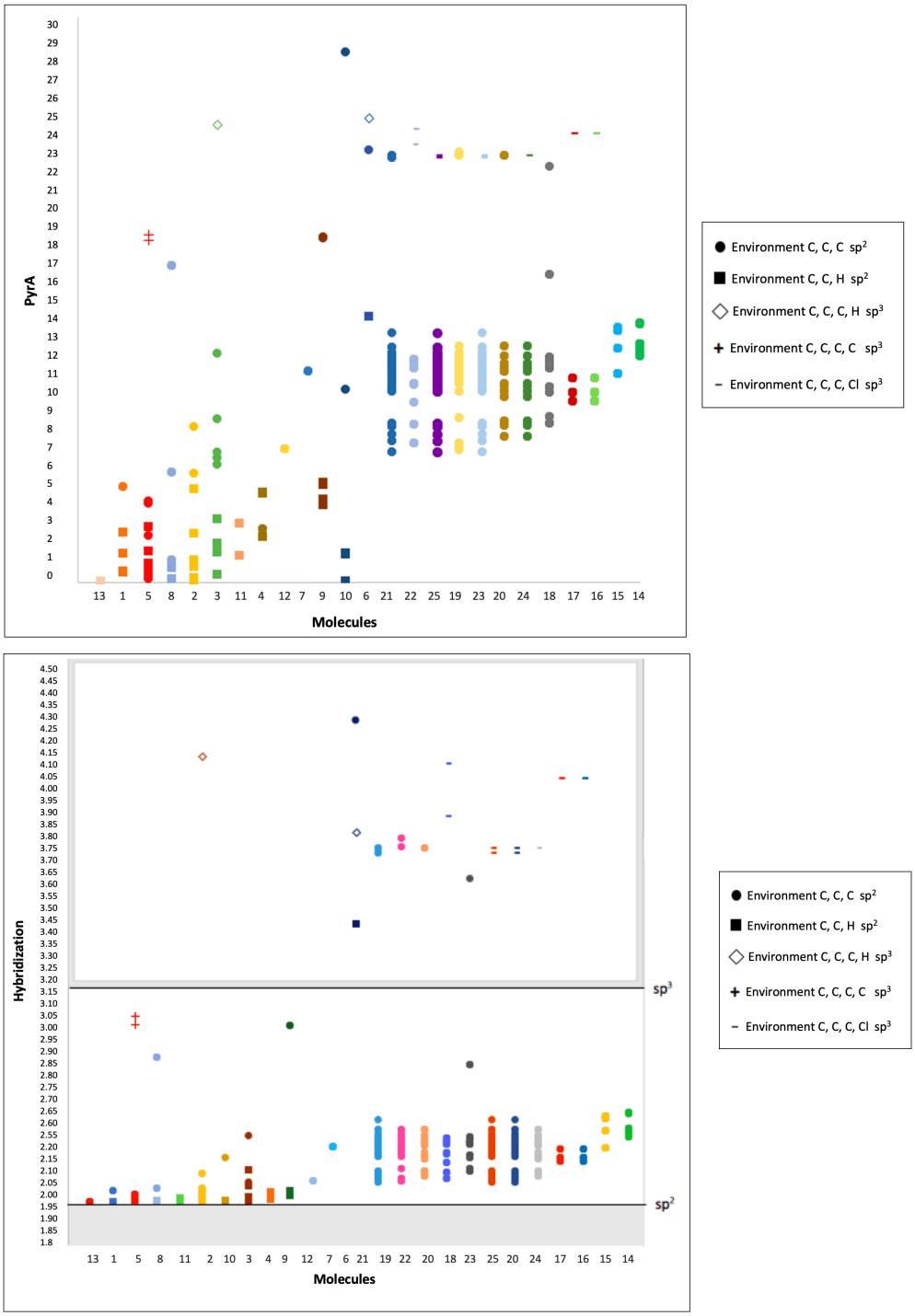

Figure 2.57: Data of the pyramidalization angles and the hybridization of each molecule considering the carbon environment

2.4 Application to reactivity

2.4.1 Presentation of the ring expansion reaction path of a Nitrile Imine

The results presented in this section are based on data from the publication: "New rearrangements of Nitriles Imines: Ring expansion of benzonitrile imines to cycloheptatetraenes and ring closure to 3-phenyl-3H-diazirines" [32].

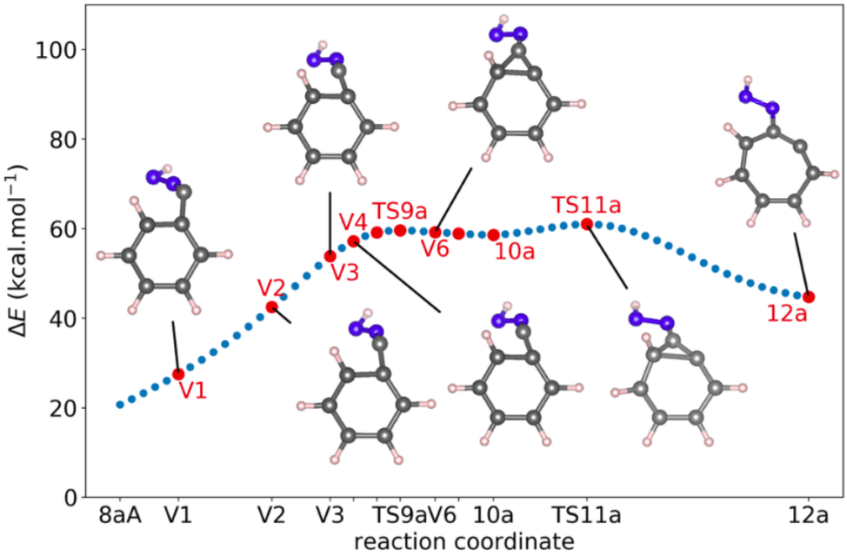

Figure 2.58: Stages ring expansion calculated by DFT B3LYP-6-311G method [32]

The **context** of this study is based on **nitrile imines** which are important intermediates in 1,3-dipolar cycloaddition reactions. They are known to undergo efficient, unimolecular rearrangements to 1H-diazirines, imidoylnitrenes and carbodiimides under thermal and photochemical reaction conditions. C. Wentrup et al. [32] have recently reported a competing rearrangement in which C-phenylnitrile imines undergo ring expansion to 1-diazenyl-1,2,4,6-cycloheptatetraenes akin to the phenylcarbene - cycloheptatetraene rearrangement. Amino-, hydroxy-, and thiol-groups in the meta positions of C-phenylnitrile imine lower the activation energies so that this rearrangement becomes competitive with cyclization to 1H-diazirines and hence rearrangement to carbodiimides. With two NMe_2 groups in the 3- and 5-positions, the activation energy for the ring expansion drops below 50 kcal/mol. The diazenylcycloheptatetraenes so formed can rearrange further to 2-diazenyl-phenylcarbenes over modest activation barriers, and these carbenes cyclize very easily to 2H- and 3H-indazoles, from which 6-methylenecyclohexadienylidene, phenylcarbene, and fulvenallene are potentially obtainable. Moreover, another new rearrangement of benzonitrile imine forms 3-phenyl-3H-diazirine, which is a precursor of phenyldiazomethane and hence phenylcarbene. This reaction is competitive with the ring expansion. The new rearrangements predicted by Wentrup et al., should be experimentally observable, e.g. under FVP or matrix-photolysis conditions.

In this **theoretical work** authors sought to **describe** and **compare** three **intramolecular rearrangement** routes of aromatic nitrile imines, as set out in figure 2.59.
Route (i) describes the new ring expansion of benzonitrile imine (*8a*) to 1-diazenylcycloheptatetraene (*12a*) and subsequent ring contraction to 2-diazenylphenylcarbene (*16a*).
Route (ii) is the previously investigated ring closure to 3-phenyl-1¬H-diazirine (*18a*) and further to phenylcarbodiimide (*20a*).
Route (iii) is the new ring closure to 3-phenyl-3H-diazirine (*22a*), which results in the easy formation of phenyldiazomethane (*24*) and then phenylcarbene (*26*).

Electronic energies of ground and transition states were studied at the DFT and CASPT2 levels of theories (figure 2.59). Compounds are designated *8a*, *10a*...etc for the parent compounds and transition states *TS9a*...etc. A designate propargylic stucture of nitrile imine.

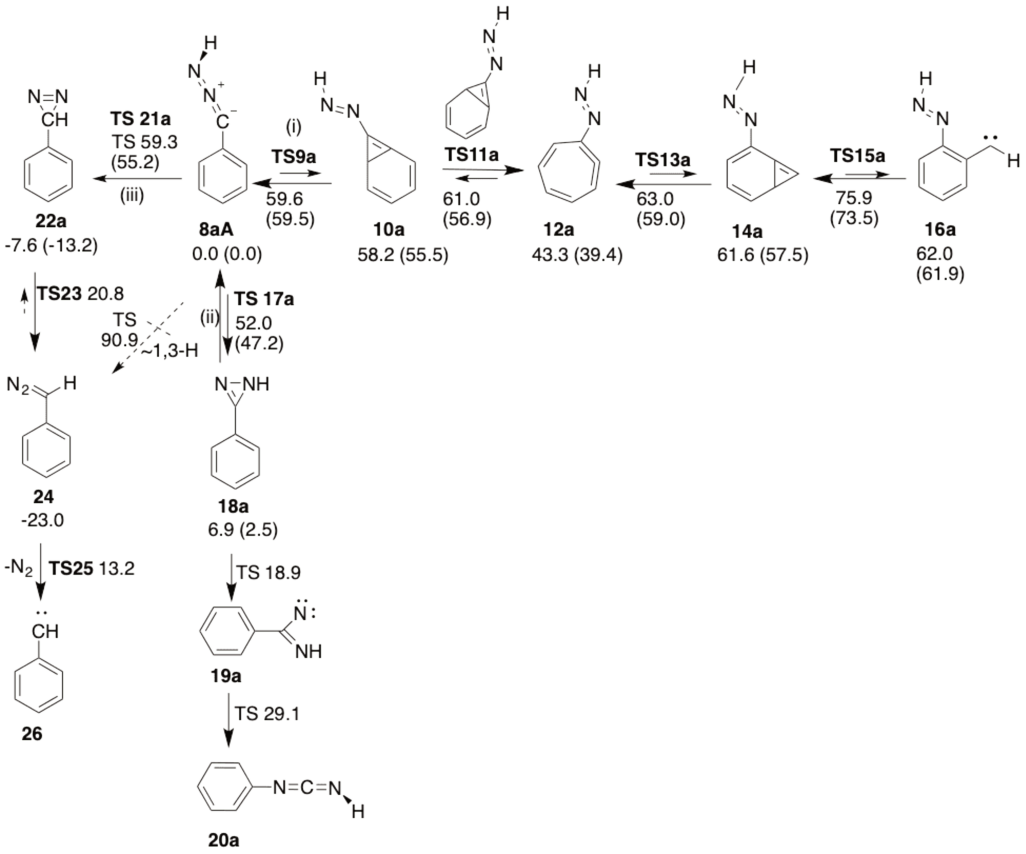

Figure 2.59: Rearrangment routes of aromatic nitrile imines [32]

If such a study provides information on the topology of the potential surfaces this kind of approach does not inform the chemist about the evolution of the chemical character of the species present during the chemical reaction (along the reaction path). Indeed, for a stable equilibrium molecule, principal theoretical interest generally focuses on the Lewis-structural bonding pattern and associated orbitals that are optimal for its description. For a chemical reaction, however, the primary focus turns to bond shifts between reactant and product species and the corresponding dynamical transformations of orbital form and location along a reactive pathway on the potential energy surface (PES). An NBO (Natural Bond Orbital) analysis of the electron distributions during these transformations is generally developed by chemist but the theoretical level of these interpretations remains sometimes questionable especially in the presence of compounds as complex as those studied in our work because of their muti-determinental character.

We believe that another way of approaching the problem is possible thanks to the **tools** we have presented so far in this work. A very **preliminary attempt** of the analysis of the route (i) is presented in this work as illustration. A thorough study of this work is still to be done. So, along this reaction path we have studied each of the points of the curve of route (i). For each of the points four parameters were studied: the pyramidalization angle, the angular defect, the spherical curvature and the hybridization.

Note that all the visualizations in this section are once again made from the program "Pychemcurv" [10].

2.4.2 Results

2.4.3 Conformation 8aA - Allenic Benzonitrile Imine

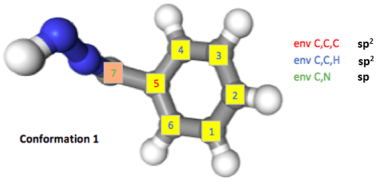

Figure 2.60: Conformation *8aA* and classification of atoms according to their environment and hybridization

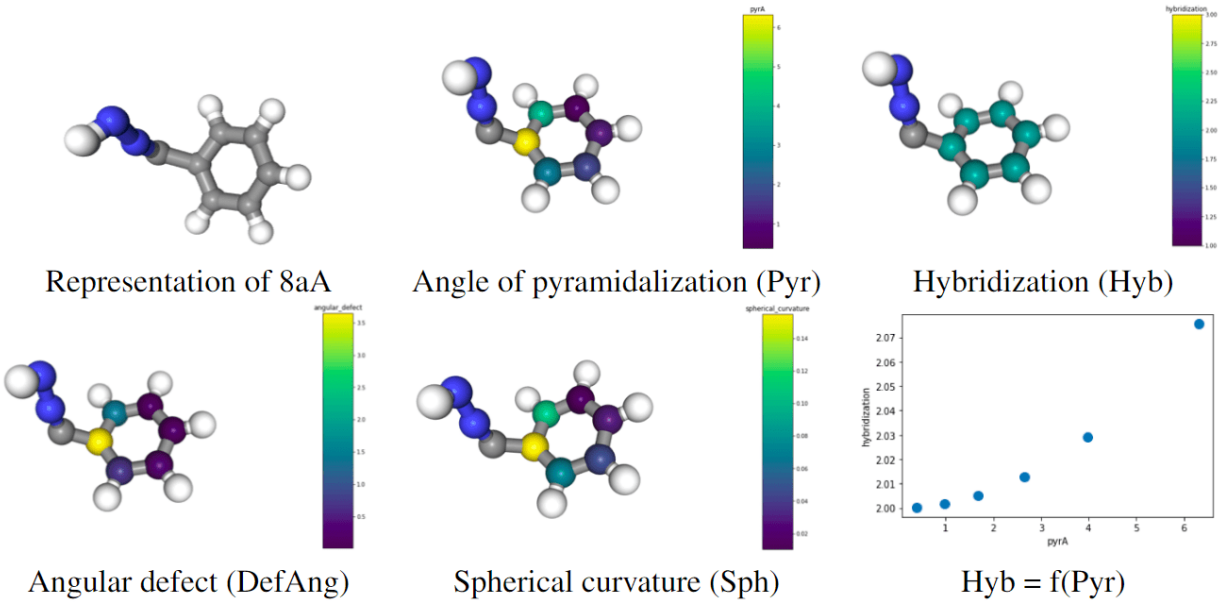

Figure 2.61: Cartographies and representation of the parameters of conformation *8aA*

Environment C-C-C	sp^2	C5
Environment C-C-H	sp^2	C1 C2 C3 C4 C6
Environment C-C-N	sp	C7
E	-	-379.827126 u.a

Table 2.29: Set of environment and energy of conformation *8aA*

Atom	Pyr	DefAng	Sph	Hyb
1	1.667498	0.252008	0.045012	2.005094
2	0.964742	0.084388	0.026089	2.001702
3	0.379465	0.013059	0.010298	2.000263
4	3.978158	1.429812	0.107605	2.029301
5	6.321044	3.649031	0.154860	2.075476
6	2.65232	0.637254	0.071664	2.012931

Figure 2.62: Set of values of parameters of conformation *8aA* (*Pyr, Hyb, AngDef, SphCurv*)

Characterics of V1

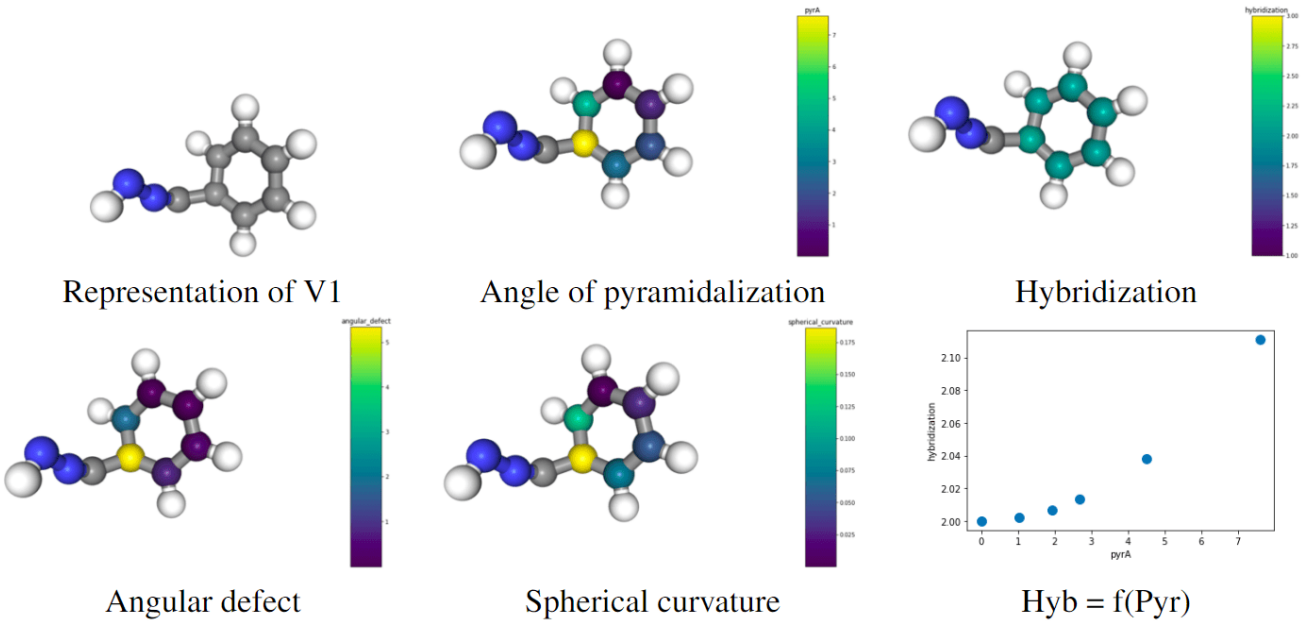

Figure 2.63: Cartographies and representation of the parameters of conformation V1

Environment C-C-C	sp^2	C5
Environment C-C-H	sp^2	C1 C2 C3 C4 C6
Environment C-C-N	sp	C7
E	-	-379.816260 u.a

Table 2.30: Set of environment and energy of conformation V1

Atom	Pyr	DefAng	Sph	Hyb
1	1.936569	0.33981180	0.052259	2.006875
2	1.024235	0.09511434	0.027681	2.001919
3	0.002085	$3.942986.10^{-7}$	0.000057	2.000000
4	4.513634	1.83891400	0.122170	2.037862
5	7.603411	5.34616100	0.186513	2.110867
6	2.681132	0.65144840	0.072442	2.013216

Figure 2.64: Set of values of parameters of conformation V1 (*Pyr, Hyb, AngDef, SphCurv*)

The "V1" state of the reaction path of figure 2.58 has been reached.

Characterics of V2

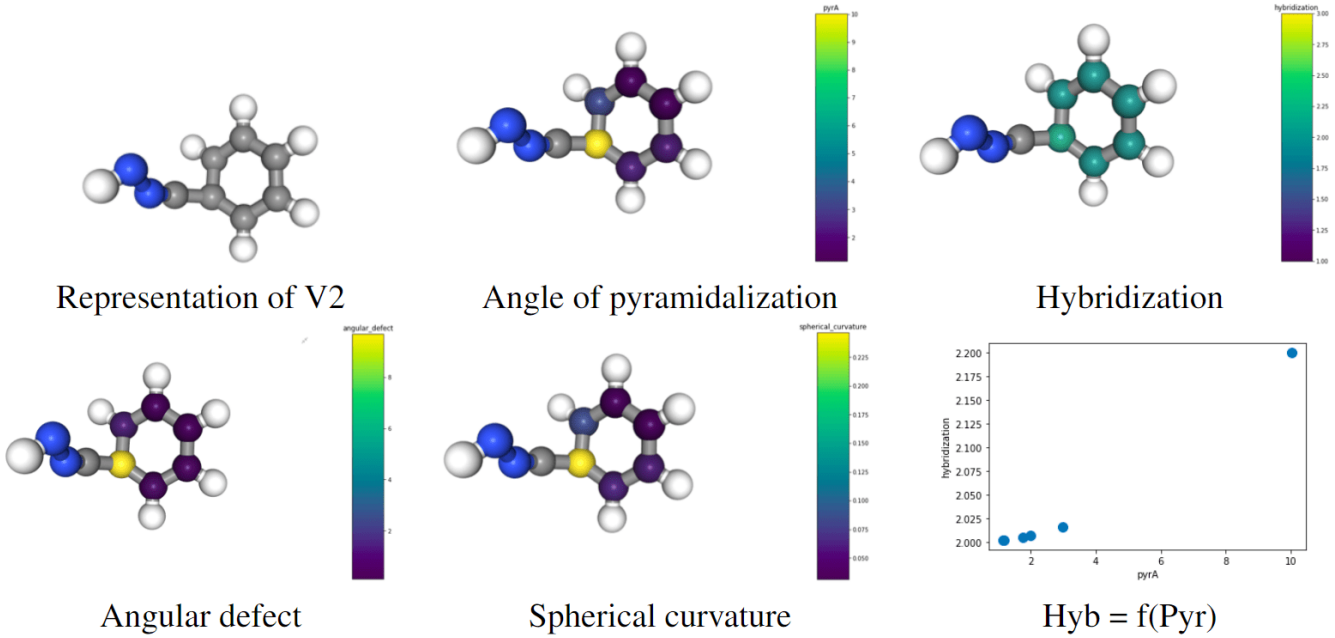

Figure 2.65: Cartographies and representation of the parameters of conformation V2

Environment C-C-C	sp^2	C5
Environment C-C-H	sp^2	C1 C2 C3 C4 C6
Environment C-C-N	sp	C7
E	-	-379.792368 u.a

Table 2.31: Set of environment and energy of conformation V2

Atom	Pyr	DefAng	Sph	Hyb
1	1.753834	0.278776	0.047307	2.005636
2	1.190437	0.128510	0.032101	2.002593
3	1.156046	0.121208	0.031440	2.002445
4	2.992608	0.811263	0.080689	2.016488
5	10.016094	9.688596	0.246477	2.199614
6	1.981983	0.35674	0.053581	2.007203

Figure 2.66: Set of values of parameters of conformation V2 (*Pyr, Hyb, AngDef, SphCurv*)

This point corresponds to point "V2" of the reaction path.

Characterics of V3

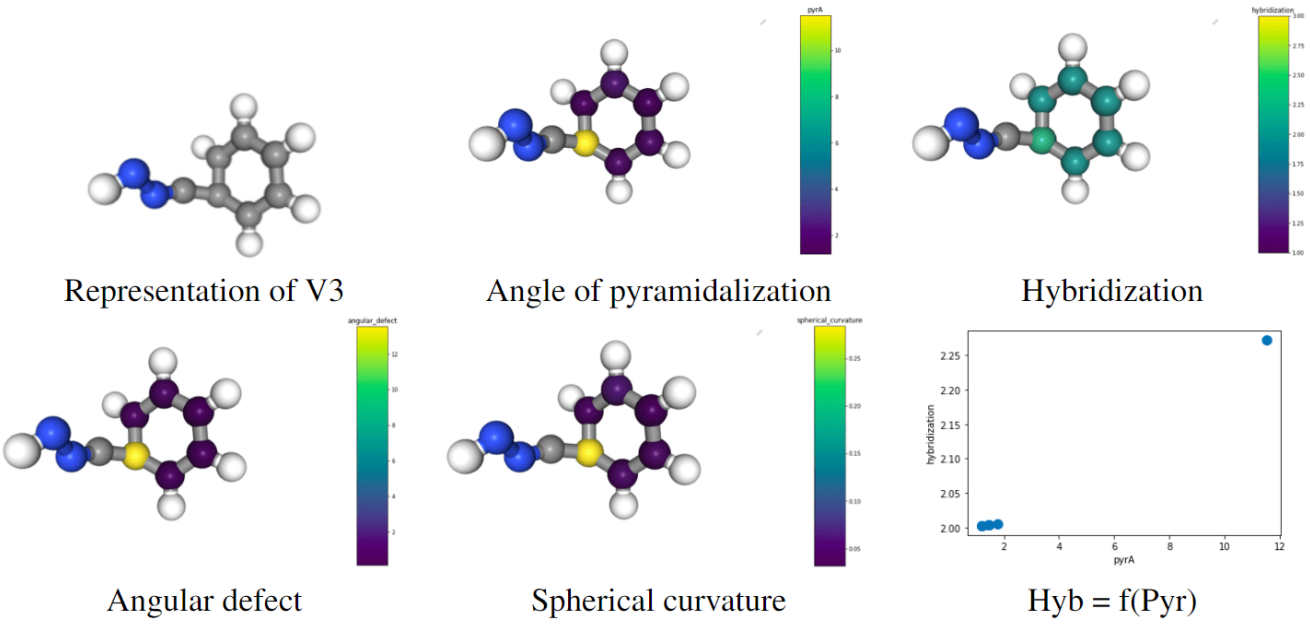

Figure 2.67: Cartographies and representation of the parameters of conformation V3

Environment C-C-C	sp^2	C5
Environment C-C-H	sp^2	C1 C2 C3 C4 C6
Environment C-C-N	sp	C7
E	-	-379.774313 u.a

Table 2.32: Set of environment and energy of conformation V3

Atom	Pyr	DefAng	Sph	Hyb
1	1.438139	0.187526	0.038757	2.003786
2	1.210689	0.132956	0.032592	2.002682
3	1.764184	0.282108	0.047811	2.005703
4	1.194216	0.129531	0.031908	2.002610
5	11.524357	13.559333	0.284061	2.272060
6	1.468643	0.196024	0.039750	2.003949

Figure 2.68: Set of values of parameters of conformation V3 (*Pyr, Hyb, AngDef, SphCurv*)

State "V3" of the reaction path is reached.

Characterics of V4

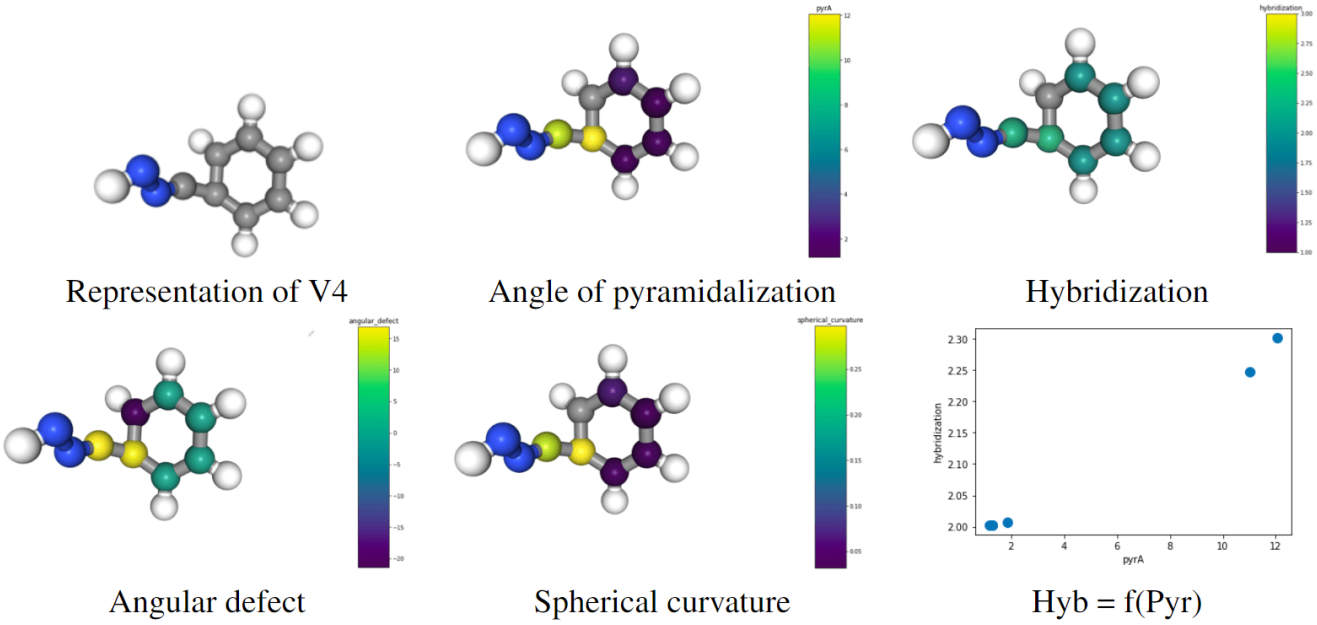

Figure 2.69: Cartographies and representation of the parameters of conformation V4

Environment C-C-C	sp^2	C5
Environment C-C-H	sp^2	C1 C2 C3 C4 C6
Environment C-C-N	sp	C7
E	-	-379.768938 u.a

Table 2.33: Set of environment and energy of conformation V4

Atom	Pyr	DefAng	Sph	Hyb
1	1.314700	0.156744	0.035407	2.003164
2	1.187049	0.127832	0.031937	2.002578
3	1.884989	0.321999	0.050948	2.006513
4	NaN	-21.387858	NaN	NaN
5	12.059293	15.280032	0.297491	2.301357
6	1.312094	0.156485	0.035541	2.003151
7	11.034023	16.893025	0.269333	2.246920

Figure 2.70: Set of values of parameters of conformation V4 (*Pyr, Hyb, AngDef, SphCurv*)

The transition state approaches the sp^3 state.
The point coincides with the V4 state of the path in the figure 2.58.

2.4.4 Conformation 2 : transition state TS9a

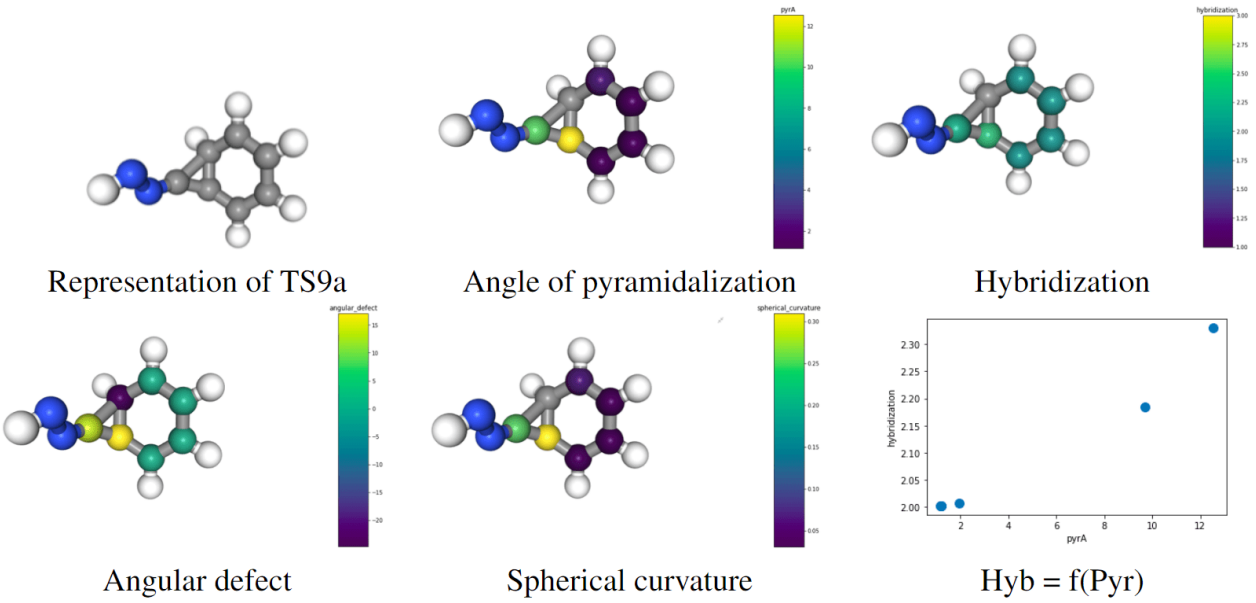

Figure 2.71: Cartographies and representation of the parameters of conformation TS9a

Environment C-C-C	sp^2	C5
Environment C-C-C-H	sp^3	C4
Environment C-C-H	sp^2	C1 C2 C3 C6
Environment C-C-N	sp	C7
E	-	-379.765890 u.a

Table 2.34: Set of environment and energy of conformation TS9a

Atom	Pyr	DefAng	Sph	Hyb
1	1.191238	0.128711	0.032057	2.002597
2	1.154461	0.120929	0.031043	2.002439
3	1.958262	0.347467	0.052759	2.007031
4	NaN	-24.73652	NaN	NaN
5	12.544951	17.073513	0.309727	2.329739
6	1.188212	0.128351	0.032213	2.002583
7	9.677130	12.801086	0.236120	2.185240

Figure 2.72: Set of values of parameters of conformation TS9a (*Pyr, Hyb, AngDef, SphCurv*)

This point corresponds to the "TS9a" state of the path, so the conformation change takes place between the point "V4" and "V6" of the path of figure 2.58.

Characterics of V6

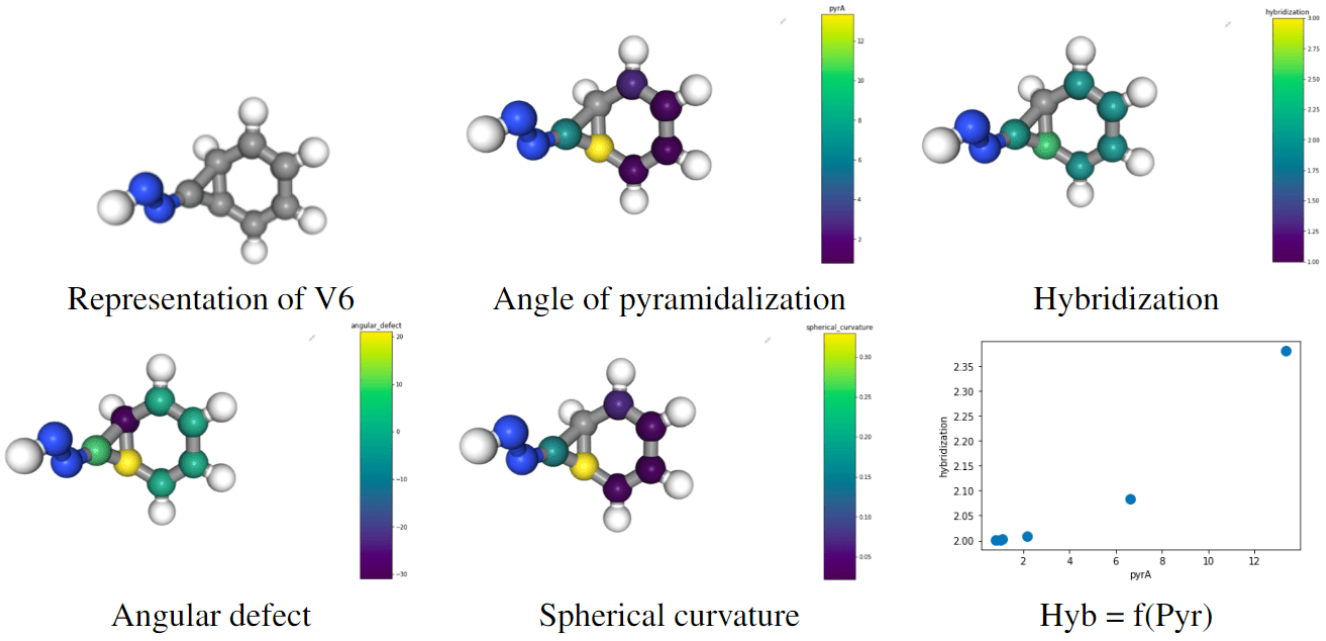

Figure 2.73: Cartographies and representation of the parameters of conformation V6

Environment C-C-C	sp^2	C5
Environment C-C-C-H	sp^3	C4
Environment C-C-H	sp^2	C1 C2 C3 C6
Environment C-C-N	sp	C7
E	-	-379.765726 u.a

Table 2.35: Set of environment and energy of conformation V6

Atom	Pyr	DefAng	Sph	Hyb
1	0.805861	0.058935	0.021642	2.001188
2	1.109085	0.111680	0.029776	2.002250
3	2.154805	0.420597	0.057685	2.008518
4	NaN	-30.916412	NaN	NaN
5	13.349291	21.076803	0.329821	2.380743
6	1.022567	0.095154	0.027767	2.001913
7	6.611699	5.875616	0.162842	2.082838

Figure 2.74: Set of values of parameters of conformation V6 (*Pyr, Hyb, AngDef, SphCurv*)

We are at point "V6" of the path (figure 2.58).

2.4.5 Conformation 3 - 10a - bicyclo[4.1.0]hepta-2,4,7-triene

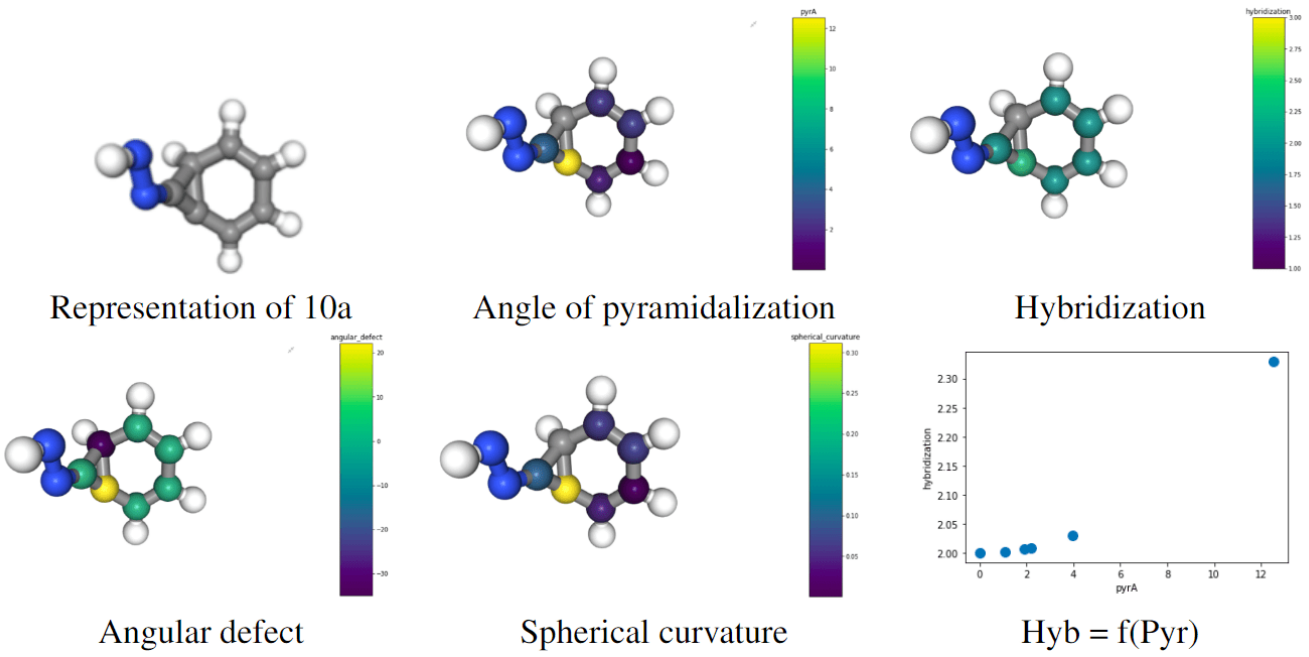

Figure 2.75: Cartographies and representation of the parameters of conformation 10a

Environment C-C-C	sp^2	C5
Environment C-C-C-H	sp^3	C4
Environment C-C-H	sp^2	C1 C2 C3 C6
Environment C-C-N	sp	C7
E	-	-379.766669 u.a

Table 2.36: Set of environment and energy of conformation 10a

Atom	Pyr	DefAng	Sph	Hyb
1	1.090407	0.108527	0.029665	2.002175
2	0.009218	0.000008	0.000247	2
3	2.200591	0.439445	0.059013	2.008886
4	1.927923	0.336771	0.051559	2.006814
5	NaN	-34.932909	NaN	NaN
6	12.532256	22.126278	0.311692	2.328974
7	3.974531	1.977641	0.099852	2.029247

Figure 2.76: Set of values of parameters of conformation 10a (*Pyr, Hyb, AngDef, SphCurv*)

This is the "10a" point of the reaction path (figure 2.58).

Characterics of TS11a

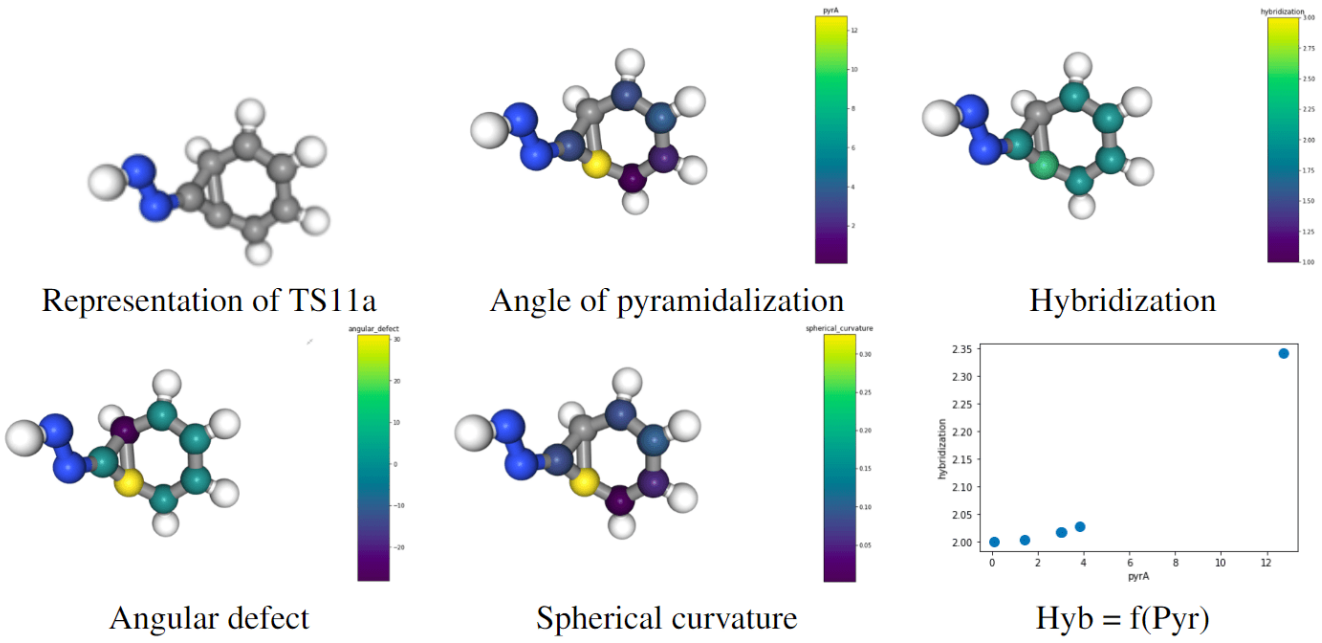

Figure 2.77: Cartographies and representation of the parameters of conformation TS11a

Environment C-C-C	sp^2	C5
Environment C-C-C-H	sp^3	C4
Environment C-C-H	sp^2	C1 C2 C3 C6
Environment C-C-N	sp	C7
E	-	-379.762883 u.a

Table 2.37: Set of environment and energy of conformation TS11a

Atom	Pyr	DefAng	Sph	Hyb
1	0.089150	0.000725	0.002434	2.000015
2	1.418131	0.182615	0.038093	2.003682
3	3.829610	1.328587	0.102723	2.027128
4	3.008701	0.821332	0.080555	2.016667
5	NaN	-28.082354	NaN	NaN
6	12.727553	31.058654	0.325574	2.340869
7	3.030169	1.006072	0.076200	2.016908

Figure 2.78: Set of values of parameters of conformation TS11a (*Pyr, Hyb, AngDef, SphCurv*)

This point represents the TS11a state of the path.

2.4.6 Conformation 4 - 12a cycloheptatetraene

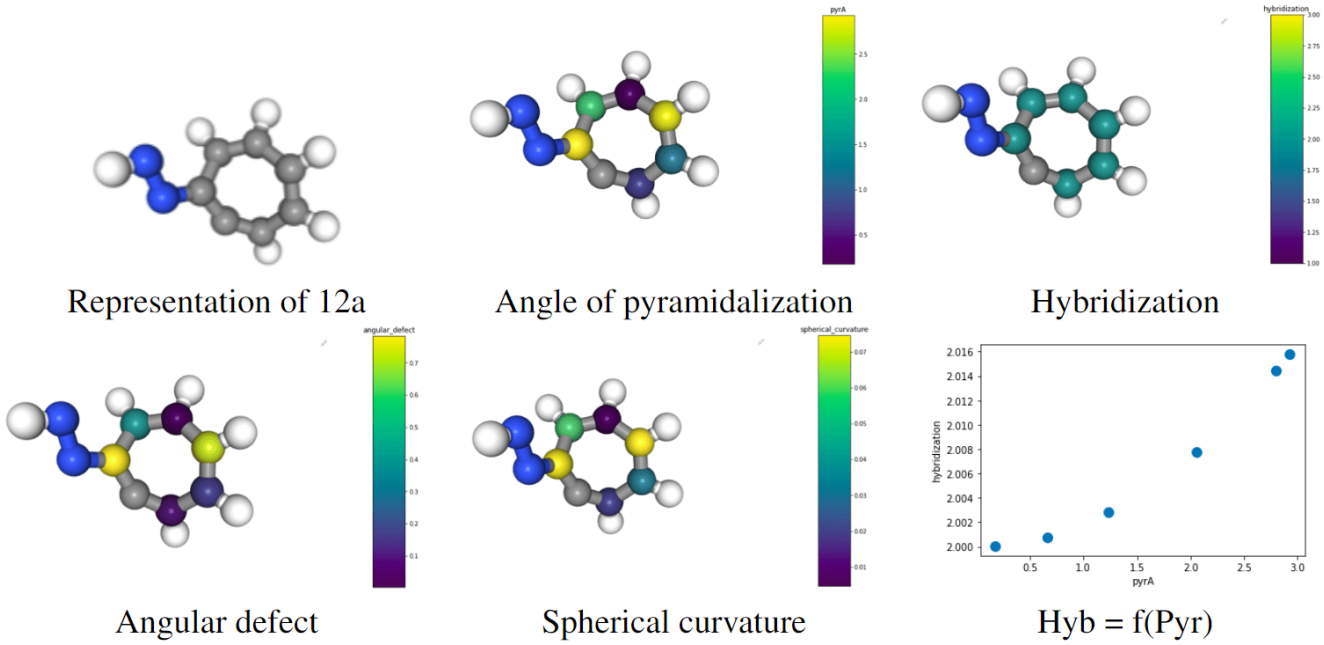

Figure 2.79: Cartographies and representation of the parameters of conformation 12a

Environment C-C	sp	C6
Environment C-C-H	sp^2	C1 C2 C3 C4 C5
Environment C-C-N	sp^2	C7
E	-	-379.788760 u.a

Table 2.38: Set of environment and energy of conformation 12a

Atom	Pyr	DefAng	Sph	Hyb
1	0.661212	0.039825	0.018010	2.000799
2	1.237321	0.138851	0.033134	2.002802
3	2.797924	0.715678	0.074597	2.014400
4	0.175846	0.002846	0.004692	2.000057
5	2.058030	0.383770	0.055007	2.007768
6	NaN	NaN	NaN	NaN
7	2.927266	0.783591	0.072709	2.015771

Figure 2.80: Set of values of parameters of conformation 12a (*Pyr, Hyb, AngDef, SphCurv*)

The last point of the path is reached point "12a".

2.4.7 Comparative graphs

- Angle of pyramidalization

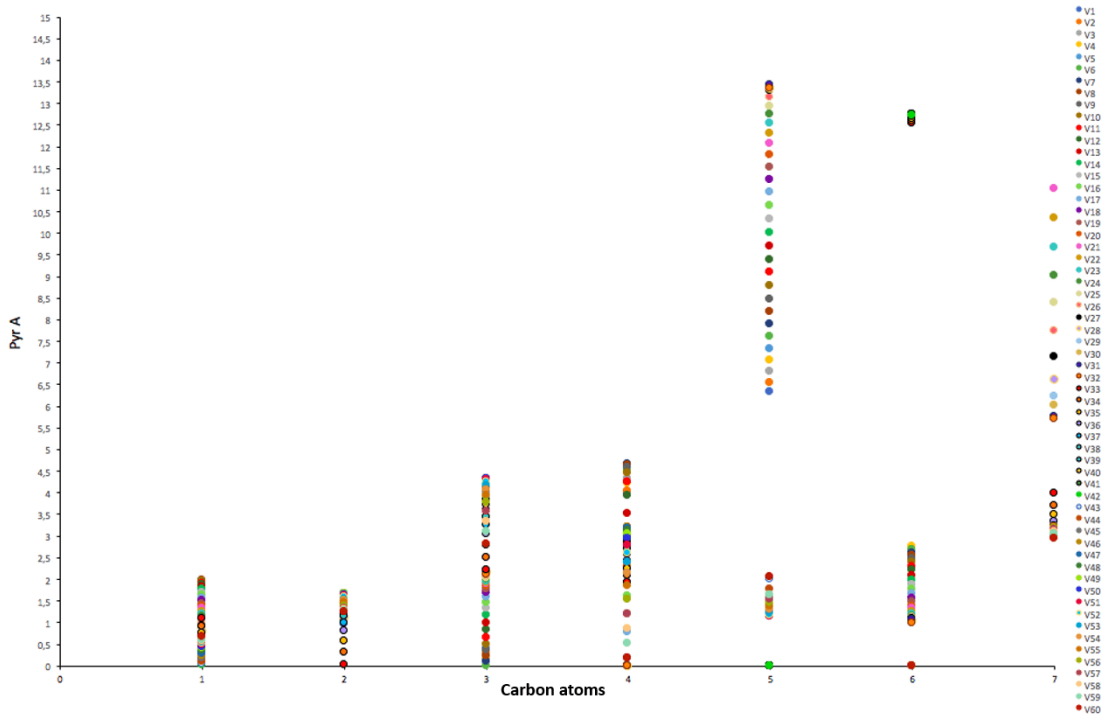

Figure 2.81: Graph displaying the angle of pyramidalization as a function of carbon atoms

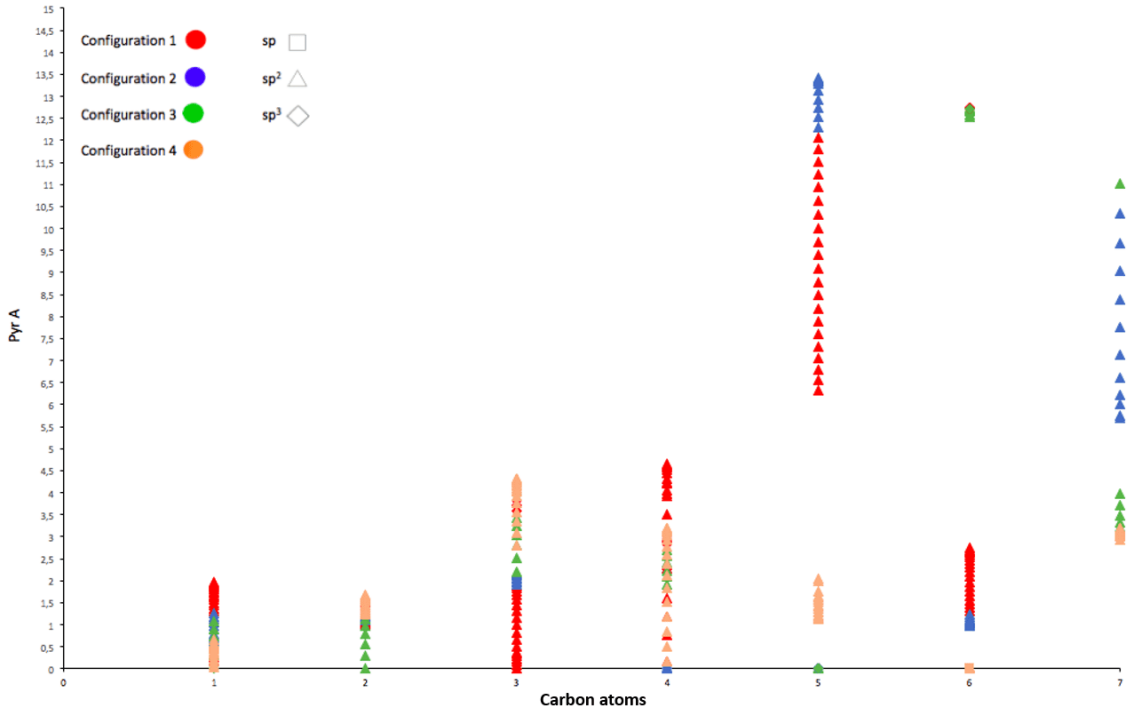

Figure 2.82: Graph displaying the angle of pyramidalization as a function of carbon atoms (taking into account the configurations)

- Hybridization

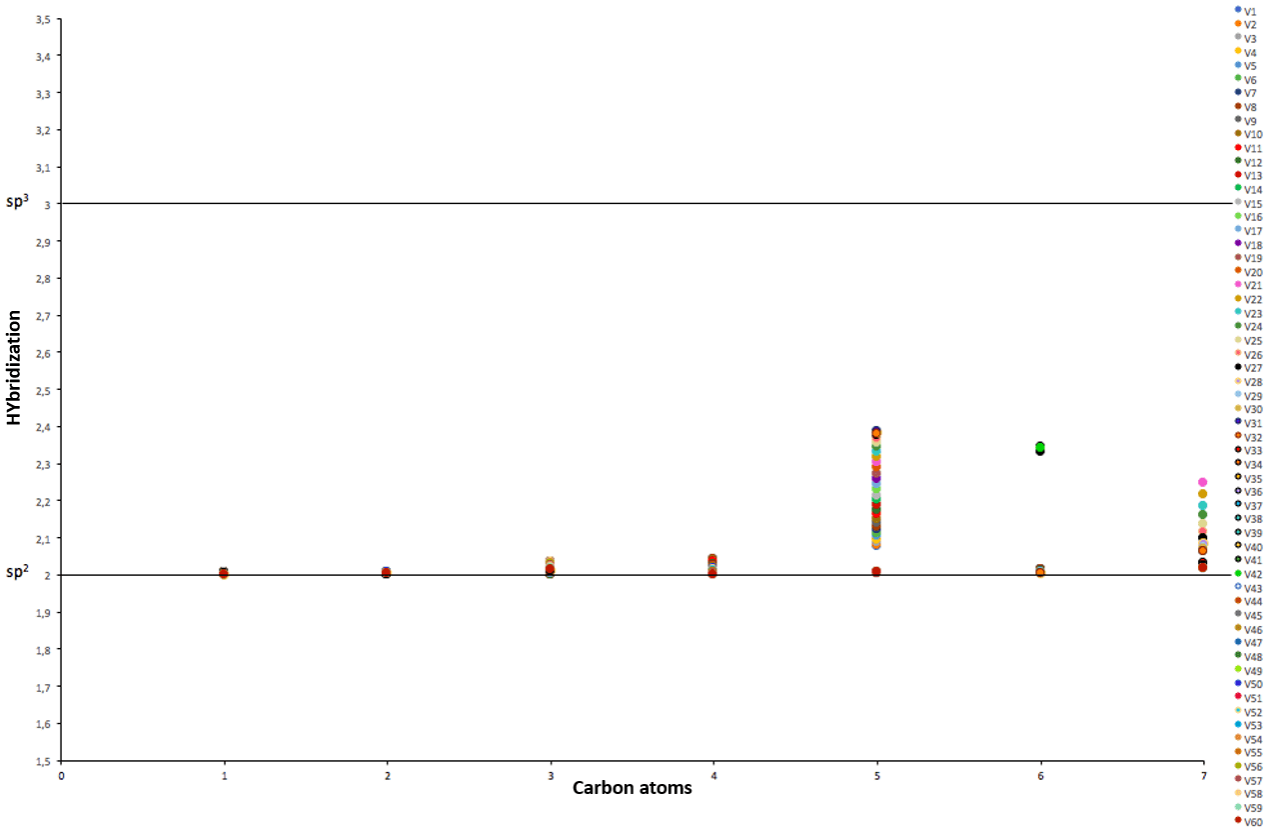

Figure 2.83: Graph displaying the hybridization as a function of carbon atoms

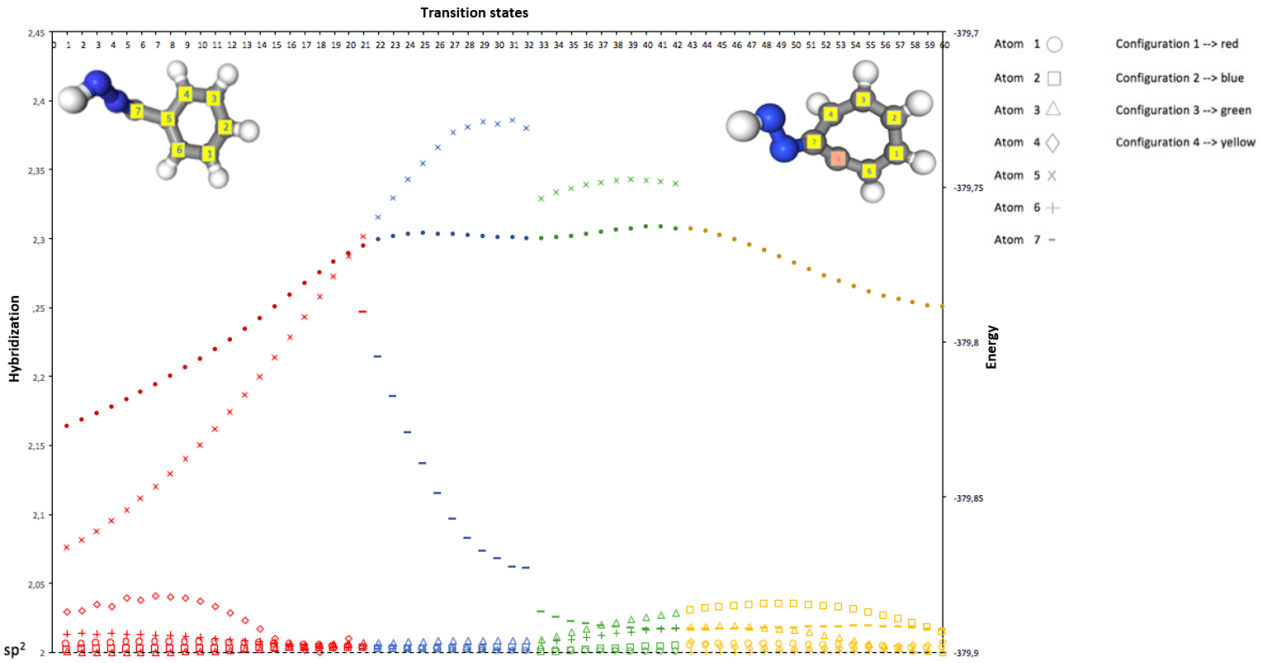

Figure 2.84: Graph showing the hybridization and the energies as a function of transition states

- Angular defect

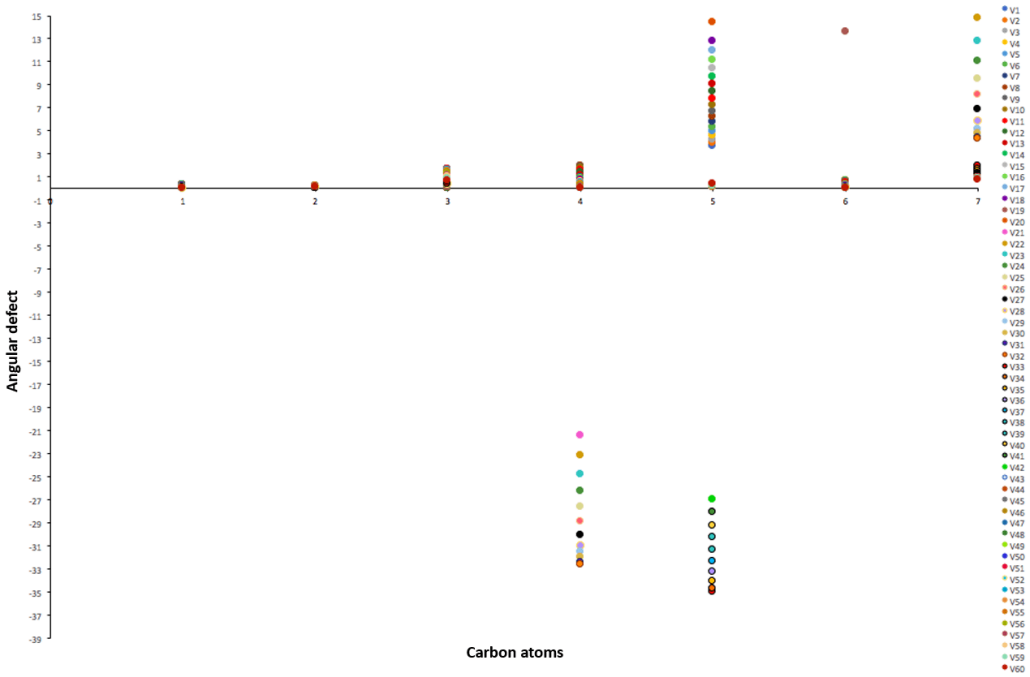

Figure 2.85: Graph showing the angular defect as a function of carbon atoms

- Spherical curvature

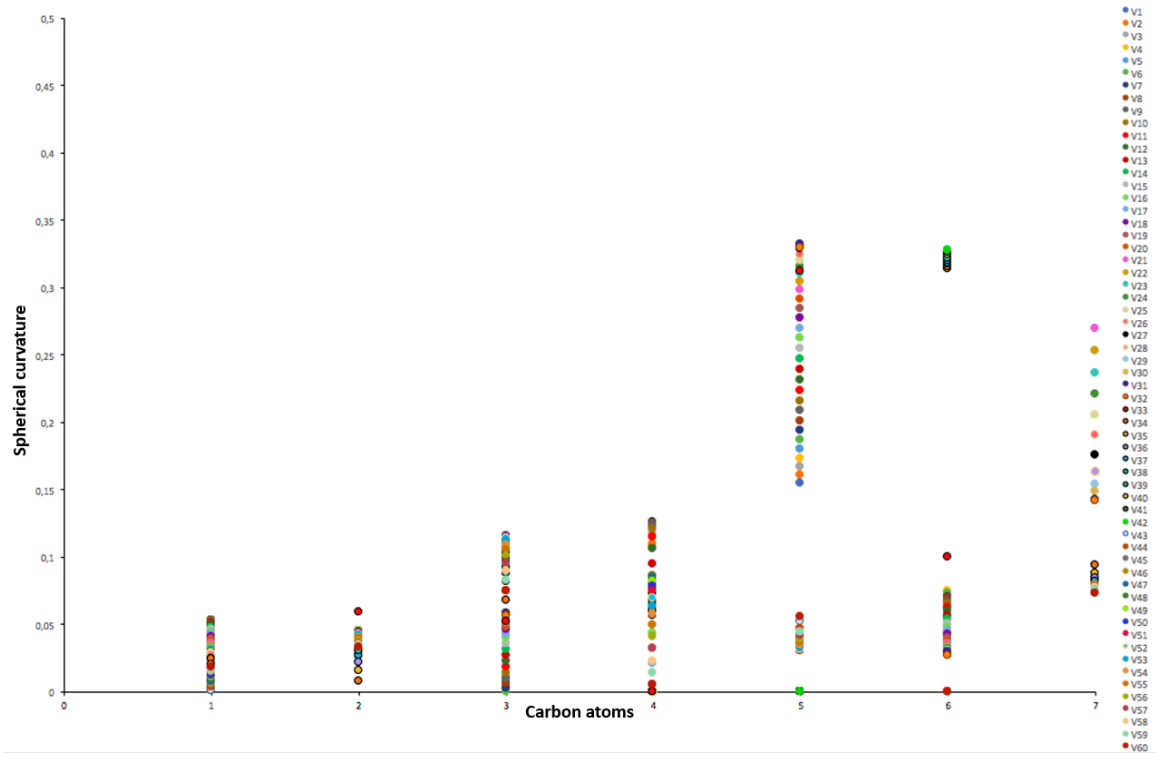

Figure 2.86: Graph representing the spherical curvature as a function of carbon atoms

These analyses allow us today to propose a **physical representation** of the reaction path (see figure 2.87) of the route (i) directly connected to the classical expected description of the chemist in terms of Lewis representation.

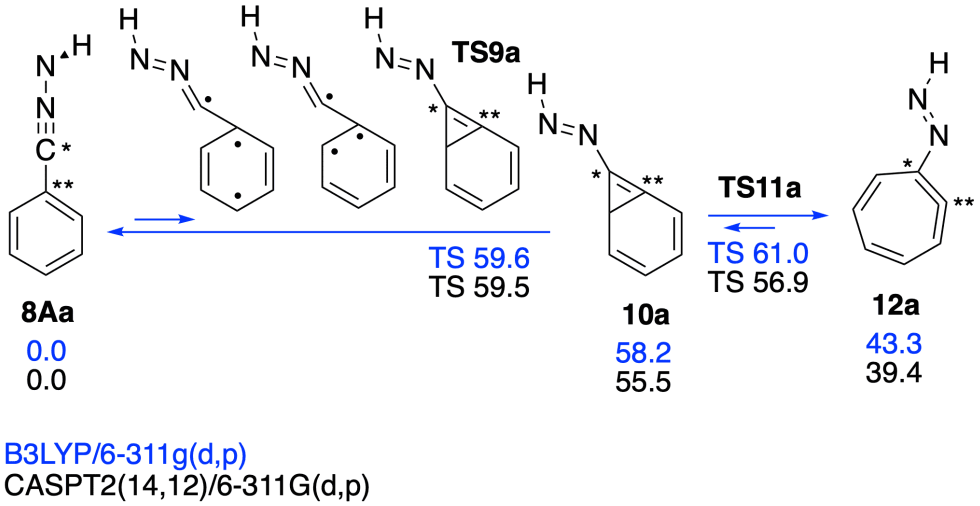

Figure 2.87: Representation of the reaction path of route (i) 2.58

2.5 Conclusion

In this chapter we studied a large range of examples following tools giving access to all the information necessary to characterize the deformation and the reactivity of the systems. 3 major categories of molecules are studied: **non-fullerenic**, **fullerenic** and **nitrile imines**.

In the case of the **non-fullerenic molecules** we observed that:

- the *Pyr* are more important at the vertices, at the junctions of the patterns and at the bridged zones,
- the **hybridization** is generally uniform around 2.00 which means sp^2 atoms hybridization. The case n°13 corannulene is totally uniform with all atoms hybridized sp^2. But in some cases the hybridization > 3 in bridged molecules,
- the **spherical curvature** is still < 1.

In general, we observe limitations of the methods for atoms whose degree is > 3. The **angular defect** provides a way to go beyond this limit but presents negative values. On the set of these molecules, the deformation is more significant on the junction zones which seem then more susceptible to be **reactive**.

For the **fullerenic molecules** we note that:

- the *Pyr* is quite uniform on this type of spherical molecule but the *Pyr* is never > 6 but is higher when the fullerene is a few distorted at the poles,
- the **hybridization** is around 2 but is still < 4 on the poles atoms,
- the **angular defect** is calculable on all the atoms but negatives values on the atoms of degree > 4,

- the **spherical curvature** is still < 1.

The same general limitations are observed with the atoms of degree > 3.
In a general way, fullerenic molecules seem to be more adapted to the use of the set of tools and are potentially **more reactive** on more deformed molecular regions.

We note an obvious limitation of our tools with the angular defect, since even if the angular defect is computable in all cases, the negative values observed have no physical meaning. This is an important point which requires additional research beyond this thesis work.

Concerning the **2 figures (2.57)** *(for reminder the non-fullerenic molecules are of number 1 to 13 and the fullerenic molecules from 14 to 25)*:

For the Pyr, the 2 groups are clearly observed: the non-fullerenic with rather low pyr values between 0 and 10° for an environment with sp^2-hybridized carbon-carbon-hydrogen type atoms and the fullerenic with higher Pyr between 8 and 15° for an environment predominantly carbon sp^2 hybridized environment. This observation is logical since the non-fullerenic exhibit less curvature.

For **hybridization** we also have 2 groups for the same environment as Pyr:
Non-fullerenes molecules have a hybridization between 2 and 2.5. For the fullerenes the hybridization is also between 2.05 and 2.6 but we observe much higher and less classic values with sp^4-type hybridizations.

For the **nitrile imines** molecules:

We show that the parameters are useful in the case of study of **reaction path**, and allow to follow the evolution of the bonds of a system. By the different graphs, we observe that a complete study of the system can be carried out.

We show by this specific example that the use of the tools described in this work is simple and gives access to useful geometrical and chemical information along reaction path.

Chapter 3

Beyond the π-Orbital Axis Vector: the POAV2 theory

In this chapter we look beyond the theories presented in the 2 previous chapters. We expose the POAV2 theory revised, initially developed by R. C. Haddon in 1986 [6].

We give a complete derivation of the POAV2 theory with complete proofs according to different parameters:

- *the σ and π-orbitals,*
- *the existence and uniqueness of POAV2,*
- *the orthogonality,*
- *and the hybridization numbers.*

Then, we make a partial comparison between POAV1 and POAV2 theories and an exploration with possible applications.

We used results from the work of R. C. Haddon [6] and our preprint work on POAV2 [36].

3.1 Study of POAV2 theory

As proven in the previous chapters, the **POAV1** theory gives tools to identify the **local geometry** of a molecule by emancipating from the bond lengths, angles between bonds of neighboring atoms and laborious quantum computations.

If we consider the situation of POAV1, it is a very particular case, typically the C_{3v} symmetry. The use of POAV1 is perfectly valid for the description of local properties but for a more global description we have to generalize the notion. It is judicious to take into consideration more information such as the length and angles between bonds. This is what R. C. Haddon proves in his 1986 article [6]. The **POAV1** is a **pure geometric object** and its construction depends only on the **local geometry** for a vertex and therefore for a considered atom. The relation with the electronic structure depends on the chosen basis of molecular orbitals. By the concept **POAV2** , R. C. Haddon describes the characteristics in a more **physical** way.

According to R. C. Haddon, the description of the σ-system is possible by choosing a set of orbitals in the direction of the bonds. Then, an orbital is added to define the π-system. The family of orbitals has an orthogonality with a certain vector v. The validity of the existence of v depends on the angles between bonds.

Thus, R. C. Haddon introduced two notions to study non-planar molecules and their electronic structure: the POAV1 for π-orthogonal average vector theory and then, the POAV2 theory aiming to solve some particular problems related to the POAV1 theory.

3.1.1 σ and π-orbitals

We consider a **trivalent molecule** as we have defined it in section 0.1 as a set of atoms A_i *(with* $i = 1, \ldots, n$*)* and 3 atoms B_i *(with* $i = 1, 2, 3$*)*, and $\theta_{i,j}$ the angle between the bonds AB_i and AB_j*(with i and j ∈ {1, 2, 3}).*
We set **σ-orbitals** as previously in section 1.2.1, h_i such as:

$$\boxed{h_i = c_i s + \lambda_i u_i} \tag{3.1}$$

with i = 1, 2, 3 and where u_i is the unitary vector along the internuclear axes between A and B_i in a trivalent case, $u_i \in \mathbb{R}^3$ and $\lambda_i > 0$. $AB_i = \lambda_i u_i$ with $\lambda_i = \|AB_i\|$ and $\|u_i\| = 1$.

Then, the **π-orbital** is given as:

$$\boxed{h_\pi = c_\pi s + \lambda_\pi u_\pi} \tag{3.2}$$

where u_π is the unitary vector.

The u_π **vector** is, when it exists, an **unitary vector** of $\mathbb{R}^2$ such that the family of orbitals $\{h_\pi, h_1, h_2, h_3\}$ is orthogonal, meaning that $\langle h_i, h_j \rangle = 0$ and $\langle h_i, h_\pi \rangle = 0$ *for i and* $j \in \{1, 2, 3\}$ and $\langle h_i, h_\pi \rangle = 0$ *for i = 1, 2, 3, where $\langle ., . \rangle$ is the classical scalar product on $\mathbb{R}^3$.*

We know that such a vector exists when the molecule possesses a C_{3v} symmetry and is given by the POAV1 vector. However, the existence of such a vector in the general case or its uniqueness is **not trivial**.

3.1.2 Existence, uniqueness of POAV2 and orthogonality conditions

Contrary to the POAV1, the **existence and uniqueness** of POAV2 does not follow pure geometric considerations. It shows by the fact that the 2 theories have very **different basis**.
In fact, the POAV1 vector satisfies only a partial orthogonality condition. Precisely, orthogonality is only required between the orbitals h_π and h_i *with i = 1, 2, 3.* We recover a complete orthogonality only in the sp^3 case.

The POAV2 vector exists and is unique up to **orientation**.
The orientation of the POAV2 vector can be fixed as : if the molecule determine an orientable surface then one can defined a coherent family of normal in each atom. We then, choose the orientation of a u_π vector in accordance with this orientation.

We then define the **POAV2** more precisely as:

The family of orbitals used $\{h_\pi, h_1, h_2, h_3\}$ is orthogonal to u_π the unitary vector of $\mathbb{R}^2$ when it exists. This means that $\langle h_i, h_j \rangle = 0$ and $\langle h_i, h_\pi \rangle = 0$ for *i and* $j \in \{1, 2, 3\}$.

The conditions on **orthogonality** are given as:

$$\boxed{H_{i,\pi} : c_i c_\pi + \lambda_i \lambda_\pi \cos(\theta_{i,\pi}) = 0} \tag{3.3}$$

with i = 1, 2, 3.

$$\boxed{H_{i,j} : c_i c_j + \lambda_i \lambda_j \cos(\theta_{i,j})} \tag{3.4}$$

with $i \neq j \in$ {1, 2, 3}.

By the relations given for the conditions of orthogonality, we can notice a strong relation between the angles of the bonds and the angles that u_π does with the bonds.

Proofs of these relations are in Appendix 2 section 11.

Then, we get the relations between the angles $\theta_{i,j}$ and *$i, j \in$ {1, 2, 3, π}* :

$$\boxed{\cos(\theta_{j,k})\cos(\theta_{i,\pi}) = \cos(\theta_{j,\pi})\cos(\theta_{i,k})} \tag{3.5}$$

with $i, j \in$ {1, 2, 3} and $i \neq k, j$.

We find this previous relation in the work of R. C. Haddon [6] (eq. 15) and the complete proofs are given in Appendix 2 section 12.

We note that if a molecule has a C_{3v} symmetry then the angles between the bonds and the u_π vector are equal. This is the only case where POAV1 and POAV2 are **identical**.

Proofs of this statement is given in Appendix 2 section 13.

The components of the vector $u_\pi = (x_\pi, y_\pi, z_\pi)$ (in an orthogonal reference system) are the solutions of a linear system whose coefficients will depend on the unit vectors u_i (x_i, y_i, z_i) along the bonds and the angles between bonds (*with i = 1, 2, 3).*

The POAV2 is a solution of the **linear system** $M.u_\pi = 0$, with u_π of coordinates (x_π, y_π, z_π):

$$M = \begin{pmatrix} x_3\cos\theta_{1,2} - x_2\cos\theta_{3,1} & y_3\cos\theta_{1,2} - y_2\cos\theta_{3,1} & z_3\cos\theta_{1,2} - z_2\cos\theta_{3,1} \\ x_1\cos\theta_{2,3} - x_3\cos\theta_{1,2} & y_1\cos\theta_{2,3} - y_3\cos\theta_{1,2} & z_1\cos\theta_{2,3} - z_3\cos\theta_{1,2} \\ x_2\cos\theta_{3,1} - x_1\cos\theta_{2,3} & y_2\cos\theta_{3,1} - y_1\cos\theta_{2,3} & z_2\cos\theta_{3,1} - z_1\cos\theta_{2,3} \end{pmatrix} \tag{3.6}$$

The kernel of the matrix is of dimension 1 in the case of a non-planar molecule meaning that the bonds u_1, u_2, u_3 define a 3-dimensional vector space. By consequence, there is $u_\pi \in ker(M)$ as $ker(M) = 1$ there exists a unitary vector u such that $ker(M) = \langle u \rangle$ unique up to orientation.

This system is given by R. C. Haddon in [6] (eq. 16) and the complete proofs are in Appendix 2 sections 14 and 15.

Concerning the orientation of POAV2, the molecule defines an **orientable** surface thus we can define a family of normals to each atom. The orientation of POAV2 will depend on the orientation of u_π.

3.1.3 Hybridization numbers

As mentioned in chapter 1, the **hybridization numbers** are related to the σ- and π-orbitals which were described at the beginning of this section (eq. 3.1 and 3.2).

We can determine the hybridization number n_i associated to the σ-orbitals. We find in the publication about POAV2 of R. C. Haddon [6] the connection with hybridization under the label n_1, n_2 and n_3. Moreover R. C. Haddon refers to sp^n hybridization as the p-part of the σ-orbitals and to $s^m p$ as the

s-part of the π-orbitals.

Here, we show that in the case of h_i the number of hybridization n.

The idea is precisely to measure in some sense the weight of the orbital p with respect to s in h_i seen as $s^{c_i^2}p^{\lambda_i^2}$ where c_i^2 and λ_i^2 are the weight of the orbitals s and p in the sense proposed by R. C. Haddon [6] putting all the weight on p as $sp^{\frac{\lambda_i^2}{c_i^2}} = sp^{n_i}$.

We have a hybridization of the sp_i^n-type as:

$$\boxed{n_i = \frac{\lambda_i^2}{c_i^2}} \tag{3.7}$$

Then, we note for n_i *with* $i = 1, 2, 3$:

$$\begin{aligned} n_1 &= -\frac{\cos\theta_{2,3}}{\cos\theta_{1,2}\cos\theta_{1,3}} \\ n_2 &= -\frac{\cos\theta_{3,1}}{\cos\theta_{2,3}\cos\theta_{2,1}} \\ n_3 &= -\frac{\cos\theta_{1,2}}{\cos\theta_{3,1}\cos\theta_{3,2}} \end{aligned} \tag{3.8}$$

These formula coincides with the one given by R. C. Haddon [6] (eq. 10).

We give the proofs of these formula in Appendix 2 section 16.

In the case of h_π, the hybridization is of type $s^m p$ and the number of hybridization associated is m as:

$$\boxed{m = \frac{c_\pi^2}{\lambda_\pi^2}} \tag{3.9}$$

Once again, this definition is different to the one given by R. C. Haddon [30] (eq. 3) but follows the same idea.

The number m can be understood as a measure of the s orbital with respect to the p content in the h_π orbital, i.e. considering h_π as $s^{c_\pi^2}p^{\lambda_\pi^2}$ and finally $s^{\frac{c_\pi^2}{\lambda_\pi^2}}p$ which corresponds to $s^m p$.

Imposing a **normalization** of the s content in the three hybrids, i.e. as:

$$\sum_{i=1}^{3} \frac{c_i^2}{c_i^2 + \lambda_i^2} + \frac{c_\pi^2}{c_\pi^2 + \lambda_\pi^2} = 1 \tag{3.10}$$

this is called by R. C. Haddon the sp^3 normalization in section 1.2.1.

We obtain then, the expression of the quantity W_σ for the π-hybridization number:

$$\boxed{W_\sigma = \sum_{i=1}^{3} \frac{1}{1 + n_i}} \tag{3.11}$$

Then, we set under the sp^3 normalization condition, the π-hybridization number is given following m such that:

$$m = \frac{1}{W_\sigma} - 1 \tag{3.12}$$

The proof is given in Appendix 2 section 17, the formula looks like the one given by R. C. Haddon in [30] (eq. 14).

3.2 Comparison of the POAV1 and POAV2

We know that the **POAV theory** allows to predict the maximum direction of the reactivity by the local study of the π-system. As we have presented, 2 approaches exist to determine the π-system: by quantum calculations and by the POAV theory.
The choice of the POAV method is obvious since it is simpler. The selection between POAV1 and POAV2 is relatively trivial since POAV2 involves more parameters and this is what we try to show in this section.

The work on **POAV2 theory** has not yet been explored sufficiently at this time of the thesis to provide complete conclusions. We present here **partial** results. This part of the work has been possible thanks to our collaboration with Dr Germain Salvato-Vallverdu who realized computations and python programs in order to carry out this section.

3.2.1 Relative variation of POAV2 versus POAV1

As we know the POAV theory provides the study of the **planarity** of molecules and here we are trying to know if the POAV2 is more adapted than the POAV1. It should be noted that the POAV1 theory is more widely used (as examples some recent works using POAV1 [37][38][39]).

The POAV2 theory takes into account additional parameters compared to POAV1. We therefore wanted to know if there was a real observable difference between the POAV1 and POAV2 theories. The first idea was to make a **comparison** between the 2 vectors.

Our first exploration was on the molecule *n°3* (from section 2.3.1) from the work of R. C. Haddon [6]:

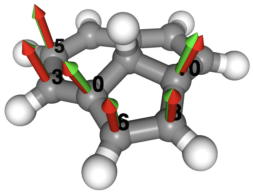

Figure 3.1: Representation of the molecule $C_{11}H_8$ with the POAV1 *(in green)* and POAV2 *(in red)* vectors

The molecule being symmetrical we have represented the vectors on only a part of the molecule to make it clearer.

On this figure we observe that the 2 vectors are very **close** in fact the maximum variation is of **4°**. The difference is observed on the atom *n°10* which is finally the most interesting since it is at the junction between 2 pentagons and according to our detailed study (section 2.3.1) it is where Pyr is the highest.

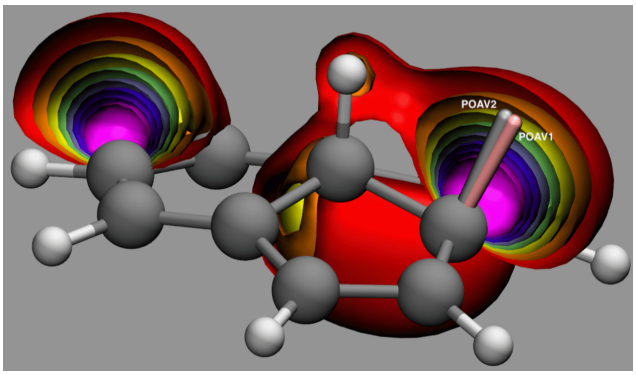

Figure 3.2: Representation of the molecule $C_{11}H_8$ with the POAV1 *(in pink)* and POAV2 *(in grey)* vectors and the HOMO

The figure represents the Highest Occupied Molecular Orbital (HOMO) of the molecule *n°3*. We observe the **isosurfaces** for values ranging from 0.02 *(in red)* to 0.09 *(in magenta)*. We note that around the atom *n°10* it is quite isotropic.
These images were carried out by DFT calculations and by extracting data from the generated *.cube* files. These calculations have been done with fine grids at a distance of 1 Å and with angles between 2 points of 1°.

The main difficulty consists in the size of the grid used on which the wave function is computed, it must be fine enough to make comparison possible and is not necessarily adaptable in Gaussview software.
On this illustration we note a difference between the 2 vectors but it remains **minor**. Based only on this example we cannot decide if the POAV2 is more appropriate than the POAV1.

3.2.2 Quality of POAV1 versus POAV2 to predict the direction of the π-system

To investigate the comparisons, we used a simpler system: ethylene.

The first step was to calculate by classical DFT quantum methods, the π-system of the molecule, what we call the "real" π-system.

By taking into account again the HOMO of the molecule *(with an isovalue of* $\pm 0.03 Å$*, in blue the negative part and in red the positive part)* and the **nodal surface** *(the white grid)* of the system, the following figure obtained with *VMD* software [40] illustrates the molecule in 3D:

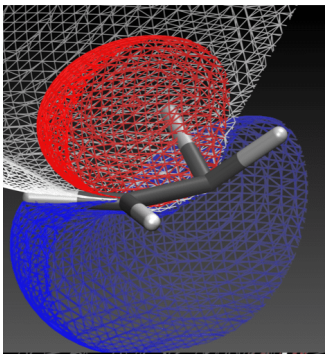

Figure 3.3: Representation of the HOMO and the nodal surface of the ethylene molecule in 3D

To determine and carry out each of the constructions (POAV1, POAV2, π-system), we investigated different methods by **linear interpolation**.
The first approach was to perform a linear regression to obtain a fitted line on the intersection between

the nodal surface and a chosen plane.
The other possibility was to look for the normal vector (the "real" π-system) to the mean plane fitted on the points of the nodal surface around a given atom.
The goal is to see if the normal vector to the nodal surface is in the plane defined by POAV1 and POAV2. As a result, it is essential to have a very fine grid to obtain precise results.
By linear interpolation and by the second approach, we made figures (figure 3.4) in the plane. The circle points represent the atoms: *black* for carbon and *grey* for hydrogen. In the left figure, we observe the HOMO in the plane in *red* and *blue*. The isosurface is represented by the curve in *grey* (at $\pm$ 0.03 Å). Finally, the *black* curve is the intersection between the plane and the nodal surface, which represents the plane defined by POAV1 and POAV2.

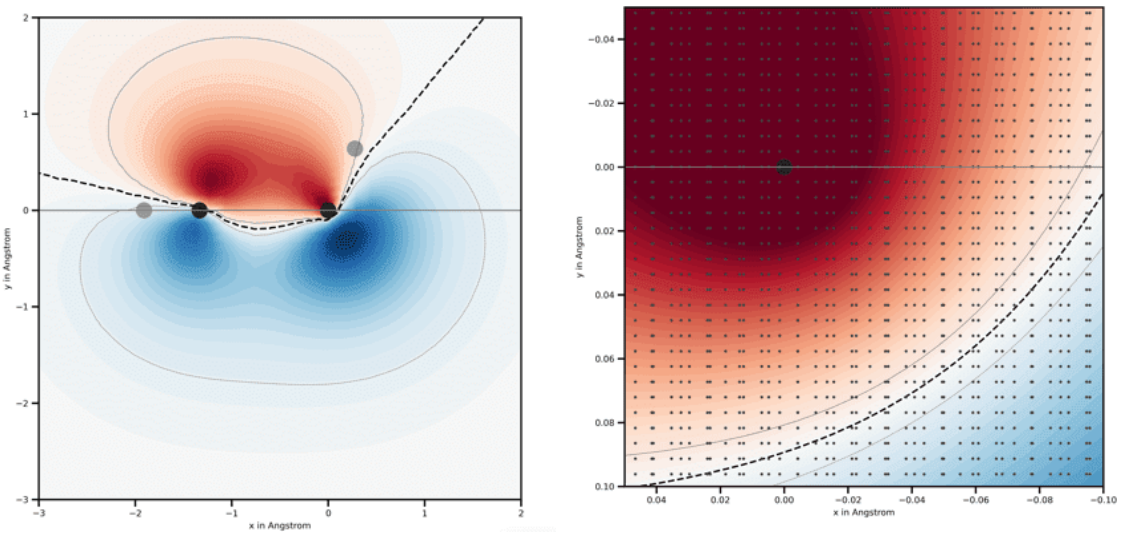

Figure 3.4: Representation of the linear interpolation for the ethylene molecule

Using a fine grid (in the right figure), i.e. a distance between 2 points of 0.005 Å, the grid is located around an atom of interest and the dotted curve represents the nodal surface.

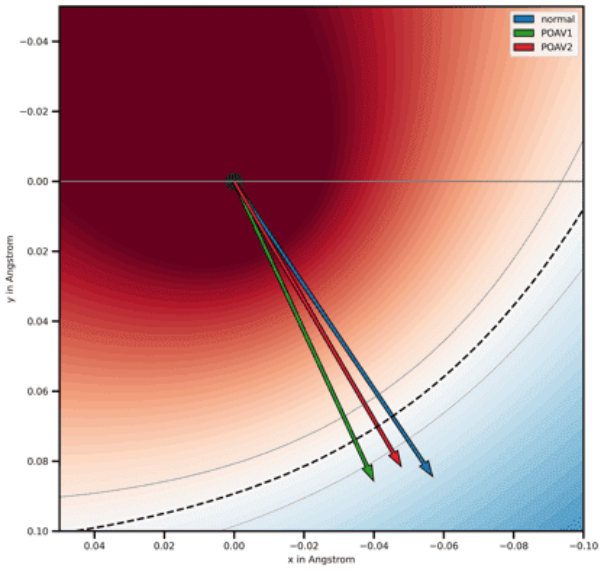

Figure 3.5: Representation by linear interpolation of POAV1 and POAV2 (*in blue the normal, in green the POAV1 and in red the POAV2)*

To clarify the construction of this last figure: we consider the closest point on the nodal surface, i.e. the orthogonal projection of the atom on the nodal curve. This means that we take the tangent to the curve and the vector we are interested in is the one that is normal to this tangent. Once this vector is determined, we relate it to the atom and compare its direction with POAV1 and POAV2.

We note in this case studied more precisely, that there is a difference between POAV1 and POAV2. This difference has not been quantified but merits to be quantified. We notice that the POAV2 is closer to the "real" π-system than the POAV1. Thus, by comparison the **POAV2** seems **more accurate** for the considered atom.

3.3 To reach further...

By the tools presented since the beginning of this manuscript, we can consider using them to **characterize** the geometries and topologies of different kind of systems as **Covalent Organic Frameworks** (COFs) and **Metal-organic frameworks** (MOFs) for their **reactivity**. This is in line with a strategy of decarbonization and energy transition. The systems could be integrated into hydrogen or methane storage or CO_2 capture processes. The purpose of these processes is not the same. Hydrogen and methane are intended to be stored for use primarily as an energy source. CO_2 capture is aimed at reducing anthropogenic emissions directly at the source.

We will make some reminders about MOFs and COFs. These complexes are crystalline solids said to be porous. Their structure makes them promising complexes for gas storage by physisorption. These materials are listed in two main databases: from Cambridge University [41, 42] and Northwestern University [43], both listing about 255,000 structures. These materials with high sorption properties can be used in surface chemistry and their reactivity can be controlled generating new electronic and chemical properties. The high number of existing structures, leads to a problem of identification of structures for a specified application. Therefore, with our tools we could propose a **topological** and **geometrical** identification according to a given property.

We could provide a selection process for COFs and MOFs based on tools whose scientific development is clear in order to organize the COFs and MOFs bases in the best possible way.
The steps that could be implemented would be based: 1 - on the development of a tool analyzing the reactivity properties of the COFs and MOFs of all the databases, 2 - then, the extraction of specific indicators such as reactivity and 3 - then, validate these tools by experimentation.

Steps 1 and 2 can be completed by our POAV tools to connect the geometrical and topological structure of the molecules with the electronic and chemical properties. In fact, POAV vectors intrinsically include all the quantum and orbital information that allow to study the chemical reactivity of the atoms of the material. The POAV vectors are computable from the local geometrical structure without using quantum calculations. The simplicity of use leads to a pretty large scale database, as we have done previously for our first article on the fullerene database [4]. In a simple way, it allows to detect on the materials the most reactive sites and to cartography them (as we have already achieved). Thus, we suggest the use of POAVs to cartography the structures of COFs and MOFs.
Following these cartographies, it will be necessary to obtain different indicators which will reflect the reactivity and selectivity of COFs and MOFs for a given target. Statistical by nature, these indicators will show the properties of the POAVs, in particular for the density of the highly reactive sites and for the average reactivity of the structure.
Finally, the last step, step 3, will validate and complete the theoretical data.

3.4 Conclusion

In this chapter, we take up the **POAV1** theory with the **POAV2** which completes in a **physical way** the POAV1 which is more **local**.
We have proven as precisely as possible mathematically the work of R. C. Haddon on the POAV2, on the basis of σ and π-orbitals but also on the conditions of orthogonality and based on the tools previously developed as the hybridization numbers.
The comparison of the work initiated here between the 2 tools shows from a more practical point of view and from the molecular point of view that the consequences are **not significant** between POAV1 and POAV2. In fact for our example, there is only 4° difference between the 2 vectors, it is then, complicated to conclude only on this observation.
However, when we compare the difference between POAV1 and the π-system and between POAV2 and the π-system it is **more significant**. We can clearly see that POAV2 is closer to the π-system. From this point of view the POAV2 theory is more interesting since it is more representative of the system. This is in accordance with the general observations related to molecules with large bond angles, POAV2 is quite different from POAV1 but this is logical since the bond parameters are taken into account.

The observations from these comparisons are **clearly not conclusive** and the development of the proofs related to these tools having required a long work it seems interesting to focus on it in the future.

Conclusion of the part II

This part II concerns the **POAV theories**. It gives a complete study of the tools and methods available to the chemistry community to understand and determine the information of molecular systems related to **deformation**, **hybridization** and **reactivity**.

Chapter 1 and 2 are complementary since the notions and tools (pyramidalization angle, POAV1, hybridizations...) are used in the wide range of examples in chapter 2 and are clearly studied, generalized and proven. Chapter 2 gives a concrete idea of the use of these tools from a computational and illustrative point of view with meaningful **cartographies** on a large panel of molecules. We show that the evolution of the transformations of the bonds (formation, weakening...) can be followed in simple ways and thus allow the understanding of the reactivity.

Chapter 3 is an **extension** of POAV1 theory with the introduction of POAV2 theory which seems theoretically more complete but does not provide clearly any practical benefit for the moment.
This remains to be investigated since the study of this last chapter is not completed.

In a general way, this part answers the initial issues generated by R. C. Haddon's work about planarity and reactivity, and it is important to mention that all the methods and tools presented in this manuscript are useful and easily implementable by chemists.

Part III

Aromaticity, helical states and applications

In this third part, we are interested both in the aromaticity criteria, and in the curiosity of helical electronic states.

The aromaticity criteria are studied :

- *in a general way by the Hückel rules,*
- *by the 2 visions of Hückel and Möbius in the case of annulenes.*

We review these criteria from a mathematical point of view with Hückel and Möbius by distinguishing the cases of linear molecules and cyclic molecules.

Then, we go beyond these aromaticity criteria with the study of Möbius systems according to Roald Hoffmann and show the criteria and the existence of helicoidal states.

Finally, applications and visualizations of helical states are presented.

The main results of this part come from the work of R. Hoffmann's research team [9] and from our preprint work [44].

Introduction

This third part gives the opportunity to go through different aspects, both **theoretical** and **applicative**. The study of concepts related to molecular deformation and tools for understanding the reactivity are associated with the aromaticity topics.

Chapter 4 leads us back to the theory with the **aromaticity criteria** (of cyclic molecules among others) according to the **rules** stated by **Hückel**. These famous Hückel's rules are widely used in chemistry and in particular by organic chemists.
We have relied on Hückel's rules to highlight the comparison between the so-called **Hückel and Möbius model systems**. First, we prove the geometrical construction of these systems, and then their **optimal** and **equivalent** structures. To improve the comprehension and to put in evidence more details, we needed to review some mathematical tools. In particular, concerning the **Hückel matrices** according to different cases. In fact, we have chosen to work according to different situations, namely in **cyclic** situations (to get closer to an annulenic system) or in **linear** situations (as cumulenic systems). After these different steps, and a brief review of the Möbius molecules, we established the **energy equations** according to the two model systems. To complete the study, we took into account both in the Möbius and Hückel case the **number of electrons** of the system: even or odd.
In the Möbius systems, we observe a **rotation** of the orbitals along the cycle, and by consequence different **angle distributions**. We have therefore decided to study these distributions and the influence of the C_2 symmetry on them.
To be more precise and applicative, we conclude with some simple examples to prove the calculation of the distribution of angles.

Chapter 5, presents how Möbius systems have found interest in recent years from research teams, in particular the Nobel prize laureate Roald Hoffmann.
It is due to the attention given to the work of R. Hoffmann that we are particularly interested in the **linear systems** called **cumulenes** and the curiosities that they provide with the **helical molecular orbitals**. We then details associated to the concepts concerning the **helical states**. We prove mathematically in a precise way the angle distributions in the general case and in the cumulene cases. The rest of the chapter presents the **criteria of existence of helices** from a mathematical and then by a chemical way.

Then, the last chapter provides a link with the chapter 5 by different **applications**. The chapter presents the applications and visualizations that we carried out on cumulenes and on more complex molecules. All these investigations are very complete since we have performed DFT and multideterminental CASSCF(CASPT2 single points) calculations both in fundamental and excited states, to be confident that the helices observed by DFT were not dependent on the method used.

Chapter 4

Criteria of aromaticity - theory

In this chapter we discuss :

- *the criteria of aromaticity,*
- *reminders of mathematical tools for Hückel matrices,*
- *and, the determination of energy equations according to the Hückel and Möbius systems.*

For the criteria of aromaticity we expose:

- *Hückel's rules,*
- *the 2 visions of Hückel and Möbius concerning the annulenic systems.*

Concerning the mathematical tools necessary to understand the Hückel matrices we review:

- *Hückel matrices for cyclic ($S_N^1(\phi)$) and linear ($L_N(\phi)$) molecules.*

Finally, for the determination of the energy equations of Möbius and Hückel systems, we expose:

- *reminders about Möbius molecules,*
- *results concerning the cases of cyclic molecules with zero distribution ($S_N^1(0)$) and with angle distribution ($S_N^1(\phi)$),*
- *the energetic comparison of the 2 cases and their stability,*
- *the study of the molecule with angle distribution following a C_2 symmetry invariance,*
- *the results for linear molecules with null distribution ($L_N(0)$) and angle distribution ($L_N(\phi)$),*
- *the study of optimal distribution for cyclic molecules ($S_N^1(\phi)$),*
- *the study of the distribution of linear molecules ($L_N(\phi)$) equivalent to cyclic molecules with angle distribution ($S_N^1(\phi)$),*
- *the asymptotic study of the angle distribution on a linear chain.*

All the results of this chapter are based on R. Hoffmann's work [9] and from our preprint dedicated to the study of the optimal structures and equivalences of some molecules [45]. This chapter has required a lot of work and time.

4.1 Hückel aromaticity

We have presented the Hückel method in part I, but here we are interested in another aspect: the **aromaticity** according to Hückel [46, 47].

Different approaches to Hückel's rules exist both on criteria based on the **number of electrons**, but also based on the **geometrical construction** related to the distribution of orbitals within the system.

4.1.1 Hückel rules

From the point of view of organic chemists, **Hückel's rules** are well-known. It is in 1931 that Erich Hückel proposes the theory of determination of the **aromatic compounds** in the case of plane cyclic molecules (also called annulenes). These **aromaticity criteria** are based on several points: the molecule must be **cyclic**, must be **plane**, must be **conjugated** and must **satisfy** the relation **4N+2**.

For more details, in a simple way, the conjugation is the alternation of single (σ) and double bonds (π) and the relation is equal to the number of π-electrons of the molecule.

The aromaticity reflects the **stability** and consequently simplifies certain reactions such as substitutions.
In the fundamental state for a cyclic molecule, if the electronic system has $4N + 2$ electrons then, the system is said to be **aromatic** and **stable**. On the contrary, if the electronic system has $4N$ electrons, the system is called **anti-aromatic**.

The $4N + 2$ rule applies when there is an **even** number of electrons. These systems are then called **Hückel systems**.
To illustrate this rule, we can take the simple example of **benzene** which is the well-known conjugated cyclic molecule. Containing 6 π-electrons, there are 2 electrons on the first lowest energy orbital and then the remaining 4 electrons are distributed on the following orbitals, as shown in the following diagram:

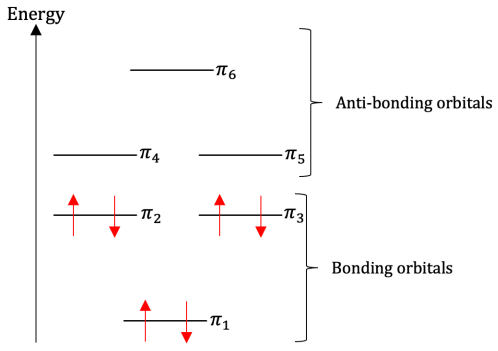

Figure 4.1: Simplified energetic diagram of the benzene

In this simple example, $4N + 2 = 6$ then, $N = 1$, we obtain a positive integer, the rule is respected.
The Hückel rule is used to determine the aromaticity thus, it only considers the π-electrons, i.e. the electrons involved in the π-bonds. The atoms implied are therefore sp^2-hybridized.
For these cyclic systems, a simple mnemonic circle method proposed by Frost and Musulin [48] in 1953 allows access to the energies of the molecular orbitals.
In 1966, on the basis of the method of Frost and Musulin [48], Zimmerman [8] proposes according to the $4N + 2$ rule of Hückel, that the systems **satisfying** the rule will be called of **Hückel** but that those satisfying $4N$ electrons will be called systems of **Möbius** [8].

4.1.2 Two visions of annulenes : Hückel and Möbius

Geometrical construction

As we have already mentioned in part I with a **geometrical** point of view, we can study different cases of **arrangement** of atoms.

The atoms of a molecule can be disposed following two possibilities:

- a **line** segment (L_N) which corresponds to a **linear chain** (as allene molecule)
- a **circle** (S^1_N) which corresponds to **cyclic** molecule (as annulene molecule)

We are interested in **two distributions** depending on the arrangement of the atoms. These distributions have a **fundamental role**.

A **distribution** is defined along a molecule γ constituted by N atoms noted s (a preliminary definition is given in the reminder 0.2.4). The distribution is given in $\mathbb{R}^3$ as a family of vectors v $\{v_1,...,v_N\}$ in the planes $\{\mathcal{P}_{s_1}, ..., \mathcal{P}_{s_N}\}$.

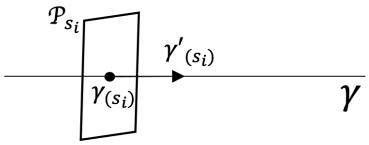

Figure 4.2: Schematic representation of the distribution along a molecule γ

In fact if we have: $\gamma : s \in$ [a,b] $\longrightarrow \gamma(s) \in \mathbb{R}^3$ a regular curve of $\mathbb{R}^3$ on which are uniformly disposed N atoms. We note $s_i \in$ [a,b] the position $\gamma(s_i)$ of the atom C_i *(with $i = 1, ..., N$)*.
We assume that $s_0 = a$ and $s_N = b$:

$$s_i = a + (i-1)\frac{b-a}{N-1} \tag{4.1}$$

Set a family of vectors u_i in $\gamma(s_i)$ contained in the plane normal to the tangent vector $\gamma'(s_i)$ to the γ curve in s_i. These vectors will represent in our case, particular orbitals in each atom. For each $i = 1, ..., N$, let us note D_i the segment described by:

$$t \in [-1, 1] \longrightarrow \gamma(s_i) + t\frac{u_i}{\| u_i \|} \in \mathbb{R}^3 \tag{4.2}$$

We note that $D_i(0) = \gamma(s_i)$ and that the line segment is symmetrical about this point.

A **homotopy** is carried out between each D_i and D_{i+1} *(with $i = 1, ..., N-1$)* in the following way:

we denote $D(s)$ the continuous family of segments defined for $s \in [a, b]$ by:

$$D(s) = \left\{ t \in [-1, 1] \longrightarrow D(s)(t) = \gamma(s) + t\left[\frac{s_{i+1} - s}{s_{i+1} - s_i}\frac{u_i}{\| u_i \|} + \frac{s - s_i}{s_{i+1} - s_i}\frac{u_{i+1}}{\| u_{i+1} \|}\right] \in \mathbb{R}^3 \right\} \tag{4.3}$$

with $s \in [s_i, s_{i+1}]$.

Note that $D(s_i) = D_i$ for $i = 1, ..., N$. We thus generate a connected parameter surface of $\mathbb{R}^3$ associated with the data of γ and the family of vectors $(u_1, ..., u_N)$ noted $\gamma_N(u_1, ..., u_N)$ such as:

$$\gamma_N(u_1, ..., u_N) = s \in [a, b] \longrightarrow D(s)(t) \tag{4.4}$$

In the situation where the γ curve is **closed**, i.e. $\gamma(a) = \gamma(b)$, the surface described is not necessarily continuous. To be continuous, it is necessary to have $u_N = \pm u_1$ so that $D(a) = D(b)$ and thus, that there is recollection of the segments, when the curve is **crossed**.

In the case where the vectors u_i are associated with a given $\phi = (\phi_1, ..., \phi_N)$ distribution such as:

$$\boxed{u_{i+1} = e^{j\phi_i} u_i} \tag{4.5}$$

with j^2 *= -1, i = 1,..., N.*

In the case where $\phi = 0$ it is enough to take $u_i = u_1$ for $i = 2, ..., N$. We obtain then in the case where γ is the segment $\gamma(s) = A + sB$ *with* A *and* $B \in \mathbb{R}^3$, $B \neq A$, $s \in [0, 1]$ the parameter surface generated by the transfer of the segment :

$$D(s) = \left\{ t \in [-1, 1] \longrightarrow D(s)(t) = \gamma(s) + t\frac{u_1}{\| u_1 \|} \in \mathbb{R}^3 \right\} \tag{4.6}$$

along the γ segment which represents a strip.

If we assume that: L_N is a linear chain with N atoms and S_N^1 is a cyclic molecule with N uniformly distributed atoms.

We consider the following geometries:

- the **zero distribution**, noted $\phi = (0, ..., 0)$ or $\phi = 0$ is represented by a **ribbon** or a strip which is called **"Hückel"**-type distribution.
- the **"Möbius"**-type distribution $\phi = (\frac{\pi}{N}, ..., \frac{\pi}{N})$ which is a Möbius ribbon i.e. a **twisted strip** of angle π [47].

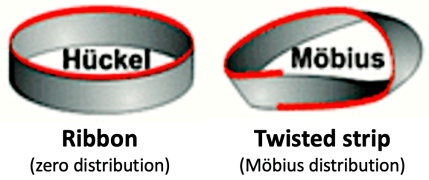

Figure 4.3: Illustration of the 2 distributions: Hückel and Möbius-types [49]

The terminology ("Hückel" or "Möbius") comes from the geometric construction.

In the case of a **Möbius distribution** we have:

$$\boxed{u_{i+1} = e^{j\frac{\pi}{N}} u_i} \tag{4.7}$$

with j^2 *= -1 and i = 1,..., N.*

The $D(s)$ segment is given *for* $s \in [0, 1]$ by :

$$D(s) = \left\{ t \in [-1, 1] \longrightarrow D(s)(t) = \gamma(s) + te^{js\frac{\pi}{N}} \frac{u_1}{\| u_1 \|} \in \mathbb{R}^3 \right\} \tag{4.8}$$

which represents a **180° twisted strip**.

This same construction in the case where γ is a circle gives respectively a ribbon and the famous **Möbius ribbon** which is a continuous surface since in this case $u_N = -u_1$.

Optimal structures

For a given $S_N^1(\phi)$ structure, several questions arise: intuitively, we expect the zero distribution to be the most energetically stable, i.e. it carries out the minimum of the molecular energy $L_N(\phi)$ or $S_N^1(\phi)$ over all possible distributions. However, it can be proven that for some values of N, this **minimum** is realized by a **Möbius-type distribution**. Moreover, the calculations comparing these two particular distributions do not answer the question.

By definition, for a given S and N, we characterize the set of ϕ distributions such as $S_N(\phi)$ satisfies the **minimum energy**. In this manuscript we study the problem in all generality for $S = S^1$ and $S = L$.

We specify the previous problem by writing explicitly the optimization problem for a given N and ϕ a given distribution. We note $E(S_N^1(\phi))$ the energy of the $S_N^1(\phi)$ molecule.

We notice E_{min} the quantity:

$$E_{min} = min_{\phi} E(S_N^1(\phi)) \tag{4.9}$$

In fact, we are looking for the set of distributions such as : $E(S_N^1(\phi)) = E_{min}$.

The **strategy** to solve the question, is to determine the structure of the orbitals for a molecule with N atoms on the circle with a given distribution ϕ. The approximation of the MOs are obtained using the Hückel method. The energy of the molecule is then calculated on the set of distributions. In a simpler way one can **compare** for a given geometry and type of atom, the **energy stability** for two fixed distributions.
We can easily **compare** for a given geometry and type of atom, the **geometrical stability** for two fixed distributions. We explicitly note a comparison between $S_N^1(0)$ and $S_N^1(\phi_M)$ in the case of carbon.

We specify here ϕ_M, it describes the Möbius-type distribution.

Equivalent structures

From a point of view of **equivalent representations**, we can represent the geometry of the π-orbitals of the molecules of the allene type (called cumulenes) either by a linear chain or a circle.

Note that a cumulene, which will be mainly discussed in the continuation of the manuscript, are carbon molecules with only double bonds.

For a given cumulene, how to describe precisely the equivalent linear and circular representations? In particular, how to specify the distribution associated with each of the representations?

To specify the previous question it is necessary to take in consideration the **symmetries** of the molecule. The problem of **equivalent representations** is expressed by the research of a **geometry adapted** to a minor symmetry than the initial molecule.
The computations to obtain the structure of the orbitals in the case of the circle can be used to determine the distribution of a linear chain whose structure of the orbitals is imposed by the decomposition obtained for the configuration of the circle in a given distribution ϕ. We then obtain for any ϕ on the circle, a distribution $L_N(\phi)$ on a chain.

4.2 Reviews of mathematical tools with Hückel matrices

4.2.1 Hückel matrices for molecules as $S_N^1(\phi)$, $L_N(\phi)$

To better understand the systems $S_N^1(\phi)$ and $L_N(\phi)$, in the following, we express the **Hückel matrices** of the 2 situations.

Molecules $S_N^1(\phi)$

As presented in part I, the atoms A_i *(with $i = 1, ..., N$)* are positioned on a circle and to simplify, we have the notations:

$$A_{N-1} = A_N \tag{4.10}$$

$$A_{N+1} = A_1 \tag{4.11}$$

To simplify the construction of the **Hückel matrix**, for a given atom, only **two neighboring atoms** on the curve have a significant overlap, thus, a given atom A_i is bonded to the atom A_{i-1} and A_{i+1} *for i = 1,..., N.*

We obtain a **symmetrical matrix** $\mathbf{M}\left[S_N^1(\phi)\right](E)$ as :

$$\begin{pmatrix} \alpha - E & \cos(\phi_1)\beta & 0 & \dots & \dots & 0 & \cos(\phi_N)\beta \\ \cos(\phi_1)\beta & \alpha - E & \cos(\phi_2)\beta & 0 & \dots & \dots & 0 \\ 0 & \cos(\phi_2)\beta & \alpha - E & \cos(\phi_3)\beta & 0 & \dots & 0 \\ \vdots & & & & & & \\ 0 & \dots & \dots & 0 & \cos(\phi_{N-2})\beta & \alpha - E & \cos(\phi_{N-1})\beta \\ \cos(\phi_N)\beta & 0 & \dots & \dots & 0 & \cos(\phi_{N-1})\beta & \alpha - E \end{pmatrix} \tag{4.12}$$

By posing $x = \frac{\alpha - E}{\beta}$, there is the **reduced matrix** $\mathbf{U}\left[S_N^1(\phi)\right](x)$ defined by :

$$\begin{pmatrix} x & \cos(\phi_1) & 0 & \dots & \dots & 0 & \cos(\phi_N) \\ \cos(\phi_1) & x & \cos(\phi_2) & 0 & \dots & \dots & 0 \\ 0 & \cos(\phi_2) & x & \cos(\phi_3) & 0 & \dots & 0 \\ \vdots & & & & & & \\ 0 & \dots & \dots & 0 & \cos(\phi_{N-2}) & x & \cos(\phi_{N-1}) \\ \cos(\phi_N) & 0 & \dots & \dots & 0 & \cos(\phi_{N-1}) & x \end{pmatrix} \tag{4.13}$$

The two matrices can be linked as:

$$\mathbf{M}\left[S_N^1(\phi)\right](E) = \beta \mathbf{U}\left[S_N^1(\phi)\right](x) \tag{4.14}$$

To simplify, we have the family of so-called **Hückel matrices** of type S^1 and parameter a ($a = (a_1, ..., a_N) \in \mathbb{R}^N$):

$$\mathbf{U_a} = \begin{pmatrix} x & a_1 & 0 & \dots & \dots & 0 & a_N \\ a_1 & x & a_2 & 0 & \dots & \dots & 0 \\ 0 & a_2 & x & a_3 & 0 & \dots & 0 \\ \vdots & & & & & & \\ 0 & \dots & \dots & 0 & a_{N-2} & x & a_{N-1} \\ a_N & 0 & \dots & \dots & 0 & a_{N-1} & x \end{pmatrix} \tag{4.15}$$

The matrix $\mathbf{U_a}$ is the **matrix associated** with the simple **Hückel matrix** of type S^1 where $a_1 = ... = a_N = a$ with the parameter a $\in \mathbb{R}$.

Molecules $L_N(\phi)$

In this configuration, the atoms are arranged on a **line** and the following simplifying hypothesis is admitted: for a given atom, only two neighboring atoms on the curve have a significant overlap, i.e. a given atom A_i is bounded to atom A_{i-1} and A_{i+1} for $i = 2, ..., N-1$. The atom A_1 is bounded to A_2 and the atom A_N to A_{N-1}.

By this hypothesis, the **Hückel matrix** $\mathbf{M}\left[L_N(\phi)\right](E)$ is purely tridiagonal:

$$\begin{pmatrix} \alpha - E & \cos(\phi_1)\beta & 0 & \dots & \dots & 0 & 0 \\ \cos(\phi_1)\beta & \alpha - E & \cos(\phi_2)\beta & 0 & \dots & \dots & 0 \\ 0 & \cos(\phi_2)\beta & \alpha - E & \cos(\phi_3)\beta & 0 & \dots & 0 \\ \vdots & & & & & & \\ 0 & \dots & \dots & 0 & \cos(\phi_{N-2})\beta & \alpha - E & \cos(\phi_{N-1})\beta \\ 0 & 0 & \dots & \dots & 0 & \cos(\phi_{N-1})\beta & \alpha - E \end{pmatrix} \tag{4.16}$$

The matrix reduction leads to $\mathbf{U}\left[S_N^1(\phi)\right](x)$:

$$\begin{pmatrix} x & \cos(\phi_1) & 0 & \dots & \dots & 0 & 0 \\ \cos(\phi_1) & x & \cos(\phi_2) & 0 & \dots & \dots & 0 \\ 0 & \cos(\phi_2) & x & \cos(\phi_3) & 0 & \dots & 0 \\ \vdots & & & & & & \\ 0 & \dots & \dots & 0 & \cos(\phi_{N-2})\beta & x & \cos(\phi_{N-1}) \\ 0 & 0 & \dots & \dots & 0 & \cos(\phi_{N-1}) & x \end{pmatrix} \tag{4.17}$$

As in the previous case $S_N^1(\phi)$, we have the **Hückel matrix** of type L^1, of parameter a *(with a = (a_1,..., a_{N-1}))* and of dimension $N \times N$ such that :

$$M_{\mathbf{a}} = \begin{pmatrix} 0 & a_1 & 0 & \dots & \dots & 0 & 0 \\ a_1 & 0 & a_2 & 0 & \dots & \dots & 0 \\ 0 & a_2 & 0 & a & 0 & \dots & 0 \\ \vdots & & & & & & \\ 0 & \dots & \dots & 0 & a_{N-2} & 0 & a_{N-1} \\ 0 & 0 & \dots & \dots & 0 & a_{N-1} & 0 \end{pmatrix} \tag{4.18}$$

Here also, we have $a_1 = ... = a_{N-1}$, the Hückel matrix L^1 is called simple.

4.3 Determination of energy equations Möbius - Hückel

4.3.1 Reviews of Möbius molecules

The so-called **Möbius molecules** have their origins in the first works published by A. F. Möbius and J. B. Listing about projective planes and one-sided surfaces in 1858 [50, 51]. Probable conflicts of publications between the 2 researchers are at the origin of the name of "Möbius" ribbon and not "Listing".

Most of the mathematical objects are two-dimensional and we are familiar with, i.e. they have an inside and an outside surface. But the Möbius ribbon is an exception since it is a **closed strip** with an **odd number of unilateral 180° twists** and **an even number of bilateral 180° twists**. This means that the Möbius ribbon is a **non-orientable** system [47].

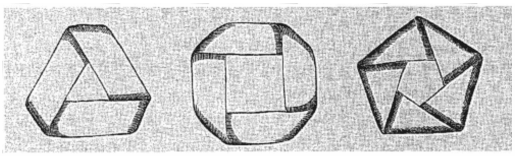

Figure 4.4: Illustrative representation of the Möbius ribbons [47]

Note that the works of Möbius and Listing have inspired many artists in terms of non-orientable surfaces.

From a chemical point of view, to define a **twisted plane** it is necessary to have a π-system. In this type of twisted π-system, the unilateral surface is defined along the nodal plane of the π-system. This type of molecule are **Möbius annulenes**. We note that the so-called **Hückel annulenes** have p-orbitals which are associated in order to create interactions. In the case of Möbius there will be at least one sign inversion of the system which will result in a 180° twist.

As a reminder, annulenes are conjugated cyclic molecules. The simplest example is the benzene which is aromatic or the cyclobutadiene which is anti-aromatic. These 2 examples are perfectly plane.

For an ideal **Möbius ribbon**, the twist is uniformly distributed, therefore, the inversion point is not precisely defined. If we assimilate the Möbius ribbon to an origami type model, the sign inversion will be observed in the most twisted region. For an example of an origami Möbius annulene, the system is not planar and shows the shape of a 8 along a C_2 axis of symmetry. Being non-planar, the π and σ-systems are not orthogonal.
Möbius π-systems have been particularly studied by Heilbronner in 1964 [7] who highlights the aromaticity according to Hückel which we have already discussed in this manuscript (section 4.1.1).

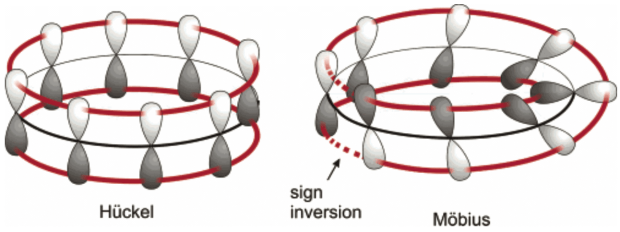

Figure 4.5: Scheme representing a Hückel and Möbius type annulene [47]

As shown in the Herges review [47] and in figure 4.5, for the Hückel case, the π-plane has two sides, thus, there are two π clouds on either side of the annulene. In the Möbius case, there is only one π-system. The presence of the torsion generates a sign inversion so a rotation of the p-orbitals.

Note that Heilbronner gives a rather good precision to the stability of the large Möbius annulenes [7].

Finally, the properties of **aromaticity** and **anti-aromaticity** are largely proven by the work of Zimmerman and Frost-Musilin that we have mentioned previously (section 4.1.1).

There are **different** types of Möbius ribbons: we can mention the cyclacenes (purely theoretical, the synthesis being complicated). They are composed exclusively of benzene units which makes them highly unstable but remain very interesting by their electronic structures.

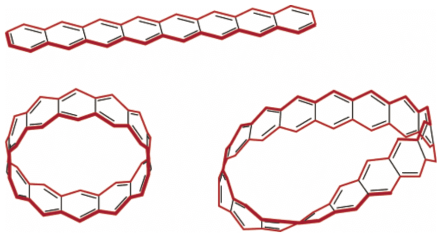

Figure 4.6: Representation of a polyacene, a cyclacene and a Möbius cyclacene [47]

Simpler than cyclacenes, polycyclic aromatic hydrocarbons are more interesting. But they present more isomers and the ways to introduce the torsions are numerous. This type of system is therefore more complex. For example, the smallest system is the Möbius coronene.

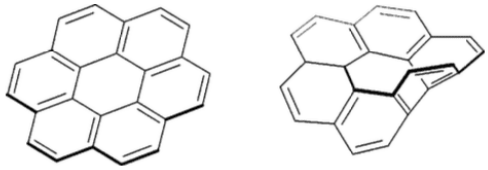

Figure 4.7: Representation of a coronene and a Möbius coronene [47]

Concerning the synthesis, it was necessary to wait 40 years between their discovery in 1964 and the first attempts of synthesis [52, 53]. The main difficulty consists in the synthesis agents which are annulenes which are stable in their non-twisted conformations. The stabilization of Möbius annulenes is based on the rigidification of the molecular frame. The synthesized systems have large π-systems and some have C_2 symmetries.
Möbius annulenes have two types of aromaticity: "normal" and "in the plane". Respectively, either the atoms are sp^2-hybridized in a planar trigonal configuration, or sp^2-hybridized atoms pyramidal with a certain sp^3 character.

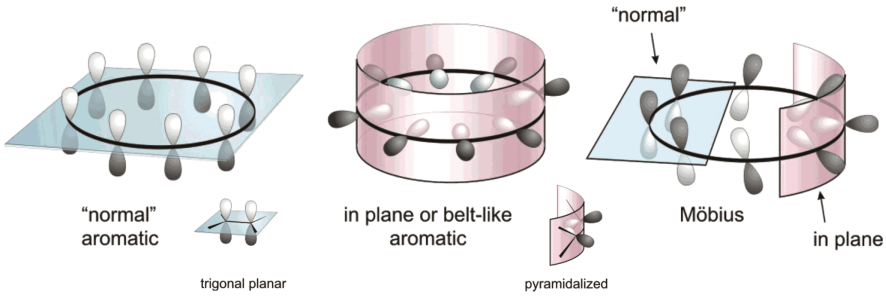

Figure 4.8: Representation of Möbius annulene [47]

Note that we have to distinguish the ***topology*** *and the* ***aromaticity criteria****.*
From a ***topological*** *point of view: we differentiate the so-called "normal" case, also called the Hückel case in the literature and here the ribbon case, from the Möbius case.*
In terms of ***aromaticity****, whether it is the ribbon or the Möbius system, it is a Hückel system, i.e. only one p-orbital participates per carbon atom. Indeed it is according to the closure of the ring that will give the meaning to the aromaticity (i.e. the value of the sign of the off-diagonal elements of the Hückel matrix) [9].*

To finish, there are other topologies, as Möbius annulenes with double twists. Different examples exist: heterooctaphyrins or the theoretically predicted [14]-annulene.

4.3.2 Cases of the molecules $S_N^1(0)$ and $S_N^1(\phi_M)$

We have determined the **electronic structures** of the molecules $S_N^1(0)$ and $S_N^1(\phi_M)$ for all N. However, first, we were interested in the computation of the **energies** according to the configurations.

Trigonometry reminder

First of all, we remind some useful information of trigonometries, by detailed proofs.

For all $\theta \in \mathbb{R}$ and m $\in \mathbb{N}$:

$$\boxed{\sum_{k=0}^{m} \sin(k\theta) = \sin\left(m\frac{\theta}{2}\right) \frac{\sin\left((m+1)\frac{\theta}{2}\right)}{\sin\left(\frac{\theta}{2}\right)}} \tag{4.19}$$

Here is the proof which seems to be the fastest:

$$\sum_{k=0}^{m} \sin(k\theta) = Im\left[\sum_{k=0}^{m} e^{jk\theta}\right] \tag{4.20}$$

where j^2 = -1 and Im[z] refers to the imaginary part of a complex number $z \in \mathbb{C}$.

We then study, the complex geometric serie $\sum_{k=0}^{m}(e^{j\theta})^k$, the classical result gives :

$$\sum_{k=0}^{m} z^k = \frac{1-z^{m+1}}{1-z} \tag{4.21}$$

For this proof we get:

$$\sum_{k=0}^{m}(e^{j\theta})^k = \frac{1-e^{j\theta(m+1)}}{1-e^{j\theta}} \tag{4.22}$$

It is possible to simplify the expression by using the arc moieties such as :

$$1-e^{j\theta} = e^{j\frac{\theta}{2}}(e^{-j\frac{\theta}{2}} - e^{j\frac{\theta}{2}}) = e^{j\frac{\theta}{2}} 2j \sin\left(\frac{\theta}{2}\right) \tag{4.23}$$

Then,

$$\frac{1-e^{j\theta(m+1)}}{1-e^{j\theta}} = \frac{e^{j(m+1)\frac{\theta}{2}}}{e^{j\frac{\theta}{2}}} \frac{\sin((m+1)\frac{\theta}{2})}{\sin\left(\frac{\theta}{2}\right)} \tag{4.24}$$

as,

$$\frac{e^{j(m+1)\frac{\theta}{2}}}{e^{j\frac{\theta}{2}}} = e^{jm\frac{\theta}{2}} \tag{4.25}$$

we get:

$$\sum_{k=0}^{m}(e^{j\theta})^k = e^{jm\frac{\theta}{2}} \frac{\sin((m+1)\frac{\theta}{2})}{\sin\left(\frac{\theta}{2}\right)} \tag{4.26}$$

By considering the imaginary part of this expression, we obtain the expected equality:

$$\sum_{k=0}^{m} \sin(k\theta) = \sin\left(m\frac{\theta}{2}\right) \frac{\sin((m+1)\frac{\theta}{2})}{\sin\left(\frac{\theta}{2}\right)} \tag{4.27}$$

This concludes the proof.

The result of this trigonometry relations is used in the following of the manuscript.

Energy proof

For all $\theta \in \mathbb{R}$ and m $\in \mathbb{N}$:

$$\boxed{\sum_{k=0}^{m} \sin(2k+1)\theta = \frac{1}{\sin\theta}[\sin((m+1)\theta)]^2} \tag{4.28}$$

We use the trigonometry reminders,

$$Im\left[\sum_{k=0}^{m} e^{j(2k+1)\theta}\right] = e^{j\theta}\sum_{k=0}^{m} e^{2jk\theta} \tag{4.29}$$

By using the relation 4.26:

$$\sum_{k=0}^{m} e^{2jk\theta} = e^{j(m+1)\theta}\frac{\sin((m+1)\theta)}{\sin\theta} \tag{4.30}$$

To conclude the proof, by taking the imaginary part:

$$\sum_{k=0}^{m} \sin((2k+1)\theta) = \frac{1}{\sin\theta}[\sin((m+1)\theta)]^2 \tag{4.31}$$

Energy level structure and conditions on N

The two configurations $S_N^1(0)$ and $S_N^1(\phi_M)$ are **different** in the structure of the energy levels of the molecule.

In the **Möbius case** $S_N^1(\phi_M)$, we get energy levels which are given by pairs. We fill several levels when $\pi(S_N^1(\phi_M))$ *($\pi(S)$: number of electrons, see the part I to complete explanations)* is a multiple of 4.

In the **ribbon case** $S_N^1(0)$, we have a minimal energy level followed by energy levels in pairs. In the same way, we saturate several energy levels if $\pi(S_N^1(0)) - 2$ is a multiple of 4.

This is resumed by what is called **electronic saturation** where $x \equiv y$ [mod.4] meaning that x is congruent to y modulo 4 ie $x = y + 4m, m \in \mathbb{N}$.

*To remind, we use here the terms of **"Möbius"** and **"ribbon"** applied for the study of aromaticity criteria.*

The **electronic saturation** is defined as: the energy levels are saturated for $S_N^1(\phi_M)$ if $\pi(S_N^1) \equiv 0$ [mod.4] and for $S_N^1(0)$ if $\pi(S_N^1) - 2 \equiv 0$ [mod.4].

We have studied different cases according to the number of electrons, the case called **"even"** $\pi(S_N^1) \equiv 0$ [mod.4] and the **"odd"** case $\pi(S_N^1) \not\equiv 0$ [mod.4].

Even case $\pi(S_N^1) \equiv 0$ [mod.4]: In this paragraph, the **energy levels** of a structure S are noted **k** and the **energy** associated to this energy level for an electron is $\epsilon_k(S)$.

In the Möbius case: From C.A. Coulson, B. O'Leary and R. B. Mallion calculation techniques [54], the **eigenvalues** of the Hückel matrix are given in this case by [54]:

$$\lambda_k = x + 2a\cos\left((2k+1)\pi\frac{k}{N}\right) \tag{4.32}$$

with k = 0,..., N-1.

In order to determine the structure of the energy levels, we study the **degeneracies** such as:

we have $\lambda_i = \lambda_j$ if and only if N is even and $j = N - i - 1$ for *i = 0,..., N-1.*

The proof of this statement is given in Appendix 2 section 18.

Thus, for N even degenerated levels set by 2, $\lambda_i = \lambda_{N-i-1}$ *for i = 0,..., N-1.*

The situation is described in the diagram :

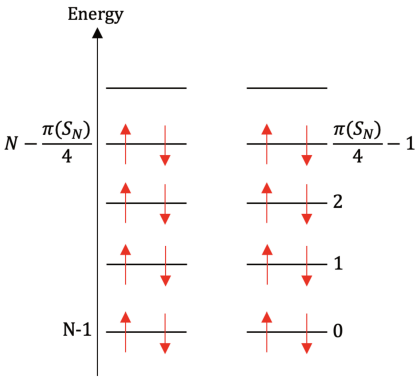

Figure 4.9: Distribution of the energy levels of $S_N^1(\phi_M)$ in the case of $\pi(S_N^1) \equiv 0$ [mod.4]

In this case here, it is an **electronic saturation**. All levels from 0 to $\frac{\pi(S_N^1)}{4} - 1$ are **occupied**.

The **energy** $\epsilon_k(S_N^1(\phi_M))$ of an electron on the energy level k verifies:

$$\boxed{\epsilon_k(S_N^1(\phi_M)) = \alpha + 2\beta\cos((2k+1)\phi)} \tag{4.33}$$

where $\phi = \frac{\pi}{N}$.

The **Möbius energy** $E(S_N^1(\phi_M))$ associated to the molecule $S_N^1(\phi_M)$ is given as:

$$\boxed{E(S_N^1(\phi_M)) = \alpha\pi(S_N^1) + 8\beta\cos\frac{\pi}{N}\sum_{k=0}^{\frac{\pi(S_N^1)}{4}-1}\cos\left((2k+1)\frac{\pi}{N}\right)} \tag{4.34}$$

To prove this result, based on symmetry considerations where all the levels are occupied, we have:

$$E(S_N^1(\phi_M)) = \sum_{k=0}^{\frac{\pi(S_N^1)}{4}-1} 2\epsilon_k(S_N^1(\phi_M)) + \sum_{k=N-\frac{\pi(S_N^1)}{4}}^{N-1} 2\epsilon_k(S_N^1(\phi_M)) \tag{4.35}$$

$$\sum_{k=0}^{\frac{\pi(S_N^1)}{4}-1} \epsilon_k(S_N^1(\phi_M)) = \sum_{k=N-\frac{\pi(S_N^1)}{4}}^{N-1} \epsilon_k(S_N^1(\phi_M)) \tag{4.36}$$

Then,

$$\boxed{E(S_N^1(\phi_M)) = 4 \sum_{k=0}^{\frac{\pi(S_N^1)}{4}-1} \epsilon_k(S_N^1(\phi_M))} \tag{4.37}$$

We can therefore substitute $\epsilon_k(S_N^1(\phi_M))$ by its expression in eq. 4.34.

In the ribbon case: In the ribbon case $S_N^1(0)$, the structure of the **energy levels is different**.

As a reminder, the eigenvalues of the Hückel matrix are given by :

$$\lambda_k = x + 2a\cos\left(2\pi\frac{k}{N}\right) \tag{4.38}$$

with $k = 0, ..., N-1$, notice that the numeration of the eigenvalues from $k = 1$ to N is equivalent to $k = 0$ to $N-1$.

As in the previous case, we study the **structure of the energy levels** such as, $\lambda_i = \lambda_j$ if and only if $j = N - i$ and $i = 1, ..., N-1$.

The proof is given Appendix 2 section 19.

We get the energy level corresponding to λ_0 and degenerate levels grouped by 2, $\lambda_i = \lambda_{N-i}$ *for i = 1,..., N-1.*

We represent this situation by the diagram:

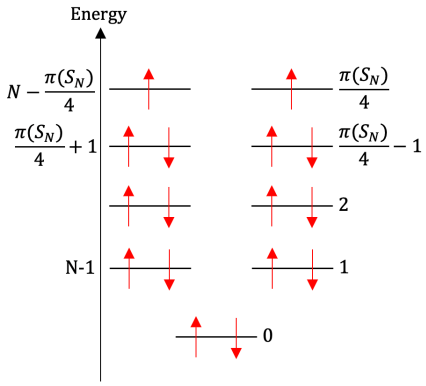

Figure 4.10: Distribution of the energy levels of $S_N^1(0)$ in the case of $\pi(S_N^1) \equiv 0$ [mod.4]

As expected, this is a **non-saturated** case with two available electrons on the last two energy levels.

We know that the $\epsilon_k(S_N^1(0))$ **energy** of an electron on the k-energy level of $S_N^1(0)$ is given by:

$$\boxed{\epsilon_k(S_N^1(0)) = \alpha + 2\beta\cos\left(\frac{2k\pi}{N}\right)} \tag{4.39}$$

The **energy** $E(S_N^1(0))$ of the molecule $S_N^1(0)$ is given by:

$$\boxed{E(S_N^1(0)) = -2\epsilon_0(S_N^1(0)) + 2\epsilon_{\frac{\pi(S_N^1)}{4}}(S_N^1(0)) + \alpha\pi(S_N^1) + 8\beta \sum_{k=0}^{\frac{\pi(S_N^1)}{4}-1} \cos\left(\frac{2k\pi}{N}\right)} \tag{4.40}$$

with $\epsilon_0(S_N^1(0)) = \alpha + 2\beta$ *and* $\epsilon_{\frac{\pi(S_N^1)}{4}}(S_N^1(0)) = \alpha + 2\beta\cos\left(\pi(S_N^1)\frac{\pi}{2N}\right)$.

To prove this relation, we know that:

$$E(S_N^1(0)) = 2\epsilon_0(S_N^1(0)) + \sum_{k=1}^{\frac{\pi(S_N^1)}{4}-1} 2\epsilon_k S_N^1(0)) + \sum_{N-\frac{\pi(S_N^1)}{4}+1}^{N-1} 2\epsilon_k(S_N^1(0)) + \epsilon_{\frac{\pi(S_N^1)}{4}}(S_N^1(0)) + \epsilon_{N-\frac{\pi(S_N^1)}{4}}(S_N^1(0)) \tag{4.41}$$

We get the relations:

$$\epsilon_{\frac{\pi(S_N^1)}{4}}(S_N^1(0)) = \epsilon_{N-\pi(S_N^1)}4(S_N^1(0)) \tag{4.42}$$

and,

$$\sum_{k=1}^{\frac{\pi(S_N^1)}{4}-1} 2\epsilon_k(S_N^1(0)) = \sum_{k=N-\frac{\pi(S_N^1)}{4}+1}^{N-1} 2\epsilon_k(S_N^1(0)) \tag{4.43}$$

Thus,

$$E(S_N^1(0)) = 2\epsilon_0(S_N^1(0)) + 4 \sum_{k=1}^{\frac{\pi(S_N^1)}{4}-1} \epsilon_k(S_N^1(0)) + 2\epsilon_{\frac{\pi(S_N^1)}{4}}(S_N^1(0)) \tag{4.44}$$

If the sum begins at $k = 0$, we have:

$$\boxed{E(S_N^1(0)) = -2\epsilon_0(S_N^1(0)) + 4 \sum_{k=0}^{\frac{\pi(S_N^1)}{4}-1} \epsilon_k(S_N^1(0)) + 2\epsilon_{\frac{\pi(S_N^1)}{4}}(S_N^1(0))} \tag{4.45}$$

If we substitute $\epsilon_k(S_N^1(0))$ by its expression we obtain the relation eq. 4.40.

Odd case $\pi(S_N^1) \not\equiv 0$ **[mod.4]:** The situation of this paragraph is **more complicated** because it considers cases where there is **saturation** of the electronic levels in the **ribbon** case. Moreover, $\pi(S_N^1) \not\equiv 0$ [mod.4] indicates that there exists $\delta \in \{1, 2, 3\}$ such as $\pi(S_N^1) = 4k + \delta$ *(with k the energy levels).*

In the Möbius case : Set $\delta \in \{1, 2, 3\}$, we get $m = \pi(S_N^1(\phi_M)) - \delta$. By hypothesis, we have $m \equiv 0$ [mod.4].

We are in a **non-saturated** situation, for example in the case $\delta = 3$ we have the representation as:

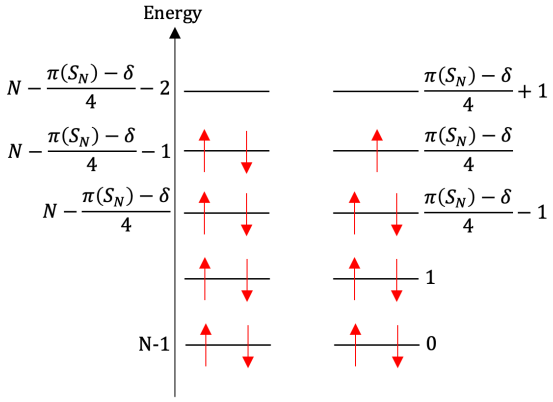

Figure 4.11: Distribution of the energy levels of $S_N^1(\phi_M)$ in the case of $\pi(S_N^1) \not\equiv 0$ [mod.4]

The **energy** of this **Möbius situation** $E(S_N^1(\phi_M))$ of the molecule $S_N^1(\phi_M)$, *with* $\delta \in 1,2,3$ as $\pi(S_N^1) - \delta \equiv 0$ [mod.4] is given by:

$$E(S_N^1(\phi_M)) = \alpha(\pi(S_N^1) - \delta) + 8\beta \cos\left(\frac{\pi}{N}\right) \sum_{k=0}^{\frac{\pi(S_N^1)-\delta}{4}-1} \cos\left((2k+1)\frac{\pi}{N}\right) \delta\epsilon_{\frac{\pi(S_N^1)-\delta}{4}}(S_N^1(\phi_M)) \tag{4.46}$$

For proof of this expression, we are interested in the first contribution of the energy given by the saturated energy levels associated with the $\pi(S_N^1) - \delta$ first electrons. To calculate this contribution, we have to use the result of the $\pi(S_N^1) \equiv 0$ [mod.4] case (eq. 4.34) by substituting $\pi(S_N^1)$ by $\pi(S_N^1) - \delta$.

We obtain a term such as:

$$\alpha(\pi(S_N^1) - \delta) + 8\beta \cos\left(\frac{\pi}{N}\right) \sum_{k=0}^{\frac{\pi(S_N^1)-\delta}{4}-1} \cos\left((2k+1)\frac{\pi}{N}\right) \tag{4.47}$$

Then, it remains δ electrons on the $\frac{\pi(S_N^1)-\delta}{4}$ level. These electrons contribute to the energy given by:

$$\delta\epsilon_{\frac{\pi(S_N^1)-\delta}{4}}(S_N^1(\phi_M)) \tag{4.48}$$

We then deduce by summing the different terms:

$$E(S_N^1(\phi_M)) = \alpha(\pi(S_N^1) - \delta) + 8\beta \cos\left(\frac{\pi}{N}\right) \sum_{k=0}^{\frac{\pi(S_N^1)-\delta}{4}-1} \cos\left((2k+1)\frac{\pi}{N}\right) \delta\epsilon_{\frac{\pi(S_N^1)-\delta}{4}}(S_N^1(\phi_M)) \tag{4.49}$$

In the ribbon case: This is **the more complex case** because three situations can happen according to the value of $\delta \in 1,2,3$ defined by $\pi(S_N^1) - \delta \equiv 0$ [mod.4].

Section 4.3.2, the **electronic saturation** gives a **particular** status to the case $\delta = 2$ since in this case (and only this one) the energy levels of the **ribbon** are **saturated**.
We will therefore see in the energy formula the implementation of δ in relation to $\delta = 2$. For this, we indicate $\mu \in \{-1, 0, 1\}$ and we put $\delta = 2+\mu$. The case $\mu = 0$ corresponds then to the saturated situation.

Let's take for example, the case $\mu = 1$ corresponding to $\delta = 3$, an electron is alone on the level of energy $\frac{\pi(S_N^1)-\delta}{4} + 1$, the levels of energy prior to this value being saturated we obtain the following diagram:

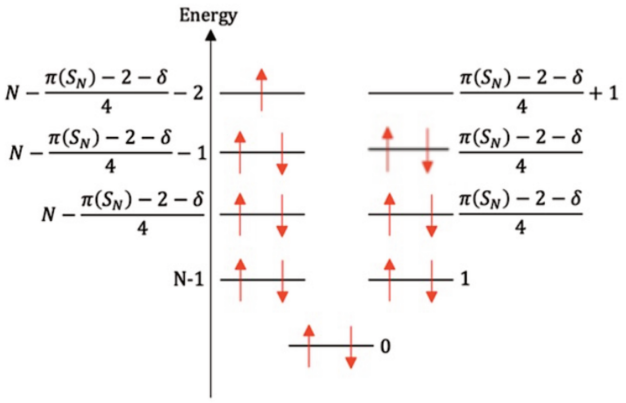

Figure 4.12: Distribution of the energy levels of $S_N^1(0)$ in the case of $\pi(S_N^1) - 3 \equiv 0$ [mod.4]

The **energy** $E(S_N^1(0))$ of the molecule $S_N^1(0)$ is given by:

$$\begin{aligned} E(S_N^1(0)) &= -2\epsilon_0(S_N^1(0)) + 4\epsilon_{\frac{\pi(S_N^1)-\delta}{4}}(S_N^1(0)) + \alpha(\pi(S_N^1) - \delta) + 8\beta \sum_{k=0}^{\frac{\pi(S_N^1)-\delta}{4}-1} \cos\left(\frac{2k\pi}{N}\right) \\ &+ \begin{cases} -\epsilon_{\frac{\pi(S_N^1)-\delta}{4}}(S_N^1(0)), \text{ if } \mu = -1, \\ 0, \text{ if } \mu = 0, \\ +\epsilon_{\frac{\pi(S_N^1)-\delta}{4}+1}(S_N^1(0)), \text{ if } \mu = 1 \end{cases} \end{aligned} \tag{4.50}$$

where $\delta \in$ {1, 2, 3} is defined by $\pi(S_N^1) - \delta \equiv 0$ [mod.4] and $\mu \in$ {-1, 0, 1} is given by $\mu = \delta - 2$.

For proof, the number $\pi(S_N^1) - \delta$ is a multiple of 4 for which we already calculated the energy. This one is given in eq. 4.40 by replacing in the formulas $\pi(S_N^1)$ by $\pi(S_N^1) - \delta$ gives a contribution to the **total energy** as:

$$-2\epsilon_0(S_N^1(0)) + 2\epsilon_{\frac{\pi(S_N^1)-\delta}{4}}(S_N^1(0)) + \alpha(\pi(S_N^1) - \delta) + 8\beta \sum_{k=0}^{\frac{\pi(S_N^1)-\delta}{4}-1} \cos\left(\frac{2k\pi}{N}\right) \tag{4.51}$$

A **corrective term** has to be applied which is dependent on δ.

If $\delta = 1$ or 2, the energy level $\frac{\pi(S_N^1)-\delta}{4}$ is completed.
If $\delta = 3$ we have to add an electron on the energy level $\frac{\pi(S_N^1)-\delta}{4} + 1$.
A manner of coding the totality of these operations is to take the saturated situation as reference. The energy of the saturated case corresponding to $\frac{\pi(S_N^1)-\delta}{4} + 1$ is obtained using the previous formula by adding 2 electrons on the $\frac{\pi(S_N^1)-\delta}{4}$ level.

We get an energy given by:

$$- 2\epsilon_0(S_N^1(0)) + 4\epsilon_{\frac{\pi(S_N^1)-\delta}{4}}(S_N^1(0)) + \alpha(\pi(S_N^1) - \delta) + 8\beta \sum_{k=0}^{\frac{\pi(S_N^1)-\delta}{4}-1} \cos\left(\frac{2k\pi}{N}\right) \tag{4.52}$$

According to the value of μ we can add or subtract the contribution of the energy levels. More precisely, we have a corrective term to the energy value of the saturated case with $\frac{\pi(S_N^1)-\delta}{4} + 2$ electrons defined as follows:

$$\begin{cases} -\epsilon_{\frac{\pi(S_N^1)-\delta}{4}}(S_N^1(0)), \text{ if } \mu = -1, \\ 0, \text{ if } \mu = 0, \\ +\epsilon_{\frac{\pi(S_N^1)-\delta}{4}+1}(S_N^1(0)), \text{ if } \mu = 1 \end{cases} \tag{4.53}$$

If we combine these contributions we obtain the expected formula eq. 4.50.

4.3.3 Energetic comparison of structures $S_N^1(0)$ and $S_N^1(\phi_M)$ - stability

Using the calculations of the previous section, we can determine which of the structures $S_N^1(0)$ and $S_N^1(\phi_M)$ is the **most energetically favorable**. We note that the number of electrons ($\pi(S_N^1)$) available in the structure takes on a primordial role.

The $\pi(S_N^1) \equiv 0$ [mod.4] case

We obtain the next result which is quite surprising, if we assume that $\pi(S_N^1) \equiv 0$ [mod.4], then:

$$\boxed{E(S_N^1(\phi_M)) - E(S_N^1(0)) = 0} \tag{4.54}$$

In this electronic configuration, from an energetic point of view, the **Möbius case is equivalent to the ribbon structure** which is the natural situation to be expectable.

For proof we use the previously proven formulas (section 4.3.2) we have:

$$\begin{aligned} E(S_N^1(\phi_M)) - E(S_N^1(0)) = 8\beta \sum_{k=0}^{\frac{\pi(S_N^1)}{4}-1} \left[\cos\left(\frac{\pi}{N}\right)\cos\left((2k+1)\frac{\pi}{N}\right) - \cos\left(\frac{2k\pi}{N}\right)\right] \\ + 2\left(\epsilon_0(S_N^1(0)) - \epsilon_{\frac{S_N^1(0)}{4}}(S_N^1(0))\right) \end{aligned} \tag{4.55}$$

As a trigonometric reminder we know that : $\cos(a)\cos(b) = \frac{1}{2}(\cos(a-b) + \cos(a+b))$.

By this trigonometric reminder we can rewrite the equality such as:

$$\begin{aligned} E(S_N^1(\phi_M)) - E(S_N^1(0)) = 4\beta \sum_{k=0}^{\frac{\pi(S_N^1)}{4}-1} \left[\cos\left((2k+2)\frac{\pi}{N}\right) - \cos\left(\frac{2k\pi}{N}\right)\right] \\ + 2\left(\epsilon_0(S_N^1(0)) - \epsilon_{\frac{\pi(S_N^1)}{4}}(S_N^1(0))\right) \end{aligned} \tag{4.56}$$

If we consider once again the trigonometric formula, we know that for all $a, b \in \mathbb{R}, 2\sin(a)\sin(b) = \cos(a-b) - \cos(a+b)$.

By setting: $a = (2k+1)\frac{\pi}{N}$ *and* $b = \frac{\pi}{N}$, *we have:* $-2\sin\left(\frac{2k\pi}{N}\right)\sin\left(\frac{\pi}{N}\right) = \cos\left((2k+2)\frac{\pi}{N}\right) - \cos\left(\frac{2k\pi}{N}\right)$.

By substituting the previous equality in the expression of $E(S_N^1(\phi_M)) - E(S_N^1(0))$, we obtain:

$$E(S_N^1(\phi_M)) - E(S_N^1(0)) = -4\beta\sin\left(\frac{\pi}{N}\right)\sum_{k=0}^{\frac{\pi(S_N^1)}{4}-1}\sin\left((2k+1)\frac{\pi}{N}\right) + 2\left(\epsilon_0(S_N^1(0)) - \epsilon_{\frac{\pi(S_N}{4}}S_N^1(0))\right) \tag{4.57}$$

We finally get:

$$E(S_N^1(\phi_M)) - E(S_N^1(0)) = -4\beta\left(\pi(S_N^1)\frac{\pi}{4N}\right)^2 + 2\left(\epsilon_0(S_N^1(0)) - \epsilon_{\frac{\pi(S_N}{4}}(S_N^1(0)\right) \tag{4.58}$$

In addition,

$$\epsilon_0(S_N^1(0)) - \epsilon_{\frac{\pi(S_N^1)}{4}}(S_N^1(0)) = 2\beta\left(1 - \cos\left(\pi(S_N^1)\frac{\pi}{2N}\right)\right) \tag{4.59}$$

and,

$$E(S_N^1(\phi_M)) - E(S_N^1(0)) = -4\beta\left(\sin(\pi(S_N^1)\frac{\pi}{4N}\right)^2 + \cos\left(\pi(S_N^1)\frac{\pi}{2N}\right) + 4\beta \tag{4.60}$$

Then, as $\pi(S_N^1) = N$, we get:

$$E(S_N^1(\phi_M)) - E(S_N^1(0)) = 0 \tag{4.61}$$

The $\pi(S_N^1) \not\equiv 0$ [mod.4] case

This is the **most complicated situation**, because each energy equation in the Möbius and ribbon case is composed of a part corresponding to the case presented earlier and of corrective terms. The energy difference in the $\pi(S_N^1) \not\equiv 0$ [mod.4] case is equal to zero, thus, the comparison of the two energies is equivalent to the **comparison** of the **corrective terms**.

If we assume that $\pi(S_N^1) \not\equiv 0$ [mod.4] then:

$$\boxed{E(S_N^1(\phi_M)) - E(S_N^1(0)) = \begin{cases} 2\beta\delta\sin\left(\frac{\pi}{N}\right)\sin\left(\left(\frac{\pi(S_N^1)-\delta}{2}+1\right)\frac{\pi}{N}\right) & \text{if } \delta = 1 \text{ or } 2, \\ 4\beta\sin(\frac{\pi}{N})\sin\left(\left(\frac{\pi(S_N^1)-\delta}{2}+1\right)\frac{\pi}{N}\right) + & \\ -\alpha - 2\beta\cos\left(\left(\frac{\pi(S_N^1)-\delta}{2}+2\right)\frac{\pi}{N}\right) & \text{if } \delta = 3 \end{cases}} \tag{4.62}$$

These expressions indicate that in this case, the sign of the energy difference is not fixed and **depends** explicitly on **N**. We are therefore, in the situation where the Möbius configuration is the most stable compared to the ribbon case.

For proof, by using the previous results, we can obtain the energy difference as:

$$\begin{aligned} E(S_N^1(\phi_M)) - E(S_N^1(0)) &= \delta\epsilon_{(\frac{\pi(S_N^1)-\delta)}{4}}(S_N^1(\phi_M)) \\ &- \begin{cases} \delta\epsilon_{(\frac{\pi(S_N^1)-\delta)}{4}}(S_N^1(0)), & \text{if } \delta = 1 \text{ or } 2, \\ 2\epsilon_{(\frac{\pi(S_N^1)-\delta)}{4}}(S_N^1(0)) + \epsilon_{(\frac{\pi(S_N^1)-\delta)}{4}+1}(S_N^1(0)), & \text{if } \delta = 3 \end{cases} \end{aligned} \tag{4.63}$$

For $\delta = 1$ or 2, the expression is now:

$$E(S_N^1(\phi_M)) - E(S_N^1(0)) = \delta \left(\epsilon_{\frac{\pi(S_N^1)-\delta}{4}}(S_N^1(\phi_M)) - \epsilon_{\frac{\pi(S_N^1)-\delta}{4}}(S_N^1(0)) \right) \tag{4.64}$$

By using the expression of the energy levels:

$$\epsilon_{\frac{\pi(S_N)-\delta}{4}}(S_N^1(\phi_M)) - \epsilon_{\frac{\pi(S_N^1)-\delta}{4}}(S_N^1(0)) =$$

$$2\beta \left[\cos\left(\frac{\pi}{N}\right) \cos\left(\left(\frac{\pi(S_N^1)-\delta}{2} + 1 \right) \frac{\pi}{N} \right) - \cos\left(\frac{\pi(S_N^1)-\delta}{2} \frac{\pi}{N} \right) \right] \tag{4.65}$$

If we use once again the trigonometry equality, $(2\cos(a)\cos(b) = \cos(a+b) + \cos(a-b))$, with $a = \left(\frac{\pi(S_N^1)-\delta}{2} + 1\right)\frac{\pi}{N}$ and $b = \left(\frac{\pi(S_N^1)-\delta}{2}\right)\frac{\pi}{N}$, we can rewrite this quantity such as :

$$\cos\left(\frac{\pi}{N} \cos\left(\frac{\pi(S_N^1)-\delta}{2} + 1 \right) \frac{\pi}{N} \right) - \cos\left(\frac{\pi(S_N^1)-\delta}{2} \frac{\pi}{N} \right) =$$
$$\frac{1}{2} \left[\cos\left(\frac{\pi(S_N^1)-\delta}{2} + 2 \right) \frac{\pi}{N} - \cos\left(\frac{\pi(S_N^1)-\delta}{2} \right) \frac{\pi}{N} \right] \tag{4.66}$$

This expression can be simplified by using the relation, for all $a, b \in \mathbb{R}$, $2\sin(a)\sin(b) = \cos(a-b) - \cos(a+b)$.

By taking, $a = \left(\frac{\pi(S_N^1)-\delta}{2} + 1\right)\frac{\pi}{N}$ and $b = \frac{\pi}{N}$, we have:

$$\cos\left(\left(\frac{\pi(S_N^1)-\delta}{2} + 2 \right) \frac{\pi}{N} \right) - \cos\left(\frac{\pi(S_N^1)-\delta}{2} \frac{\pi}{N} \right) = \sin\frac{\pi}{N} \sin\left(\left(\frac{\pi(S_N^1)-\delta}{2} + 1 \right) \frac{\pi}{N} \right) \tag{4.67}$$

Thus, we get a term as:

$$E(S_N^1(\phi_M)) - E(S_N^1(0)) = 2\beta\delta \sin\frac{\pi}{N} \sin\left(\left(\frac{\pi(S_N^1)-\delta}{2} + 1 \right) \frac{\pi}{N} \right) \tag{4.68}$$

$$2\epsilon_{\frac{\pi(S_N^1)-\delta}{4}}(S_N^1(0)) + \epsilon_{\frac{\pi(S_N^1)-\delta}{4}+1}(S_N^1(0)), \text{ if } \delta = 3. \tag{4.69}$$

4.3.4 Molecule S_N^1 twisted by a distribution and a C_2 invariance

Geometry of a twisted molecule S_N^1

The geometry of a **molecule S_N^1 twisted** by a ϕ distribution ($\phi = (\phi_1, ..., \phi_N)$) is characterized by **two families of angles**. Firstly, a family of θ_i angles related to the **position** of the atoms on the circle, and the ϕ_i angles providing the **orientation** of the orbitals in relation to each other in each atom taking as reference the first one.We give some precisions in the rest of the manuscript.

Parametrization of the circle and θ_i angles: We consider a reference frame (x, y, z) of $\mathbb{R}^3$ and a circle in the (y, z) plane centered in $O = (0, 0, 0)$ of radius $R > 0$ parametrized by an angle $\theta_i \in [0, 2\pi]$ as:

$$\boxed{C_R = \{(0, R\sin(\theta_i), -R\cos(\theta_i))\}} \tag{4.70}$$

with $\theta_i \in [0, 2\pi[$.

Note that x is normal to the plane containing the circle.

We get a $\phi = (\phi_1, ..., \phi_N)$ distribution. We dispose N atoms C_i along the circle and we note θ_i (*with i = 1,..., N*) the angles corresponding to this distribution. The C_i atoms have the coordinates $(0, R\sin(\theta_i), -R\cos(\theta_j))$ *with* j^2 = *-1.*

ϕ distribution and representation: Let n_i be the tangent vector to the circle at point C_i i.e. $n_i = (0, R\cos(\theta_i), R\sin(\theta_i))$. Let $\mathcal{P}_i$ be the normal plane to n_i at point C_i. Let u_i be a family of vectors in the normal plane to n_i. A basis of $\mathbb{R}^3$ at the point C_i consists of $e_1 = (1, 0, 0)$, n_i and the vector OC_i. The vectors e_1 and OC_i form a basis of $\mathcal{P}_i$. A vector $u_i \in \mathcal{P}_i$ is therefore represented by a vector U_i of $\mathbb{R}^2$ whose coordinates are given by the coordinates of u_i in the basis $\langle e_1, OC_i \rangle$.

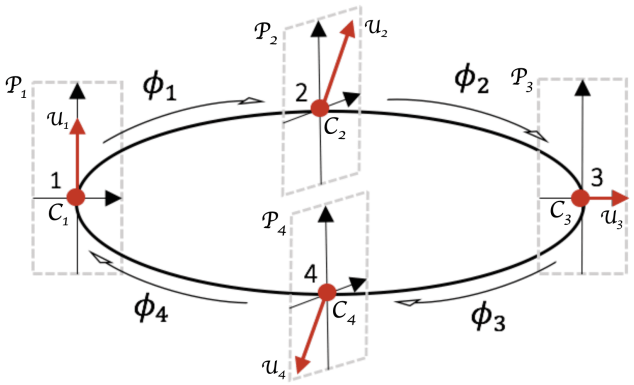

Figure 4.13: Evolution of the orbitals along the circle - Möbius case

Using these notations, the ϕ **distribution** is related to the vectors u_i by identifying the planes $\mathcal{P}_i$ by the relation:

$$\widehat{U_i, U_{i+1}} = \phi_i \tag{4.71}$$

with i=1,. . . , N-1.

With the vector u_1 fixed, we get the vector u_k by positioning the vector in the $\mathcal{P}_k$ plane:

$$\boxed{U_k = e^{-j(\phi_1 + \cdots + \phi_{k-1})} U_1} \tag{4.72}$$

At this step of the manuscript, we have not imposed any particular symmetry, we will then impose the C_2 **invariant molecule**.

Note that in many publications, the direction of the circle is clockwise, which is contrary to the usual trigonometric direction used in mathematics. This is what explains the presence of the "-" in the rotation that expresses U_k as a function of U_1. It is also what explains the particular form of the parameterization of the circle.

C_2 invariance of a twisted molecule

We are interested in identifying the conditions imposed by the C_2 **invariance** condition on the data of the **twisted** molecule.

Axis positioning: The first evident but important result indicates the potential axis around which the molecule $S_N^1(\phi)$ can be eventually C_2 invariant.

We can define if a molecule $S_N^1(\phi)$ is C_2 invariant then, the axis of symmetry depends:

- either to the plane of the molecule, i.e. a line passing through the center of the circle
- or, is perpendicular to the plane of the molecule passing through the center of the circle

For proof, the molecule being $S_N^1(\phi)$, the set of atoms corresponds to the plane containing the circle. The image of this molecule by a C_2 **symmetry** whose the axis is outside the plane does not belong to the molecule unless the axis is perpendicular to the plane and through the center of the circle.
If we are not in this situation, we consider an axis in the plane containing the circle. In the same way, the circle is invariant by a reflection around an axis if and only if this axis passes through the center of the circle.
The two situations are represented in the following figures:

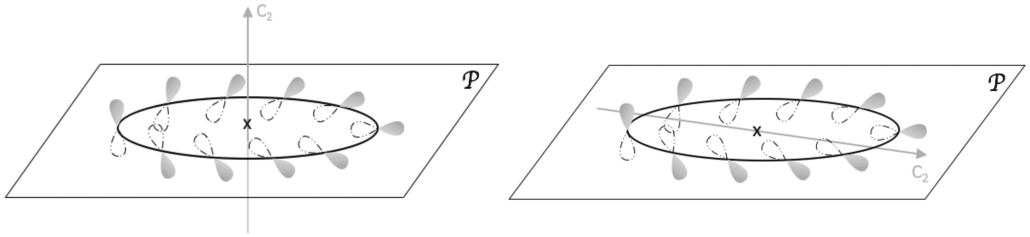

Figure 4.14: Position of the C_2 axis - transverse to the plane (on the left) and in the plane (on the right)

We can thus assume that the axis of C_2 symmetry is carried by the z-axis and that the molecule is contained in the $x = 0$ plane.

Restrictions on the positions of the atoms: We suppose that the invariant C_2 molecule is subject to the action of a **rotation** of angle π around the axis carried by z.
We note this rotation: $r_z(\pi)$ and it is given by:

$$r_z(\pi) = \begin{pmatrix} -1 & 0 & 0 \\ 0 & -1 & 0 \\ 0 & 0 & 1 \end{pmatrix} \tag{4.73}$$

The first family of **constraints** imposed by the C_2 invariance is on the **position** and **number** of atoms.
We define the geometric constraints for a C_2 invariance. Let $S_N^1(\phi)$ be a C_2 molecule invariant by a rotation of angle π carried by the $x = y = 0$ axis.

Then, we have the two following properties:

- let k be the number of atoms on the $x = y = 0$ axis. We have $k = 1$ or 2. Then, there exists $n \in \mathbb{N}$ such as the number of atoms N is given by $N = 2n + k$.
- let C_i be an atom whose position is marked by the angle θ_i then its image by $r_z(\pi)$ is indicated by the angle $2\pi - \theta_i$.

For proof, these properties are relatively trivial. The molecule is by definition symmetric to the axis $x = y = 0$ in the plane $x = 0$. If we get n atoms outside the axis in the $\theta_i \in]0, \pi[$ part, then we have the images of these atoms by symmetry in the $\theta_i \in]0, 2\pi[$ part. Therefore, we have $2n$ atoms by symmetry for the molecule out of the axis, which justifies our result.

Moreover, $r_z(\pi)[(0, R\sin(\theta_i), -R\cos(\theta_i))] = (0, -R\sin(\theta_i), -R\cos(\theta_i))$ corresponds to an angle $\tilde{\theta}$ between $[0, 2\pi[$ equals to $\tilde{\theta_i} = 2\pi - \theta_i$.

Orbital constraints and orbitals distribution: Regarding the **constraints** on the atomic orbitals carried by the atoms and associated to u_i (with $i = 1, ..., N$) vectors data, the first obvious constraint is : let S_N^1 be a C_2 invariant molecule where the axis is carried by z. If an atom C_i is part of the rotation axis, then its u_C vector is of the form $(0, 0, a)$ for a certain $a \in \mathbb{R}$.

For proof, the molecule being C_2 invariant, $r_z(\pi)[C_i]$ has to belong to the molecule. As C_i is carried by the axis, it is invariant by $r_z(\pi)[C_i] = C_i$. The image of the orbital $u_C = (\alpha, \beta, \gamma)$ has to verify the invariance condition, which is i.e. $r_z(\pi)[u_C]$. This is only possible if u_C is of the form $(0, 0, a)$ for a given $a \in \mathbb{R}$. In fact, $r_z(\pi)[u_C] = (-\alpha, -\beta, \gamma)$ thus, $\alpha = \beta = 0$.

The constraint implies the following corollary:
let S_N^1 be a C_2 invariant molecule where the axis is carried by z. If a C_i atom has a u_C orbital which is not carried by the axis of symmetry, then the considered atom cannot be on the axis of symmetry.

Structure of molecules S_N^1 - C_2 invariant: In most of the Möbius type molecules, we consider the first atom with a $u_1 = (1, 0, 0)$ orbital along the x axis. This atom has to be positioned out of the symmetry axis, since we assume that the C_2 symmetry is carried by the z axis. We thus have to consider the first atom with a given $\theta_i \neq 0$ coordinate.

We consider the following situation:
let the molecule S_N^1 made of N atoms whose first C_1 is denoted by an angle $\theta \neq 0$ and carrying a vector $u_1 = (1, 0, 0)$. There are n atoms with $\theta_i \in]0, \pi[$ coordinates and thus n atoms by symmetry with $\theta_i \in]\pi, 2\pi[$ coordinates.

There are **two** possible situations:

- either there is **an atom on the axis** which in this case has an orbital belonging to the axis. We then have $N = 2n + 1$, and the distribution has to satisfy $\phi_1 + ... + \phi_{n+1} = \frac{\pi}{2}$ in order to guarantee that the image of $u_1 = (1, 0, 0)$ by the successive rotations of angles ϕ_i gives a vector belonging to the z axis.
- either there are **no atoms** on the axis and $N = 2n$.
  A global constraint on the distribution comes from the fact that the image of $u_1 = (1, 0, 0)$ by $r_z(\pi)$ corresponds to the orbital of the atom N, i.e. $u_N = (-1, 0, 0)$ which imposes the distribution as $\phi_1 + ... + \phi_{N-1} = \pi$. Moreover, the C_2 symmetry refers the C_i atom to the C_{N-i+1} atom, thus, we have $\theta_{N-i+1} = 2\pi - \theta_i$.

We can summarize these results as follows:

let a molecule $S_N^1(\phi)$, C_2 **invariant** by a symmetry carried by the z-axis. We suppose $u_1 = (1, 0, 0)$, then we have :

- the ϕ distribution has to satisfy $\phi_1 + ... + \phi_{N-1} = \pi$,
- the C_1 atom is not on the axis,
- if the number of atoms is of the form $N = 2n$, then there is no atom on the symmetry axis,
- if the number of atoms is as $N = 2n + 1$, then $n + 1$ is on the axis and its orbital is carried by the axis. We have then $\phi_1 + ... + \phi_n = \frac{\pi}{2}$,
- and, the positions of the atoms are related by the relation $\theta_{N-i+1} = 2\pi - \theta_i$.

The hypothesis that a molecule $S_N^1(\phi)$ is C_2 symmetric, imposes a **Möbius condition** if the vector $u_1 = (1, 0, 0)$.

The C_2 symmetry imposes **other constraints** as well:

Let $S_N^1(\phi)$ be a C_2 molecule invariant by a rotation of angle π carried by the axis $x = y = 0$. Then, we have the property of the **torsion distribution** such that:

$$\boxed{\phi_{N-i+1} = \phi_i} \tag{4.74}$$

with $i = 1, ..., N-1$.

The simple proof of this relation is given in Appendix 2 section 20.

At this stage of the manuscript we can describe some distributions widely found in the literature.
The **standard Möbius case** is obtained by imposing a **constant angle** and the C_2 **symmetry** of axis carried by z.

A molecule $S_N^1(\phi)$ is a standard Möbius if it is invariant by C_2 symmetry of axis carried by z and, if $N = 2n$ and $\phi_1 = ... = \phi_n$.

To show the standard Möbius, we know that by **invariance** we get $\phi_1 + ... + \phi_{2n} = \pi$ and $\phi_1 + ... + \phi_n = \frac{\pi}{2}$.

The symmetry relation on the angles implies $\phi_{n+1} + ... + \phi_{2n} = \phi_1 + .. + \phi_n$.

As $\phi_1 = ... = \phi_n = \phi$, we obtain $\frac{N-1}{2}\phi = \frac{\pi}{2}$ or $\phi = \frac{\pi}{N-1}$.

Molecule $S_N^1(\phi)$ constituted of one type of atoms and C_2 invariance: All the definitions presented previously do not assume **any specificity** on the atoms positioned on the circle. However, the fact of considering a molecule with only one type of atom or with several type of atoms does not have the same consequences.
Let us suppose that the molecules are constituted of only **one type** of atom. Then, the **length of the bonds** between the successive atoms should *a priori* be **constant** (or approximately constant). This imposes the distribution of θ_i angles involving the atoms, such as:

$$\theta_{i+1} - \theta_i = \theta_2 - \theta_1 \tag{4.75}$$

with i = 1,..., N.

We have used the $\theta_{N+1} = \theta_1$ convention. In other words, each atom is **uniformly** distributed on the circle, which implies:

$$\boxed{\theta_{i+1} - \theta_i = \frac{2\pi}{N}} \tag{4.76}$$

with $i = 1, ..., N$.

Concerning the positioning of the C_1 atom: if we still consider an C_2-invariant $S_N^1(\phi)$ molecule composed of only one type of atoms, we have, $\theta_{i+1} - \theta_i = \frac{2\pi}{N}$ (with $i = 1, ..., N$) and $\theta_1 = \frac{\pi}{N}$.

To prove this situation, we consider a single atom which is in relation by symmetry with its predecessor is C_1 which is referred to C_N. Now, the angle between C_N and C_1 is $2\theta_1$ and we then obtain:
$\theta_{N+1} - \theta_i = 2\theta_1 = \frac{2\pi}{N}$ or $\theta_1 = \frac{\pi}{N}$.

4.3.5 Molecules $L_N(0)$ and $L_N(\phi)$

Geometry of the molecules $L_N(\phi)$

We get N atoms on a **linear** segment and a ϕ **distribution** for the **orbitals** along the molecular chain. We consider a reference frame (x, y, z) of $\mathbb{R}^3$ such as the atoms are arranged along the z-axis with the C_1 atom at $z = 0$. We then assume $u_1 = (1, 0, 0)$.

Note that the above hypothesis is not restrictive since the data of u_1 simply depends on the reference frame (x, y, z) to localize the first orbital.

We can ask, why studying these linear molecules?

As we have seen in this manuscript, $S_N^1(\phi)$ molecules of **Möbius-type cannot be C_2 invariant**.

A **Möbius-type $S_N^1(\phi)$ molecule verifies the C_2 invariance** conditions globally at the geometric level but partially at the orbital level. Only the C_1 atom placed on the axis obstructs the global symmetry. One idea is therefore to look for a geometry that gets around this difficulty. To do so, it is necessary to divide an $S_N^1(\phi)$ molecule of Möbius type at the level of the C_1 atom which causes the problem. We then obtain a linear invariant C_2 molecule whose axis of symmetry passes through the middle of the chain and is orthogonal to it.

In the continuation of the manuscript, we study in all generality the characterization of C_2 invariant $L_N(\phi)$ molecules.

Twisted C_2 invariant $L_N(\phi)$ molecules

We look for distributions such as $L_N(\phi)$ is C_2 **invariant**.
Using the previous definitions of C_2 invariance, we adapt it to $L_N(\phi)$ molecules.

By definition, if $L_N(\phi)$ is C_2 invariant then, its symmetry axis is orthogonal to the molecule.

By proof, if the axis coincides neither with the chain or with the orthogonal direction, a given atom of $L_N(\phi)$ is moved by the action of the symmetry out of $L_N(\phi)$. It is therefore impossible.
On the other hand, if the axis coincides with the chain, then as C_1 is returned to C_1, the vector u_1 has to be returned to itself. However, by the action of C_2 it is returned to $-u_1$ which implies $u_1 = 0$. However, we have assumed $u_1 = (1, 0, 0)$ and we have a contradiction. The only possible case is when the axis of symmetry is orthogonal to the chain.

Let $L_N(\phi)$ a C_2 **invariant linear chain**. Thus, we have the following properties:

- if $N = 2n$, we get n atoms **symmetrically distributed** around the axis passing through the middle of the chain.
- if $N = 2n + 1$, then the axis passes through the atom $n + 1$ which is positioned in the **middle** of the chain with u_{n+1} carried by the axis. The $2n$ remaining atoms are symmetrically distributed on the chain around this axis.

To prove this, for reasons of symmetry, if the axis does not pass through the center of the chain, we necessarily have atoms whose reflection by the symmetry is outside the chain. We therefore assume that the axis passes through the center of the chain. If we have n atoms on one side, then their images also belong to the chain and so we have $2n$ atoms on the chain. Two cases are to be studied: the one where there is an atom on the middle of the chain and the one where there is not.
In the case where there are no atoms in the center of the chain, we necessarily have an even number

of atoms $N = 2n$. If an atom C_i is placed in the middle, then the previous proposition imposes that the associated vector u_c is situated along the axis.

We specify more precisely the action of the C_2 symmetry of axis carried by y passing through the center of the chain. For that, we note $l = Nd$ the length of the chain *(where d is the distance between two consecutive atoms)*. The atoms C_i are represented in the reference frame (x, y, z) of $\mathbb{R}^3$ whose origin is situated in C_1 and such that $x = 0, y = 0$ carries the chain. The coordinates of C_i are of the form: $(0, 0, z_i)$, $z_i = (i-1)d$, $i = 1, ..., N$.
The vectors u_i are of the form (x_i, y_i, z_i). By symmetry, the atom C_i is projected on the atom C_{N-i+1} and the vector u_i on u_{N-i+1}. But, the image of u_i is given by $(-x_i, y_i, z_{N-i+1})$. We note U_i the vectors of $\mathbb{R}^2$ given by (x_i, y_i). The angle ϕ_i is the angle between the vector U_i and U_{i+1}.

Let $L_N(\phi)$ be a C_2 **invariant linear chain**, we have :

- $\phi_1 + ... + \phi_{N-1} = \pi$
- $\phi_i = \phi_{N-i}$ *(with i = 1, ..., N-1).*

In other words, the existence of a C_2 symmetry for the molecule means that we are in a **Möbius-type** configuration.

By proof, the rotation of axis y passing through $M = (0, 0, \frac{l}{2})$ puts C_i on C_{N-i+1}. As by hypothesis $u_1 = (1, 0, 0)$, its image is the vector $(-1, 0, 0)$. Thus, we have a total rotation of angle π between the atom C_1 and C_N. As the vector u_n is obtained from u_1 by a rotation of angle $\phi_1 + ... + \phi_{N-1}$, we get $\phi_1 + ... + \phi_{N-1} = \pi$. We are then in a Möbius-type configuration.
The C_2 symmetry being an isometry, it preserves the geometrical angles (i.e. not oriented) between the vectors.
Then, we have :

$$\phi_i = \widehat{U_i, U_{i+1}} = \widehat{U_{N-i+1}, U_{N-i}} = \phi_{N-i} \tag{4.77}$$

We can specify according to the number of atoms the configuration if $N = 2n + 1$ then the molecule $L_N(\phi)$ is invariant if $\phi_1 + ... + \phi_n = \frac{\phi}{2}$.

To prove this, it is sufficient to use the previous proposition by noticing that $\phi_1 = \phi_{N-1}, ..., \phi_n = \phi_{n+1}$, or $\phi_1 + ... + \phi_N = 2(\phi_1 + ... + \phi_n) = \pi$ and $\phi_1 + ... + \phi_n = \frac{\pi}{2}$. The standard linear Möbius is obtained by assuming that a chain has $N = 2n + 1$ atoms, is of constant distribution and C_2 invariant.

If $L_N(\phi)$ is a molecule of constant distribution ϕ and C_2 invariant then $\phi = \frac{\pi}{N-1}$. If $N = 2n + 1$ then $\phi = \frac{\pi}{2n}$ and the central orbital is carried by y i.e. $\phi_1 + ... + \phi_n = \frac{\pi}{2}$.

As we can see, C_2 invariance in this type of geometry **practically imposes** a Möbius configuration.

4.3.6 Optimal distribution of $S_N^1(\phi)$ molecules

In the following, we study whether there is only an **optimal distribution** or several **distributions** for $S_N^1(\phi)$ molecules in the C_2 invariant case. We distinguish here: the **standard Möbius case** (symmetrical) and the **Möbius case** (with a variable distribution). Against all expectations, the standard Möbius distribution which is at the origin of the study of structures of this type, is not the optimal distribution.

Optimal distributions C_2 invariant

We interested in two cases $N = 3$ and $N = 4$.

$N = 3$ **case:** We consider an invariant $S_3^1(\phi)$ C_2 molecule. We get $\phi_1 = \phi_2$ and $\phi_1 + \phi_2 = \pi$ thus, $\phi_1 = \phi_2 = \frac{\pi}{2}$.

Let relax this condition and just assume that we have the $\phi_1 + \phi_2 = \pi$ relation providing that we have a Möbius type molecule.

A $\phi = (\phi_1, \phi_2)$ distribution, gives the **Hückel matrix** of the form:

$$\begin{pmatrix} x & \cos(\phi_1) & -\cos(\phi_1) \\ \cos(\phi_1) & x & \cos(\phi_2) \\ -\cos(\phi_1) & \cos(\phi_2) & x \end{pmatrix} \tag{4.78}$$

We need to have $\phi_1 + \phi_2 = \pi$, and $\cos(\phi_2) = -\cos(\phi_1)$. Note that $a = \cos(\phi_1)$, the Hückel matrix is of the form:

$$\begin{pmatrix} x & a & -a \\ a & x & -a \\ -a & -a & x \end{pmatrix} \tag{4.79}$$

We obtain the **eigenvalues**: $\boxed{\lambda_1 = \lambda_2 = a \text{ and } \lambda_3 = -2a}$

The **energy** is then given by: $\boxed{\text{E} = 2\lambda_1 + \lambda_2 = 3a \text{ if a} > 0 \text{ and } E = 2\lambda_3 + \lambda_1 = -3a \text{ if a} < 0}$

By plotting the function of ϕ_1 obtained, we see that the minimum is reached for $\phi_1 = 0$. We then obtain: among the $S_3^1(\phi)$ molecules such as $\phi_1 + \phi_2 = \pi$, the one that carries out the **minimum** of energy corresponds to the $\phi = 0$ and $\phi_2 = \pi$ distribution.

In other words, the **optimal distribution is not the Möbius distribution**.

$N = 4$ **case:** We consider the $S_4^1(\phi)$ molecule as:

$$\phi_1 = \phi_3 \tag{4.80}$$

and,

$$\phi_1 + \phi_2 + \phi_3 = \pi \tag{4.81}$$

The **Hückel matrix** is given by:

$$\begin{pmatrix} x & \cos(\phi_1) & 0 & -\cos(\phi_1) \\ \cos(\phi_1) & x & \cos(\phi_2) & 0 \\ 0 & \cos(\phi_2) & x & \cos(\phi_3) \\ -\cos(\phi_1) & 0 & \cos(\phi_3) & x \end{pmatrix} \tag{4.82}$$

Symmetry **constraints** gives:

$\cos(\phi_3) = \cos(\phi_1)$ and $\cos(\phi_2) = \cos(\pi - 2\phi_1) = -\cos(2\phi_1) = 1 - 2(\cos(\phi_1))^2$.

By posing $a = \cos(\phi_1)$, we get the simplified Hückel matrix:

$$\begin{pmatrix} x & a & 0 & -a \\ a & x & 1-2a^2 & 0 \\ 0 & 1-2a^2 & x & a \\ -a & 0 & a & x \end{pmatrix} \tag{4.83}$$

Note $\delta(a) = 4a^4 - 4a^3 + a^2 + 2a + 1$.

Then, the **eigenvalues** are given as:

$$\boxed{\begin{array}{rcl} \lambda_{1,\pm} & = & \frac{1}{2}\left(2a^2 + a - 1 + \pm\sqrt{\Delta(a)}\right) \\ \lambda_{2,\pm} & = & -\frac{1}{2}\left(2a^2 + a - 1 - \pm\sqrt{\Delta(a)}\right) \end{array}} \tag{4.84}$$

We have the relations $\lambda_{2,+} = -\lambda_{1,-}$ and $\lambda_{2,-} = -\lambda_{1,+}$. It is sufficient to trace $\lambda_{1,\pm}$ to have an idea of the energies:

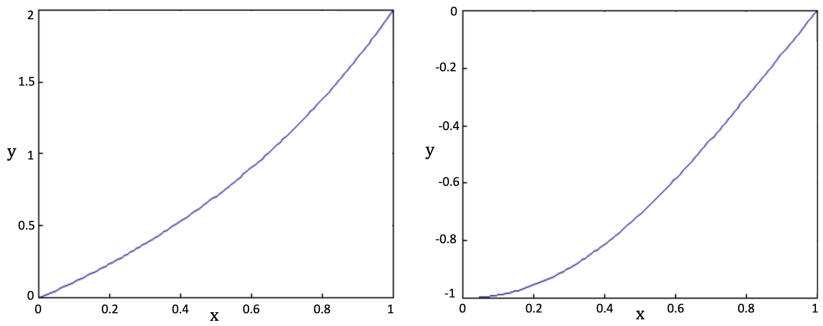

Figure 4.15: Representations of the $\lambda_{1,+}$ and $\lambda_{1,-}$ energy solutions

The **energy** of the molecule is given by:

$$\boxed{E(a) = 2\lambda_{2,-} + 2\lambda_{1,-} = -2\sqrt{\Delta(a)}} \tag{4.85}$$

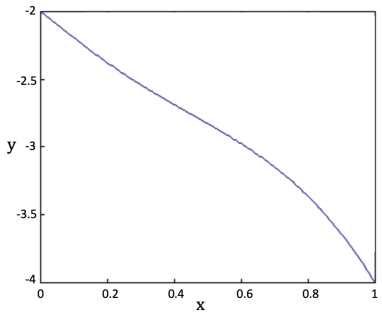

Figure 4.16: Representations of the energy of a Möbius-C_2 invariant

By minimization, we obtain: for $N = 4$, the **optimal distribution** in the case of a C_2 invariant molecule is given by $\phi_1 = \phi_3 = 0$ and $\phi_2 = \pi$.

For proof, the graph of the function shows that the minimum is reached for $a = 1$ which corresponds to $\phi_1 = 0$. The symmetry conditions then imply $\phi_3 = 0$ and then $\phi_2 = \pi$. This is very different from the Möbius type configurations. But, the energy of such a configuration is -4 which corresponds to the **standard Möbius**.

Optimal Möbius and symmetric Möbius distributions

The results of **optimality** with more or less constraints in the class of Möbius-type distributions are as follows:

a distribution $(\phi_1, ..., \phi_{2n+2})$ is considered as Möbius if:

$$\boxed{\phi_1 + ... + \phi_{n+1} = \frac{\pi}{2}} \tag{4.86}$$

$$\boxed{\phi_{n+2} + ... + \phi_{2n+2} = \frac{\pi}{2}} \tag{4.87}$$

A **Möbius distribution** is defined as **symmetric** if we have:

$$\boxed{\phi_i = \phi_{2n+2-i+1}} \tag{4.88}$$

with i = 1, ..., n+1.

We remind the schematic representation of a **symmetric Möbius** (standard) configuration:

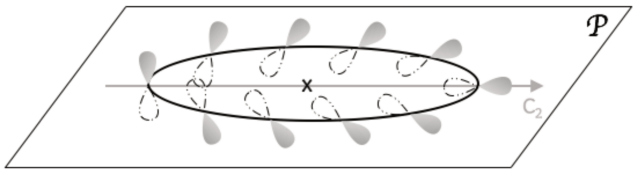

Figure 4.17: Representation of a symmetric Möbius configuration

Symmetrical Möbius $N = 4$**:** In this case, we have: $\phi_1 + \phi_2 = \frac{\pi}{2}$ and $\phi_3 = \phi_2$.

As $\cos(\frac{\pi}{2} - \phi_1) = \sin(\phi_1)$, the **Hückel matrix** is only expressed in terms of ϕ_1:

$$\begin{pmatrix} x & \cos(\phi_1) & 0 & -\cos(\phi_1) \\ \cos(\phi_1) & x & \sin(\phi_1) & 0 \\ 0 & \sin(\phi_1) & x & \sin(\phi_1) \\ -\cos(\phi_1) & 0 & \sin(\phi_1) & x \end{pmatrix} \tag{4.89}$$

As $\phi_1 \in [0, \frac{\pi}{2}]$, we get $\sin(\phi_1) = \sqrt{1 - \cos^2(\phi_1)}$.

By posing $a = \cos(\phi_1) \in [0, 1]$, we have the matrix:

$$\begin{pmatrix} x & a & 0 & -a \\ a & x & \sqrt{1-a^2} & 0 \\ 0 & \sqrt{1-a^2} & x & \sqrt{1-a^2} \\ -a & 0 & \sqrt{1-a^2} & x \end{pmatrix} \tag{4.90}$$

The **eigenvalues** are given as:

$$\boxed{\lambda_\pm = \pm\sqrt{2a}} \tag{4.91}$$

$$\boxed{\mu_\pm = \pm\sqrt{2}\sqrt{1-a^2}} \tag{4.92}$$

In terms of **degeneracy**, for $N = 4$, a Möbius system is degenerate if and only if it is a standard Möbius with $\phi\frac{\pi}{4}$.

For proof, it is necessary to solve the equation $a = \sqrt{1-a^2}$ for $a \in [0, 1]$. We obtain $a = \frac{1}{\sqrt{2}}$ which corresponds to $\phi_1 = \frac{\pi}{4}$.

The **energy** of the molecule is:

$$\boxed{E(a) = -2\sqrt{2}a - 2\sqrt{2}\sqrt{1-a^2} = -2\sqrt{2}(\cos(\phi_1) + \sin(\phi_1))} \tag{4.93}$$

As $E'(\phi_1) = -2\sqrt{2}(-\sin(\phi_1) + \cos(\phi_1))$, the extremums are situated on $\cos(\phi_1) = \sin(\phi_1)$, then, $\phi_1 = \frac{\pi}{4}$ because $\phi_1 \in [0, \frac{\pi}{2}]$.

It is a minimum because $E''(\phi_1) = -E(\phi_1)$ then, $E''(\frac{\pi}{4}) = 4 > 0$.

Thus, we have: for $N = 4$, the **optimal distribution** among the symmetrical distributions of Möbius type is given by the **standard Möbius**.

Möbius case $N = 4$: In the Möbius case, we have the **Hückel matrix** as:

$$\begin{pmatrix} x & \cos(\phi_1) & 0 & -\cos(\phi_1) \\ \cos(\phi_1) & x & \sin(\phi_1) & 0 \\ 0 & \sin(\phi_1) & x & \cos(\phi_3) \\ -\cos(\phi_1) & 0 & \cos(\phi_3) & x \end{pmatrix} \tag{4.94}$$

By posing $a = \cos(\phi_1)$ and $b = \cos(\phi_3)$, the matrix is:

$$\begin{pmatrix} x & a & 0 & -a \\ a & x & \sqrt{1-a^2} & 0 \\ 0 & \sqrt{1-a^2} & x & b \\ -a & 0 & b & x \end{pmatrix} \tag{4.95}$$

The **eigenvalues** are given by:

$$\boxed{\lambda_\pm = -\frac{\sqrt{2}}{2}\sqrt{1+a^2+b^2 \pm \sqrt{\Delta}}, \quad \mu_\pm = \frac{\sqrt{2}}{2}\sqrt{1+a^2+b^2 \pm \sqrt{\Delta}}} \tag{4.96}$$

where,

$$\Delta = 5a^4 - 2a^2b^2 - 8a^2b\sqrt{1-a^2} - 2a^2 + (1+b^2)^2 \tag{4.97}$$

The molecule **energy** is:

$$\boxed{E(a,b) = -\sqrt{2}\left[\sqrt{1+a^2+b^2+\sqrt{\Delta}} + \sqrt{1+a^2+b^2-\sqrt{\Delta}}\right]} \tag{4.98}$$

If we set $b = 1$, we get the energy $E(a, 1)$:

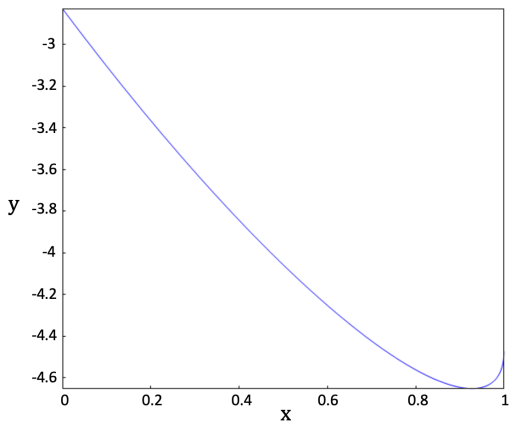

Figure 4.18: Representation of the energy E(a, 1) for a Möbius case

We note that on the section in $b = 1$ the energy increases, but in the direction of b the energy is always decreasing as we can see on the following figure:

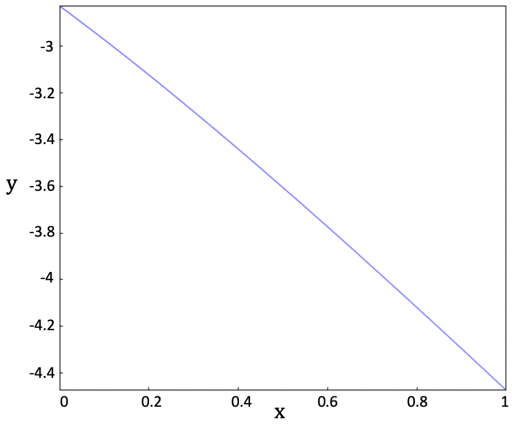

Figure 4.19: Representation of the energy E(a, b) for a Möbius case

We therefore expect to obtain a minimum of the energy for a value of $b = 1$ and a value of a close but different from 1. This is what the research of the minimum proves.

For $N = 4$, the **Möbius-type optimal distribution** is given by $\phi_1 = 0.3831$ rad, $\phi_2 = \frac{\pi}{2} - \phi_1$, $\phi_3 = 0$ and $\phi_4 = \frac{\pi}{2}$.

In fact for $E(a, b)$, a and $b \in [0, 1]$ the minimum in $a = 0.9275$ and $b = 1$ which is equal to $\phi_1 = 0.3831$ rad and $\phi_3 = 0$ rad, thus we understand the result.

The angle ϕ_1 is about 21.951°. The energy of the optimal Möbius distribution is -4.6513 u.a which is quite below the energy of the symmetric Möbius which is -4 u.a.

Note that unlike the symmetric Möbius case, the optimal Möbius case is non-degenerate.

4.3.7 Distribution of an $L_N(\phi)$ molecule equivalent to a $S_N^1(\phi_M)$ molecule

In this section, we study the distribution of an $L_N(\phi)$ molecule equivalent to a standard Möbius-type $S_N^1(\phi_M)$ molecule. In other words, we consider the **effect of imposing the C_2 invariance** condition on the description of the molecule. In this manuscript, obtaining a C_2 invariant representation complicates the shape of the distribution. From a uniform distribution for the $S_N^1(\phi_M)$ Möbius case, we progress to an irregular distribution for the equivalent $L_N(\phi)$.
A precise description of this distribution is given for any N. We also study the asymptotics of these distributions, which corresponds to the structure of an infinite linear chain.

Notion of equivalent molecule

The problem of **equivalence** is not easy because the notion requires a formal definition which is not *a priori* available in the literature. Before giving the definition that we will use, we will take **classical examples** as the conjugated polyenes.

In the case of a **planar molecule**, we take into account the separation between the π and σ-systems which is possible. The π-system is constituted by the set of MOs said to be **antisymmetric** with respect to the plane of the molecule and each carbon atom participates in its formation via a single p_z-orbital (if x and y constitute the molecular plane) (chap. 9 [11]).

Equivalence of polygonal H_n and cyclic C_nH_n: For $n \geq 3$, the **linear** molecules H_n and **linear** C_nH_{n+2} or **cyclic** C_nH_n are equivalent in the following meaning:

- they have the same symmetry group,
- the coefficients of the MOs decomposition of H_n according to the $1s_H$ orbitals of each hydrogen atom are the same as the coefficients of the MO decomposition of C_nH_n in the π-system.
- the relative energy of the π-MOs of C_nH_n is equal to the model system H_n.

In the linear case H_n, the notion of equivalence changes slightly.

(Weak) equivalence of linear H_n and linear C_nH_{n+2}: For $n \geq 3$, the **linear** H_n and **linear** C_nH_{n+2} molecules are equivalent as:

- the coefficients of the MOs decomposition of H_n according to the $1s_H$ orbitals of each hydrogen atom are the same as the coefficients of the MOs decomposition of C_nH_n in the π system.
- the relative energy of the π-MOs of C_nH_n is equal to the H_n model system.

This weak equivalence is therefore about the fact that the molecule has not conserved the symmetry group of the initial molecule. Nevertheless, the MOs of a "hypothetical" linear version of C_nH_{n+2} differ slightly from those of C_nH_{n+2}. We can then, reason on an "ideal" linear version of C_nH_{n+2} and thus, establish the "usual" equivalence of the molecules.

We can now specify the notion of **equivalence** that we will use in the rest of the manuscript.

Equivalence of a molecule M_1 and a molecule M_2: Let M_1 be a molecule of symmetry group G_1 and M_2 a molecule of symmetry group G_2. Let G be a mutual subgroup of G_1 and G_2.
We impose that M_1 is equivalent to M_2 modulo G if:

- the coefficients of the MOs decomposition of M_1 according to the orbitals of each atom of M_1 are the same as the coefficients of the MOs decomposition of the molecule M_2 in the π-system.
- the relative energy of the π-MOs of M_2 is equal to that of its model system M_1.

In the continuation, we investigate equivalent molecules and study what changes in the deformation of the adopted geometry.

4.3.8 Equivalence between $S_N^1(\phi_M)$ and $L_N(\phi)$

The issue that we study here, is to identify a linear chain $L_N(\phi)$ that is equivalent to a Möbius-type $S_N^1(\phi_M)$ molecule. As we have already indicated, it is sufficient to consider the coefficients obtained in the decomposition of the $S_N^1(\phi)$ molecular orbitals and to assume that they are also obtained in the $L_N(\phi)$ case. The question is then to know how the ϕ distribution will diverge from the standard Möbius distribution on $L_N(\phi)$.

Properties of the coefficients a_n:

Let a **linear chain** of atoms numbered from 1 to $N+1$. We identify an atom of the chain by an integer n between 1 and $N+1$. The following calculations depend on an integer k. We adopt the convention: a quantity q associated to the atom n, naturally depends on k and N and the complete notation is then: $q_n(N,k)$.

We define the family of coefficients $\{a_n\}_{n=1,...,N}$ and $\{b_n\}_{n=1,...,N}$ given as:

$$\boxed{a_n = \sqrt{\frac{2}{N+1}} \sin\left(n\frac{k\pi}{N+1}\right)} \tag{4.99}$$

and

$$\boxed{b_{n+1} = a_n} \tag{4.100}$$

$n = 1, ..., N$ *and* $b_1 = 0$.

These coefficients have symmetry properties that explain the behavior of the angles for the orbitals along the molecular chain.

We get for all $l = 1, ..., N$, the symmetry relation:

$$\boxed{a_{N-(l-1)} = (-1)^{k+1} a_l} \tag{4.101}$$

and

$$\boxed{b_{N+1-(l-1)} = (-1)^{k+1} b_{l+1} = (-1)^{k+1} a_l} \tag{4.102}$$

For proof, we have:

$$\begin{aligned} a_{N-(l-1)} &= \sqrt{\frac{2}{N+1}} \sin\left((N+1-l))\frac{k\pi}{N+1}\right) \\ &= \sqrt{\frac{2}{N+1}} \left[\sin(k\pi)\cos\left(l\frac{k\pi}{N+1}\right) - \cos(k\pi)\sin\left(l\frac{k\pi}{N+1}\right)\right] \\ &= \sqrt{\frac{2}{N+1}}(-1)^{k+1}\sin\left(l\frac{k\pi}{N+1}\right) = (-1)^{k+1} a_l \end{aligned} \tag{4.103}$$

We have the following relations for $N = 4$:

- if k is **odd**, then $a_1 = a_4$ and $a_2 = a_3$ and of course $a_5 = 0$
- if k is **even**, then $a_1 = -a_4$ and $a_2 = -a_3$ and always $a_5 = 0$

In the case of a chain of **infinite length**, the previous results are expanded by periodicity in the structure, i.e. the symmetry is found at a multiple of $N + 1$ in the coefficients.

Torsion angle and properties:

The **vector** associated to the atom numbered n is defined by:

$$u_n = \frac{1}{\sqrt{2}} \begin{pmatrix} b_n \\ a_n \end{pmatrix} \tag{4.104}$$

Let us remark for more details, that the expression of u_n represents the decomposition of the associated MO according to the local basis used in each atom. Moreover, we consider only the contribution carried by the p_x and p_y orbitals (along the chosen axes), which corresponds to a part located only in the plane.

We consider as reference vector u_1 given by $\sqrt{2}u_1 = (0, a_1)$, and we observe the **angle** formed by the vector u_n with u_1 noted $\phi_{1,n}$. A simple calculation gives the expression of $\phi_{1,n}$.

The angle $\phi_{1,n}$ has for expression:

$$\boxed{\phi_{1,n} = \arccos\left(\epsilon(a_1)\epsilon(a_n)\frac{|\alpha_n|}{\sqrt{1+\alpha_n^2}}\right)} \tag{4.105}$$

where $\epsilon(a_1)$ and $\epsilon(a_n)$ give the sign of a_1 and a_n respectively and α_n is given by:

$$\alpha_n = \frac{a_n}{b_n} \tag{4.106}$$

The proof of the expression of the angle $\phi_{1,n}$ is given in Appendix 2 section 21.
We can note some points about the signs of a_1 and a_n.

The sign of a_1 is positive if:

$$(N+1)2l \leq k \leq (N+1)(1+2l) \tag{4.107}$$

for any integer $l \in \mathbb{N}$.

We notice by eq. 4.107, when N tends to infinity, the condition will always be verified and the sign of a_1 will therefore not intervene. This will also be true for $0 \leq k \leq (N+1)$ which includes for example the case $k = 3$ when $N = 4$ studied by the research team of R. Hoffmann [9].

The situation is more complicated for a_n. The positivity condition which depends explicitly on k is:

$$(N+1)2l \leq nk \leq (N+1)(1+2l) \tag{4.108}$$

We can say that the observable angles are obtained from the **family of angles**:

$$\boxed{\phi_n = \arccos\left(\frac{|\alpha_n|}{\sqrt{1+\alpha_n^2}}\right)} \tag{4.109}$$

The following formula (eq. 4.110) shows that the angles can be obtained from the ϕ_n family, optionally adding the family of conjugate angles $\pi - \phi_n$:

$$\arccos(-x) = \pi - \arccos(x) \tag{4.110}$$

In order to analyze how the angles are distributed, we prove some properties of the vectors u_n.

For l = 1,..., N+1 we have:

$$\|u_{N+1-(l-1)}\| = \|u_l\| \tag{4.111}$$

The proof of this relation is based on the fact that (except for the sign), we have:

$$a_{N+1-(l-1)} = (-1)^{k+1}a_{l-1} = (-1)^{k+1}b_l \tag{4.112}$$

$$b_{N+1-(l-1)} = (-1)^{k+1}b_{l+1} = (-1)^{k+1}a_l \tag{4.113}$$

and then the vector $u_{N+1-(l-1)}$) is obtained from u_l by axial symmetry $y = x$ and multiplication by $(-1)^{k+1}$ gives:

$$u_{N+1-(l-1)} = (-1)^{k+1}\frac{1}{\sqrt{2}}\begin{pmatrix} a_l \\ b_l \end{pmatrix} \tag{4.114}$$

From the previous result we deduce symmetries on the distribution of angles between ϕ_1 and ϕ_{N+1}.

Precisely, noting by $\phi_{l,l+1}$ the angle between u_l and u_{l+1} we get for $l = 1, ..., N$:

$$\phi_{l,l+1} = \phi_{N+1-l,N+1-(l-1)} \tag{4.115}$$

The proof of this expression relies on the symmetry property of the coefficients given in Appendix 2 section 22.

Some examples with $N = 4$ and $k =$ 1, 2, 3, 4

In the following, we show how the **parity** on k affects the **arrangement of the orbitals** along the chain. We consider the **simplest** cases: $N = 4$ and $k = 1$, $k = 2$, $k = 3$ and $k = 4$.

Case $N = 4$ and $k = 1$: In this situation, we have: $a_1 = 0.37$ and $a_2 = 0.6$ and by the relations: $a_3 = a_2$ and $a_4 = a_1$.

The angle between the vector $u_1 = (0, a_1)$ and $u_5 = (b_5, 0) = (a_4, 0) = (a_1, 0)$ is 90°.

We find via the symmetry relations on the angles: $\phi_{1,3} = \frac{\phi_{1,5}}{2} = 45°$ which is the analog of the symmetry of the **even** case showing the angle of 135°.

By calculations: $\phi_{1,2} = 31.7°$, then, by using the symmetrical relations: $\phi_{1,4} = 2\phi_{1,3} - \phi_{1,2} = 58.3°$.

Case $N = 4$ and $k = 2$: In this case, we have : $a_1 = 0.60$ and $a_2 = 0.37$ which gives : $a_3 = -a_2$ and $a_4 = -a_1$.

The angle between the vector $u_1 = (0, a_1)$ and $u_5 = (a_4, 0) = (-a_1, 0)$ is 270°.

The previous relations imply that: $\phi_{1,2} = \phi_{4,5}$ and $\phi_{2,3} = \phi_{3,4}$.

As $\phi_{1,5} = \phi_{1,2} + \phi_{2,3} + \phi_{3,4} + \phi_{4,5} = 2(\phi_{1,2} + \phi_{2,3})$, then, $\phi_{1,2} + \phi_{2,3} = \phi_{1,3} = 135°$.

It is necessary to calculate one of the $\phi_{1,2}$ or $\phi_{2,3}$ angles to obtain all the information.

We have $\phi_{1,2} = 58°$, thus: $\phi_{1,4} = \phi_{1,3} + \phi_{3,4} = \phi_{1,3} + \phi_{2,3} = 2\phi_{1,3} - \phi_{1,2} = 270 - 58 = 212°$.

Case $N = 4$ and $k = 3$: By setting $k = 3$, then, $a_1 = 0.60$ and $a_2 = 0.37$.

We still have : $a_4 = a_1$ and $a_3 = a_2$.

The angle $\phi_{1,5}$ is 90° but we need to understand this angle as: $360 + 90$ because following the vectors u_1 to u_5 on the trigonometric circle, we carry out a complete rotation and it is a significant difference.

In particular, when we write via the symmetrical relations: $\phi_{1,3} = \frac{\phi_{1,2}+\phi_{2,3}+\phi_{3,4}+\phi_{4,5}}{2}$, that we previously used: $\phi_{1,2}+\phi_{2,3}+\phi_{3,4}+\phi_{4,5} = \phi_{1,5}$ which is true but modulo 2π, i.e. to a certain integer number of turns.

Here: $\phi_{1,3} = \frac{360+90}{2} = 225°$. The angle $\phi_{1,2}$ gives by calculations, $\phi_{1,2} = 122°$.

We deduce, $\phi_{2,3} = \phi_{1,3} - \phi_{1,2} = 225 - 122 = 103°$, so, $\phi_{1,4} = \phi_{1,3} + \phi_{3,4} = \phi_{1,3} + \phi_{2,3} = 225 + 103 = 328°$.
We note that, $\phi_{4,5} = 360 + 90 - 328 = 122° = \phi_{1,2}$ as expected.

This situation corresponds to the case $k = 1$ but for vectors rotated by $-90°$.

Case $N = 4$ and $k = 4$: Now, let $k = 4$ then $a_1 = 0.37$; $a_2 = -0.60$; $a_4 = -a_1$, and $a_3 = -a_2$.

The angle $\phi_{1,5}$ is still 270°. Once again by following the vectors u_1 to u_5 we perform a turn of the circle and the angle $\phi_{1,3} = 315°$.

The angle $\phi_{1,2}$ is given by calculations at 148°. We then obtain: $\phi_{1,4} = \phi_{1,3} + \phi_{3,4} - 360 = 120°$.

We verify again that: $\phi_{4,5} = 270 - 122 = 148°$ is equal to $\phi_{1,2}$.

To sum up: To resume the 4 previous examples:

k	ϕ_1	ϕ_2	ϕ_3	ϕ_4	ϕ_5
1	0	32	45	58	90
2	0	58	135	212	270
3	0	122	225	328	90
4	0	148	315	122	270

Table 4.1: Overview of the angles (in degrees) of the 4 examples

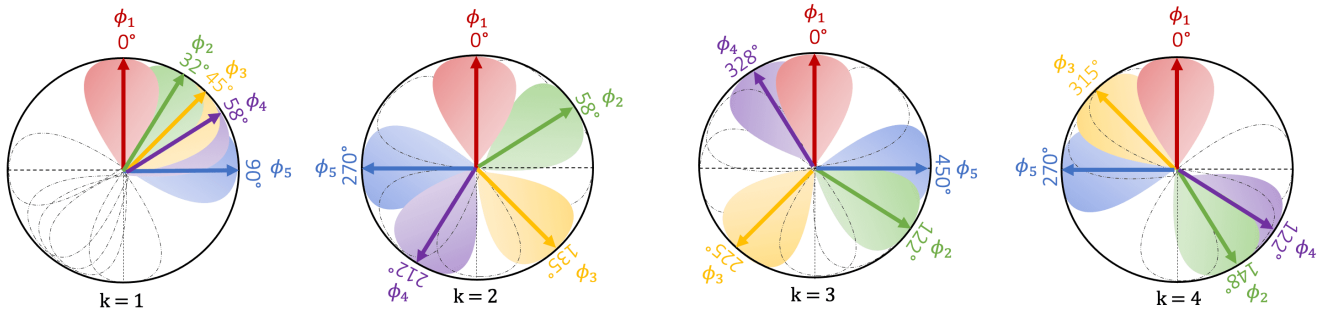

Figure 4.20: Orbital distributions for $N = 4$ and $k = 1, 2, 3, 4$

For a general remark both on the cases k even or odd. We note an asymmetry between the even and odd cases k which is always present for any value of N.

4.3.9 Asymptotic distribution of angles along a chain

Orbital cases of the form (b_n, a_n)

The angle $\phi_{1,n}$ converges for fixed n and k when N tends to infinity to the angle:

$$\boxed{\phi_{\infty,n} = \arccos\left(\frac{n}{\sqrt{n^2 + (n-1)^2}}\right)} \tag{4.116}$$

The proof is given is Appendix 2 section 23.

We note that this angle corresponds to the situation of an **infinite chain** and that it is independent of k. We obtain the following values for the atoms of the chain (with n = 1,...,7):

n	$\phi_{1,n}$
1	0
2	26.57
3	33.69
4	36.87
5	38.66
6	39.81
7	40.6

Table 4.2: Examples of angles values (in degrees) along a molecular chain

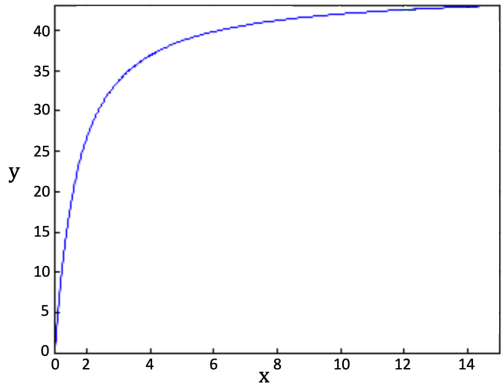

Figure 4.21: Representation of asymptotic angles

These symptomatic angles only have meaning in the case of an **infinite chain** which is a **purely abstract object**. We note a progressive stabilization around an angle of 45° which is easily proved as: the angles are accumulated when n becomes large around $\frac{\pi}{4}$.

The proof is direct,

$$\lim_{n\longrightarrow\infty} \frac{n}{\sqrt{n^2+(n-1)^2}} = \frac{1}{\sqrt{2}} \tag{4.117}$$

then,

$$\lim_{n\longrightarrow\infty} \phi_{\infty,n} = \arccos\frac{1}{\sqrt{2}} = \frac{\pi}{4} \tag{4.118}$$

Case of orbitals of the form $(b_n, -a_n)$

As in the previous case, we can introduce the family of angles which considers the fact that the sign of an is replaced by "-" in the expression:

$$\boxed{\phi_n = \arccos -\frac{|\alpha_n|}{\sqrt{1+\alpha_n^2}}} \tag{4.119}$$

4.4 Conclusion

This chapter is very dense in information. Our interest was focused on the different aspects of **aromaticity** since it is related to the reactivity of the molecule. The criteria of aromaticity are linked to the rules stated by Hückel and associated with the systems that we distinguish as **"Möbius"** and **"Hückel"**.

Generally, we have either **linear** L_N or **cyclic** S_N^1 chains, where each of these representations will have different **orbital distributions**: either **null** (0) (called ribbon or Hückel), or with **angle distribution** (ϕ) (called twisted ribbon or Möbius).
All these distributions are detailed and proven as generally as possible in order to determine the **equivalent** and most **optimal** structure depending on the **energy** parameter.

Using mathematical details on the **Hückel matrices** in each of the cyclic and linear cases, we showed how the energies of each system were determined and compared. In fact, the **energy difference** between the **cyclic** case with **null** distribution and the **Möbius** case with **electronic saturation** is **null**, which shows that the two cases are **equivalent**.
On the contrary, with the case of **electronic unsaturation**, it is more complex. The comparison takes into account δ **corrective terms**. It results that the comparison depends mainly on the **parameter N** (i.e. the number of atoms).

To be precise in the understanding of the twisted cyclic systems $S_N^1(\phi)$, we took into account the C_2 **symmetry** with a set of parametrizations, showing that the **optimal** distribution **is not** the Möbius distribution (which contradicts what is intuitively stated in the work of Hoffmann et al. [55]).
Analogously, for the linear cases L_N, the same steps are followed (determination of the energy and taking into account the symmetry). Among other things, the C_2 invariance symmetry **imposes** a configuration with **Möbius distribution**.

The notion of **equivalence** between linear and cyclic molecules is shown by different classical examples and clearly detailed to identify how the divergence between the standard Möbius distribution $S_N^1(\phi)$ and the linear case $L_N(\phi)$ is presented.

Finally, we define the properties and expression of the ϕ_n **torsion angles** for all systems as well as for infinite linear chains.

Chapter 5

Beyond aromaticity criteria - Helical states

In this chapter we go beyond the aromaticity criteria and focus on helical states. In a first approach we discuss the following points:

- *the Möbius systems following R. Hoffmann,*
- *the linear cases with cumulenes,*
- *helical molecular orbitals,*
- *molecular orbitals in even and odd cases (in terms of number of double bonds).*

Then, we expose:

- *the properties of helical states,*
- *the criteria for the existence of helices.*

All these results come from the work of R. Hoffmann [9], Solomon et al. [56], Jin et al. [57] and our preprint [44].

5.1 Möbius systems according to the study of Roald Hoffmann

In this section we refer to recent 2018 work of the Nobel prize laureate research team Roald Hoffmann which we considered as particularly interesting [9].
As we saw in the previous chapter, section 4.3.5, **Möbius systems** are based on p-orbitals where there is a **continuous overlap** (as shown figure 4.5) which forms a continuous ribbon that closes upon sign inversion. Following the discovery of these original systems in 1964 [7], other researchers such as Fisher and Kollmar in 1968 [58] and Zimmerman in 1971 [46], have shown with the theory of Hückel, that the topology of Möbius systems have a similarity of behavior with the orbitals of allene type molecules. In parallel, in 1968, Buenker, showed with *ab initio* studies of MOs, the rotation barrier of the allenes [59]. Then, in 1976 it is semi-empirical calculations which are carried out to demonstrate the optical properties of rotation of allenes [60].

As a reminder, allenic molecules are linear hydrocarbons containing only consecutive double bonds. From a reactivity point of view this type of system is more reactive than those composed by an alternation of single and double bonds. Moreover, note that the allenes display an axial chirality.

The following figure illustrates the parallel between the **fictive Möbius cyclic systems** and the **linear allene systems**. We observe the **rotation** and the change of sign of the orbitals within the systems.

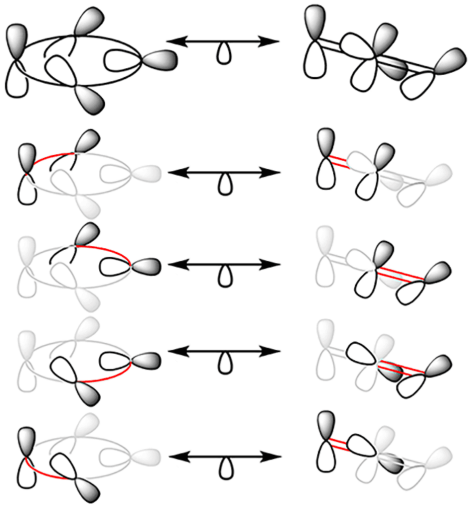

Figure 5.1: Comparison between the behavior of orbitals in Möbius ribbons and allenes (*here a cyclobutadiene and a [2]-cumulene)* [9]

On the left-hand side of the figure, we observe the **rotation** of the p-type orbitals along a Möbius cyclobutadiene. Analogously, on the right-hand side, the rotation of the orbitals of the allene, which can be described as a so-called coarctate system. The term coarctate is proposed by Herges to describe two fused π-systems (as related to the breaking and creation of bonds on one or more atoms simultaneously), an action that takes place in pericyclic reactions (alternating cyclic sequence processes) [61].

5.1.1 [n]-cumulenes : linear case

To be more precise, here, when we refer to allenic molecules, the most appropriate term is **cumulene**. As explained in the previous paragraph, the cumulenes are **linear systems** constituted exclusively of **double bonds** between the carbons and can be substituted at the end of the chain.

To detail the following figure, the molecule is composed of N **carbon atoms** sp**-hybridized** with C_0 and C_N are sp^2**-hybridized** since they are at the end of the chain. To be precise, the chain of atoms is oriented along the z-axis. We note that L_1, L_2 and R_1 and R_2 are the left and right **substituents** of the chain ends, which can simply be hydrogens but can also be more complex as we will discuss in the continuation of the manuscript.

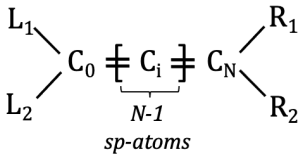

Figure 5.2: Representation of a [n]-cumulene

To complete, in terms of nomenclature we note [n]-cumulene, [n] corresponds to the number of double bonds and N the number of carbons involved in the molecule. In our study we have studied **even and odd** cumulenes i.e. composed by an **even or odd number of atoms**.

We simulated the π-system with a basis set composed by p_x and p_y-orbitals for each atom of the chain. Then, the p_z-orbitals are directed along the direction of the chain and is included in the σ-system. An illustration of this hybrid system is given in the following figure 5.3. We observe in the case of a [4]-cumulene for the HOMO-1, HOMO and LUMO, the mixing of the p_x and p_y-systems which are

at the origin of the formation of the curiosity of helical orbitals whose the detailed study is in the continuation of the manuscript.

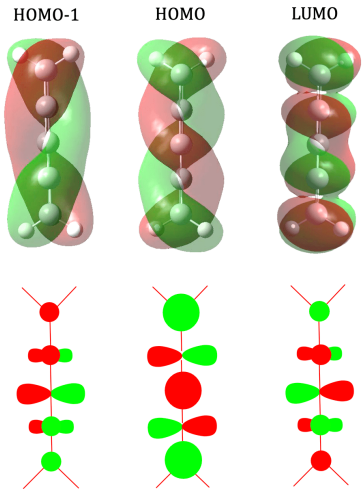

Figure 5.3: Representation of the hybrid systems at the origin of the formation of orbitals in helix *(lower part : p_x and p_y-systems are represented schematically, the green and red lobes indicate the sign - higher part: the representation of the orbitals by DFT computations)*

Concerning the **synthesis** of this type of molecule: we note that the literature is **rich** in terms of synthesis of allenes since they are useful complex molecular targets (for example: as precursor in cycloadditions, or as redox reagent) in many fields such as pharmaceuticals, nanomaterials or electronics. Among their advantages, they present fundamental properties that are interesting both for structural electronic properties and in terms of reactivity [62].
There is a great variety of [n]-cumulenes. In terms of even cumulenes it has been possible to synthesize from [4]-cumulene to metallo-[6]-cumulene. For odd cumulenes, we note synthesis up to [9]-cumulene. Substituted cumulenes have also generated a lot of interest (such as S-α,ω-dimethyl-[n]-cumulene). We quote here only some examples since we do not focus on the synthesis work [63, 64, 65, 66, 67].

It should be noted, however, by studying the cumulene litterature, Hendon et al. [63] proves a difference between the terms of allenes and cumulenes. According to them, allenes have an odd number of carbon atoms with orthogonal chain ends showing an electrohelicity (a term whose meaning will be explained in the rest of this work). On the other hand, cumulenes with an even number of carbons are planar and without orbital helicity. By misuse of language we will use the term cumulene in a generic way and will demonstrate the presence of orbital helicity in the continuation of the manuscript.

5.1.2 Helical molecular orbitals

The major curiosity for **cumulenes** is the presence of **helical frontier orbitals**. The important point is that these orbitals are **not due** to a helical molecular structure.

According to the literature, in particular the study carried out by Hoffmann et al. [9], the research team shows that cumulenes have **two perpendicular** π-systems along their molecular axis.
Thus, for **unsubstituted** [n]-cumulenes (with even [n]), the π-systems are **equivalents** and the ends chain are **perpendicular** to each other providing a D_{2d} symmetry and then, π-MOs all **degenerated**.

However, when a **substitution** is applied at the ends of the chain we observe a relaxation of the

degeneracy reducing the symmetry to C_2 resulting in a **chiral** molecule.
Notice that the same behavior is observed when a **mechanical constraint** is imposed, for example a torsion of the terminal carbons. The mechanical constraint such as setting the two ends perpendicular to each other resulting in the appearance of helical orbitals has been highlighted recently in 2013 by Hendon and Walsh research team [63]. Indeed, the forced torsion of the terminal groups lowers the symmetry of D_{2d} to D_2, which will generate **helical orbitals**.

It is particularly on the aspect of **mechanical constraint** that we have focused. We tried to obtain all possible configurations in order to achieve **helical MOs**. The final aim being to obtain **new properties** of materials since the helical MOs provide a **delocalization** of π-electrons all along the twisted chain.
It should be noted that the **electrohelicity** phenomenon shown by Hendon [63] can be discussed according to different methods, in a classical way following the Hückel theory [9] that we have seen previously (section 0.2.1) or in a more complex method from a physical point of view by the Hamiltonian [68].

Note that the phenomenon of electrohelicity is said for a system that presents perpendicular end groups and that the system shows helical frontier orbitals.

We are interested in the helical MOs specific to the **linear carbon chain** with no specific terminal substituents.

Finally, it should be noted that there are contradictions in the literature since many articles specify that the presence of helices is only visible for odd cumulenes [63]. However, we show in the continuation of the manuscript that helical MOs are present independently for the even or odd case.

Helical molecular orbitals in even and odd cases

Most publications examine several **even-odd** cases and **parallel-perpendicular** chain ends.

Publications dealing with **even systems** and **perpendicular extremities** are numerous [9, 63, 69, 70, 62, 71]. There are several examples showing that the helical behaviour is observable only when the chain ends [9] are **twisted** at a certain angle (i.e. the ends are no longer flat [63]), and others depending on the nature of the substituents of the chain ends [9, 62, 55, 71]. The substituents listed may be –dimethyl [9, 71], -dichloro [55], or -nitrogen [62]. The cumulenes studied range from $[n] = 2$ [63, 69, 62, 55, 71] to $[n] = 8$ [70]. The case mentioned by Imamura et al. [70] shows a certain influence of the angle of twist of the CH_2 end groups in the formation of helixes. The presence of non-hydrocarbon substituents provides a break in symmetry with free pairs, allowing different interactions resulting in a helical character [62]. The **even parallel** cases seem to show helixes from a certain angle or even no helix for ketone substituents [72]. According to Garner et al. [56], the axial torsion angle is a crucial factor in the constitution of helical orbitals (between 30° and 150°).

The analysis of the **odd cases** between $[n] = 3$ to $[n] = 9$ with perpendicular chain ends, shows once again the impact of the torsion angle to see the existence of helixes [70]. **Parallel cases** show the same behaviour with the presence of helix at a certain angle [9, 56] and others not [63, 55].

It is obvious that the helical shape of an electronic system will depend on the molecular symmetry. But finally, it is also true that the definition of a cylindrical helical system is quite subjective, this is why it is imperative to define parameters to quantify them and that is what we try to do in this manuscript.

5.2 Helical states

5.2.1 Properties of helical states

General case

As discussed previously (section 5.1.2), the helical MOs are visible on the [n]-cumulenes. From a general point of view, we can formalize mathematically the **criteria of appearance** of these helical systems.

Let E the energy of a molecule and z the position of the atoms on the linear chain with $z = 0$ corresponding to the left end chain, and $z = N$ the right end chain.

We define the MO as $\psi(z)$ associated to the atoms as :

$$\boxed{\psi(z) = \begin{pmatrix} \psi_x(z) \\ \psi_y(z) \end{pmatrix} = MR(z\omega)v_0} \tag{5.1}$$

v_0 a fixed two-dimensional unit vector, $\omega \in \mathbb{R}$, $R(z\omega)$ the rotation matrix of angle $z\omega$ and M a real symmetric matrix.

The helices mainly found are said to be **classical**, and are sometimes called **perfect helices** [56], but it is difficult to estimate the perfect cylindrical shape of a helix.

We can therefore define the **shape of a helix** as:

$$\boxed{\begin{array}{rcl} x(t) & = & r(t)\cos(t) \\ y(t) & = & \epsilon r(t)\sin(t) \\ z(t) & = & P(t) \end{array}} \tag{5.2}$$

with $P(t)$ a smooth increasing function and $r(t)$ an arbitrary function corresponding to a non-constant radius, so $r : \mathbb{R} \longrightarrow \mathbb{R}^+$.

The best approximation of the helix is finally obtained in a **non-linear context**, i.e. by using polynomial functions $P(t)$ and $r(t)$.

There are **different morphologies** of helical MOs. Actually, helices are not necessarily "perfect" as we will see in the continuation of the manuscript.

Distributions of angles

Let a linear chain of atoms C_i oriented according to z, we define the **distributions of angles** according to the **numerical** and **theoretical** point of view, which are respectively part of the continuous and discrete geometry.

Numerically, the distribution depends on the choice of **basis** such as $z \in$ [0, N], then, it exists the MOs $\psi(z)$ which give the **distribution** $\mathcal{D}_{Base}$ according to a chosen basis: $\{\psi(z_1)...\psi(z_N)\}$.

Theoretically, the distribution called **Hückel distribution** $\mathcal{D}_{Huckel}$, valid on each atoms, we have $\psi(C_i)$ orbitals depending on p_{xi} and p_{yi}. The Hückel distribution is such that $z = \{z_1...z_N\}$.

We can define the **distribution of a constant helix** such as:

$$\boxed{\mathcal{D}_{helix} = \{\phi(z_i) = \frac{z_i}{b}\}} \tag{5.3}$$

with b the constant pitch and i = 0,..., N.

We consider the **cumulated angle** ϕ_c as:

$$\boxed{\phi_c(i) = \sum_{1}^{i} \mid \phi(z_i) - \phi(z_{i-1}) \mid} \tag{5.4}$$

If we have $\phi_c(z_0) = 0$,

$$\phi_c(z) = \frac{1}{b} z \tag{5.5}$$

This corresponds to a straight line passing through the origin with a constant slope $\frac{1}{b}$.

We compare the set of points $\{(z_i, \phi_c(z_i))$ *(with* $i = 0, ..., N)\}$ for a given **helical distribution** with a set of helical points $(z_i, \frac{z_i}{b})$ by minimizing a parameter as:

$$L(b) = \sum_{i=0}^{n} (\phi_c(i) - f_i)^2 \tag{5.6}$$

with $f_i = \frac{z_i}{b}$ by using a **regression method** analysis to obtain a fitted straight line as:

$$\phi_c = \alpha(z - z_0) + \phi_0 \tag{5.7}$$

where $\alpha \in \mathbb{R}$ *determined following the values of* $\phi_c(z_i)$.

The shape of the line is imposed by the initial point $(z_0, \phi_c(0))$ which is the first value of the cumulative angle distribution.

Finally, the first atom is positioned at $z_0 = 0$ and $\phi_c(0) = 0$, thus, the optimization issue is reduced to:

$$\phi = \alpha z \tag{5.8}$$

Which fits the results of $\phi_c(z_i)$.

We based our work on the study carried out by the team of Solomon et al. [56], who define the **mean of the absolute deviation** as the **MAD** index. To be informative the MAD index is used to determine how much an orbital helix deviates from the so-called perfect helix. A high MAD means that the studied helix deviates strongly from a perfect helix and a low MAD value shows the MO is very close to the perfect helix.
The **mean of the absolute deviation** is given as:

$$\boxed{\mid \phi_c(z_i) - f_i \mid} \tag{5.9}$$

We give an **analytical solution** as:

$$\boxed{\alpha = \frac{\sigma(\phi_c(z), z) + \overline{\phi_c(z) z}}{\sigma^2(z)}} \tag{5.10}$$

If we have two mathematical series: $x = (x_0, ..., x_N)$ and $y = (y_0, ..., y_N)$:

$$\overline{x} = \frac{1}{N+1} \sum_{i=0}^{N} x_i \tag{5.11}$$

$$\sigma(x,y) = \sum_{i=0}^{N} \frac{(x_i - \overline{x})(y_i - \overline{y})}{N+1} \tag{5.12}$$

$$\sigma^2(x) = \sum_{i=0}^{N} \frac{(x_i - \overline{x})^2}{N+1} \tag{5.13}$$

Each of these equations represent the mean of x ($\overline{x}$), the covariance of x and y ($\sigma(x,y)$) and the variance of x ($\sigma^2(x)$) respectively.

We also defined the **correlation factor** as:

$$\boxed{\rho(x,y) = \frac{\sigma(x,y)}{\sigma(x)\sigma(y)}} \tag{5.14}$$

By linear regression, we have the approximation approach such that $\rho(\phi_c(z),z)$, $\rho^2(\phi_c(z),z)$ must be close to 1.

For reminder, to determine the quality of a measurement we use linear regression by approximating a straight line, and the correlation coefficient has to be greater than 0.95 which represents a very good approximation.

We therefore propose an **indicator of helicity** (**HEL**) such as:

$$\boxed{HEL = \rho(\phi_c(z),z)} \tag{5.15}$$

We prove by this indicator that the correlation coefficient is sufficiently well-known to be easily interpreted even if it is subject to discussion, is well documented. Moreover, the values of HEL can easily be compared to the data of linear regressions since HEL $\in [0,1]$. This is more convenient than the MAD index since the MAD values can be arbitrary which is not obvious to interpret and compare.

Distribution of angles for twisted [n]-cumulenes

We studied the angle distribution of p-orbitals along $[n]$-cumulene twisted with a Hückel distribution. The twisted term used here corresponds to a rotation between 0 and $\frac{\pi}{2}$ of one of the chain ends. Indeed, we have shown before in the manuscript that helical MOs are visible in the case of rotation of one of the extremities of the chain (seen in section 5.1.2).

Simple example: First of all, let us take an simple example for the angle distributions obtained for equivalent [4]-cumulene version of Möbius systems when $n = 1$ is:

$$\mathcal{D}_{4,1} = \{0, 32, 45, 58, 90\} \tag{5.16}$$

The associated cumulated distribution is:

$$\phi_c = \{0, 32, 77, 135, 225\} \tag{5.17}$$

The "best" perfect helix fitting this set of data and the correlation factor which shows very good agreement are:

$$\phi(z) = 49.7z \tag{5.18}$$

$$\rho(z, \rho_c(z)) = 0.98872 \tag{5.19}$$

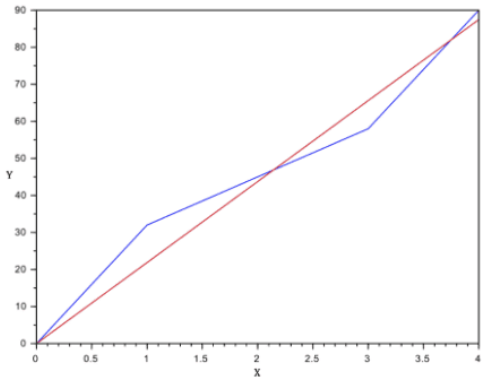

Figure 5.4: Best fitted helix for distribution of equivalent [4]-cumulene version of Möbius system and n=1

The same approach can be done for the distribution of the equivalent [4]-cumulene version of Möbius system when n=2. In this situation, the distribution is:

$$\mathcal{D}_{4,2} = \{0, 58, 135, 212, 270\} \tag{5.20}$$

The associated cumulated distribution is given by:

$$\phi_c = \{0, 58, 193, 405, 675\} \tag{5.21}$$

The "best" perfect helix fitting and the correlation factor of this set of data which again show a very good fit are:

$$\phi(z) = 145.3z \tag{5.22}$$

$$\rho(z, \rho_c(z)) = 0.97942 \tag{5.23}$$

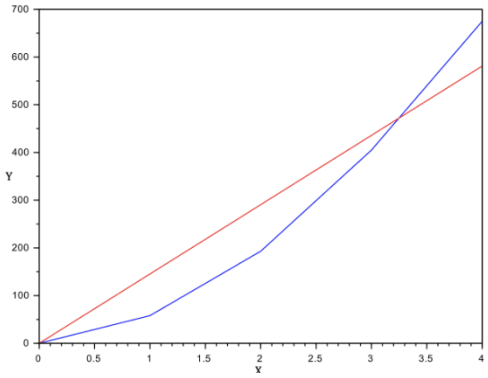

Figure 5.5: Best fitted helix for distribution of equivalent [4]-cumulene version of Möbius system and n=2

Hückel distribution of $0 < \theta < \frac{\pi}{2}$: The Hückel distribution for $[n]$-cumulene twisted is obtained by **vectors** as:

$$\psi_n(z) = a_n R\left(\frac{\theta}{2}\right) D_{\frac{b_n}{a_n}} R(k_n z + \delta_n) \tag{5.24}$$

with $D_{\frac{b_n}{a_n}} : \mathbb{R}^2 \longrightarrow \mathbb{R}^2$.

$D_{\frac{b_n}{a_n}}$ corresponds to the **dilatation map of weight** $\frac{b_n}{a_n}$ defined as $(x, y) \longrightarrow (x, \frac{b_n}{a_n} y)$.

δ_n and k_n are given as:

$$\tan(\delta_n) = -\frac{a_n}{b_n}\tan\left(\frac{\theta}{2}\right) \tag{5.25}$$

$$\sin^2((N+1)k_n) = \cos^2(\theta)\sin^2(k_n) \tag{5.26}$$

with $1 \leq n \leq 2N$.

Generally, it is not possible to obtain angle distribution values except in the cases $\theta = 0$ and $\theta = \frac{\pi}{2}$, one can only give indications on the structure with the following.

We can then define the **Hückel distribution** $\mathcal{D}_{Huckel}$ according to N and θ:

$$\boxed{\phi(N-z) - \phi\left(\frac{N}{2}\right) = \phi\left(\frac{N}{2}\right) - \phi(z)} \tag{5.27}$$

with $z = 0, ..., N$.

This angle distribution has an axis of symmetry along the $\phi\left(\frac{N}{2}\right)$ vector.

For $\phi(0) = 0$ and $\phi(N) = \theta$, this axis will be at $\frac{\theta}{2}$ or $\frac{\theta}{2} + \frac{\pi}{2}$ in accordance with the number of turns and the direction of winding of the helix.

Finally, the distribution of angles obtained is from a **circular distribution** as:

$$\phi_n(z) = k_n z + \delta_n \tag{5.28}$$

Note that with respect to zero, the distribution is:

$$\boxed{\phi_n(N-z) = -\phi_n(z)} \tag{5.29}$$

with $z = 0, ..., N$.

We know that **rotations** are **angle-preserving** transformations, but **dilatations do not preserve the angles** but preserve the structure of a **circular distribution**.
In our case, the circular distribution provides the $\mathcal{D}_{Huckel}(\theta)$ by dilatation $(D\frac{b}{a})$ along the vectors : $v_n(z) = ae^{i\phi_n(z)}$ with $i^2 = -1$ followed by a rotation of $e^{i\frac{\theta}{2}}$.

The previous observation can be justified by the work of Gunasekaran et al. [68] with circular polarized MOs. They increase the coupling between the terminal p-orbitals from t to $\sqrt{2}t$ rather than a constant coupling between atoms of the molecule and thus consider a modified Hückel matrix.

The **mathematical analysis** is simplified for distributions $\phi_n(0) = 0$ and $\phi_n(N) = \theta$:

$$\phi_n(z) = k_n z \tag{5.30}$$

$$Nk_n = \begin{cases} \theta + m\pi, & n = 2m+1 \\ m\pi - \theta, & n = 2m \end{cases} \tag{5.31}$$

with $z = 1, ..., N-1$.

We have for $z \in \{1, .., N-1\}$:

$$\phi_n(z) = Nk_n\frac{z}{N} = \begin{cases} (\theta + m\pi)\frac{z}{N}, & n = 2m+1 \\ (m\pi - \theta)\frac{z}{N}, & n = 2m \end{cases} \tag{5.32}$$

We define for $z = \frac{N}{2}$:

$$\phi_n\left(\frac{N}{2}\right) = \begin{cases} (\theta + m\pi)\frac{1}{2}, & n = 2m+1 \\ \\ (m\pi - \theta)\frac{1}{2}, & n = 2m \end{cases} \tag{5.33}$$

The **Hückel distribution** $\mathcal{D}_{Hckel}(\theta)$ satisfies:

$$\boxed{\phi_n\left(\frac{N}{2}\right) - \phi_n(z) = \begin{cases} (\theta + m\pi)\left(\frac{1}{2} - \frac{z}{N}\right), & n = 2m+1 \\ \\ (m\pi - \theta)\left(\frac{1}{2} - \frac{z}{N}\right), & n = 2m \end{cases}} \tag{5.34}$$

and,

$$\boxed{\phi_n(N-z) - \phi_n(\frac{N}{2}) = \begin{cases} (\theta + m\pi)\left(1 - \frac{z}{N} - \frac{1}{2}\right), & n = 2m+1 \\ \\ (m\pi - \theta)\left(1 - \frac{z}{N} - \frac{1}{2}\right), & n = 2m \end{cases} = \phi_n\left(\frac{N}{2}\right) - \phi_n(z)} \tag{5.35}$$

Hückel distribution in the cases $\theta = 0$ or $\theta = \frac{\pi}{2}$: As explained, the helical MOs are only observed when we impose a **deformation constraint or substituents** at the ends of the $[n]$-cumulenes. Thus, when the constraint is at $\theta = 0$ or $\frac{\pi}{2}$ there are no helices. In reality, we know that the helices are due to the coupling of the π_x and π_y systems in a C_2 symmetry. We note that the distribution in a **cyclic Möbius case is quasi-perfect**, but this is not valid for its $[n]$-cumulene analogue.

Case $\theta = \frac{\pi}{2}$: The p_x part is defined from $z = 1$ to $z = N$ and, the p_y part from $z = 0$ to $z = N-1$.

The **coefficients** related to the wave function for $z = 1$ to N are given as:

$$c_{N,n}(z) = \sqrt{\frac{2}{N+1}} a_{N,n}(z) \tag{5.36}$$

with $a_{N,n}(z) = \sin(k_n z)$ *and* $z = 1, ..., N$.

and with:

$$k_n = \frac{n\pi}{N+1} \tag{5.37}$$

with $1 \leq n \leq N$.

In this case we have a **Hückel matrix** implying the coefficients $c_x(z)$ and $c_y(z)$:

$$c_x(z) = \sqrt{\frac{2}{N+1}} a_{N,n}(z) \tag{5.38}$$

with $z = 1, ..., N$.

$$c_y(z) = \sqrt{\frac{2}{N+1}} a_{N,n}(z+1) \tag{5.39}$$

with $z = 0, ..., N-1$.

We notice that $c_x(0) = 0$ and $c_y(N) = 0$.

For proof we refer to [73], if we get a classical $N \times N$ matrix corresponding to a chain of atoms as:

$$A_N(w) = \begin{pmatrix} w & 1 & 0 & \dots & 0 \\ 1 & w & \ddots & \ddots & \vdots \\ 0 & \ddots & \ddots & \ddots & 0 \\ \vdots & & & & 1 \\ 0 & \dots 0 & & 1 & w \end{pmatrix} \tag{5.40}$$

with $w = \frac{\alpha-\lambda}{\beta}$ *and* $S_N(\lambda)$ *the secular determinant of the Hückel matrix* H_N *as* $S_N(\lambda) = det(H_N - \lambda Id)$ *(with Id the identity matrix).*

Then, the **secular determinant** is:

$$S_N(\lambda) = \beta^N \left(P_N(w)\right)^2 \tag{5.41}$$

with $P_N(w) = det(A_N(w))$.

The solutions of $S_N(\lambda)$ are **symmetric** and **doubly-degenerated** such as:

$$\boxed{\lambda_n = \alpha + 2\beta \cos\left(k_{N,n}\right)} \tag{5.42}$$

with $k_{N,n} = \frac{n\pi}{N+1}$.

In the case where C_2 **symmetry is reached**, we have wave functions $\psi_{+,n}$ and $\psi_{-,n}$ that can be described according to the direction of winding of the helix respectively to the right $(+)$ and to the left $(-)$:

$$\boxed{\psi_{+,n} = \frac{1}{\sqrt{2}}(c_y(z)p_y + c_x(z)p_x)} \tag{5.43}$$

$$\boxed{\psi_{-,n} = \frac{1}{\sqrt{2}}(c_y(z)p_y - c_x(z)p_x)} \tag{5.44}$$

If we focus on the $\psi_{+,n}$, $\psi_n(z)$ is:

$$\psi_n(z) = \sqrt{\frac{2}{N+1}} \begin{pmatrix} a_{N,n}(z) \\ a_{N,n}(z+1) \end{pmatrix} \tag{5.45}$$

Then, we deduce $\psi_n(N-z)$:

$$\psi_n(N-z) = \sqrt{\frac{2}{N+1}} \begin{pmatrix} a_{N,n}(N-z) \\ a_{N,n}(N-z+1) \end{pmatrix} \tag{5.46}$$

For more details, *for z = 0,...,N and* $N \geq 1$, we can prove that a_n:

$$\boxed{a_{N,n}(N-z+1) = (-1)^{n+1} a_{N,n}(z)} \tag{5.47}$$

We know that:

$$a_n(z) = \sin\left(\frac{zn\pi}{N+1}\right) \tag{5.48}$$

Then,

$$\begin{aligned} a_n(N-z+1) &= \sin\left((N-z+1)\tfrac{n\pi}{N+1}\right) \\ &= \sin\left(\tfrac{(N+1)n\pi}{N+1} - \tfrac{zn\pi}{N+1}\right) \\ &= \sin(n\pi)\cos\left(\tfrac{zn\pi}{N+1}\right) - \cos(n\pi)\sin\left(\tfrac{zn\pi}{N+1}\right) \\ &= -\cos(n\pi)\sin\left(\tfrac{zn\pi}{N+1}\right) = (-1)^{n+1}a_n(z) \end{aligned} \tag{5.49}$$

Thus,

$$\psi_n(z) = (-1)^{n+1}\sqrt{\frac{2}{N+1}}\begin{pmatrix} a_{N,n}(z+1) \\ a_{N,n}(z) \end{pmatrix} \tag{5.50}$$

By using an **axial symmetry** along $x = y$, we have the diagonal symmetry $S : (x, y) \longrightarrow (y, x)$, the wave function $\psi_{+,n}(N-z)$ is given as:

$$\boxed{\psi_{+,n}(N-z) = (-1)^{n+1}S(\psi_{+,n}(z))} \tag{5.51}$$

We get the Hückel distribution relation eq. 5.27.

We give an expression of the **angles** along the distribution according to the various parameters considered.
Thus, we note by $\mathcal{A}_{N,n,+,0,z}$ the **angle** between $\psi_{+,n}(0)$ and $\psi_{+,n}(z)$.
The angle will have the formula:

$$\mathcal{A}_{N,n,+,0,z} = cos^{-1}\left(\frac{\epsilon(a_{N,n}(1))\epsilon(a_{N,n}(z+1))}{\sqrt{1+\left(\frac{a_{N,n}(z)}{a_{N,n}(z+1)}\right)^2}}\right) \tag{5.52}$$

$$\boxed{\mathcal{A}_{N,n,+,0,N} = (-1)^{n+1}\frac{\pi}{2}} \tag{5.53}$$

with $z = 0, ..., N-1$ and $\epsilon(x)$ is a function of the same sign of x, equal to 1 when $x > 0$ and equal to -1 when $x < 0$.

The proof of this relation is given in Appendix 2 section 24.

Case $\theta = 0$: In this situation, the p_x part will be between $z = 1$ and $z = N-1$ and the p_y part from $z = 0$ to $z = N$, thus, the $[n]$-cumulenes are composed by $N+1$ atoms.

The following **coefficients** depend on the form of the Hückel matrix:

$$c_y(z) = \sqrt{\frac{2}{N+2}}\sin\left(\frac{n\pi(1+z)}{N+2}\right) \tag{5.54}$$

$$c_x(z) = \sqrt{\frac{2}{N}}\sin\left(\frac{(n-1)\pi z}{N}\right) \tag{5.55}$$

we note that $c_x(0) = 0$ and $c_x(N) = 0$.

The proofs of these relations are available in Appendix 2 section 25.

If we are interested in **MOs** with C_2 symmetry, $\psi_{+,n}$:

$$\psi_{+,n} = \begin{pmatrix} \sqrt{\frac{2}{N}} \sin\left(\frac{(n-1)\pi z}{N}\right) \\ \sqrt{\frac{2}{N+2}} \sin\left(\frac{n\pi(z+1)}{N+2}\right) \end{pmatrix} \tag{5.56}$$

with $z = 1, ..., N-1$.

If we consider the values that n can take we have the **angles**:

$$\boxed{\mathscr{A}_{N,n,+,0,N} = \frac{(1-(-1)^{n+1})}{2}\pi = \begin{cases} 0 & \text{if } n \text{ is odd} \\ \pi & \text{otherwise} \end{cases}} \tag{5.57}$$

In the continuation of the manuscript we show different examples of distributions as defined here.

5.3 Criteria for the existence of helices

As we have seen previously in this chapter, the literature shows specific cases in which helices appear. In this section, we indicate the necessary criteria to obtain helices following two approaches: physical and chemical.

5.3.1 By a physical approach : Löwdin partitioning technique

This section is based on the work of Gunasekaran and al. [68] which presents a discussion of the **existence** of helical states studying directly the eigenstates of the Schrödinger equation associated to the molecule. We prove using their approach that molecules admits **generically helical states**.

In terms of mathematics, we have to be interested in the so-called **Löwdin partitioning technique** [74][57] for matrices. This is applied to Hamiltonian matrices which we can write in the case of a cumulenic system. The technique is to compute a Hamiltonian matrix of the part of the molecule that we are interested in, which then allows to return to a Hamiltonian matrix taking into account the total space.

A **schematic** example to improve the meaning of the Hamiltonian matrix is given in the work of Jin and Song [57]:

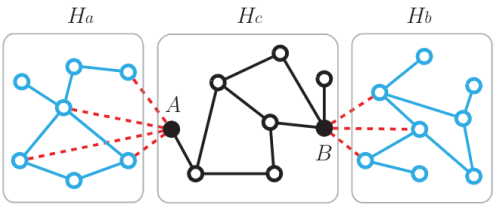

Figure 5.6: Schematic illustration of a molecule to define a Hamiltonian square matrix in the Löwdin partitioning technique [57] *(the graph consists of two branch graphs a and b in cyan and a center graph c in black - the dashed edges in red represents the connections between them, with A and B being the branch-root nodes).*

Then for a **complete system** we define the **Hamiltonian square matrix** as:

$$H = \begin{pmatrix} H_{aa} & H_{ac} & 0 \\ H_{ca} & H_{cc} & H_{cb} \\ 0 & H_{bc} & H_{bb} \end{pmatrix} \tag{5.58}$$

Note that $H_{ca}^t = H_{ac}$ with t is the transpose.

As a reminder, our system is composed of a linear chain with **2N orbitals** with a left (L) and right (R) part as we have shown in the schematic figure 5.2 and more generally in figure 5.6. The elements of the left part is noted a and those of the right part b. Thus, we have on the left $p_a = (p_1, ..., p_a)$ orbitals and on the right $p_b = (p'_1, ..., p'_b)$ orbitals. Then, we have $2(N-2)$ orbitals as $p_{x,i}$ and $p_{y,i}$ (*with i = 1,...,N-1*), constituting the vector p_c.

As we know the Schrödinger equation, we have :

$$\psi = \sum_{i=1}^{a} c_i p_i + c_L p_L + \sum_{i=1}^{n} c_{x,i} p_{x,i} + c_{y,i} p_{y,i} + c_R p_R + \sum_{j=1}^{b} c_j p'_j \tag{5.59}$$

We get the **linear system** as follows:

$$\begin{cases} H_{aa}p_a + H_{ac}p_c = Ep_a \\ H_{ca}p_a + H_{cc}p_c + H_{cb}p_b = Ep_c \\ H_b p_c + H_{bb}p_b = Ep_b \end{cases} \tag{5.60}$$

If we consider once again the identity matrix I_d, with $d > 0$ the I_d matrix is of size d. For a given E the matrices $EI_a - H_{aa}$ and $EI_b - H_{bb}$ are **invertible**, we get p_a, p_b and p_c as:

$$p_a = (EI_a - H_{aa})^{-1} H_{ac} p_c \tag{5.61}$$

$$p_b = (EI_b - H_{bb})^{-1} H_{bc} p_c \tag{5.62}$$

We then replace in the linear system eq. 5.60 :

$$H_{ca}(EI_a - H_{aa})^{-1} H_{ac} p_c + H_{cc}p_c + H_{cb}(EI_b - H_{bb})^{-1} H_{bc} p_c = Ep_c \tag{5.63}$$

We can then, join the respective terms of the left and right parts of the molecule, it results in a **Hamiltonian term** called **effective**:

$$\boxed{H_{eff} = \Sigma_L + H_c + \Sigma_R} \tag{5.64}$$

with $\Sigma_L(E)$ and $\Sigma_R(E)$ the $2N \times 2N$ matrix depending on the coupling of the terminal groups as:

$$\Sigma_L = H_{ca}(EI_a - H_{aa})^{-1} H_{ac} \tag{5.65}$$

and

$$\Sigma_R = H_{cb}(EI_b - H_{bb})^{-1} H_{bc} \tag{5.66}$$

Gunasekaran et al. [68] gives the following **criterion of existence** of helical MOs, it is a **physical criterion**: to obtain helical states it is necessary that the matrices Σ_L and Σ_R do not commute i.e.:

$$\boxed{[\Sigma_L, \Sigma_R] \neq 0} \tag{5.67}$$

where $[,]$ *denotes the brakets on matrices defines by* $[A, B] = AB - BA$.

The condition eq. 5.67 is **open** because generically we have helices, it is only necessary to introduce the right substituents at the end of the chain.

It should be noted that the calculation of the 2 matrices Σ_L and Σ_R is relatively complex [57] and are computable only in **very simple** cases.

5.3.2 By chemistry: using molecular symmetries

In this section, we bypass the computational problem linked with the matrices Σ_L and Σ_R by stating a criterion based on the **symmetry group** of the molecule.

We consider a **linear chain molecule** $L_{\mathbf{A}}$ containing N atoms denotes by A_i *(with* $i = 1, ..., N$*).* We can denote by the set $\mathbf{A} = \{A_i\}_{i=1,...,N}$ whose coordinates depend on the z axis.

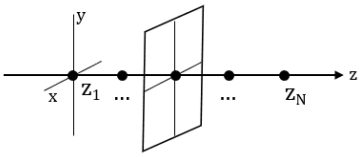

Figure 5.7: Schematic representation of a linear chain depending on the z axis

We get n atoms being two-dimensional, with a basis set p_x, p_y, p_z orbitals participating in the σ-system. For a linear molecule, there are two planes $\mathcal{P}_x$ and $\mathcal{P}_y$ which contain the family of p orbitals as $p_x(z)$ and $p_y(z)$ orbitals according to their position on the z axis.

In this case, using symmetry, we have therefore **frontier orbitals** on the left ($p_y = p_0$) and on the right (p_N) of the linear chain at $N = n + 2$ atoms oriented in the xy-plane.

The **Hückel matrix** of a molecule as $L_{\mathbf{A}}$ takes the form of a basis set $p_0 = p_x$, p_x^i, p_y^i, p_N *with* $i = 1, ..., n$ such as:

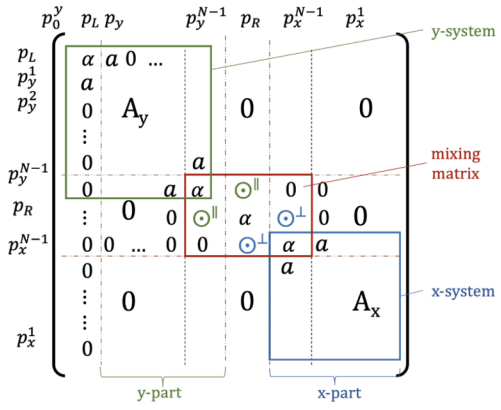

(5.68)

where the matrix A_x and A_y are given such as (the matrix of A_y is given as example):

$$A_y = \begin{array}{c} \\ p_y^1 \\ \vdots \\ p_y^k \end{array} \begin{array}{c} \begin{array}{cccc} p_y^1 & \cdots & p_y^k \end{array} \\ \begin{pmatrix} \alpha & a & & 0 \\ a & \ddots & & \\ & & \ddots & a \\ 0 & & a & \alpha \end{pmatrix} \end{array} \tag{5.69}$$

We can decoupled the **characteristic polynomial** of the Hamiltonian matrix in two situations:

- $\odot^{\parallel} = 0$ corresponds to the situation where p_N is orthogonal to p_x^N (i.e. $p_N = p_y$). The matrix of mixing is reduced to :

$$Mix^{\perp} = \begin{pmatrix} \alpha & 0 & 0 \\ 0 & \alpha & \odot^{\perp} \\ 0 & \odot^{\perp} & \alpha \end{pmatrix} \tag{5.70}$$

  with the characteristic polynomial:

$$P(x) = P_A(x) P_{A^{\perp}, \odot^{\perp}}(x). \tag{5.71}$$

- $\odot^{\perp} = 0$ corresponds to the situation where p_N is orthogonal to p_y^N (i.e. $p_N = p_x$). The mixing matrix is reduced to:

$$Mix^{\parallel} = \begin{pmatrix} \alpha & \odot^{\parallel} & 0 \\ \odot^{\parallel} & \alpha & 0 \\ 0 & 0 & \alpha \end{pmatrix} \tag{5.72}$$

  with the characteristic polynomial is given by:

$$P(x) = P_{A^{\perp}}(x) P_{A, \odot^{\parallel}}(x) \tag{5.73}$$

Thus, the first case is the orthogonal configuration of the ethylene and the other one to the planar configuration.

Finally in others configurations, the **necessary condition** to obtain helical MOs is to have a mixing of the components of the p_x and p_y orbitals.

Note that it is obvious that the presence of the p_x, p_y and p_z orbitals limit the method to certain elements of the periodic table, in particular to those of the p-block.

The **mixing** of these orbitals seems simple but the point to keep in mind is the **symmetry**. Indeed, the presence of a **helicogenic axis** [9], i.e. an axis of symmetry C_2 is necessary. This axis implies that : $C_2(p_x) = p_y$ and and this axis is involved in the formation of helical orbitals.

For instance, we consider the case of **ethylene** which doesn't present helical MOs. In its **orthogonal** configuration, ethylene has **mirror plane symmetry**, and **3** C_2 **axes of rotation**: one along the molecular chain and 2 axes (dihedral) helicogenics. In this situation, there is a mixing generated by the axes, but due to the mirror plane symmetry, the characteristic polynomial is factorized which induces a disconnection between the family of the p_x and p_y orbitals. By consequence, there are **no** helical MOs.

In its **planar** configuration, there are **3** C_2 **axes** (one along the molecular chain and 2 passing through the centre directed the x and y axes), none of these axes are helicogenics. The symmetries don't induce mixing of orbitals then, we **cannot** wait helical MOs.

We deduce by this example, that the **absence of a mirror plane** in the molecule is necessary from a symmetric point of view to obtain helical orbitals.

Other point of symmetry, in the linear case of [n]**-cumulenes**, which present helical MOs, [n]-cumulenes **do not** have a mirror plane, but a C_2 axis of symmetry. In addition, the absence of mirror plane, implies that the molecule is chiral.

As a reminder, the chirality of a molecule indicates that the image of the molecule by a mirror plane is not invariant.

We then define a **symmetry criterion for helical states** as:
for a linear chain $L_{\mathbf{A}}$ chiral and satisfying the structural hypothesis, admitting a C_2 helicogenic axis presents explicit helical MOs.

With these different criteria of symmetry we can refer to **Curie's principle** [75]. This principle stated in a paper of 1894 by Pierre Curie proves the relationship between the **symmetry of an effect and its cause**: "when certain causes produce certain effects, the elements of symmetry of the causes must be found in the effects produced". The Curie's principle gives a physical support to the sentence of Garner et al. [55]: "the formation of helical symmetry-adapted MOs requires chirality; not surprising considering a helix is a chiral object" this is not surprising indeed and is a consequence of the Curie's principle.
More details about the validity of the Curie's principle are given in the work of Chalmers [76] and Ismael [77].

5.3.3 In the non-planar linear molecules

As discussed, in **linear molecules** the criteria of appearance of helical MOs are **well-defined** but what about in the case of other molecules?

In the case of molecules that do not naturally have helical MOs, the molecular main chain has **2 helical axes** C_2, **one axis** C_2 **along the chain** and **3 orthogonal planes**. The presence of **mirror planes** does not permits helices. It is therefore necessary to bypass these mirror planes. From the point of view of the symmetry of molecules, the orthogonal planes are noted mirror planes such as : σ_{xy}, σ_{xz} and σ_{yz}.

Thus, to respect the **helicity criteria**, we need to break the mirror planes. For example, if we break the σ_{xz} plane, then the molecule is no more plane.
Each terminal fragment (L_1, L_2) and (R_1, R_2) (as terminal groups denoted in the figure 5.2) has to be taken into account. Considering for example the fragments L in the plane of symmetry σ_{xz}. Then, if this mirror plane is broken the fragment R will not be contained in the plane $\mathcal{P}_y$ defined in the previous section.
These different actions will generate "mechanical" constraints that we see as torsions of the chain ends (as we have seen in the literature). As we will see in the next chapter, we show that we can prove the existence of helical MOs on this type of systems in their ground states.
We have to take into consideration that the symmetry of the molecule also depends on the energy state.
Thus, if we examine a symmetry group whose symmetry elements are valid for the helicity criteria, it is then possible to see helical MOs in energy states other than the fundamental.

5.4 Conclusion

This chapter is very dense in information. The first part of the chapter is very informative on Möbius systems following the work of R. Hoffmann. Based on the linear case of $[n]$-cumulenes and the curiosities of the **helical orbitals** that this type of carbon systems presents.

In the second part of the chapter, we provide a detailed description of the **properties** of the helical states such as the **angle distribution** or the **helicity index** (HEL). We detail the **angle distribution** of $[n]$-cumulenes according to the rotation of one of the chain end substituents.

Finally, the last part presents the criteria of existence of helices: by physical and chemical approach. The **physical approach** is based on the **Löwdin partitioning technique** which shows the use of Hamiltonian matrices: in particular the **criterion of non commutation** of the matrices of each of the extremities of the molecular system. This computational step being complex, it can only be applied in very simple cases.

The **chemical approach** uses the **symmetries** of the molecules. The necessary condition to obtain helices is the **mixing** of the p_x and p_y orbitals but also the presence of a helical axis: that is to say an axis of symmetry of type C_2. The last point related to symmetry is the **absence of a mirror plane**. The link with **Curie's principle** is then established with respect to the criterion of symmetry of helical states. Finally, in the case of non-planar linear molecules, the criterion of helicity is applicable in **any energy state**.

Chapter 6

Applications and visualizations

In this chapter, we use the points discussed in the previous chapter 5 and present our results in an illustrated way.

We expose results on:

- *[n]-cumulenes (with n = 3, 4, 11): in the fundamental and excited states,*
- *[n]-hetero-cumulenes (with n = 2, 3): in the fundamental state,*
- *[B=N] or [N=B]-cumulenes: in the fundamental and excited states,*
- *DPBD, tolanophane and molecules with metals.*

The results illustrate among other the work of R. Hoffmann [9], Escudié et al. [78], Toyota et al. [79], Garner et al. [55], Caviglasso et al. [80], Cretu et al. [81] and our preprint [44].

Our studies present in a simple way the possibility of reaching **helical orbitals** within **simple native systems** but summarize most of the cases. The systems considered are [n]**-cumulenes** with [n] = 3 and [n] = 4 without substituents at the ends of the chains. The interest focuses on the terminal hydrogen and on the singlet or triplet energy state of the [n]-cumulene, which is clearly not mentioned in the bibliography.
Then, we display the presence of such helices in the case of [n]-cumulenes composed of **hetero-elements** and more complex carbon molecules as **diphenylbutadiyne** and **tolanophane**.

Our results prove the presence of helix orbitals in all the cases studied, all the properties are represented by our systems. The bibliography does not rely on simple cases to answer precisely to the questions.

Most publications refer to DFT calculations to determine the presence of helical orbitals. Our work is based for the ground and excited-states geometries, both on DFT calculations (B3LYP exchange-correlation functional with 6-311G(d.p) basis set using Gaussian 09 program package) [82] but also on a more solid calculation program with results obtained by Molpro CASPT2 (10.8/6-311G(d.p) using Molpro program packages) [15]. These computations allow us to confirm the validity of the DFT results.

The procedure followed for the calculations is given in detail in Appendix 1.

6.1 Results on [n]-cumulenes

We describe the results obtained for **[n]-cumulenes** with $[n] = 3$, $[n] = 4$ and $[n] = 11$ (i.e. containing 3, 4 or 11 successive double bonds).

We study **several cases**: either the ends of the chains are **parallel**, or **perpendicular** and into energetic states **singlet** or **triplet**.

6.1.1 Fundamental states

We distinguish the **positions of the chains ends**, by imposing **rotation from 0° to 90°**. We observe the shape of the orbitals and the evolution of changes throughout the rotations. We note that the calculations are carried out in a C_2 symmetry to satisfy the helicity criteria.

We notice that the investigation of the helical states required a long research work, since the helical MOs are generally visible between HOMO-1 and LUMO+1.

[3]-cumulene

DFT computations: To describe the molecule : the core linear chain composed by 3 double bounds and 4 carbon atoms, has 2 C_2 **helicogenic axes** and a C_2 **axis** along the chain.

In addition, the linear chain possesses **3 orthogonal mirror planes** (σ_{xy}, σ_{xz} and σ_{yz}).

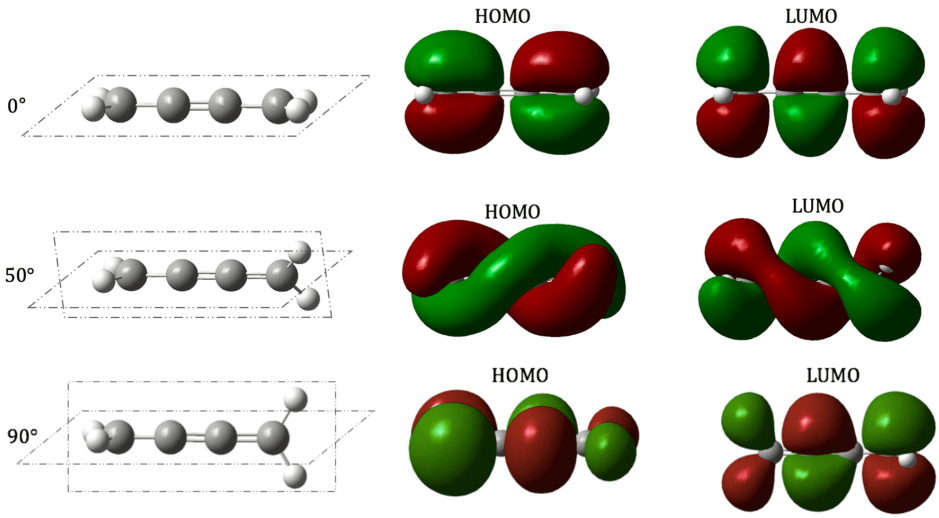

Figure 6.1: Representation of helical MOs of a [3]-cumulene at different states of rotation (0, 50°, 90° carried out by DFT computations) in the ground state

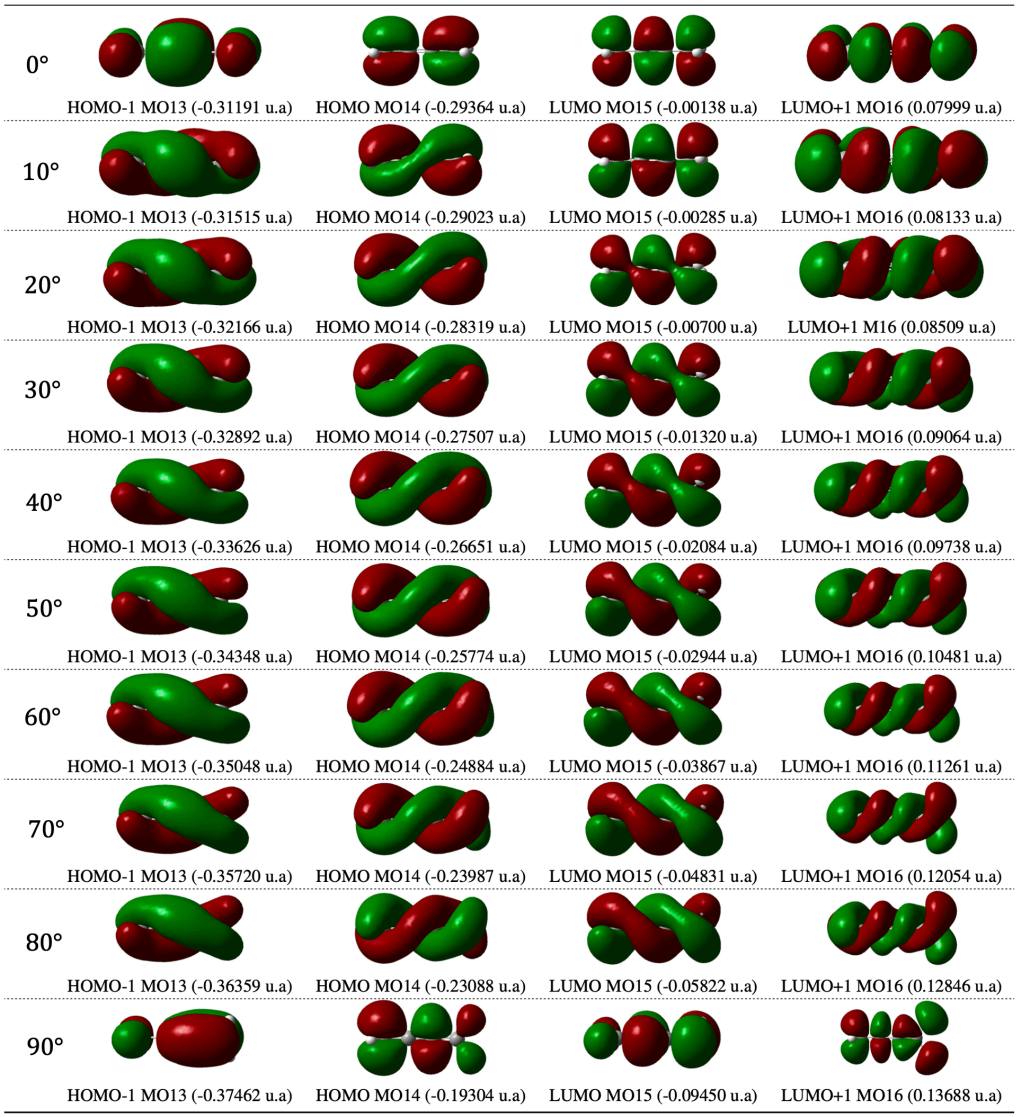

Figure 6.2: Molecular orbitals and energies of a [3]-cumulene associated for rotations from 0° to 90° (carried out by DFT computations) in the ground state

As we expose in the chapter 5, the figure 6.1 illustrates perfectly the fact that the **torsional constraint** of one of the chain ends induces the appearance of a helix. Indeed in the extreme cases, at 0° plane and 90° perpendicular case we see the electronic clouds on both sides of the plane of the molecule. But at 50° when there is mixing of the p_x and p_y orbitals the helices are perfectly defined. It should obviously be noted that as we see in the previous figure (6.2), all cases of intermediate rotation (the calculations of the rotations with steps of 1° were carried out) also show helices.

The **helical orbital criterion** is satisfied, in fact we have broken the mirror planes symmetries by torsional constraints.

[4]-cumulene

DFT computations: In the case of **[4]-cumulene** we are in the same situation and the same observations can be reported as for the [3]-cumulene case, but the molecule contains 4 double bounds and 5 carbon atoms.

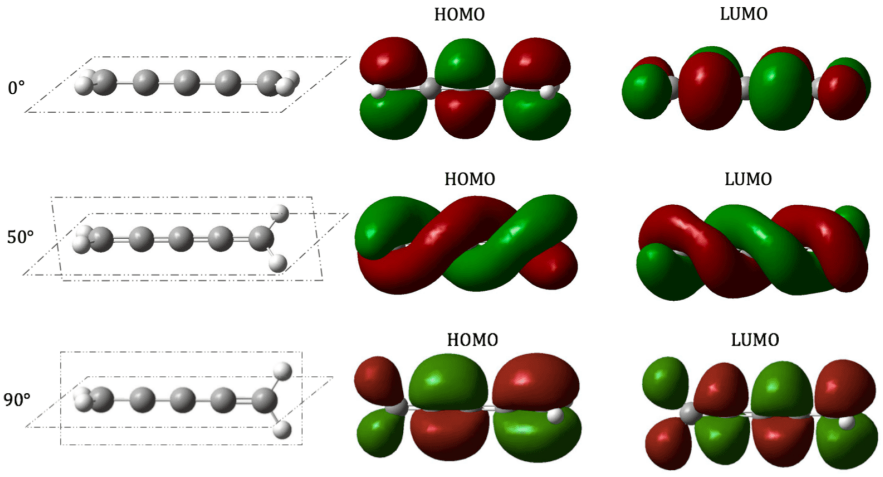

Figure 6.3: Representation of helical MOs of a [4]-cumulene at different states of rotation (0, 50°, 90° carried out by DFT computations) in the ground state

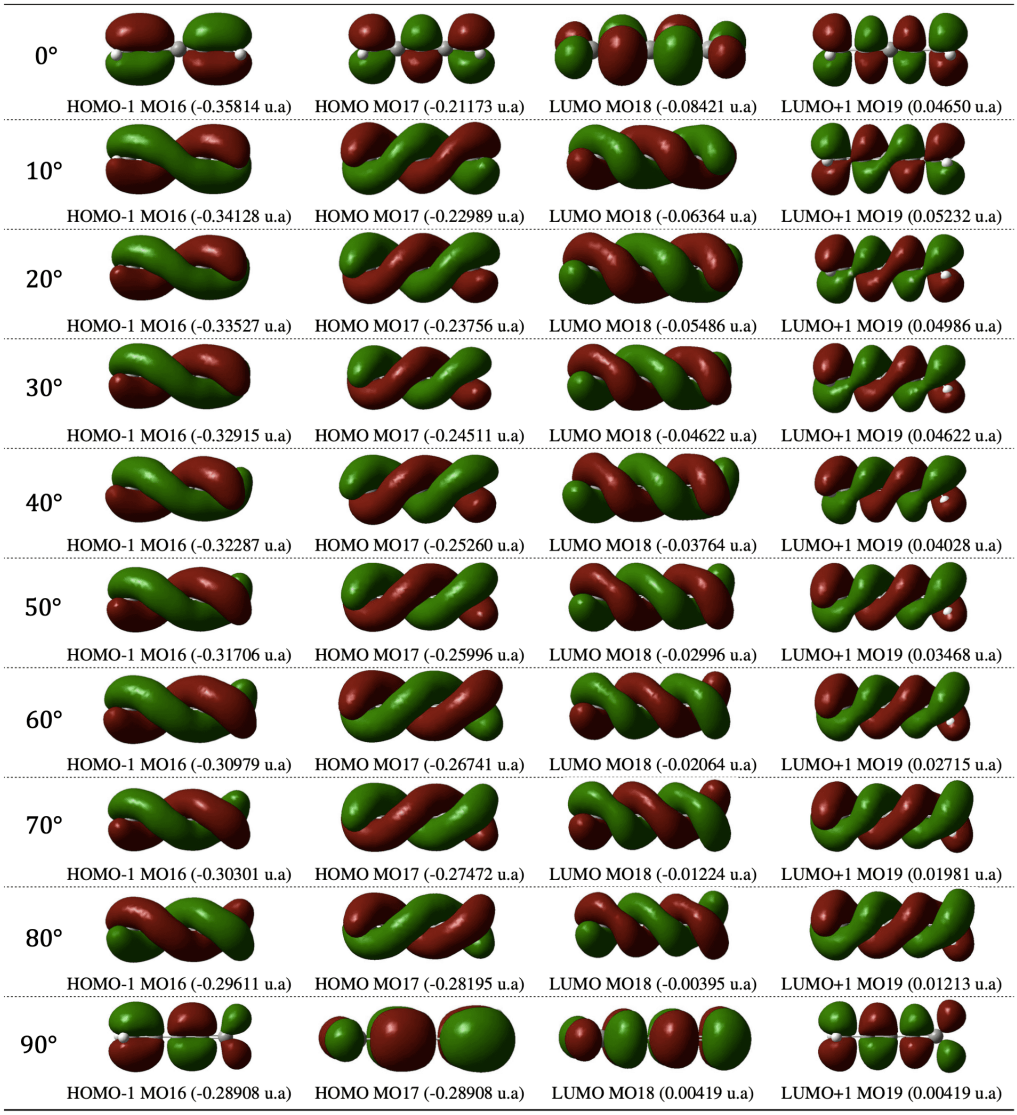

Figure 6.4: Molecular orbitals and energies associated for rotations from 0° to 90° (carried out by DFT computations) in the ground state

Once again as in the case of [3]-cumulene the **helical orbital criterion** is satisfied.

For more details in these 2 cases presented, the **criterion is satisfied** thanks to the **breaking of the symmetries** of the mirror planes. Actually, it depends on the fragments of the chain ends and it is done in several conditions:

- the mirror plane σ_{xz} is broken which means that the molecule is no longer a planar linear chain,
- considering the left fragment L of the molecule which is contained in the σ_{xz} plane which is broken implies that the right fragment R is not contained in the $\mathcal{P}_y$ plane. This, also implies the breaking of the σ_{xy} mirror plane.

There is therefore an axial torsion of the terminal group of the linear chain which generically induces helical MOs.

[11]**-cumulene**

DFT calculations: We considered the case of a **longer [n]-cumulene** and at only 10° of rotation of one of the chain ends. We also see in this case the presence of helices and even if the constraint is not very high (10° of rotation), the **helical orbital criterion is satisfied**.

Note for a better visualization the transparency of the helices.

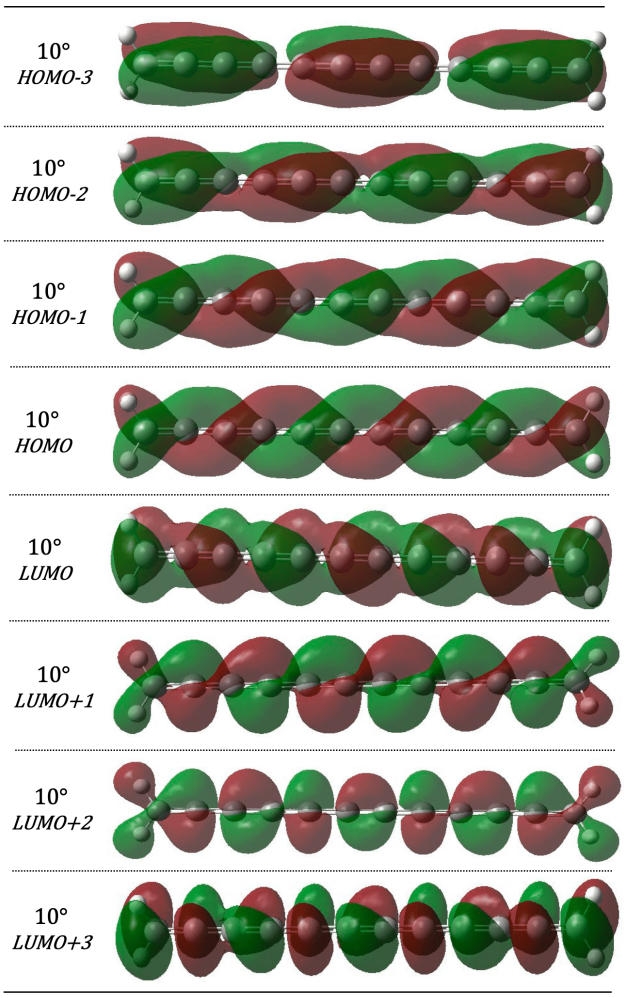

Figure 6.5: Helical molecular orbitals for a rotation of 10° (carried out by DFT computations) in the ground state

6.1.2 Excited states

As in the previous section, we performed the same DFT calculations, but in a **triplet excited state**, which has not been proven in the literature. This excited state results in the MOs being in 2 different spins α and β.

[3]-cumulene

DFT computations: We are in the case where the [n]-cumulene is in an **excited state**, i.e. in a triplet state (multiplicity $\mu = 3$). We notice here also that as in the ground state situations, when the rotations are of **0° and 90°**, we **do not observe helices** but at **50°** of rotation the **helices** are clearly present under the 2 multiplicities.

Note that the shape, the number of turns and the direction of winding of the helices are not the same in the α and β-spin state.

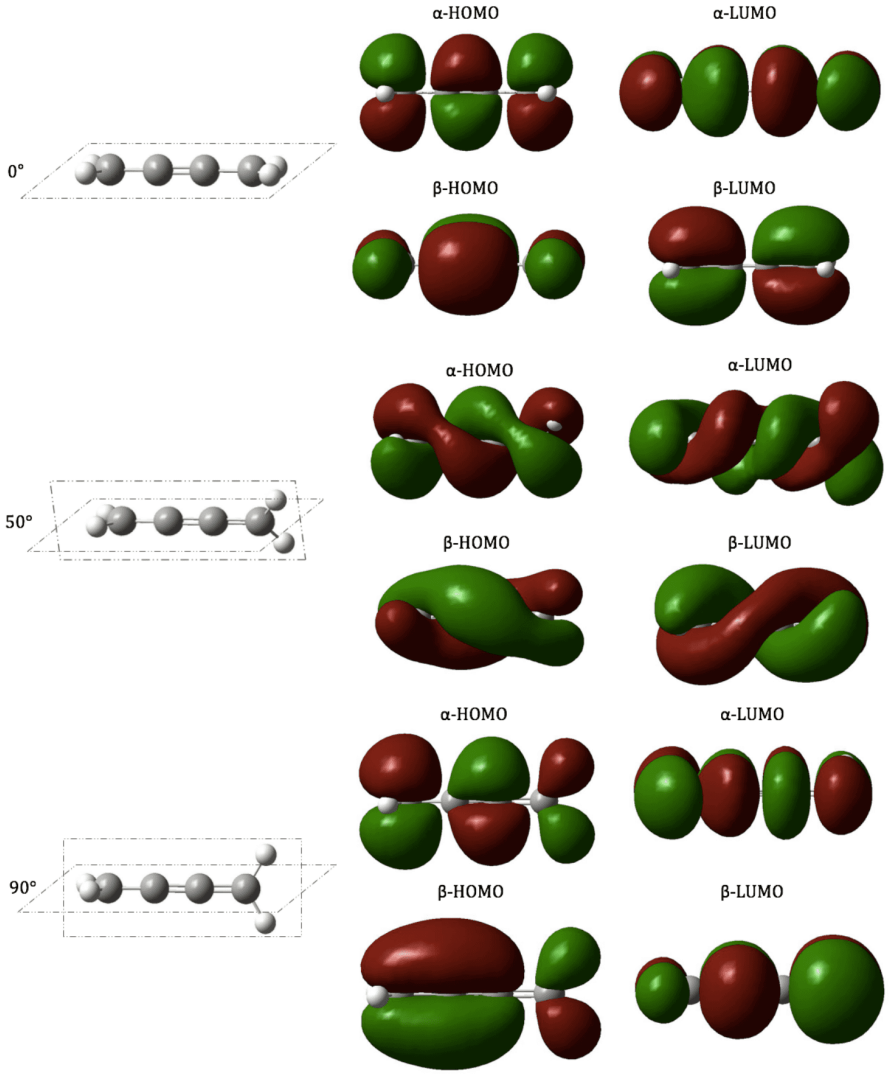

Figure 6.6: Representation of helical MOs of a [3]-cumulene at different states of rotation (0, 50°, 90° carried out by DFT computations) in a triplet state.

[4]**-cumulene**

DFT computations: The same behaviours are observed.

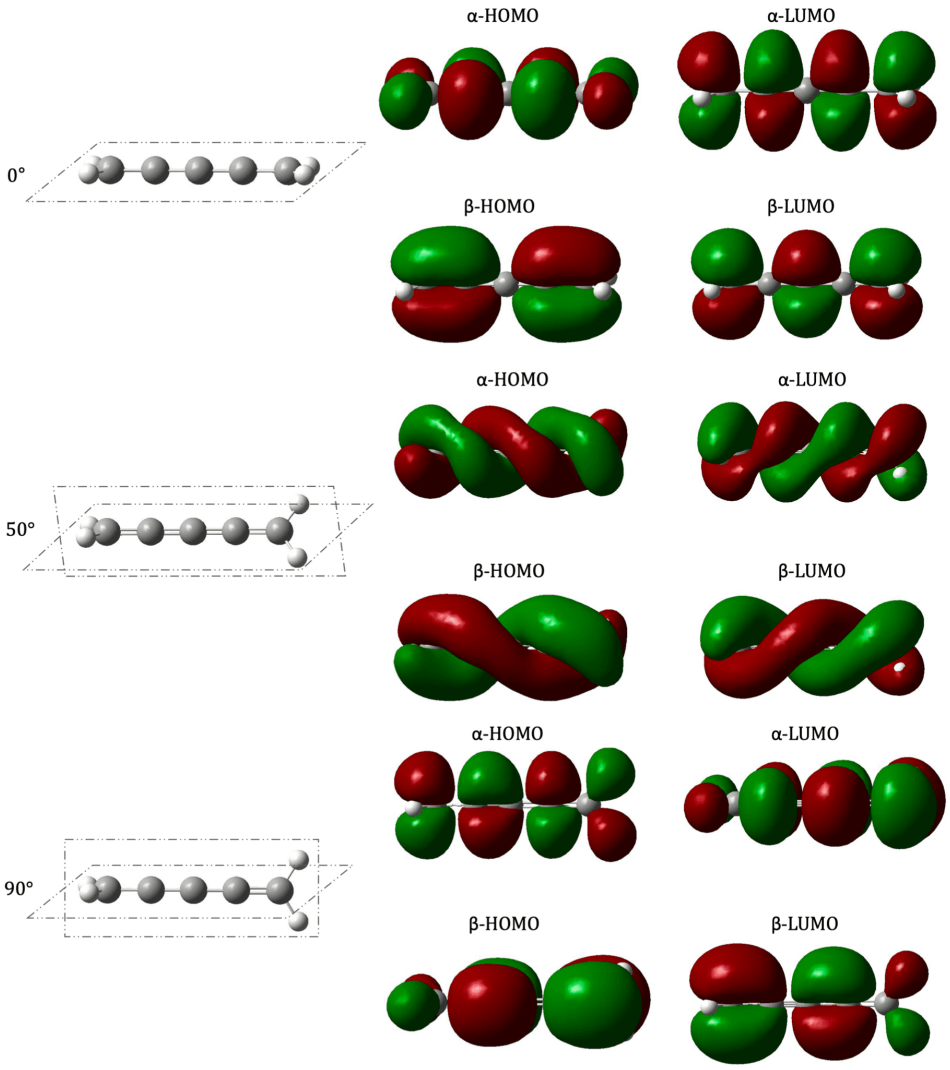

Figure 6.7: Representation of helical MOs of a [4]-cumulene at different states of rotation (0, 50°, 90° carried out by DFT computations) in a triplet state.

We note in the 2 situations of the figures 6.6 and 6.7, that the helical MOs are more defined under α-spin than β-spin.

We know that the symmetry group of the MOs of a molecule depends on its **energy state**. Therefore if the symmetry group of the molecule does not have helical MOs but contains symmetry elements that satisfy the criterion for the existence of helices, then there will be excited states of the molecule with helical MOs that will fit the symmetry. In the same way, this statement also applies for the **electronic multiplicities**.

6.2 Molecules with hetero-elements and more examples

6.2.1 [n]-hetero-cumulenes

[n]-cumulenes being molecules with a linear carbon chain, we chose to work with more **varied** [n]-cumulenes. By referring to the literature [78] where 15 families of [n]-cumulenes are reviewed, we studied [n]-cumulenes containing in the principal linear chain (from atoms C_0 to C_N): **silicon, germanium, phosphorus, arsenic or more simply oxygen** or **nitrogen**.

We resume all the studied [n]**-hetero-cumulenes** in the following table:

	C_0 / C_N	L_1	L_2	R_1	R_2
[n]**-cumulene**	C / C	H	H	H	H
[2]-heterocumulene:					
Phosphaallene	P / C	H	-	H	H
Diphosphaallene	P / P	H	-	H	-
Phosphaazallene	P / N	H	-	H	-
Arsaallene	As / C	H	-	H	H
Arsaphosphaallene	As / P	H	-	H	-
Diarsaallene	As / As	H	-	H	-
Siaallene	Si / C	H	H	H	H
Phosphasilaallene	Si / P	H	H	H	-
Silaketene	Si / O	H	H	-	-
Germaallene	Ge / C	H	H	H	H
Germaphosphaallene	Ge / P	H	H	H	-
[3]-heterocumulene:					
Phosphabutatriene	P / C	H	-	H	H
Diphosphabutariene	P / P	H	-	H	-
Arsabutariene	As / C	H	-	H	H
Silabutariene	Si / C	H	H	H	H

Table 6.1: Set of studied [n]-hetero-cumulenes

For more details concerning the table: we note [2]-hetero-cumulene and [3]-hetero-cumulene constituted by hetero-elements (*P : phosphorus, N: nitrogen, As: arsenic, Si: silicon, Ge: germanium, O: oxygen*) and the presence or absence of hydrogen in terminal groups.

[2]-hetero-cumulenes

DFT calculations: The representation of the MOs of the [2]-hetero-cumulenes from the table 6.1, shows the **existence of helices** between the **HOMO-1** and the **LUMO+1**, for a **rotation of 25°** of only one of the terminal group.

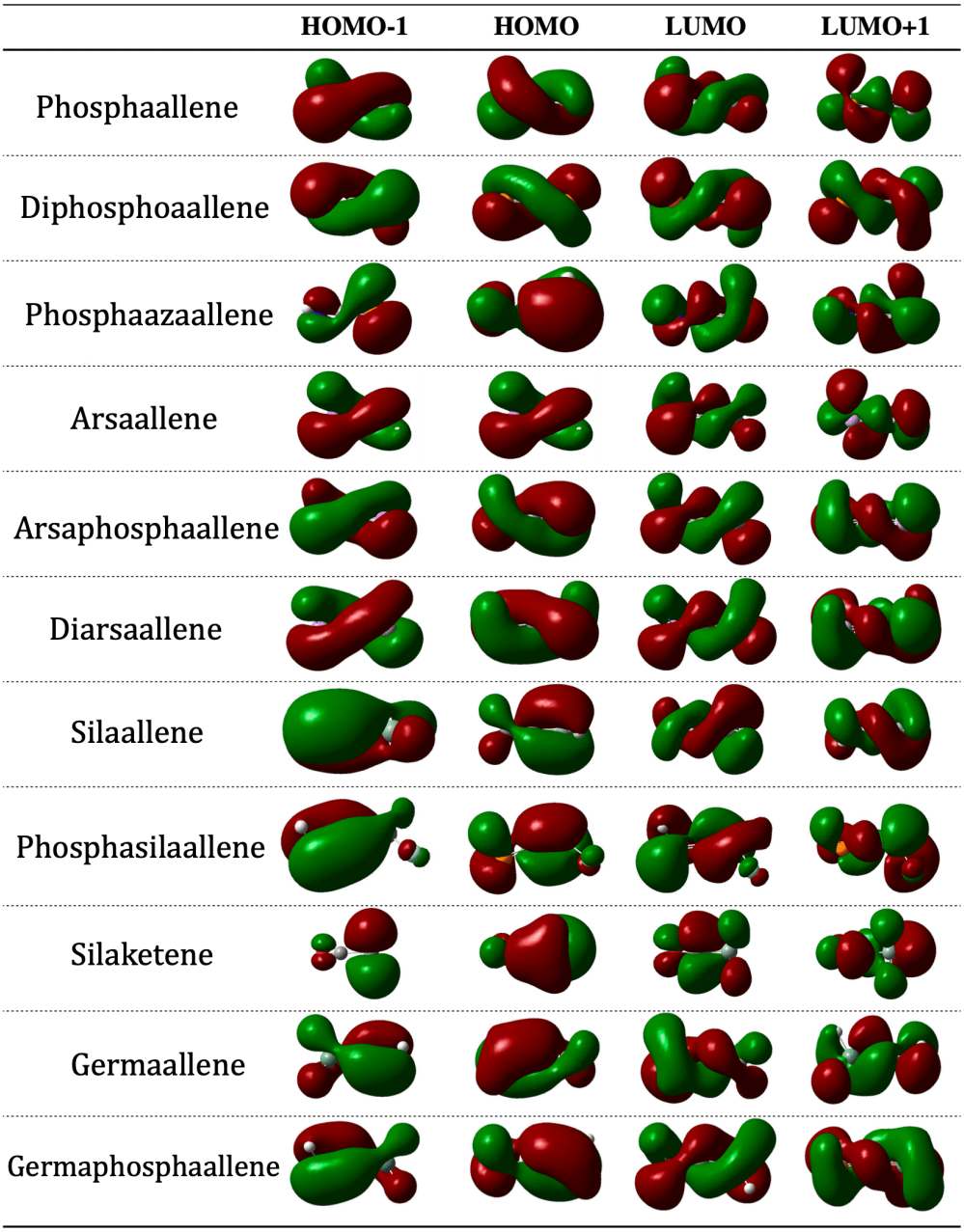

Figure 6.8: Representation of helical MOs of [2]-hetero-cumulenes at 25° of torsion by DFT computations in the ground state

We observe for most of the molecules that the helices exist for both HOMO and LUMO but the shapes and windings of LUMO and LUMO+1 seem more complex.

[3]-hetero-cumulenes

DFT calculations: Here, also for a **25° of torsion**, we represented the MOs between the **HOMO-1** and the **LUMO+1**.

In this case, the helices are existing and better defined for HOMO-1 and HOMO.

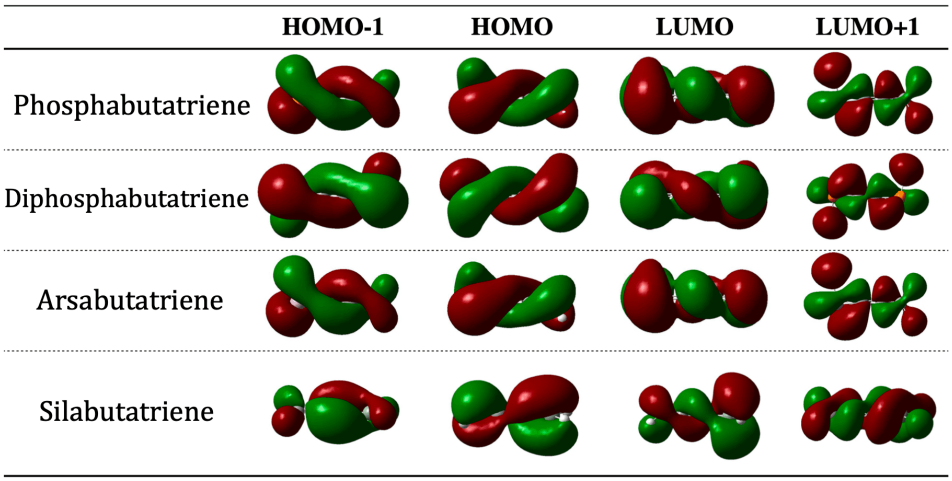

Figure 6.9: Representation of helical MOs of [3]-hetero-cumulenes at 25° of torsion by DFT computations in the ground state

In the 2 figures presented 6.8 and 6.9 we observe that the helical MOs are **less well-defined** than in the cases of [2] and [3]-hetero-cumulenes.

6.2.2 $[B = N]$ or $[N = B]$-cumulenes

After using hetero-elements, we chose to design linear chains as $[n]$-cumulenes from **boron** and **nitrogen** only, based on the work of Cretu et al. [81]. These linear boron nitride chains highlight the existence of **non-standard helices**.

Note that bron nitride nanostructures are known to present a wide diversity of chemical and physical properties.

Here, we see a **large variety of MOs in helices** according to the number of atoms and the alternation between boron and nitrogen in the ground and excited states.

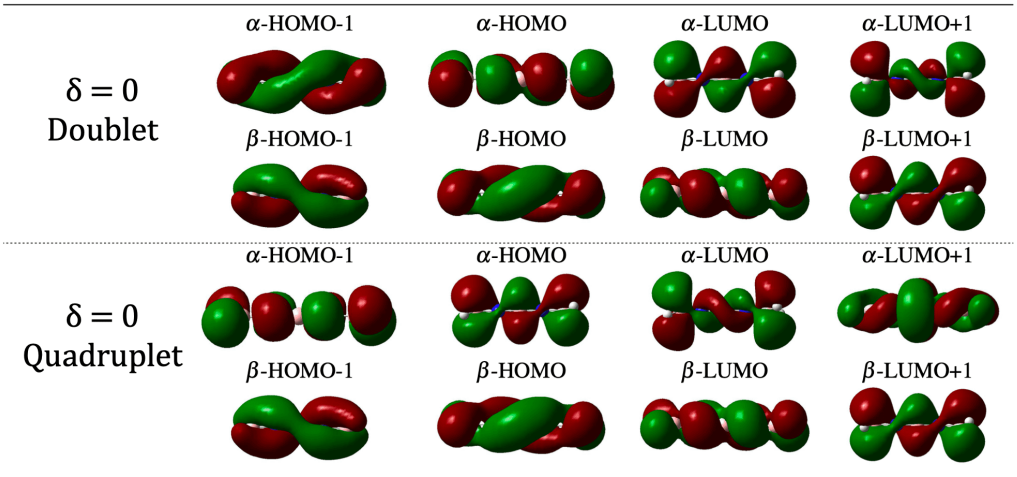

Figure 6.10: Representation of the molecular orbitals of the **B=N=B=N=B-cumulene** (by DFT computations) for a rotation of 30° (charge 0 - doublet and quadruplet states)

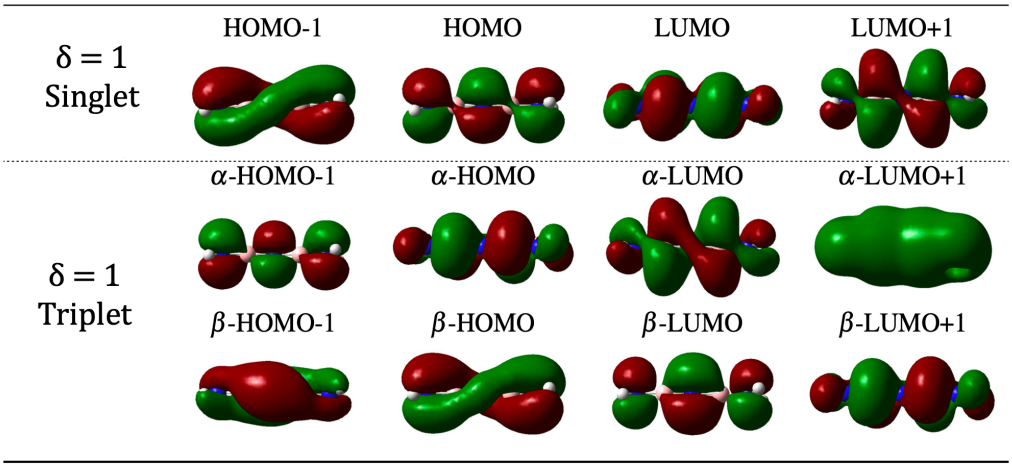

Figure 6.11: Representation of the molecular orbitals of the **N=B=N=B=N-cumulene** (by DFT computations) for a rotation of 30° (charge 1 - singlet and triplet states)

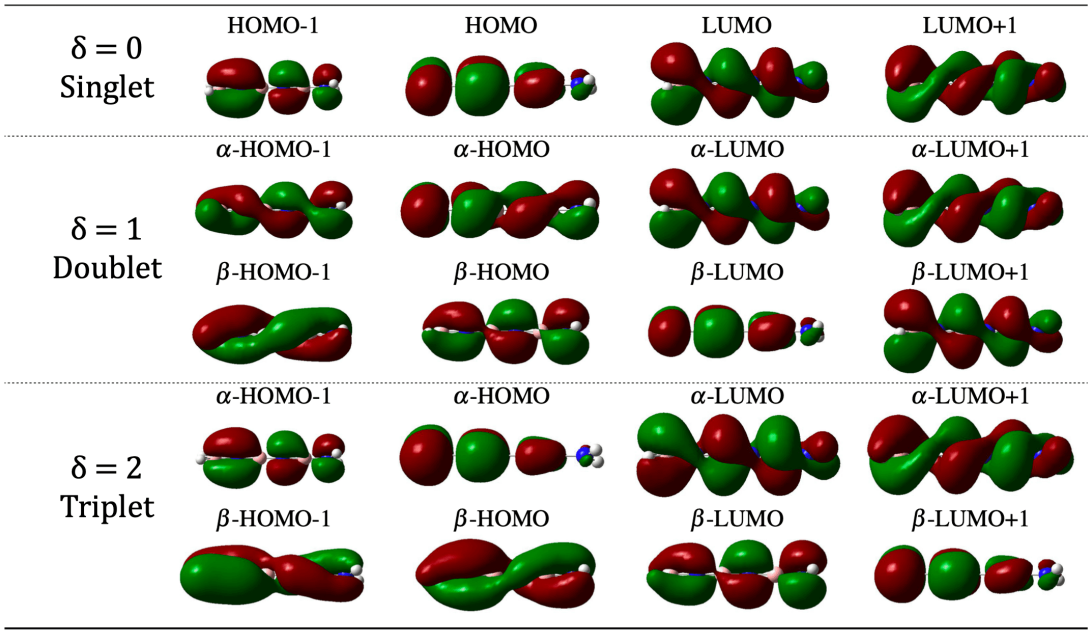

Figure 6.12: Representation of the molecular orbitals of the **B=N=B=N=B=N-cumulene** (by DFT computations) for a rotation of 30° (charge 0, 1 and 2 - singlet, doublet and triplet states)

6.2.3 Other examples

For other examples, there is also interest in **diphenylbutadiyne (DPBD)** [83] which has a **linear chain** combining **single and triple** bonds and **phenyl end groups**.

The **tolanophane** molecule is also interesting because it is composed by 2 units of diphenylethyne with 2 linear chains [79].

DPBD molecule

The following figure 6.13 presents the representation of the MOs from HOMO-1 to LUMO+1 according to the C_2 symmetry for rotations from 0° to 90° which highlights the **helices**. The helices are only present on the linear chain where the helical orbital criterion can be applied.

We note that the helices are well defined for the **LUMO+1** between 20° and 80° of rotation and once again that the **rotation** of one of the chain ends induces the appearance of **helices**.

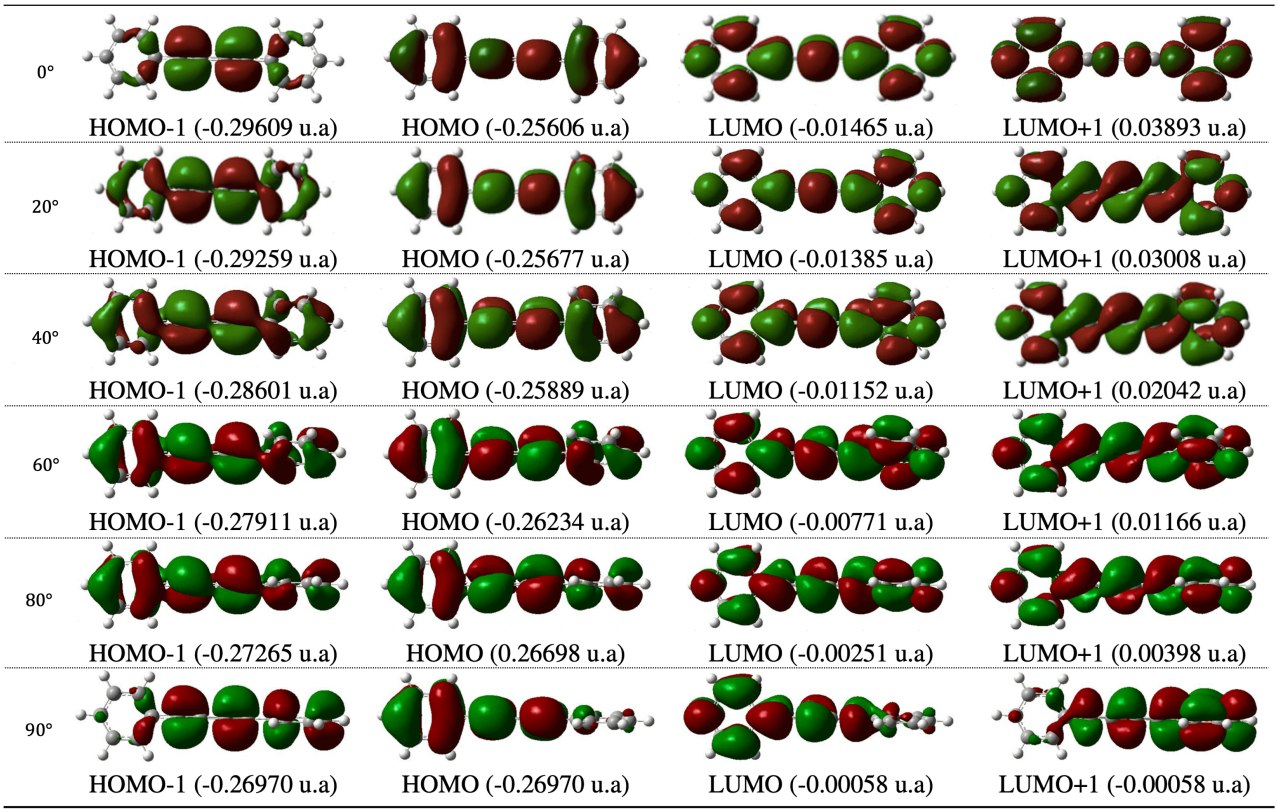

Figure 6.13: Representation of the molecular orbitals of the DPBD molecule (by DFT computations)

Tolanophane molecule

In the following figure, the molecule of symmetry C_2 is **rotated** by one end of the chain. As indicated at 0° there are no helices but for intermediate angles helices are present.

Beyond 65° the helices are less well defined. We note that the helices are **clearly visible** only on the **LUMO+3** orbitals and once again along the linear chains where the criterion of helical orbitals is applicable.

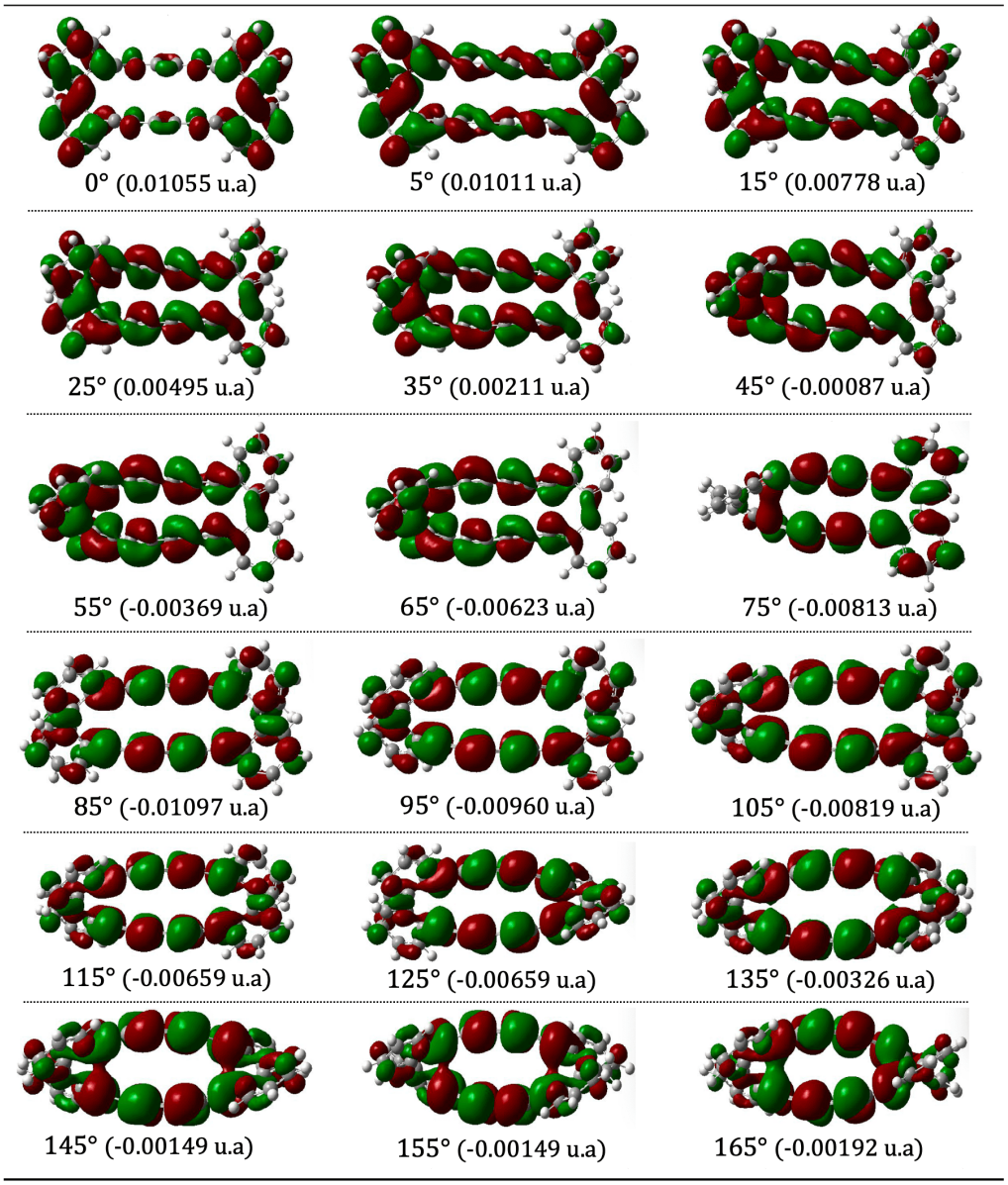

Figure 6.14: Representation of the molecular orbitals LUMO+3 of the tolanophane molecule (by DFT computations)

Molecules with metals

As discussed in the previous chapter, to study the helical MOs, we focused on the p**-orbitals** of the systems. But it is also possible to be interested in these same states in the case of d**-orbitals** [56]. For this type of orbitals, it is the **metals** that carry them thus, we have to be attentive to the **metal-cumulenes**.

The study of MOs in helices in molecules with metal-like atoms is **more confidential**. In a recent paper by Garner et al. [56] the research team highlights the possibility of obtaining helical states with d-type orbitals. They propose **complex systems** based on ruthenium such as: $trans - [EtC = (C =)_4C = Ru = (C =)_4CMe]^{2+}$.

To try to prove this as well, we have carried out different calculation tests with metals, such as $[M_2X_8]^{2-}$ [80]. We have worked on metal complexes from rhenium $[Re_2H_8]^{2-}$. We have chosen to carry out our analysis in a **lower energy configuration** with eclipsed hydrogen atom ligands, thus

in D_{4h} symmetry. This configuration provides a better overlap of the sigma systems between metals. The formation of the helical MOs is observed at the region of the rheniums and leads to the breaking of the applied symmetry.

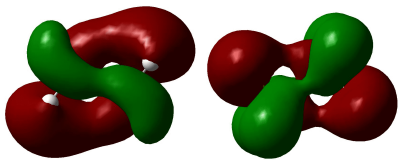

Figure 6.15: Representation of the molecular orbitals HOMO and HOMO-5 of the rhenium complex $[Re_2H_8]^{2-}$ (by DFT computations)

6.3 Conclusion

In this 6^{th} chapter, we **applied** the elements presented and proven in chapter 5 with concrete examples: $[n]$-cumulenes, $[n]$-hetero-cumulenes and more complex molecules especially with metals.

We show the results of DFT calculations for $[n]$**-cumulenes** with 3, 4, and 11 double bonds in **ground** and **excited** states following chain end rotations.

In parallel, we have carried out CASPT2 type calculations which also confirm the presence of helices, and proves that the formation of helices **does not depend** on the computation method.

We give illustrations of the formation of helices for each of the examples except for the 0° and 90° rotation cases.The so-called criterion for obtaining helices is thus satisfied.

In the case of **[n]-hetero-cumulenes** the helices are studied for a rotation of 25° and helices are obtained in most situations. We note that for silaketene the helices are not clearly visible between HOMO-1 and LUMO+1.

The cases of **[B=N]** and **[N=B]-cumulenes** show non-standard helices of the different energetic states.

The examples of **DPBD** and **tolanophane** are complementary. They show that the formation of helices depends on the mixing of p_x and p_y induced by the multiple bonds of the central linear chain during the rotation of one of the chain ends, whether it is the extremities are complex or not.

Finally to complete the study, we studied d-type orbitals with **metal-cumulenes**. These metallic complexes present **pseudo-helices** but further investigations for these situations could be considered.

To conclude on these results, we note that the influence of the rotation of the chain ends is essential in the existence of helices and that the complexity of the substituents and the number of atoms or double bonds (odd or even) are not determining factors.
Finally, the formation of such helices provides a different electronic distribution which certainly has an influence on the molecular reactivity. This gives access to new perspectives that require investigations beyond this manuscript.

Conclusion of the part III

This part III is composed of 3 chapters very dense in information.

Chapter 4 is **theoretical** and identifies all the elements and tools necessary to understand aromaticity for linear and cyclic systems in different situations.

Chapter 5 focuses on **helical states** which interested us a lot and required some ressources. We expose the properties of these helical states and the ways to characterize them (HEL, $\mathcal{A}_{N,n,\pm,0,z}$ for example). Moreover, we determine and prove the **criteria** of existence of helices based on mathematical (Löwdin) and chemical (Hückel and symmetries) works.

Chapter 6 gives a series of **illustrated examples** to summarize what we have shown by theory and to validate hypotheses concerning the nature of the substituents and the atoms constituting the system and on the constraints to be applied to provide helices.

Part IV

General conclusion

This manuscript is the result of three years of work, which required a great investment and a close collaboration between the work of chemists and mathematicians to provide general tools easily usable by the scientific community.

The **3 parts** of this manuscript are complementary and were detailed for a good understanding.

The **reminder** gives a general basic review of what is needed to understand in this work. The reminders related to the Schrödinger equation, the Hückel matrices, the atomic and molecular orbitals are essential for the subjects studied in this thesis. In addition, the computational methods used for this work are also largely explained.

A **second part** of this thesis work is based on the understanding of the **reactivity** and its representation by the π-Orbital Axis Vector (POAV) theory initially proposed by R. C. Haddon.
We have worked to implement an adapted, clarified and generalized response of the tools related to **POAV1**. This answer gives the possibility to avoid heavy computational methods in the case of complex molecules, and to predict the reactivity, essential information for chemists.
All of this work also, gave us the opportunity to publish our first article on the subject of the pyramidalization angle, the POAV1 and the associated tools. This work has been illustrated with fullerenic, non-fullerenic and nitrile imines molecules by the means of the *Pychemcurv* software developed in the context of the thesis and which is detailed in chapter 2. This illustrative dense chapter shows clearly the extent of the work that has been done and the investments of our research team.
POAV2 theory's work has not been fully finalized and will certainly require additional time for analysis and research, particularly the quantified difference of POAV2 versus POAV1. The theoretical difference between the two theories has clearly been established by our work, however the results of comparisons are not sufficient enough to make clear conclusions at this stage. This leads to the following question, is the computational cost of the algorithm compensated by the precision's degree obtained? It doesn't, meaning that POAV1 can be used without any problem. The struggle being majorly on the reactivity cartographies of molecules, the result is important because they can be carried out without difficulties on large molecules. At this time, a preprint of our work on POAV2 is in progress and we should have solutions to the unsolved questions.

The **third part** of this manuscript is focused on **aromaticity** and **helical states**.
The study of aromaticity is closely related to the reactivity issues encountered in part II and aromatic molecules will be privileged for many useful reactions.
The work on the **aromaticity criteria** has required an important research work by using old works of Hückel and Zimmerman. We have established with the help of mathematics all the definitions and relations in order to make the presentation and the link between the visions of Hückel and Möbius, to establish relations and energetic comparisons. Moreover, we make the distinction according to the electronic configuration between the cyclic and linear cases in a complete way by many parameters.
The work related to aromaticity has emphasized the curiosity of the **helical orbitals** studied by R. Hoffmann. We have spent a lot of time for understanding these particular electronic states. All the properties of these states such as the distribution of angles, could be studied in different situations in particular according to the rotational constraint applied to the molecular ends which proved to be essential. In a physical and chemical way, we have established the criteria of existence of these helices related to the molecular symmetry. The last chapter illustrates this important work and gives the opportunity to validate properties and observations.

The manuscript provides an important contribution of information on the theoretical level and gives simple tools to establish the link between different major notions as curvature, reactivity and aromaticity. It therefore, opens perspectives for the determination of the reactivity and the characterization of new materials.

Part V

Appendices

Appendix 1 : Chemistry part

This first appendix presents the detailed computational techniques used to perform this work and, the different molecule representations used for the quantum calculations of the third part of this thesis manuscript chapter 6.

Computational techniques

The different simulations of molecules carried out in this manuscript were possible thanks to the cartesian coordinates (x, y, z) of each molecule under a precise symmetry of sections 2.2, and 2.3, and in a precise torsion angle in the particular case of the third part chapter 6. We make available in a supplementary information file all the cartesian data that we have generated to perform the simulations.

For all the simulations carried out in the application part of the database of Tománek and Frederick (section 2.2), the cartesian coordinates were available in free access [5].

However, for the coordinates used in the applications to the compounds resulting from the work of R. C. Haddon (section 2.3), and in the case of [n]-cumulenes and the other examples associated to chapter 6 it was necessary to create molecular structures (in 3D) files.

By consequence, the data files were generated by modeling the molecules, by creating each of the molecular structures in 3D by the **Avogadro** or VMD [84][40] software. For each molecule, their geometry was optimized on the software. Then, the cartesian data of the molecules are extracted in a *.xyz* file. These data are the cartesian coordinates (x, y, z) of each molecule under precise constraints.

Note that a lot of work has been necessary to select and design all these molecules.

When all the cartesian data were obtained, we used them for the Gaussian [12] quantum calculations. For each of the molecules, we created *.com* type calculation launching files in order to obtain all the necessary information in terms of energy, frequency, and orbitals in *.out* and *.fchk* type output files. The exploitation (in particular the visualization of the orbitals) of the *.out* files was carried out by **Molden** [85] and the *.fchk* files by the **Gaussview** software [86] which give access to 3D structural data of the molecules, energy and orbital data but also give information on the viability of the molecules designed. All the calculations were performed by DFT at a $B3LYP-6-311G^*$ level but also CASPT2 calculations have completed and validated certain of the previous results.

All the simulations of computations were carried out on the scientific computing cluster Pyrene of the university. All the information related to the cluster is easily accessible [87].

Notice that the theoretical details about the quantum computation methods are given in the reminder part of the manuscript 0.3.

Representation of the molecules used for DFT computations in chapter 6

The representations of this section, concern the molecules used for the DFT calculations presented for all of the [3]-cumulene, [4]-cumulene, [11]-cumulene, [2]-heterocumulenes, [3]-heterocumulenes, [B=N]-cumulenes, [N=B]-cumulenes, DPBD molecule, and tolanophane molecule following the detailed method presented in the first section of the appendix.

All the representations of the molecules are provided for molecules with 0°, 25°, 30° of rotation.

[n]-cumulenes:

[3]**-cumulene**

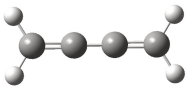

Figure a1.16: Representation of the [3]-cumulene in the fundamental state at 0°.

[4]**-cumulene**

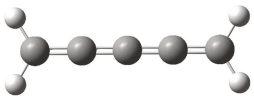

Figure a1.17: Representation of the [4]-cumulene in the fundamental state at 0°.

[11]**-cumulene**

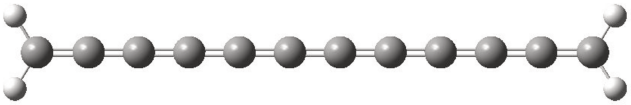

Figure a1.18: Representation of the [11]-cumulene in the fundamental state at 0°.

[2]**-heterocumulenes:**

Phosphaallene

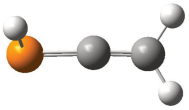

Figure a1.19: Representation of the phosphaallene in the fundamental state at 25°.

Diphosphoaallene

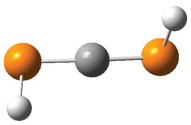

Figure a1.20: Representation of the diphosphoaallene in the fundamental state at 25°.

Phosphaazaallene

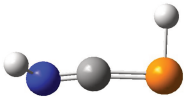

Figure a1.21: Representation of the phosphaazaallene in the fundamental state at 25°.

Arsaallene

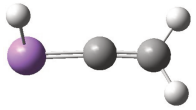

Figure a1.22: Representation of the arsaallene in the fundamental state at 25°.

Arsaphosphaallene

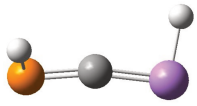

Figure a1.23: Representation of the arsaphosphaallene in the fundamental state at 25°.

Diarsaallene

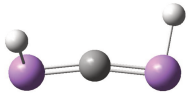

Figure a1.24: Representation of the diarsaallene in the fundamental state at 25°.

Silaallene

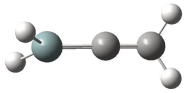

Figure a1.25: Representation of the silaallene in the fundamental state at 25°.

Phosphasiaallene

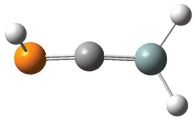

Figure a1.26: Representation of the phosphasilaallene in the fundamental state at 25°.

Silaketene

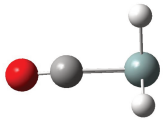

Figure a1.27: Representation of the silaketene in the fundamental state at 25°.

Germaallene

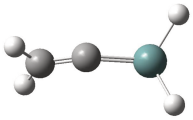

Figure a1.28: Representation of the germaallene in the fundamental state at 25°.

Germaphosphaallene

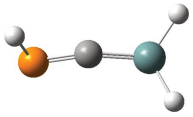

Figure a1.29: Representation of the germaphosphaaallene in the fundamental state at 25°.

[3]-heterocumulenes:

Phosphabutatriene

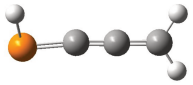

Figure a1.30: Representation of the phosphabutatriene in the fundamental state at 25°.

Diphosphabutatriene

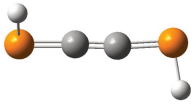

Figure a1.31: Representation of the diphosphabutatriene in the fundamental state at 25°.

Arsabutatriene

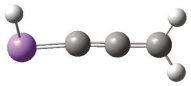

Figure a1.32: Representation of the arsabutatriene in the fundamental state at 25°.

Silabutatriene

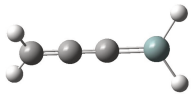

Figure a1.33: Representation of the silabutatriene in the fundamental state at 25°.

$[B = N]$ or $[N = B]$-cumulenes:

B=N=B=N=B cumulene (charge = 0 - doublet and quadruplet states)

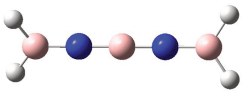

Figure a1.34: Representation at 30° of rotation.

N=B=N=B=N cumulene (charge = 1 - singlet and triplet states)

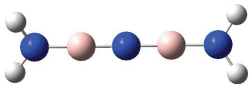

Figure a1.35: Representation at 30° of rotation.

B=N=B=N=B=N cumulene (charge = 0 - singlet state)

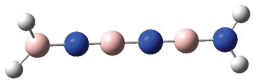

Figure a1.36: Representation at 30° of rotation.

B=N=B=N=B=N cumulene (charge = 1 - doublet state)

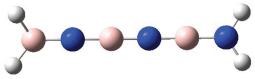

Figure a1.37: Representation at 30° of rotation.

B=N=B=N=B=N cumulene (charge = 2 - triplet state)

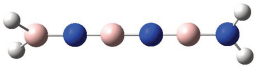

Figure a1.38: Representation at 30° of rotation.

DPBD molecule

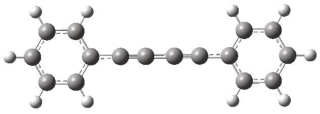

Figure a1.39: Representation at 30° of rotation.

Tolanophane molecule

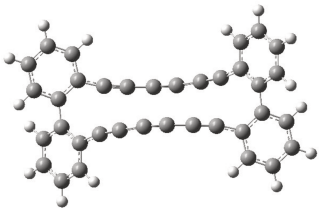

Figure a1.40: Representation at 30° of rotation.

Rhenium complex $[Re_2H_8]^{2-}$

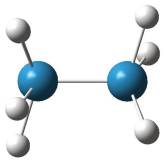

Figure a1.41: Representation of the rhenium complex.

Appendix 2 : Technical and proofs part of the results used

For the convenience of the reader, proofs of the results are detailed in this appendix and some of the results in this thesis are provided from our article and preprints [4, 44, 36].

1-Proofs associated to the section 0.2.4: Characteristic polynomial of H

Note that by using the graph approach for Hückel's calculations, we are in the case of uniform distribution:

$$\mathbf{H} = \alpha \mathbf{Id}_N + \beta \cos(\phi) \mathbf{A}(\mathbf{G}) \tag{a2.1}$$

Taking $\sigma_1, \ldots, \sigma_n$ the real ordered eigenvalues of $\mathbf{A}(G)$, since $\mathbf{A}(G)$ is symmetrical, we obtain the relation between the eigenvalues of $\mathbf{H}$ and $\mathbf{A}(G)$:

$$\lambda_i = \alpha + \beta \cos(\phi) \sigma_i \tag{a2.2}$$

with $i = 1, \ldots, N$.
Assuming that $\mathbf{H}$ is diagonalizable, P is the passing matrix between the initial basis and the eigenvector basis such that:

$$\mathbf{D} = P^{-1} \mathbf{H} P \tag{a2.3}$$

where $\mathbf{D}$ *is the diagonalizable matrix.*

$$\mathbf{D} = \begin{pmatrix} \lambda_1 & 0 & \ldots & 0 \\ \ldots & \ldots & \ldots & \ldots \\ 0 & \ldots & 0 & \lambda_N \end{pmatrix} \tag{a2.4}$$

If we multiply on each side the relation a2.1 and using $P^{-1}P = \mathbf{Id}_N$, we have:

$$\mathbf{D} = \alpha \mathbf{Id}_N + \beta \cos(\phi) P^{-1} \mathbf{A}(G) P \tag{a2.5}$$

The matrix $P^{-1}\mathbf{A}(G)P$ must be diagonal and of eigenvalues σ_i, $i = 1, \ldots, N$ which results in the relation on the eigenvalues of $\mathbf{H}$ and $\mathbf{A}(G)$.

2-Proofs associated to the section 0.2.4: Total energy of a molecule

This relation is simplified when we assume a uniform distribution $\phi_i = \phi$ because $\nu_i(\phi) = \cos(\phi)\sigma_i$ where the σ_i are the eigenvalues of the adjacent matrix of the graph G of the molecule:

$$E = \pi(S)\alpha + \beta \cos(\phi) \sum_{i=1}^{N} g_i \sigma_i \tag{a2.6}$$

Note that in most interesting cases, we can relate the value of g_i to the sign of σ_i via the rule $g_i = 2$ if $\sigma_i > 0$ and $g_i = 0$ if $\sigma_i < 0$.

In this case, the energy is: $E = \pi(S)\alpha + 2\beta \cos(\phi) \sum_{i=1}^{N} \sigma_i \mathbf{1}_{\sigma_i > 0}$ where $\mathbf{1}_{\sigma_i > 0}$ is the indicator of $\sigma_i > 0$. By separating the eigenvalues ≤ 0, noted $\sigma_1, \ldots, \sigma_k$, for a certain k, from the positive eigenvalues $\sigma_{k+1}, \ldots, \sigma_N$ and by using the relation $(\sigma_1 + \cdots + \sigma_k) + (\sigma_{k+1} + \cdots + \sigma_N) = 0$, we rewrite the energy as:

$$\begin{aligned} E &= \pi(S)\alpha + 2\beta\cos(\phi)\sum_{i=1}^{N}\sigma_i \mathbf{1}_{\sigma_i>0} \\ &= \pi(S)\alpha + 2\beta\cos(\phi)\sum_{i=k+1}^{N}\sigma_i \\ &= \pi(S)\alpha + \beta\cos(\phi)\left[\sum_{i=k+1}^{N}\sigma_i + \sum_{i=k+1}^{N}\sigma_i\right] \\ &= \pi(S)\alpha + \beta\cos(\phi)\left[\sum_{i=k+1}^{N}\sigma_i - \sum_{i=1}^{k}\sigma_i\right] \\ &= \pi(S)\alpha + \beta\cos(\phi)\sum_{i=1}^{N} \mid \sigma_i \mid \end{aligned} \tag{a2.7}$$

The quantity $E(G) = \sum_{i=1}^{N} \mid \sigma_i \mid$ is called energy of the graph G of the molecule. We have then the relation:

$$E = \pi(S)\alpha + \beta\cos(\phi)E(G) \tag{a2.8}$$

which explains that in some simple configurations, the G graph contains all the information of the orbitals.

3-Proofs associated to the section 1.1.1: POAV$_\epsilon$(A)

The $POAV_\epsilon(A)$ vector is only defined by the **local geometry** of the molecule in a given atom A and precisely only on the relative angles of the bonds starting in A. By construction, all regularized vector $\overrightarrow{AReg_\epsilon(B)}$ for $B \in \star(A)$ satisfy the relation (1.4) meaning that if $POAV_\epsilon(A)$ makes a constant angle with all the vectors $\overrightarrow{AReg_\epsilon(B)}$ for $B \in \star(A)$, this vector makes also a constant angle with all vectors in $\overrightarrow{AReg_{\epsilon'}(B)}$ with $B \in \star(A)$ for any $\epsilon' > 0$. As a consequence, the vector $POAV(A)_\epsilon$ vector is independent of ϵ.

4-Proofs associated to the section 1.2.1: Condition of normalization

The normalization on the s component of (h_1, h_2, h_3, h_π) gives:

$$c_\pi^2 + 3\mu^2\lambda_\pi^2 = 1, \tag{a2.9}$$

and the one on the p_z component gives:

$$\lambda_\pi^2 + 3\mu^2 c_\pi^2 = 1. \tag{a2.10}$$

We then obtain by addition of the two previous equations:

$$(c_\pi^2 + \lambda_\pi^2)(1 + 3\mu^2) = 2 \tag{a2.11}$$

As $c_\pi^2 + \lambda_\pi^2 = 1$, this gives:

$$\mu = \frac{1}{\sqrt{3}} \tag{a2.12}$$

This concludes the proof.

5-Proofs associated to the section 1.2.1: Hybridization coefficients and POAV1

The POAV1 vector is such that the angle between the h_π orbital and each orbital h_1, h_2, h_3 is:

$$\frac{\pi}{2} + Pyr(A)$$

The vector associated to h_π is $v_\pi = (0, 0, \lambda_\pi)$ and the one with h_1 is $v_1 = (c_{1,2}, 0, \frac{-c_\pi}{\sqrt{3}})$.
The scalar product between the two vectors gives $v_\pi \cdot v_1 = -\frac{1}{\sqrt{3}} c_\pi \lambda_\pi$.
This scalar product is also equal to $\| v_\pi \| \| v_1 \| \cos(v_\pi, v_1)$.

As $\| v_\pi \|^2 = \lambda_\pi^2$ and $\| v_1 \|^2 = \frac{3c_{1,2}^2 + c_\pi^2}{3}$, we obtain taking the square on each side of the equality:

$$\frac{\lambda_\pi^2 c_\pi^2}{3} = \frac{3c_{1,2}^2 + c_\pi^2}{3} \lambda_\pi^2 \cos^2\left(\frac{\pi}{2} + Pyr(A)\right) \tag{a2.13}$$

We then have:

$$\lambda_\pi^2 \left[c_\pi^2 - (3c_{1,2}^2 + c_\pi^2) \cos^2\left(\frac{\pi}{2} + Pyr(A)\right)\right] = 0 \tag{a2.14}$$

As $\lambda_\pi \neq 0$, we obtain:

$$c_\pi^2 \left(1 - \cos^2\left(\frac{\pi}{2} + Pyr(A)\right)\right) = 3c_{1,2}^2 \cos^2\left(\frac{\pi}{2} + Pyr(A)\right) \tag{a2.15}$$

Using the fact that:

$$1 - \cos^2\left(\frac{\pi}{2} + Pyr(A)\right) = \sin^2\left(\frac{\pi}{2} + Pyr(A)\right)$$

and the equality:

$$\cos\left(\frac{\pi}{2} + Pyr(A)\right) = -\sin(Pyr(A)$$

and

$$\sin\left(\frac{\pi}{2} + Pyr(A)\right) = \cos(Pyr(A))$$

We deduce:

$$c_\pi^2 \cos^2(Pyr(A)) = 3c_{1,2}^2 \sin^2(Pyr(A)) \tag{a2.16}$$

Assuming that $Pyr(A) \neq \frac{\pi}{2}$, we obtain:

$$c_\pi^2 = 3c_{1,2}^2 \frac{\sin^2(Pyr(A))}{\cos^2(Pyr(A))} = 3c_{1,2}^2 \tan^2(Pyr(A)), \tag{a2.17}$$

which concludes the proof.

6-Proofs associated to the section 1.2.1: sp^3 hybridization conditions

This follows from $c_{2,3}^2 + c_{3,3}^2 = 2c_{2,3}^2 = 1$, which gives for example $c_{2,3} = \pm\frac{1}{\sqrt{2}}$ and $c_{3,3} = \pm\frac{1}{\sqrt{2}}$.

The second normalization gives $c_{1,2}^2 + 2c_{2,2}^2 = 1$.

The symmetry condition (eq. 1.23) with $c_{2,3}^2 = \frac{1}{2}$ leads to the relation $c_{2,2}^2 + \frac{1}{2} = c_{1,2}^2$. Putting this expression in the normalization equation gives $c_{2,2}^2 + \frac{1}{2} + 2c_{2,2}^2 = 1$.

We deduce that $3c_{2,2}^2 = \frac{1}{2}$ or $c_{2,2}^2 = \frac{1}{6}$ and so $c_{1,2}^2 = \frac{2}{3}$.

7-Proofs associated to the section 1.3: Admissible molecules

The proof of this angle is well-defined, and follows the same line as in the trivalent case. Let $\epsilon > 0$ be given and denoted by $z_{A,\epsilon}$, the distance $O_\epsilon A$. Then, we have for a given bond AB, B $\in \star(A)$, as:

$$\sin(Pyr(A)) = \frac{z_{A,\epsilon}}{\epsilon} \tag{a2.18}$$

This quantity does not depend on B and is, in fact, independent of ϵ. Indeed, let us consider $\epsilon' = \lambda\epsilon$, then $z_{A,\epsilon'} = \lambda z_{A,\epsilon}$ and $\frac{z_{nA,\epsilon'}}{\epsilon'} = \frac{z_{A,\epsilon}}{\epsilon}$.

The previous definition is, of course, far from being satisfied as it works for a very restrictive class of molecules. We discuss more precisely the restriction associated with the use of the pyramidalization angle in the section 1.3.

8-Proofs associated to the section 1.4.1: Non-linear relationship between the spherical curvature and the pyramidalization angle

B $\in \star(A)$ and I the middle between A and B and, O the center of the osculating sphere of radius R_A.

We have $AB = a$, $AI = \frac{a}{2}$ and $AO = R_A$.

In the triangle AIO, we have the angle $\widehat{OAI} = \frac{\pi}{2} - Pyr(A)$.

By consequence, $\cos\left(\frac{\pi}{2} - Pyr(A)\right) = \frac{AI}{AO} = \frac{a}{2R_A}$,

thus, $\cos\left(\frac{\pi}{2} - Pyr(A)\right) = \sin(Pyr(A))$.

9-Proofs associated to the section 1.4.2: Spherical curvature in non-regular case

By definition, in the figure 1.8 the line $\mathcal{L}$ corresponds to the set of points at equal distance of B, C and D. The center of the osculating sphere must belong to $\mathcal{L}$. The center O_z is then of the form $O_z = (0, 0, z)$ with $z \in \mathbb{R}$ in the reference frame $\mathcal{R}$.

We look for a point O_z such that $O_zA = O_zB = O_zC = O_zD$.

As $O_zB = O_zC = O_zD$ by construction, we have only to ensure $O_zA = O_zB$.

By the Pythagorean theorem, we have $O_zB^2 = z^2 + l^2$ and,

$O_zA^2 = O_zO_{z_A}^2 + O_{z_A}A^2 = L^2 + (z_A - z)^2 = L^2 + z_A^2 + z^2 - 2zz_A$ thus,

$O_zB^2 = O_zA^2$ implies $2zz_A = L^2 + z_A^2 - l^2$.

As $A \notin \mathcal{P}$ then $z_A \neq 0$ and $z = \frac{L^2 + z_A^2 - l^2}{2z_A}$.

This concludes the proof.

10-Proofs associated to the section 1.5: Relationship angular defect and pyramidalization angle

By definition, we have:

$$\theta_1(A) + \theta_2(A) + \theta_3(A) = 2\pi \tag{a2.19}$$

By construction, we have $OB_1 = OB_2 = OB_3 = R$, with R the radius of the **circumcircle** for the triangle $B_1B_2B_3$.

The triangle AOB_1 is rectangle in O by construction. By definition of the Pyr, we have:

$$OB_1 = l\cos(Pyr(A)) \tag{a2.20}$$

Then,

$$R = l\cos(Pyr(A)) \tag{a2.21}$$

Using this quantity, one can compute the quantity $B_1B_2 + B_2B_3 + B_3B_1$ which is the perimeter of the triangle $B_1B_2B_3$ in $\mathcal{P}(A)$. We have two ways to compute this quantity:

- First, using the fact that in the triangle B_1OB_2, the length B_1B_2 is given by $2R\sin\left(\frac{\theta_1(A)}{2}\right)$ and similar expressions for B_2B_3, B_3B_1. We then obtain:

$$B_1B_2 + B_2B_3 + B_3B_1 =$$

$$2R\left[\sin\left(\frac{\theta_1(A)}{2}\right) + \sin\left(\frac{\theta_2(A)}{2}\right) + \sin\left(\frac{\theta_3(A)}{2}\right)\right] \tag{a2.22}$$

- Second, using the fact that in the triangle B_1AB_2, the length B_1B_2 is given by $2l\sin\left(\frac{\alpha_1(A)}{2}\right)$ and similar expressions for B_2B_3, B_3B_1. We then obtain:

$$B_1B_2 + B_2B_3 + B_3B_1 =$$

$$2l\left[\sin\left(\frac{\alpha_1(A)}{2}\right) + \sin\left(\frac{\alpha_2(A)}{2}\right) + \sin\left(\frac{\alpha_3(A)}{2}\right)\right] \tag{a2.23}$$

Replacing R by its expression, and writing the equality of these two expressions, we deduce:

$$\cos(Pyr(A))\left[\sin\left(\frac{\theta_1(A)}{2}\right) + \sin\left(\frac{\theta_2(A)}{2}\right) + \sin\left(\frac{\theta_3(A)}{2}\right)\right] =$$

$$\left[\sin\left(\frac{\alpha_1(A)}{2}\right) + \sin\left(\frac{\alpha_2(A)}{2}\right) + \sin\left(\frac{\alpha_3(A)}{2}\right)\right] \tag{a2.24}$$

The Pyr is then understood as a measure of the difference between the angles $\theta_i(A)$ and $\alpha_i(A)$, $i = 1, 2, 3$.

Denoting by I_1 the middle of the segment B_1B_2 and by using the triangle AOI_1 which is rectangle in O, we obtain using the Pythagorean theorem:

$$\cos\alpha_F(A) = \cos^2 Pyr(A)\ \cos\theta_F(A) + \sin^2 Pyr(A) \tag{a2.25}$$

This concludes the proofs.

11-Proofs associated to the section 3.1.2: Conditions of orthogonality

We have by definition: s orbitals and the set $\{p_x, p_y, p_z\}$ of orbitals as: $u_i = u_{i,2}p_x + u_{i,3}p_y + u_{i,4}p_z$ and $u_\pi = u_{\pi,2}p_x + u_{\pi,3}p_y + u_{\pi,4}p_z$ where $u_{i,k}$ and $u_{\pi,k}$, $\mathbf{k = 1, 2, 3}$ are scalars.

We identify the orbital u_i with the vector $(u_{i,2}, u_{i,3}, u_{i,4})$ of $\mathbb{R}^3$ as well for u_π.

By definition, we have $\langle s, s\rangle = 1$, $\langle p_x, p_x\rangle = 1$, $\langle p_y, p_y\rangle = 1$, $\langle p_z, p_z\rangle = 1$ and $\langle p_x, p_y = \langle p_x, p_z\rangle = \langle p_y, p_z\rangle = 0$.

We then deduce that: $\langle u_i, u_i\rangle = 1$ and $\langle u_\pi, u_\pi\rangle = 1$ as the vectors u_i and u_π are unitary.
Moreover, we have by definition: the angle $\theta_{i,j}$ as $\langle u_i, u_j\rangle = \cos(\theta_{i,j})$. In the same way, we obtain $\langle u_i, u_\pi\rangle = \cos(\theta_{i,\pi})$.

As a consequence, we obtain:

$$\begin{array}{rcl} \langle h_i, h_j\rangle & = & c_i c_j \langle s, s\rangle + \lambda_i \lambda_j \langle u_i, u_j\rangle \\ & = & c_i c_j + \lambda_i \lambda_j \cos(\theta_{i,j}) \end{array} \tag{a2.26}$$

As $\langle h_i, h_j\rangle = 0$ by orthogonality conditions, we obtain the first set of conditions $(H_{i,j})$.

The set of conditions $(H_{i,\pi})$ follows the same lines.

12-Proofs associated to the section 3.1.2: Relation between the angles $\theta_{i,j}$

This is a simple computation, we have orthogonality between h_π and the h_i:

$$\lambda_\pi = -\frac{c_i c_\pi}{\lambda_i \cos(\theta_{i,\pi})},$$

thus,

$$\frac{c_i}{\lambda_i \cos(\theta_{i,\pi})} = \frac{c_j}{\lambda_j \cos(\theta_{j,\pi})}$$

for i, j ∈ {1, 2, 3}.

We deduce:

$$c_j \lambda_i \cos\theta_{i,\pi} = c_i \lambda_j \cos\theta_{j,\pi} \tag{a2.27}$$

for i, j ∈ {1, 2, 3}.

Moreover, the orthogonality condition between the h_i orbitals leads to:

$$c_i = -\frac{\lambda_i \lambda_k \cos(\theta_{i,k})}{c_k} \quad for\ all \quad i \neq k \in \{1, 2, 3\}. \tag{a2.28}$$

Replacing c_i and c_j in eq. a2.27 by these expressions for $k \neq i$ or j, we obtain:

$$\frac{\lambda_j \lambda_i \lambda_k}{c_k} \cos(\theta_{j,k}) \cos(\theta_{i,\pi}) = \frac{\lambda_i \lambda_j \lambda_k}{c_k} \cos(\theta_{i,k}) \cos(\theta_{j,\pi}) \tag{a2.29}$$

for i, j ∈ {1, 2, 3},

which leads to:

$$\cos(\theta_{j,k}) \cos\theta_{i,\pi} = \cos(\theta_{i,k}) \cos(\theta_{j,\pi}) \tag{a2.30}$$

This concludes the proof.

13-Proofs associated to the section 3.1.2: C_{3v} symmetry

If the angles between the vector u_π and the bonds are equal, then we obtain directly using eq. 3.5 that $\theta_{i,k} = \theta_{j,k}$ and the molecule possesses a C_{3v} symmetry.

If the molecule possesses a C_{3v} symmetry, we have $\theta_{i,k} = \theta_{j,k}$ and as a consequence using relation 3.5, $\theta_{i,\pi} = \theta_{j,\pi}$ *for all* i, j.
This concludes the proof.

14-Proofs associated to the section 3.1.2: Components of the u_π vector solutions of linear system

The proof is a simple computation.

We have $u_i.u_\pi = x_i x_\pi + y_i y_\pi + z_i z_\pi = \cos\theta_{i,\pi}$, *(with i=1, 2, 3)* by definition of the angles $\theta_{i,\pi}$ and the fact that the u_i and u_π are unitary.
Multiplying the previous equation for i by $\cos\theta_{j,k}$ and subtracting for j multiplied by $\cos\theta_{i,k}$, we obtain the relation:

$$(x_i\cos\theta_{j,k} - x_j\cos\theta_{i,k})x_\pi + (y_i\cos\theta_{j,k} - y_j\cos\theta_{i,k})y_\pi + (z_i\cos\theta_{j,k} - z_j\cos\theta_{i,k})z_\pi \qquad \text{(a2.31)}$$
$$= \cos(\theta_{j,k})\cos(\theta_{i,\pi}) - \cos(\theta_{j,\pi})\cos(\theta_{i,k})$$

which is equal to zero by eq. 3.5.

15-Proofs associated to the section 3.1.2: Linear system $M.u_\pi = 0$

The determinant of M is zero. Indeed, if we denote by $M = (m_{i,j})_{i,j\in\{1,2,3\}}$, we observe that $m_{2,i} - m_{1,i} = m_{3,i}$ *for i=1, 2, 3.* As a consequence, the matrix M has a kernel of dimension 1 or 2.

A condition for the kernel to be of dimension 2 is that the rank of the matrix M is 1. This can be done if all the 2 by 2 minor of the matrix have a determinant equal to zero. A direct computation of these determinants lead to three conditions corresponding to the determinant of three minors.

Precisely, we have:

$$\begin{vmatrix} x_3\cos\theta_{1,2} - x_2\cos\theta_{3,1} & y_3\cos\theta_{1,2} - y_2\cos\theta_{3,1} \\ x_1\cos\theta_{2,3} - x_2\cos\theta_{3,1} & y_1\cos\theta_{2,3} - y_2\cos\theta_{3,1} \end{vmatrix}$$

$$= \cos\theta_{1,2}\cos\theta_{2,3}(x_3y_1 - y_3x_1) + \cos\theta_{1,2}\cos\theta_{3,1}(y_3x_2 - y_2x_3) + \cos\theta_{2,3}\cos\theta_{3,1}(x_1y_2 - y_1x_2) \qquad \text{(a2.32)}$$

In the same way, we obtain:

$$\cos\theta_{1,2}\cos\theta_{2,3}(y_3z_1 - z_3y_1) + \cos\theta_{1,2}\cos\theta_{3,1}(z_3y_2 - z_2y_3) + \cos\theta_{2,3}\cos\theta_{3,1}(y_1z_2 - z_1y_2) \qquad \text{(a2.33)}$$

and

$$\cos\theta_{1,2}\cos\theta_{2,3}(x_3z_1 - z_3x_1) + \cos\theta_{1,2}\cos\theta_{3,1}(z_3x_2 - z_2x_3) + \cos\theta_{2,3}\cos\theta_{3,1}(x_1z_2 - z_1x_2) \qquad \text{(a2.34)}$$

As $u_1 \wedge u_3 = (y_1z_3 - y_3z_1, x_3z_1 - x_1z_3, x_1y_3 - x_3y_1)$ we can resume the previous equality by the following vector relation:

$$\cos\theta_{1,2}\cos\theta_{2,3}u_1 \wedge u_3 + \cos\theta_{1,2}\cos\theta_{3,1}u_2 \wedge u_3 + \cos\theta_{2,3}\cos\theta_{3,1}u_1 \wedge u_2 = 0 \qquad \text{(a2.35)}$$

This relation can be rewritten as:

$$u_1 \wedge (\cos\theta_{1,2}\cos\theta_{2,3}u_3 + \cos\theta_{2,3}\cos\theta_{3,1}u_2) = -\cos\theta_{1,2}\cos\theta_{3,1}u_2 \wedge u_3. \tag{a2.36}$$

The vector $u_2 \wedge u_3$ is orthogonal to the plane $\mathcal{P}_{2,3}$ generated by u_2 and u_3.
As $w = \cos\theta_{1,2}\cos\theta_{2,3}u_3 + \cos\theta_{2,3}\cos\theta_{3,1}u_2$ belongs to $\mathcal{P}_{2,3}$, the vector $u_1 \wedge w$ is perpendicular to the plane $\mathcal{P}_{2,3}$ if and only if u_1 belongs to this plane, meaning that u_1, u_2 and u_3 belongs to $\mathcal{P}_{2,3}$ and the molecule is planar.

16-Proofs associated to the section 3.1.3: Hybridization numbers n_1, n_2, n_3

We give the proof only for n_1, the other ones following the same strategy.

We remind that due to eq. 3.3 and 3.4, we have the following system of relations:

$$\begin{array}{rcl} c_1c_2 + \lambda_1\lambda_2\cos\theta_{1,2} &=& 0 \\ c_1c_3 + \lambda_1\lambda_3\cos\theta_{1,3} &=& 0 \\ c_2c_3 + \lambda_2\lambda_3\cos\theta_{2,3} &=& 0 \end{array} \tag{a2.37}$$

The first equation gives:

$$\frac{\lambda_1}{c_1} = -\frac{c_2}{\lambda_2}\frac{1}{\cos\theta_{1,2}} \tag{a2.38}$$

Using the third equation, we obtain the relation:

$$\frac{c_2}{\lambda_2} = -\frac{\lambda_3}{c_3}\cos\theta_{2,3} \tag{a2.39}$$

it can be used to replace $\frac{c_2}{\lambda_2}$ in eq. a2.38, then we have:

$$\frac{\lambda_1}{c_1} = \frac{\lambda_3}{c_3}\frac{\cos\theta_{2,3}}{\cos\theta_{1,2}} \tag{a2.40}$$

Using the second equation, we explicit $\frac{\lambda_3}{c_3}$ as:

$$\frac{c_3}{\lambda_3} = -\frac{\lambda_1}{c_1}\cos\theta_{1,3} \tag{a2.41}$$

Replacing in eq. a2.40, we finally obtain:

$$\frac{\lambda_1}{c_1} = -\frac{c_1}{\lambda_1}\frac{\cos\theta_{2,3}}{\cos\theta_{1,2}\cos\theta_{1,3}} \tag{a2.42}$$

which leads to:

$$\frac{\lambda_1^2}{c_1^2} = -\frac{\cos\theta_{2,3}}{\cos\theta_{1,2}\cos\theta_{1,3}} \tag{a2.43}$$

This concludes the proof.

17-Proofs associated to the section 3.1.3: sp^3 normalization

The sp^3 normalization condition (eq. 3.10) can be rewritten as:

$$\sum_{i=1}^{3}\frac{1}{1+n_i} + \frac{m}{m+1} = 1 \tag{a2.44}$$

By factorizing c_i^2 in the third first terms and λ_π^2 in the last one.

We then obtain:

$$\frac{m}{m+1} = 1 - W_\sigma \tag{a2.45}$$

using the definition of W_σ, which leads to:

$$m = \frac{1 - W_\sigma}{W_\sigma} \tag{a2.46}$$

18-Proofs associated to the section 4.3.5: Study of the degeneracies of the energy levels in the even case $\pi(S_N^1) \equiv 0$ [mod.4] for the Möbius case

For proof, the solutions correspond to i and j such as:

$$\cos\left((2k+1)\pi\frac{i}{N}\right) = \cos\left((2k+1)\pi\frac{j}{N}\right)$$

This leads to,

$$(2i+1)\frac{\pi}{N} = -(2j+1)\pi\frac{j}{N} + 2l\pi \tag{a2.47}$$

Thus,

$$2i + 1 = -2j - 2 + lN$$

As *i and j ∈ 0,..., N-1*, there is $l = 1$.

We then, have:

$$j = \frac{N}{2} - 1 - i \tag{a2.48}$$

if N is an even number.

19-Proofs associated to the section 4.3.5: Study of the degeneracies of the energy levels in the even case $\pi(S_N^1) \equiv 0$ [mod.4] for the ribbon case

The solutions of $\lambda_i = \lambda_j$ correspond to i and j as:

$$\cos\left(\frac{2\pi i}{N}\right) = \cos\left(\frac{2\pi j}{N}\right)$$

This last equation gives:

$$\frac{2\pi i}{N} = -\frac{2\pi j}{N} + 2l\pi$$

Thus, $i = -j + lN$.

As, $i, j \in 0, ..., N-1$, $l = 1$, therefore, $j = N - i$ and $1 \leq i \leq N - 1$.

20-Proofs associated to the section 4.3.5: Structure of molecules S_N^1 C_2 invariant, property of torsion distribution

$$\phi_{N-i+1} = \phi_i \tag{a2.49}$$

with $i = 1, ..., N-1$.

To prove this, it is a simple computation. Each vector u_i *(with* $i = 1, ..., N$*)*, is obtained in a reference frame centered in the atom C_i by giving the tangent vector n_i in the direction of the curve and the normal plane in which we note by convention the coordinates by (x, y), and the coordinate x being normal to the plane of the molecule. Each vector u_i is then, in its adapted reference frame of the form

$(a_i, b_i, 0)$ which is identified with a vector of $\mathbb{R}^2$ noted $U_i = (a_i, b_i)$. By convention, we have $U_1 = (1, 0)$.

By definition of the ϕ distribution, the angle ϕ_i is such as $U_{i+1} = e^{-j\phi_i} U_i$. The C_2 symmetry of axis z refers the atom C_i to the atom C_{N-i+1}. By invariance we also have $U_i = U_{N-i+1}$. Moreover, the C_2 symmetry being an isometry, it maintains the angles and we have :

$$\phi_i = \widehat{U_i, U_{i+1}} = \widehat{U_{N-i+1}, U_{N-i}} = \phi_{N-i+1} \tag{a2.50}$$

with i = 1,..., N-1.

In other words, we obtain the relation:

$$\phi_i = \phi_{N-i+1} \tag{a2.51}$$

with i = 1,..., N-1.

21-Proofs associated to the section 4.3.9: Torsion angle and properties - $\phi_{1,n}$ relation

This angle is computed in the plane (x, y) by the formula:

$$\cos(\phi_{1,n}) = \frac{u_1 . u_n}{\| u_1 \| \| u_n \|} = \frac{a_1 a_n}{| a_1 | \sqrt{b_n^2 + a_n^2}} \tag{a2.52}$$

then,

$$\phi_{1,n} = \arccos\left(\frac{a_1 a_n}{| a_1 | \sqrt{b_n^2 + a_n^2}}\right) \tag{a2.53}$$

An other way to write this formula is:

$$\phi_{1,n} = \arccos\left(\epsilon(a_1)\epsilon(a_n)\frac{| \alpha_n |}{\sqrt{1 + \alpha_n^2}}\right) \tag{a2.54}$$

where $\epsilon(a_1)$ et $\epsilon(a_n)$ give the sign of a_1 et a_n respectively and α_n is given by:

$$\alpha_n = \frac{a_n}{b_n} \tag{a2.55}$$

This concludes the proof.

22-Proofs associated to the section 4.3.9: Torsion angle and properties - $\phi_{l,l+1}$

Since the norms of the vectors involved in the calculation of the angle are preserved, we just have to check if the scalar product is the same.

We have:

$$\begin{aligned} & u_{n+1-l} \cdot u_{n+1-(l-1)} \\ &= b_{n+1-l} b_{n+1-(l-1)} + a_{n+1-l} a_{n+1-(l-1)} \\ &= (a_{l+1} a_l + b_{l+1} b_l)(-1)^{2k+2} \\ &= u_l \cdot u_{l+1} \end{aligned} \tag{a2.56}$$

This gives the result.

23-Proofs associated to the section 4.3.9: Orbital cases of the form (b_n, a_n): $\phi_{\infty,n}$

We can study the asymptotics of this angle by investigating the evolution of α_n.

We have:

$$\alpha_n = \frac{a_n}{b_n} = \frac{\sin\left(\frac{nk\pi}{n+1}\right)}{\sin\left(\frac{(n-1)k\pi}{n+1}\right)} \tag{a2.57}$$

As we have:

$$\begin{aligned} &\sin\left(\frac{nk\pi}{n+1}\right) \\ &= \sin\left(\frac{(n-1)k\pi}{(n+1)} + \frac{\pi k}{(n+1)}\right) \\ &= \sin\left(\frac{(n-1)k\pi}{(n+1)}\right)\cos\left(\frac{\pi k}{(n+1)}\right) + \cos\left(\frac{(n-1)k\pi}{(n+1)}\right)\sin\left(\frac{\pi k}{(n+1)}\right) \end{aligned} \tag{a2.58}$$

We get:

$$\alpha_n = \cos\left(\frac{\pi k}{n+1}\right) + \cos\left(\frac{(n-1)k\pi}{n+1}\right)\frac{\sin\left(\frac{\pi k}{n+1}\right)}{\sin\left(\frac{(n-1)k\pi}{n+1}\right)} \tag{a2.59}$$

For all n and k fixed, we have N going to infinity: $\frac{\pi k}{n+1}$ and $\frac{(n-1)k\pi}{n+1}$ which tend to zero.

We can then use the equivalents:

$$\sin\left(\frac{\pi k}{n+1}\right) \equiv \frac{\pi k}{n+1},$$

and,

$$\sin\left(\frac{(n-1)k\pi}{n+1}\right) \equiv \frac{(n-1)\pi k}{n+1} \tag{a2.60}$$

which gives by using the fact that: $\cos(\frac{\pi k}{n+1})$ tends to 1 when N tends to infinity:

$$\lim_{N\to\infty} \alpha_n = 1 + \frac{1}{n-1} \tag{a2.61}$$

By adding back into the formula of $\phi_{1,n}$, we finally get:

$$\lim_{N\to\infty} \phi_{1,n} = \arccos\left(\frac{n}{\sqrt{n^2+(n-1)^2}}\right) \tag{a2.62}$$

by using the fact that the sign of a_1 and a_n are positives for large values of N.

24-Proofs associated to the section 5.2.1: $\mathcal{A}_{N,n,+,,z}$ Angle between $\psi_{+,n}(0)$ and $\psi_{+,n}(z)$

For proof, we have:

$$\mathcal{A}_{N,n,+,0,z} = cos^{-1}\left(\frac{\psi_n(0).\psi_n(z)}{\|\psi_n(0)\|\|\psi_n(z)\|}\right) \tag{a2.63}$$

$\psi_n(0)$ and $\psi_n(z)$ are two vectors such as:

$$\psi_0(z) = \sqrt{\frac{2}{N+1}}\begin{pmatrix} 0 \\ a_n(1) \end{pmatrix} \tag{a2.64}$$

$$\psi_n(z) = \sqrt{\frac{2}{N+1}}\begin{pmatrix} a_n(z) \\ a_n(z+1) \end{pmatrix} \tag{a2.65}$$

For more details, the scalar product and the norm of the vectors give:

$$\psi_n(0).\psi_n(z) = \frac{2}{N+1} a_n(1) a_n(z+1) \tag{a2.66}$$

$$\|\psi_n(0)\| = \sqrt{\frac{2}{N+1}} \mid a_n(1) \mid \tag{a2.67}$$

$$\|\psi_n(z)\| = \sqrt{\frac{2}{N+1}} \sqrt{(a_n(z)^2 + (a_n(z+1))^2} \tag{a2.68}$$

Then,

$$\mathcal{A}_{N,n,+,0,z} = \cos^{-1}\left(\frac{a_n(1) a_n(z+1)}{\mid a_n(1) \mid \sqrt{(a_n(z))^2 + (a_n(z+1))^2}}\right) \tag{a2.69}$$

We know that $a_n(z+1) \neq 0$ and $z = 1, ..., N-1$, then:

$$\mathcal{A}_{N,n,+,0,z} = \cos^{-1}\left(\frac{\epsilon(a_n(1))\epsilon(a_n(z+1))}{\sqrt{1 + \left(\frac{a_n(z)}{a_n(z+1)}\right)^2}}\right) \tag{a2.70}$$

For $z = N$ we have:

$$a_n(N+1) = \sin(n\pi) = 0 \tag{a2.71}$$

thus,

$$\mathcal{A}_{N,n,+,0,N} = \cos^{-1}(0) = \pm\frac{\pi}{2} \tag{a2.72}$$

For $z = N$, we get:

$$\mathcal{A}_{N,n,+,0,N} = (-1)^{n+1}\frac{\pi}{2} \tag{a2.73}$$

The sign will depend on the symmetry (see eq. 5.51).

25-Proofs associated to the section 5.2.1: Hückel distribution coefficients in the case $\theta = 0$

The coefficients are detailed and depend on the form of the Hückel matrix:

$$c_y(z) = \sqrt{\frac{2}{N+2}} a_{N+1,n}(z+1) = \sqrt{\frac{2}{N+2}} \sin\left(\frac{n\pi(1+z)}{N+2}\right) \tag{a2.74}$$

$$c_x(z) = \sqrt{\frac{2}{N}} a_{N-1,n-1}(z) = \sqrt{\frac{2}{N}} \sin\left(\frac{(n-1)\pi z}{N}\right) \tag{a2.75}$$

with $c_x(0) = 0$ *and* $c_x(N) = 0$.

For more details, we consider the secular determinant of the Hückel matrix $S_N(\lambda)$:

$$S_N(\lambda) = \beta^N P_{N+1}(w) P_{N-1}(w) \tag{a2.76}$$

Note that we have for solution $2N$ non-degenerate roots. $P_{N-1}(w)$ and $P_{N+1}(w)$ are symmetric roots corresponding respectively to the systems p_x and p_y and β being as we have previously seen the total overlap.

Part VI

Abstract

English version:

Title

Structural and Electronic Chemistry: Role of Symmetries and Curvature

Abstract

This thesis is the result of 3 years of work based on the subject: "Structural and Electronic Chemistry: Role of Symmetries and Curvature".

The originality of the topic consists in the multidisciplinary nature of the subject which involves both chemists theoreticians and mathematicians. An important part of the work is based on the understanding of theoretical chemistry and its use by modeling.
One of the objectives attributed to this work, is the understanding of molecular systems by geometrical tools mainly initiated by Robert C. Haddon in 1997. We first propose a clarification and a generalization of these tools based on carbon materials such as fullerenes whose study of topological characteristics is largely exploited in this manuscript.
All the theoretical points and tools developed (the pyramidalization angle, the spherical curvature, the angular defect, and the hybridization) are widely illustrated with cartographies by the use of programming tools and softwares which provide the study of the deformation, the curvature and the investigation of the chemical and physical properties of the systems.
The use of the tools resulting from this work will facilitate the simulation of molecules without size limitation and for systems whose modelisation by ab-initio or DFT calculations remains inaccessible.
We also tried to show the relation which could exist between the geometry of the systems and the orbital information. We were interested in many systems as examples most of them are carbon-based and potentially aromatic.
Consequently, we propose the study of the criteria of aromaticity according to the theories stated among others by Hückel. By this study, we focus on less known linear systems: the [n]-cumulenes which present the curiosity of helical orbitals. We established the criteria for the existence of this type of helices according to the molecular symmetry.

The aim *in fine* was to establish the link between the topological characteristics and the chemical reactivity of these molecules and materials.

Keywords

Theoretical Chemistry - Simulation - Electronic Structure - Symmetry - Curvature - Materials - Pyramidalization Angle - POAV - Helical Orbitals

Version française:

Titre

Chimie Structurale et Electronique: Rôle des Symétries et de la Courbure

Résumé

Cette thèse est le fruit de 3 années de travail reposant sur le sujet intitulé : "Chimie Structurale et Electronique: Rôle des Symétries et de la Courbure".

L'originalité de la thématique abordée dans ce travail se trouve dans la pluridisciplinarité du sujet qui fait appel à la fois aux chimistes théoriciens et aux mathématiciens. Une importante partie des travaux se base sur la compréhension de la chimie théorique et de son utilisation par modélisation.
Un des objectif alloué à ce travail, est la compréhension des systèmes moléculaires par des outils géométriques principalement initiés par Robert C. Haddon dès 1997. Nous avons tout d'abord proposé une clarification et une généralisation de ces outils basées sur des matériaux carbonés comme les fullerènes dont l'étude des caractéristiques topologiques est largement exploitée dans ce manuscrit.
L'ensemble des points théoriques et des outils développés (l'angle de pyramidalisation, la courbure sphérique, le défaut angulaire, et l'hybridation) ont été largement illustrés avec des cartographies par l'utilisation d'outils de programmation et de logiciels qui ont permis l'étude de la déformation, de la courbure et l'étude des propriétés chimiques et physiques des systèmes.
L'utilisation des outils issus de ce travail devrait permettre de pouvoir faciliter la modélisation de molécules sans limitation de tailles et pour des systèmes dont la modélisation par des calculs ab-initio ou DFT reste inaccessible.
Nous avons également cherché à montrer le lien pouvant exister entre la géométrie des systèmes et l'information orbitalaire. Nous nous sommes intéressés à titre d'exemples à de nombreux systèmes pour la plupart carbonés et potentiellement aromatiques.
Enfin, nous avons proposés l'étude des critères d'aromaticité suivant les théories énoncées entre autre par Hückel. Par cette étude, nous nous sommes penchés sur des systèmes linéaires moins connus i.e. les [n]-cumulènes qui présentent en particulier la curiosité de posséder des orbitales hélicoïdales. Nous avons établis les critères d'apparition de ce type d'hélices en fonction de la symétrie moléculaire.

Le but *in fine* de ce travail, était de réussir à faire le lien entre des caractéristiques topologiques et la réactivité chimique de ces molécules et matériaux.

Mots clefs

Chimie Théorique - Modélisation - Structure Electronique - Symétrie - Courbure - Matériaux - Angle de Pyramidalisation - POAV - Orbitales Hélicoïdales

List of Figures

List of Tables

Nomenclature

$L_N(\phi)$ Arrangement of atoms in line with a ϕ distribution

$S^1_N(\phi)$ Arrangement of atoms in circle with a ϕ distribution

$x \equiv y$ [mod.4] x is congruent to y - modulo 4

Ang Def: Angular Defect

AO: Atomic Orbital

CAS: Complete Active Space

CASPT2: Complete Active Space Perturbation Theory

CASSCF: Complete Active Space Self-Consistent Field

CI: Configuration Interaction

COF: Covalent Organic Framework

DFT: Density Functional Theory

DPBD: Diphenylbutadiyne

FVP: Flash Vacuum Pyrolysis

GGA: Generalized Gradient Approximation

GTO: Gaussian Type Orbitals

HF: Hartree-Fock

HOMO: Highest Occupied Molecular Orbital

HSE: Heyd Scuseria Ernzerhof

Hyb: Hybridization

IEPA: Independent Electron Pair Approximation

KS: Kohn-Sham

LCAO: Linear Combination of Atomic Orbitals

LDA: Local Density Approximation

LUMO: Lowest Unoccupied Molecular Orbital

MAD: Mean Absolute Deviation

MCSF: Multi Configurational Self Consistent field

MO: Molecular Orbital

MOF: Metal-Organic Framework

NBO: Natural Bond Orbital

PBE: Perdew Burke Ernzerhof

PES: Potential Energy Surface

POAV: π-Orbital Axis Vector

Pyr: Pyramidalization angle

RHF: Restricted Hartree-Fock

Sph Curv: Spherical Curvature

STO: Slater Type Orbitals

Index

Bibliography

[1] I. H. Son, J. H. Park, S. Park, K. Park, S. Han, J. Shin, S.-G. Doo, Y. Hwang, H. Chang, and J. W. Choi. Graphene balls for lithium rechargeable batteries with fast charging and high volumetric energy densities. *Nature Communications*, 8:–, 2017.

[2] J. Abraham, K. S. Vasu, C. D. Williams, K. Gopinadhan, Y. Su, C. T. Cherian, J. Dix, E. Prestat, S. J. Haigh, I. V. Grigorieva, P. Carbone, A. K. Geim, and R. R. Nair. Tunable sieving of ions using graphene oxide membranes. *Nature Nanotechnology*, 12:546–550, 2017.

[3] R. C. Haddon. C_{60} sphere or polyhedron? *Journal of the American Chemical Society*, 119:1797–1798, 1997.

[4] J. Sabalot-Cuzzubbo, G. Salvato-Vallverdu, D. Bégué, and J. Cresson. Relating the molecular topology and local geometry: Haddon's pyramidalization angle and the Gaussian curvature. *Journal of Chemical Physics*, 152:244310, 2020.

[5] D. Tománek and N. Frederick. c_n fullerenes. `https://nanoten.com/science/fullerene/index.html`. Accessed: 2021-10-15.

[6] R. C. Haddon. Hybridization and the orientation and alignment of π-orbitals in nonplanar conjugated organic molecules: π-orbital axis vector analysis (POAV2). *Journal of the American Chemical Society*, 108:2837–2842, 1986.

[7] E. Heilbronner. Hückel molecular orbitals of Möbius-type conformations of annulenes. *Tetrahedron Letters*, 5:1923–1928, 1964.

[8] H. E. Zimmerman. On molecular orbital correlation diagrams, the occurrence of Möbius systems in cyclization reactions, and factors controlling ground- and excited-state reactions.I. *Journal of the American Chemical Society*, 88:1564–1565, 1966.

[9] M. H. Garner, R. Hoffmann, S. Rettrup, and G. C. Solomon. Coarctate and Möbius: The helical orbitals of allene and other cumulenes. *ACS Central Science*, 4:688–700, 2018.

[10] G. Salvato-Vallverdu, J. Sabalot-Cuzzubbo, D. Bégué, and J. Cresson. Pychemcurv. `https://pychemcurv.readthedocs.io/en/latest/`. Accessed: 2021-10-15.

[11] Y. Jean and F. Volatron. *Structure électronique des molécules - Vol2 : Géométrie, réactivité, et méthode de* H*ückel*. Dunod, 2003.

[12] M. J. Frisch, G. W. Trucks, H. B. Schlegel, G. E. Scuseria, M. A. Robb, J. R. Cheeseman, G. Scalmani, V. Barone, G. A. Petersson, H. Nakatsuji, X. Li, M. Caricato, A. V. Marenich, J. Bloino, B. G. Janesko, R. Gomperts, B. Mennucci, H. P. Hratchian, J. V. Ortiz, A. F. Izmaylov, J. L. Sonnenberg, D. Williams-Young, F. Ding, F. Lipparini, F. Egidi, J. Goings, B. Peng, A. Petrone, T. Henderson, D. Ranasinghe, V. G. Zakrzewski, J. Gao, N. Rega, G. Zheng, W. Liang, M. Hada, M. Ehara, K. Toyota, R. Fukuda, J. Hasegawa, M. Ishida, T. Nakajima, Y. Honda, O. Kitao, H. Nakai, T. Vreven, K. Throssell, J. A. Montgomery, Jr., J. E. Peralta, F. Ogliaro, M. J. Bearpark,

J. J. Heyd, E. N. Brothers, K. N. Kudin, V. N. Staroverov, T. A. Keith, R. Kobayashi, J. Normand, K. Raghavachari, A. P. Rendell, J. C. Burant, S. S. Iyengar, J. Tomasi, M. Cossi, J. M. Millam, M. Klene, C. Adamo, R. Cammi, J. W. Ochterski, R. L. Martin, K. Morokuma, O. Farkas, J. B. Foresman, and D. J. Fox. Gaussian 16 Revision C.01, 2016. Gaussian Inc. Wallingford CT.

[13] A.D. Becke. Density-functional thermochemistry.III. The role of exact exchange. *Journal of Chemical Physics*, 98:5648–5652, 1993.

[14] C. Lee, W. Yang, and R.G. Parr. Development of the Colle-Salvetti correlation-energy formula into a functional of the electron density. *Physical Review B*, 37:785–789, 1998.

[15] H.-J. Werner, P.J. Knowles, G. Knizia, F. R. Manby, M. Schütz, P. Celani, T. Korona, R. Lindh, A. Mitrushenkov, and et al. G. Rauhut. MOLPRO, version 2012.1, A package of ab initio programs,, 2012.

[16] K. Kim and K. D. Jordan. Comparison of Density Functional and MP2 calculations on the water monomer and dimer. *The Journal of Physical Chemistry*, 98:10089–10094, 1994.

[17] C. F. Chabalowski P. J. Stephens, F. J. Devlin and M. J. Frisch. Ab initio calculation of vibrational absorption and circular dichroism spectra using density functional force fields. *The Journal of Physical Chemistry*, 98:11623–11627, 1994.

[18] J. P. Perdew, M. Ernzerhof, and K. Burke. Rationale for mixing exact exchange with density functional approximations. *The Journal of Physical Chemistry*, 105:9982–9985, 1996.

[19] C. Adamo and V. Barone. Toward reliable density functional methods without adjustable parameters: The PBE0 model. *The Journal of Chemical Physics*, 110:6158–6170, 1999.

[20] J. Heyd, G. Scuseria, and M. Ernzerhof. Hybrid functionals based on a screened Coulomb potential. *The Journal of Chemical Physics*, 118:8207–8215, 2003.

[21] Y. Zhao and D. G. Truhlar. The M06 suite of density functionals for main group thermochemistry, thermochemical kinetics, non covalent interactions, excited states, and transition elements: two new functionals and systematic testing of fourM06-class functionals and 12 other functionals. *Theoretical Chemistry Accounts*, 120:215–241, 2008.

[22] Y. Zhao and D. G. Truhlar. Density functional for spectroscopy: No long-range Self-Interaction error, good performance for Rydberg and charge transfer states, and better performance on average than B3LYP for ground states. *The Journal of Physical Chemistry A*, 110:13126–13130, 2006.

[23] R. C. Haddon and L. T. Scott. π-orbital conjugation and rehybridization in bridged annulenes and deformed molecules in general: π-orbital axis vector analysis. *Pure and Applied Chemistry*, 58:137–142, 1986.

[24] H. W. Kroto, J. R. Heath, S. C. O'Brien, R. F. Curl, and R. E. Smalley. C_{60}: Buckminsterfullerene. *Nature*, 318:162–163, 1985.

[25] R. C. Haddon. Comment on the relationship of the pyramidalization angle at a conjugated carbon atom to the σ-bond angles. *The Journal of Physical Chemistry A*, 105:4164–4165, 2001.

[26] Y. Liu, H. Pottmann, J. Wallner, Y. L. Yang, and W. Wang. Geometric modeling with conical meshes and developable surfaces. *ACM Trans. Graph.*, 25:681–689, 2006.

[27] P. Romon. *Introduction à la géométrie différentielle discrète*. Ellipses, 2013.

[28] J. G. Radziszewski, J. W. Downing, M. Jawdosiuk, P. Kovacic, and J. Michl. 4-azahomoadamant-3-ene: spectroscopic characterization and photoresolution of a highly reactive strained bridgehead imine. *Journal of the American Chemical Society*, 107:594–603, 1985.

[29] R. C. Haddon. GVB and POAV analysis of rehybridization and π-orbital misalignment in non-planar conjugated systems. *Chemical Physics Letters*, 125:231–234, 1986.

[30] R. C. Haddon. Measure of nonplanarity in conjugated organic molecules: which structurally characterized molecule displays the highest degree of pyramidalization? *Journal of the American Chemical Society*, 112:3385–3389, 1990.

[31] A. R. Khamatgalimov, L. I. Yakypova, and V. I. Kovalenko. Features of molecular structure of small non-IPR fullerenes: the two isomers of C_{50}. *Theoritical Chemistry Accounts*, 139:159, 2020.

[32] D. Bégué, A. Dargelos, and C. Wentrup. Rearrangements of nitrile imines: Ring expansion of benzonitrile imines to cycloheptatetraenes and ring closure to 3-phenyl-3h-diazirines. *Journal of Organic Chemistry*, 84:8668–8673, 2019.

[33] J. Guan, Z. Jin, Z. Zhu, C. Chuang, B-Y. Jin, and D. Tománek. Local curvature and stability of two-dimensional systems. *Physical Review B*, 90:245403–1–245403–6, 2014.

[34] X. Han, S-J. Zhou, Y-Z. Tan, X. Wu, F. Gao, Z-J. Liao, R-B. Huang, Y-Q. Feng, X. Lu, S-Y. Xie, and L-S. Zheng. Crystal structures of saturn-like $C_{50}Cl_{10}$ and pineapple-shaped $C_{64}Cl_4$: geometric implications of double and triple-pentagon-fused chlorofullerenes. *Angewandte Chemie International Edition*, 47:5340–5343, 2008.

[35] K. Momma and F. Izumi. VESTA 3 for three-dimensional visualization of crystal, volumetric and morphology data. *Journal of Applied Crystallography*, 44:1272–1276, 2011.

[36] J. Sabalot-Cuzzubbo, J. Cresson, and D. Bégué. Haddon's POAV2 versus POAV theory for non planar molecules. *Preprint*, 2021.

[37] H. Santos Silva, J. Cresson, A. Rivaton, D. Bégué, and R. C. Hiorns. Correlating geometry of multidimensional carbon allotropes molecules and stability. *Organic Electronics*, 26:395–399, 2015.

[38] Y. Tanuma, T. Maekawa, and C. Ewels. Methodological investigation for hydrogen addition to small cage carbon fullerenes. *Crystals*, 11:1334, 2021.

[39] I. R. Amaral, A. Forestier, A. Piednoir, R. Galafassi, C. Bousige, D. Machon, O. Pierre-Louis, R. S. Alencar, A. G. Souza Filho, and A. San-Miguel. Delamination of multilayer graphene stacks from its substrate through wrinkle formation under high pressures. *Carbon*, 185:242–251, 2021.

[40] W. Humphrey, A. Dalke, and K. Schulten. VMD: Visual molecular dynamics. *Journal of Molecular Graphics*, 14:33–38, 1996.

[41] P. Z. Moghadam, A. Li, S. B. Wiggin, A. Tao, A. G. P. Maloney, P. A. Wood, S. C. Ward, and D. Fairen-Jimenez. Development of a cambridge structural database subset: A collection of Metal–Organic Frameworks for past, present, and future. *Chemistry of Materials*, 29:2618–2625, 2017.

[42] P. Z. Moghadam, A. Li, S. B. Wiggin, A. Tao, A. G. P. Maloney, P. A. Wood, S. C. Ward, and D. Fairen-Jimenez. Cambridge Structural Database (CSD) MOF subset. `https://sites.google.com/view/csdmofsubset/contact`. Accessed: 2021-12-16.

[43] N. Tracy-Amoroso, B. Bucior, D. Siderius, and S. Bobbitt. MOFDB API databases. `https://mof.tech.northwestern.edu`. Accessed: 2021-12-16.

[44] J. Sabalot-Cuzzubbo, J. Cresson, and D. Bégué. Generation of helical states - breaking of symmetries, Curie's principle, and excited states. *Preprint*, 2021.

[45] J. Sabalot-Cuzzubbo, J. Cresson, and D. Bégué. Etude des structures optimales et équivalentes de quelques molécules - e cas linéaire et le cercle pour la distribution nulle ou de möbius. *Preprint*, 2020.

[46] H. E. Zimmerman. The Möbius-Hückel concept in organic chemistry. application of organic molecules and reactions. *Accounts of Chemical Research*, 4:272–280, 1971.

[47] R. Herges. Topology in chemistry: Designing Möbius molecules. *Chemical Reviews*, 106:4820–4842, 2006.

[48] A. Frost and B. Musulin. A mnemonic device for molecular orbital energies. *The Journal of Chemical Physics*, 21:572, 1953.

[49] K. Möbius, Ma. Plato, G. Klihm, C. Laurich, A. Savitsky, W. Lubitz, B. Szyszko, M. Stępień, and L. Latos-Grażyński. Möbius–Hückel topology switching in an expanded porphyrin cation radical as studied by EPR and ENDOR spectroscopy. *Physical Chemistry Chemical Physics*, 17:6644–6652, 2015.

[50] A. F. Möbius. Über die bestimmung des inhaltes eines polyëders. *Berichte über die Verhandlungen der Königlich Sächsischen Gesellschaft der Wissenschaften, Mathematisch-physikalische Klasse*, 17:31–68, 1865.

[51] J. B. Listing. Der census räumlicher complexe, oder verallgemeinerung des euler´schen satzes von den polyädern. *Abhandlungen der Königlichen Gesellschaft der Wissenschaften in Göttingenen*, 10:97–182, 1861.

[52] D. Ajami, O. Oeckler, A. Simon, and R. Herges. Synthesis of a Möbius aromatic hydrocarbon. *Nature*, pages 819–821, 2003.

[53] D. Ajami, K. Hess, F. Köhler, C. Näther, O. Oeckler, A. Simon, C. Yamamoto, Y. Okamoto, and R. Herges. Synthesis and properties of the first Möbius annulenes. *Chemistry A European Journal*, 12:5434–5445, 2006.

[54] C. A. Coulson, B. O'Leary, and R. B. Mallion. HÜCKEL THEORY FOR ORGANIC CHEMISTS. Academic Press, 1978.

[55] M. H. Garner, A. Jensen, L. O. Hyllested, and G. C. Solomon. Helical orbitals and circular currents in linear carbon wires. *Chemical Science*, 10:4598–4608, 2019.

[56] W. Bro-Jørgensen, M. H. Garner, and G. C. Solomon. Quantification of the helicality of helical molecular orbitals. *The Journal of Physical Chemistry A*, 125:8107–8115, 2021.

[57] L. Jin and Z. Song. Partitioning technique for discrete quantum systems. *Physical Review A*, 83:062118, 2011.

[58] H. Fischer and H. Kollmar. Zur invarianz in der LCAO MO theorie. *Theoretica chimica acta volume*, 12:344–348, 1968.

[59] R. J. Buencker. Theoretical study of the rotational barriers of allene, ethylene, and related systems. *The Journal of Chemical Physics*, 48:1368, 1968.

[60] H. Dickerson, S. Ferber, and F. S. Richardson. Molecular orbital calculations on the optical rotatory properties of chiral allene systems. *Theoretica chimica acta volume*, 48:33–344, 1976.

[61] R. Herges. Organizing principle of complex reactions and theory of coarctate transition states. *Angewandte Chemie*, 33:255–276, 1994.

[62] Y. Orimoto, Y. Aoki, and A. Imamura. Extraction of one-handed helical frontier orbital in even [n]cumulenes by breaking mirror images of right- and left-handed helical orbitals: Theoretical study. *The Journal of Physical Chemistry C*, 123:11134–11139, 2019.

[63] C. H. Hendon, D. Tiana, A. T. Murray, D. R. Carberya, and A. Walsh. Helical frontier orbitals of conjugated linear molecules. *Chemical Science*, 4:4278–4284, 2013.

[64] S. Yu and S. Ma. How easy are the syntheses of allenes? *Chemical Communications*, pages 5384–5418, 2011.

[65] P. Rivera-Fuentes and F. Diederich. Allenes in molecular materials. *Angewandte Chemie*, 51:2818–2828, 2012.

[66] W. D. Chu, L. Zhang, Z. Zhang, Q. Zhou, F. Mo, Y. Zhang, and J. Wang. Enantioselective synthesis of trisubstituted allenes via Cu(I)-catalyzed coupling of diazoalkanes with terminal alkynes. *Journal of the American Chemical Society*, 138:14558–14561, 2016.

[67] J. Ye and S. Ma. Conquering three-carbon axial chirality of allenes. *Organic Chemistry Frontiers*, 1:1210–1224, 2014.

[68] S. Gunasekaran and L. Venkataraman. Tight-binding analysis of helical states in carbyne. *Journal of Chemicals Physics*, 153:124304, 2020.

[69] D. Wendiger and R. R. Tykwinski. Odd [n]-cumulenes (n = 3, 5, 7, 9): synthesis, characterization, and reactivity. *Accounts of Chemical Research*, 50:1468–1479, 2017.

[70] A. Imamura and Y. Aoki. Helical molecular orbitals around straight-chain polyyne oligomers as models for molecular devices. *Chemical Physics Letters*, 590:136–140, 2013.

[71] M. H. Garner and C. Corminboeuf. Correlation between optical activity and the helical molecular orbitals of allene and cumulenes. *Organic Letters*, 22:8028–8033, 2020.

[72] F. Weinhold. Why do cumulene ketones kink? *The Journal of organic chemistry*, 82:12238–12245, 2017.

[73] C. A. Coulson. The electronic structure of some polyenes and aromatic molecules IV-the nature of the links of certain free radicals. *Proceedings of the Royal Society A*, 164:383–396, 1938.

[74] P-O. Löwdin. Studies in perturbation theory. IV. Solution of eigenvalue problem by projection operator formalism. *Journal of Mathematical Physics*, 3:969, 1961.

[75] P. Curie. Sur la symétrie dans les phénomènes physiques, symétrie d'un champ électrique et d'un champ magnétique. *Journal de Physique Théorique et Appliquée*, 3:393–415, 1894.

[76] A.F. Chalmers. Curie's principle. *The British Journal for the Philosophy of Science*, 21:133–148, 1970.

[77] J. Ismael. Curie's principle. *Synthese*, 110:167–190, 1997.

[78] J. Escudié, H. Ranaivonjatovo, and L. Rigon. Heavy allenes and cumulenes $E = C = E'$ and $E = C = C = E'$ ($E = P, As, Si, Ge, Sn$; $E' = C, N, P, As, O, S$). *Chemical Reviews*, 100:3639–3696, 2000.

[79] S. Toyota, K. Kawai, T. Iwanaga, and K. Wakamatsu. Tolanophane revisited-resolution and racemization mechanism of a twisted chiral aromatic compound. *European Journal of Organic Chemistry*, 2012:5679–5684, 2012.

[80] G. Cavigliasso and N. Kaltsoyannis. On the paucity of molecular actinide complexes with unsupported metalmetal bonds: a comparative investigation of the electronic structure and metalmetal bonding in U_2X_6 (X = Cl, F, OH, NH_2, CH_3) complexes and $d-$block analogues. *Inorganic Chemistry*, 45:6828–6839, 2006.

[81] O. Cretu, H.-P. Komsa, O. Lehtinen, G. Algara-Siller, U. Kaiser, K. Suenaga, and A. V. Krasheninnikov. Experimental observation of boron nitride chains. *ACS Nano*, 8:11950–11957, 2014.

[82] M. J. Frisch, G. W. Trucks, H. B. Schlegel, G. E. Scuseria, M. A. Robb, J. R. Cheesemana, G. Scalmani, V. Barone, B. Mennucci, and G. A. Petersson et al. Gaussian 09, revision a.2, 2009. Gaussian Inc. Wallingford CT.

[83] A. Ozcelik, D. Aranda, S. Gil-Guerrero, X. A. Pola-Otero, M. Talavera, L. Wang, S. Kumar Behera, J. Gierschner, Á. Peña-Gallego, F. Santoro, R. Pereira-Cameselle, and J. L. Alonso-Gómez. Distinct helical molecular orbitals through conformational lock. *Chemistry A European Journal*, 26:17342–17349, 2020.

[84] Avogadro Chemistry. Avogadro. `http://avogadro.cc/`. Accessed: 2022-01-17.

[85] Gijs Schaftenaar. Molden. `https://www3.cmbi.umcn.nl/molden/`. Accessed: 2022-01-17.

[86] Roy Dennington, Todd A. Keith, and John M. Millam. Gaussview Version 6, 2019. Accessed: 2022-01-17.

[87] `https://git.univ-pau.fr/num-as/pyrene-cluster/-/wikis/1-Environment/1.1-Overview`, 2021. Accessed: 2022-01-17.

ECOLE DOCTORALE :
Sciences Exactes et leurs Applications de l'Université de Pau et des Pays de l'Adour

LABORATOIRES :
IPREM Institut des Sciences Analytiques et de Physico-Chimie pour l'Environnement et les Matériaux
LMAP Laboratoire de Mathématiques et de leurs Applications

ABSTRACT

This thesis is the result of 3 years of work based on the subject: **"Structural and Electronic Chemistry: Role of Symmetries and Curvature"**.

The originality of the topic consists in the multidisciplinary nature of the subject which involves both theoretical chemists and mathematicians. An important part of the work is based on the understanding of theoretical chemistry and its use by modeling.
One of the objectives attributed to this work, is the understanding of molecular systems by geometrical tools mainly initiated by Robert C. Haddon in 1997. We first propose a clarification and a generalization of these tools based on carbon materials such as fullerenes whose study of topological characteristics is largely exploited in this manuscript.
All the theoretical points and tools developed (the pyramidalization angle, the spherical curvature, the angular defect, and the hybridization) are widely illustrated with cartographies by the use of programming tools and softwares which provide the study of the deformation, the curvature and the investigation of the chemical and physical properties of the systems.
The use of the tools resulting from this work will facilitate the simulation of molecules without size limitation and for systems whose modelisation by ab-initio or DFT calculations remains inaccessible.
We also tried to show the relation which could exist between the geometry of the systems and the orbital information. We were interested in many systems as examples most of them are carbon-based and potentially aromatic.
Consequently, we propose the study of the criteria of aromaticity according to the theories stated among others by Hückel. By this study, we focus on less known linear systems: the [n]-cumulenes which present the curiosity of helical orbitals. We established the criteria for the existence of this type of helices according to the molecular symmetry.

The aim *in fine* was to establish the link between the topological characteristics and the chemical reactivity of these molecules and materials.

CONTACT

Didier BEGUE
Professeur
IPREM, Pôle CAPT, Pau
didier.begue@univ-pau.fr

Jacky CRESSON
Professeur
IPRA, LMAP, Pau
jacky.cresson@univ-pau.fr

Julia SABALOT-CUZZUBBO
Doctorante
IPREM, Pôle CAPT, Pau
sabalot.julia@univ-pau.fr